1. AGENCY USE ONLY (Leave blank)	2. REPORT DATE	3. REPORT TYPE AND DATES COVERED
	April 1991	Final Report 1988-1991

4. TITLE AND SUBTITLE

PREPARATION AND CHARACTERIZATION OF CARBON FILAMENTS

5. FUNDING NUMBERS

F49620-88-C-0017

6. AUTHOR(S)

Dinesh Patel and Carol McConica*

7. PERFORMING ORGANIZATION NAME(S) AND ADDRESS(ES)

Colorado State University
Physics Department,* Ag. & Chem. Engineering
Fort Collins, CO 80523

8. PERFORMING ORGANIZATION REPORT NUMBER

AFOSR-TR-

9. SPONSORING/MONITORING AGENCY NAME(S) AND ADDRESS(ES)

Dr. Liselotte J. Schioler
Air Force Office of Scientific Research
Bolling Air Force Base
Washington, D.C. 20332-6448

10. SPONSORING/MONITORING AGENCY REPORT NUMBER

2306/A2

11. SUPPLEMENTARY NOTES

12a. DISTRIBUTION/AVAILABILITY STATEMENT

Unlimited

12b. DISTRIBUTION CODE

13. ABSTRACT *(Maximum 200 words)*

The final report for our contract "Preparation and Characterization of Carbon Filaments" is presented. We have performed important and extensive research on Catalytic Chemical Vapor deposited fibers with comparative work on ex-polymer fibers. A new diagnostic technique has been developed involving low frequency electrical noise in carbon fibers. The exciting results from this technique infer microstructural properties as inter-ribbon and inter-layers are probed. Mechanical properties including Young's modulus, torsional modulus and compressive properties have been measured also on CCVD filaments. We have proved that Young's modulus of CCVD fibers generally decrease with diameter. However, increases in the Young's modulus for a small range of diameters may be present due to separating entities during the growth of CCVD fibers. Higher torsional moduli were also measured for these annular structures. Typical values were as high as one quarter theoretical maximum for a perfectly ordered system. Temperature dependent piezoresistance was observed for the first time in high moduli fibers. The dependence was dramatic in annealed CCVD carbon fiber. These dependencies are due to electronic mechanisms. Effort has also been made to perform in situ Raman spectroscopic study during CCVD process.

14. SUBJECT TERMS	15. NUMBER OF PAGES
Carbon Fibers, CCVD(Catalytic Chemical Vapor Deposition), Electrical Noise, Mechanical Properties, Young's Modulus	225 Pages
	16. PRICE CODE

17. SECURITY CLASSIFICATION OF REPORT	18. SECURITY CLASSIFICATION OF THIS PAGE	19. SECURITY CLASSIFICATION OF ABSTRACT	20. LIMITATION OF ABSTRACT
Unclassified	Unclassified	Unclassified	Unlimited

INTRODUCTION

Carbon fibers possesses excellent strength-to-mass parameter which makes it a highly desirable candidate for technological applications such as airborne vehicles by the Air Force. As an example of an advanced material, Carbon fiber-Carbon matrix Composites referred to as C-C Composites are being developed. A major area of research is why the excellent mechanical properties of carbon fibers have not been translated in to composites? Carbon fiber can be prepared with a large range of Young's moduli (E_y) dependent on the orientation of the hexagonal ribbons with respect to the fiber axis and can approach the theoretical limit of perfect graphite ($E_y \sim 1000$ GPa). Generally, the strength of the fiber decreases with increasing E_y. Most carbon fibers are heterogeneous materials, therefore, stress leading to fracture develop at flaws reduces the strength below the theoretical limit. Carefully controlling the microstructure during fiber processing will lead to improved mechanical properties corresponding to calculated values.

Whereas commercial ex-PAN fibers (accounting for over 90% of the current market) and ex-pitch fibers are prepared from polymer precursors and are continuous; a relatively new type is prepared from vapor phase (Catalytic Chemical Vapor Deposited) CCVD fibers. These fibers are more graphitic than ex-polymer ones, so are more readily intercalated. They also have different microstructure compared to those of other commercial fibers. CCVD fibers reveal a tree-ring like morphology. The concentric layers are parallel to the fiber axis and therefore, the tree-ring appearance. The vapor grown fibers have good thermal and electrical conductivity, and tensile strength and moduli. A disadvantage is their inability to be produced continuously, however thickening ex-PAN fibers by this CCVD process may a solution. The vapor-phase deposition technique offers a way to carefully control the microstructure of the fibers and to harness the high-strength-to mass ratio for application. To some degree, CCVD may play a major role in carbon technology similar to it's partner in the semiconductor industry especially where applications are dictated by specific fiber and matrix microstructure.

Research was undertaken to provide a detailed characterization of CCVD carbon fibers and compare them with polymer based fibers. Understanding the gas-phase reactions during the CCVD process was also included in our study. The order of this report will begin by defining a list of objectives followed by a summary of the most important accomplishments. We also list pertinent publications which have been published and the work performed under the present contract that will be published. Participants in this project have been acknowledged including students and professionals. A special dedication is made to Professor Ian L. Spain who died in September, 1990. Ian was the Principal Investigator on the present contract.

The detailed technical portion of the report includes six sections which are all inter-related. We have established a new technique in performing low frequency-electrical noise in carbon fibers. New temperature dependent piezoresistance on carbon fibers have also been determined for the first time. A set of mechanical tests have been established in our facility. Electrical and magnetic field studies have also been carried out and presented in this report. The fibers were prepared at Colorado State University by vapor deposition on metal-catalyzed substrates and thickened ex-PAN fibers. An account of the growth technique and in situ Raman spectroscopic study is also given. Appendix includes reprints of publications.

TABLE OF CONTENTS

RESEARCH SECTIONS

A. LIST OF OBJECTIVES

Research was undertaken here at Colorado State University in the preparation and characterization of carbon fibers with emphasis on Catalytic Chemical Vapor Deposited carbon fibers. Our efforts were aimed at achieving superior fibers with high-strength-to-weight properties important in highly technological material like the Carbon-Carbon composites and electronic applications. The thrust of our work involved high degree of electrical, mechanical, structural characterization and effort to improve the CCVD technique by understanding the underlying mechanisms of growth. The following are specific objectives.

Objective 1

CCVD of carbon fibers were obtained by both in-house and on special consignment from Applied Sciences, Inc. These relatively new filaments were the subject of detailed research involving quantification of their mechanical and electrical properties. Where appropriate comparisons have been made with ex-polymer and bulk carbons.

I Low frequency electrical noise in carbon fibers.

II Mechanical characterization including determination of the diameter dependent Young's modulus (from tensile and compressive effect via loop tests), and torsional modulus. Electro-mechanical characterization from new piezoresistance measurements.

III Electrical and high magnetic field properties of CCVD and thickened ex-PAN carbon fibers.

IV Structural understanding of these relatively new fibers in comparison to PAN and pitch.

Objective 2

In-house capabilities were initiated with the aim of producing specialized fibers with specific features such as size, microstructure, and additives during vapor deposition process.

I Reactor design optimized to produce straight thin CCVD fibers for the previous contract were modified to produce samples of CCVD fibers for the present efforts.

II Substrate and catalyst standardization for the production of CCVD fibers with optimum morphology.

III A thickening reactor for the process of thickening ex-PAN fibers to simulate composite.

IV Gas-phase reactions using Raman spectroscopic techniques.

B. SUMMARY OF THE MOST IMPORTANT ACCOMPLISHMENTS

1. Low frequency Electrical Noise in Carbon Fibers

For the first time our group has established that low frequency electrical noise, referred to as 1/f noise, measured in carbon fibers reflects their microstructure quantitatively. One of our paper published in J. Applied Physics (see appendix) reported the first exciting result of the variation in the magnitude of the noise power for carbon fibers with different microstructure. Electrical noise is a manifestation of conductivity fluctuation. Therefore, noise magnitudes in fibers prepared from ex-PAN, pitch and vapor deposited filaments showed dependencies corresponding to their different structural morphology. In the order given, these fibers usually vary from random, radial to annular arrangement of structure respectively. This increasing degree of crystallinety leads to reduced electron scattering and thus lowering of the 1/f noise in carbon fibers.

Low temperature (10-300K) profiling of 1/f noise in these important carbon fibers show multiple type electronic interactions. In fact results show that higher temperature (>300K) measurements may be important in these fibers. This will be of great importance since high temperature applications of carbon-carbon composites are of considerable interest.

To maintain a progressive development of this new and exciting tool, we have for the first time performed the noise measurements in carbon fibers under applied stress and also during a fiber loop test. This research is being submitted for publication in the J. Applied Physics 1991. Uniaxial stress showed a small reduction in noise as the fibril alignment improved with small stress. However, considerable increase in the noise was observed for higher stress as the fibril-fibril contacts ruptured and created electronic scattering centers in the fiber. Models have been proposed to explain the noise behavior in carbon fibers.

An exciting prospect is the application of this 1/f noise technique in diagnosing the high temperature oxidation sensitivity of the carbon-carbon composite. We believe that we can contribute positively to this problem with our new technique and expertise here at Colorado State University.

2. Mechanical Properties of Vapor grown Carbon Fibers

In any characterization involving carbon fibers, the mechanical testing should be routine, especially since a major advantage of these materials is their high-strength-to-mass ratio. We have performed a number of measurements to mechanically characterize CCVD fibers and where appropriate comparison made with ex-PAN and pitch fibers. Manuscripts have been prepared on the following measurements:

(i) Stress-Strain Profile

A simple yet accurate test apparatus for stress profiling has been developed using linear variable transformers. Displacement resolutions of about 2μm can be detected with ease. This is sufficient for a single carbon fiber which typically have elastic strain values less than 1%. Young's modulus of vapor grown carbon fibers with varying diameters have been measured successfully. Results show a decrease in the Young's modulus with increasing diameters. A value of 200$\pm$15 GPa was obtained on an 8μm sample in agreement with other reports, however, somewhat lower values $<$100 GPa were obtained for larger ~2μm diameter fibers. Step like stress-strain profiles were recorded on the annealed ($>$2500°C) vapor grown carbon fibers. All the results are discussed in terms of the tree ring morphology of the vapor grown carbon fibers.

(ii) Loop Testing CCVD Fibers

A remarkable observation was made in our diameter dependent (θ) Young's modulus (E_y), of as-grown CCVD carbon fibers obtained from a single batch. The measurements were made during a simple, yet requiring considerable dexterity, loop test of a single fiber. We observed decreasing E_y with fiber diameter increasing from 5 to 10μm. Then an increase in E_y with $10<\theta<20\mu$m. Other reports of $dE_y/d\theta$ show a negative behavior with large range of θ(0-100μm). However, our study for the first time on a single batch of fibers ranging from 5 to 20μm have shown a detailed behavior previously unseen or masked by the volume of measurements. Our interpretations are based on microstructural entities, within the annular morphology of the CCVD carbon fibers. A Matthiessen's type of behavior has been inferred for the E_y, $[E_y=1/(\Sigma\alpha_i/E_i)]$.

(iii) Torsional Behavior of CCVD Fibers

The torsional modulus (G) of CCVD carbon fibers of both as-grown and annealed samples were determined with a torsional pendulum. G is found to be both stress and size dependent. The extrapolated zero stress of G is 105$\pm$5 GPa for a 5.4μm diameter as-grown and 200$\pm$10 GPa for an 8.4μm diameter annealed fiber. G decreases with increasing diameter. These unusually high values of G, compared to those of other types of carbon fibers, are believed to be due to the tree-ring structural morphology and the degree of graphitization of these CCVD fibers. In fact, the maximum theoretical value for a perfectly graphitic structure should be ~400GPa. Therefore, the measured G values for the CCVD fibers are quite high showing highly desirable annular structure.

(iv) New Piezoresistance of Carbon Fibers

A paper was being reviewed by Philosophical Magazine at the untimely death of Professor Ian L. Spain on the relationship between structural, elastic and piezoresistance (PR) properties of carbon fibers. In the

paper PR was found to be weakly positive for turbostratic fibers, falling to increasingly negative values as Young's modulus increased. The negative PR was attributed to an electronic contribution to the PR which becomes more important as the graphitization of the fiber increases.

The work performed in the next phase of this research was to test the validity of the presence of electronic contribution to PR in carbon fibers. If geometrical effects were solely responsible for the PR than it should be temperature independent, otherwise electronic interactions must be present in carbon fiber. Electronic interactions are frequently temperature sensitive. Therefore, we performed one of the first temperature dependent PR measurements on carbon fibers. Our results are very exciting. Indeed electronic contributions are present in the high moduli fibers which showed negative PR at room 300K. At 11K the amount of negative PR was reduced compared to 300K. This was interpreted as a reduction in the ionized impurities (at 11K) that was available to the inter-basal planes as their alignment improved with applied stress (or improved graphitization).

Annealed CCVD fibers with high modulus showed even more exciting and interesting result. At 300K, the PR of this fiber is positive compared to the negative values for high modulus PAN and pitch fibers. The positive PR in this CCVD fiber is due to the high degree of 3D ordering. Here we have observed, for the first time, a positive-to-negative transition in PR at low temperature. This result is an indication that perhaps new phenomenon exist in these annular or tree-ring annealed CCVD fibers. Further work is required before making any firm conclusion.

3. <u>Electrical and Magnetic Properties of Thickened ex-PAN and CCVD Carbon Fibers</u>

Electrical characterization of thickened ex-PAN and CCVD fibers have been carried out. Four-point resistivities measured between 10 and 300K have been compared with other commercially available fibers. The magnetoresistance of these fibers was also obtained at 4.2K with fields up to 15 Tesla at the National Magnetic Facilities (MIT). The magnetoresistance curves can be fitted with Bright's theory with the addition of ionized impurity scattering.

Ex-PAN fibers were thickened to varying degrees by vapor deposition of hydrogen/acetylene gaseous mixtures. The pyrolysis of the hydrogen/acetylene mixture can produce two distinct forms of carbon: (1) vitreous pyrolytic carbon and (2) colloidal soot. The production of vitreous pyrolytic carbon is favored when the partial pressure of acetylene is low. The reaction conditions (partial pressure of acetylene, total gas flow, and time) were varied to optimize the thickening rate and minimize non-uniform growth along the length of the fiber. The same reaction mechanism controlling the thickening of CCVD filaments appears to control this thickening of ex-PAN carbon fibers. Both are composed of concentric rings of pyrolytic carbon.

4. CCVD growth straight and high aspect ratio fibers

Three years were spent optimizing the conditions for the CCVD rowth of straight carbon fibers with aspect ratios of 100 to 1000. Evaporated ferrocene catalyzed fiber growth on graphite, quartz and ceramic substrates. A hot wall high vacuum to atmospheric pressure ceramic reactor was built and characterized. Graphite substrates were found to consume iron catalyst particles upon heat treating above 1000 C. Straight fibers up to 1.5 cm in length and 60 microns in diameter were grown. Increasing the partial pressure of benzene linearly decreases fiber length but results in a hyperbolic decrease in fiber diameter. The optimal temperature for CCVD was found to be 1150C. Three stages of fiber growth were observed: nucleation, axial growth and then thickening. For any set of chemical conditions, axial growth self limits as radially growth rate simultaneously increases. There appears to be separate and competitive chemistry between fiber lengthening and thickening.

5. In-situ gas characterization with Raman spectroscopy during fiber growth

Because near-fiber gas phase composition and temperature must be known before any laboratory process can be scaled to pilot conditions, a laser Raman system was built for local observation during CCVD. This project has been cost shared with Sematech, Semiconductor Research Corporation and Sandia National Labs in order to build this state-of-the-art laser Raman facility. The laser, optical system, diagnostics, high vacuum-atmospheric pressure CCVD reactor have been built and calibrated for nitrogen, hydrogen and methane. The students will continue this work until carbon filament growth has been characterized in terms of local gas composition. Papers written after the termination of this project will be sent to AFOSR.

6. Other Accomplishments

Computer simulation of carbon whisker growth was initiated. This simulation is based on techniques successfully applied to the molecular beam epitaxy of semiconductors.

Attempts were made here at CSU to study the x-ray diffraction of fibers subjected to tensile and bending stresses. Recommendations are made to perform these critical studies using synchrotron radiation.

Other related work completed during this contract period: Carbon Boron-Nitride, Highly Oriented Pyrolytic Graphite, X-ray diffraction of graphite at high pressure, and whisker growth by ion-bombardment. Also completed by Professor Ian L. Spain was a book on "Graphite Fibers and Filaments".

C. PUBLICATIONS

Books

1. *Graphite Fibers and Filaments*, M. S. Dresselhaus, G. Dresselhaus, K. Sugihara, I. L. Spain, H. A. Goldberg. (Springer Verlag, NY) (1988).

Research Papers

1. Graphite nature of chemical-vapor-deposited carbon filaments grown on carbon and Silicon surfaces, Y. X. Zhao, C. W. Bowers, and I. L. Spain; Carbon 26, 291, (1988).
2. X-ray diffraction data for graphite to 20GPa. Y. X. Zhao and I. L. Spain; Phys. Rev. B40, 993, (1989-I)
3. Properties and characterization of co-deposited Boron Nitride and carbon materials, A. W. Moore, S. L. Strong, G. L. Dol, M. S. Dresselhaus, I. L. Spain, C. W. Bowers, J. P. Issi, and L. Piraux, J. Appl. Phys. 65, 5109 (1989).
4. The role of sputter redeposition in the growth of cones and filaments on carbon surfaces during ion-bombardment, W. A. Solberg and I. L. Spain; J. Vac. Sci. Tech., A8, 3907 (1990).
5. The electrical noise of carbon fibers, R. O. Dillon, R. D. Kirby, and I. L. Spain, J. Appl. Phys. 66, 4284, (1989).
6. The electrical noise of carbon fibers as a function of temperature, R. Dutcher, R. O. Dillon, R. D. Kirby, I. L. Spain, and D. Patel (in preparation).
7. Relationship between structural, elastic and piezo-resistive properties of carbon fibers, H. A. Goldberg, F. Haimbach, J. Stamatoff, and I. L. Spain; (submitted to Philosophical Magazine), (1990).
8. Stress dependent low frequency electrical noise in carbon fibers under applied stress, D. Patel, Y. Dumont, R. O. Dillon, and R. Kirby (to be submitted) (1991).
9. Temperature dependent piezoresistance in carbon fibers of different microstructure, D. Patel (in preparation).
10. Tensile stress apparatus for stress-strain profiling vapor grown carbon fibers, D. Church, and D. Patel, (to be submitted to Rev. Sci. Inst.) (1991).
11. Stress dependent torsional modulus of vapor grown carbon fibers, J. Chen and D. Patel, (to be submitted to J. Appl. Phys.) (1991).
12. Determination of the tensile properties of vapor grown carbon fibers from looped filaments, B. Gordon and D. Patel, (in preparation).

Conference Papers and Abstracts

1. Relationship between structural, elastic and piezo-resistive properties of carbon fibers, H. A. Goldberg, F. Haimbach, J. Stamatoff, and I. L. Spain; Proc. of Advanced Materials Conf., 839 (1989).

2. Electrical noise from carbon fibers, R. O. Dillon, R. D. Kirby, and I. L. Spain, CARBONE 90, Paris, July (1990).
3. New electrical and mechanical trends in carbon fibers, D. Patel, D. Church, J. Chen, B. Gordon, and Y. Lu, Carbon/Carbon workshop, December, (1990).
4. Intercalation of VGCF as a function of diameter, M. L. Lake, K. K. Brito, D. Patel, and J. Chen, (to be presented at CARBON 91 (1991).

D. PARTICIPANTS

Students

1. C. C. Schmitt, Awarded M.S
2. K. Baughman M.S*
3. D. Udpa PhD*
4. F. Dillon (6 months exchange Ph.D. student)
5. R. Hennicke (6 months exchange M.S student)
6. Y. Lu (1 year graduate student)
7. B. Gordon (B.S., Physics Major)
8. D. Church (B.S., Physics Major)
9. J. Chen Post Doc (6 months)
10. Amit Inamdar* (PhD student)
11. Carmen Menoni, Postdoctoral physicist 1990
12. Richard Jones, Postdoctoral physicist 1990

Professionals

1. Ian L. Spain, Principle Investigator+
2. Carol McConica, co-PI
3. Dinesh Patel, replacement PI for Spain
4. Max Lake, President, Applied Sciences, Inc. Ohio
5. Rod Dillon, University of Nebraska, Lincoln
6. Roger Kirby, University of Nebraska, Lincoln
7. H. Goldberg, Celanese Research Company, N.J
8. D. Vvedensky, Imperial College, London
9. Y. X. Zhao, visiting scientist

* thesis to be completed- presently at industry

\+ regretfully deceased September, 1990

Carbon, Vol. 29, No.2, p. 125, 1991
Printed in Great Britain

In Memory of Ian L. Spain

Professor Ian L. Spain died on September 5, 1990, at the age of 50 from cancer. Ian was a senior faculty member of the physics department at Colorado State University. Ian was treated for the same illness eighteen months prior to his death and was given a clean bill of health even to the extent that he fell in love and was married three months prior to this sudden recurrence. He had accomplished so much of importance to science and technology and had contributed so much of himself to so many people. During his tenure on the staff of Colorado State University, and before that at the University of Maryland, Ian made a memorable impression on his students, visitors, professionals, colleagues, and friends. Hardest to accept is the realization that he still had so much to offer to his friends, family, colleagues, and God. A deeply religious man, Ian was also studying theology for the last three years, and this together with his love of science and music led him to a full spectrum of life. He was also a skilled sailor which often took him and his sons back to Maryland or Washington for sailing.

Ian was born in Kent, England, on June 19, 1940. He received his B.S. in Physics and A.R.C.S. in 1961, and his Ph.D. with A.R. Ubbelohde at Imperial College, University of London, in 1964. In addition to his commitments to science, Ian raised three boys after the death of his first wife Wendy. This year Ian witnessed his eldest son, Anthony, earn a doctorate in Music. His second son, Andrew, graduated with a degree in Political Science in the presence of his father. His youngest son, Russell, now studying at Colorado State University, was married just prior to Ian's death.

In 1988 Ian co-authored a book, *Graphite Fibers and Filaments*, (with M.S. and G. Dresselhaus, K. Sugihara, and H.A. Goldberg: pub. Springer-Verlag). His area of scientific interest was the Physics of the Condensed Phase. Specifically the physics of Carbons and related materials (electronic properties, mechanical properties, structure-property relationships, highly-oriented pyrolytic graphite, carbon fibers, glassy carbon, intercalation of graphite) and the physics of materials subject to high pressure (phase transitions, equations of state, electronic properties of semiconductors and semiconductor structures, superconductivity). He left ongoing research projects on catalytic chemical vapor deposited carbon fibers with emphasis on the growth and testing of superior carbon fibers for aerospace technology.

Ian's high pressure expertise is reflected in the book *High Pressure Technology* (two volumes), (with J. Paauwe, Marcel Dekker, NY, 1977). He also contributed to four book chapters, and an encyclopedia article *High Pressure Technology*, which was published in the Kirk Othmer Encyclopedia of Chemical Technology (John Wiley and Sons, 1980). He was involved in the research and development of the high pressure diamond anvil cell. Perhaps one of the more unique experiments that Ian was concerned with recently was the first electrical measurement on semiconductors in a liquid environment and in a diamond anvil high pressure cell. He was also involved in development of a miniature cell for low temperature operation. As a world leader in this field he was always being consulted by many laboratories all over the world for his expert advice. His consulting arena included universities, government and industrial laboratories.

Ian was truly an internationally known scientist. Prior to his illness he was in Europe on a NATO grant where he was collaborating with research laboratories in France and England. He was in the North American Editor for the *Contemporary Physics* journ. He also consulted for books and journals for Taylor and Francis of London. At the time of his death Ian had four manuscripts in the publication pipeline and at least a half dozen papers that will be completed by his colleagues. His ability to show students, both undergraduate and graduate, the exciting side of research was well recognized. Students and visitors to his laboratory frequently returned for his advice and collaboration. His graduate students will testify to Ian's ability to produce quality results. He was always available to discuss the nature of their research and frequently visited the laboratory to see if anyone needed his help. Indeed he never lost the desire to work beside students and visiting scientists in the laboratory. On some occasions when his expertise was not especially called for, he would joke about feeling neglected. Ian will be remembered by those whom he met and worked with as a leader, teacher, and a friend who was always available even on the end of a telephone. Ian always tried to help financially poor students complete their studies as he was in a similar situation when he was growing up.

To the scientific community the death of Professor Ian L. Spain is an immense loss. His expertise and professional attitude towards his research was admirable. His creativity, originality, and excellence in research was exemplary. His enthusiasm and energetic style of life made him quite unique and we salute a man of great stature. Ian leaves behind his sons and widow Elisabeth, a French lady, who is new to America. Ian felt very proud to be sharing his life with Elisabeth after being seemingly reprieved from cancer. The relatively sudden reappearance of the cancer which claimed his life in a short period is sometimes incomprehensible.

The contributions of the Physics department at Colorado State University and Ian's family in the preparation of this obituary are gratefully appreciated.

Dinesh Patel

1. LOW FREQUENCY ELECTRICAL NOISE IN CARBON FIBERS

ABSTRACT

In our study, published in the Journal of Applied Physics 66, 4284−87 (1989), the low−frequency excess electrical noise was measured in carbon fibers with a wide range of crystalline perfection and corresponding electrical and mechanical properties. Fibers included those prepared from ex−PAN and ex−pitch polymers and a catalytic-chemical-vapor deposited filament. The extensional (Young's) moduli of these fibers varied from about 220 to 890 GPa (35−130 MSi) while the electrical resistivities varied from about 19 to 1 $\mu\Omega$−m. The low frequency electrical noise of each fiber was found to be proportional to I^2 (I=current) and to vary as $1/f^{\alpha}$, where f is the frequency and α is about 1.15. The most striking feature of the results was the strong dependence of the normalized noise power on the degree of crystalline perfection.

Temperature (80−300K) dependence of the electrical noise in carbon fibers have also been performed in order to further substantiate the origins of noise in fibers. Evidence shows that new modeling is required in order to explain the new findings.

A third phase of the noise criterion in carbon fibers is the application of tensile and compressive stress while simultaneously profiling noise. The specific noise initially decreases with applied stress, corresponding to improved alignment of the layers or ribbons; then the noise increased considerably with further increase in stress. This increase is due to the fracture of interlayer filaments leading to an eventual catastrophic failure of the fiber. Quantification of the results indicate a probable two band model with one positive and one negative contributing terms. A strong recommendation is made to exploit this technique to further probe the carbon fiber and the carbon−carbon fiber composite in order to solve the high temperature oxidation problem for utilizing the high−strength-to-mass ratio in aerospace and also hostile environment.

I. INTRODUCTION

Carbon fibers are inhomogeneous materials in which the basic building blocks can be thought of as ribbons. Each ribbon consists of a stack of graphene planes (planes of hexagonal carbon with vacancies and vacancy clusters), and the stacking can be random (turbostratic ordering) or regular (graphitic). The ribbons are roughly aligned along the fiber axis and the mean misorientation angle is an important parameter which controls the extensional (Young's) modulus. The arrangement of the ribbons across the section of the fiber depends critically on the type of fiber and such parameters as the processing conditions. For instance, ex−PAN fibers usually have a random arrangement, ex−pitch fibers a radial, and catalytic-chemical-vapor-deposited (CCVD) filaments a tree ring one.[1]

Although scanning electron microscopy and x−ray diffraction techniques are employed to define these microstructures, there is a lack of probe type method for structural analysis of carbon fibers and composites. In order to understand the microstructure of various carbon fibers ranging from complete turbostratic to highly ordered systems, low frequency electrical noise program has been successfully initiated. Room temperature electrical noise in a number of carbon fibers have been measured and the results published[2] (hereafter denoted as I). It was shown that the noise varies strikingly with the degree of perfection of the fiber. Since noise is a manifestation of conductivity fluctuation, it was suggested that electrical noise may be a sensitive probe of fracture and pre−fracture in fibers, which are not well understood.

In order to understand the origin of electrical noise, an extension of the work in paper I, low temperature dependent noise profiles were obtained for consistency on the same samples studied in the previous paper. This is important in enabling the data to be fitted to existing models. Results are analyzed to give the exponent α, of the $1/f^{\alpha}$ noise dependence (f = frequency), and the variation of the noise power at 22 Hz, as a function of temperature. These data are then analyzed in terms of an existing model, showing that the model needs to be improved.

This temperature dependent noise in carbon fibers will be re−examined and published in due course by DP. This delay was due to the regretful death of Professor Ian L. Spain.

The next phase of noise technique development and application is the stress dependent electrical noise in carbon fibers. This new work is currently being submitted for publication in the J. Appl. Phys. The current measurements are exploiting the somewhat unique feature of the electrical noise to examine the microstructure of carbon fibers. Tensile stress is applied to improve the alignment of the fiber microstructure, whereby the low frequency 1/f noise power should diminish until fiber fracture when a sharp increase in noise can be expected. Models are discussed to describe these stress dependent noise in carbon fibers.

II. EXPERIMENTAL DETAILS

Details of the fiber types with their size, Young's modulus, and electrical resistivities can be found in Paper I. The same batch of samples were studied for the low temperature work. In the stress dependent experiment a good cross section of the samples were selected. These included low and high modulus PAN fibers and as−grown and annealed vapor grown fibers.

Sample preparation (Paper I) were similar for all the noise experiments with few special details as described below. A four point probe type electrical contacts were maintained.

1. No special feature was necessary for the room temperature measurement.
2. Performing cryogenic measurements required few special requirements. Sample was mounted on a small phenolic circuit board with electrical leads and placed in a copper can in a stainless steel tube of a cryostat. The tube was cooled on the outside with liquid nitrogen via a small partial pressure of exchange gas inside it. Measurements were taken at ~ 10 K increments with the temperature maintained to ± 0.1 K by a heater. The temperature was measured with a calibrated thermocouple.
3. Stress dependent noise requirements were somewhat special. A schematic of the monofiber mount is shown in Fig. 1. Mylar was used to mount the fiber. The electrical contacts were made using silver epoxy. Non−conducting epoxy was employed to isolate the portion of the fiber under stress from the electrical contacts. A special feature of the techniques involves a method which allows for handling of the single fiber sample and the holder during preparation. This was achieved by attaching a small nylon (fishing line) thread on both sides of the single carbon fiber sample. Prior to measurements the nylon threads were severed using a hot soldering iron. Uniaxial stress was applied using a suspended weight from the lower portion of the mylar mount and a calibrated electromagnet, also shown in Fig. 1.

The electrical circuit used for the noise extraction was similar to the one employed for the measurements in our Paper I. A constant dc current was maintained through the sample using batteries, a wire wound potentiometer, and a regulated field effect transistor. The voltage across the potential leads of the sample, after blocking the dc voltage with capacitors, was amplified first by a pre−amplifier (voltage gain of 1000 between 10−100 Hz), than by a Princeton Applied Research amplifier (variable gain). The amplified signal is analyzed by a Fast Fourier Transform Hewlett-Packard Spectrum Analyzer to produce a voltage−frequency spectrum. A block diagram of the experimental set up is shown in Fig. 2.

In Paper I the basic characteristics of 1/f behavior in carbon fibers were established. The 1/f characteristic in carbon fibers was shown for intermediate frequencies. In fact noise power shows a $1/f^2$ dependence at very high frequencies and no dependence for very low frequencies. In the range of interest, the 1/f noise power is defined as

$$S_v(f) = \langle V^2(f) \rangle / \Delta f \quad . \tag{1}$$

The 1/f behavior for low modulus PAN fiber at room temperature and for different sample currents is shown in Fig. 1 of Paper I. The noise spectra were free from any mechanical interference and the zero current noise was consistent with Johnson noise. Each spectrum was obtained by averaging up to 256 measurements. In Fig. 2 of Paper I the corresponding I^2 behavior, which according to Eq. 1, is linear. The slope of the S_v variation with frequency is the constant α given by the phenomenological relation

$$S_v(f) \propto V^2/Nf^{\alpha} \tag{2}$$

where N represents the number of charge carriers and $\alpha \sim 1$ (for the frequency range of interest). A more detailed discussion of the background can be found in I and ref. [3] relating to these types of measurements and analysis.

III. THE ELECTRICAL NOISE OF CARBON FIBERS (Paper I)

The results of these experiments have been reported in Paper I (see appendix). The highlight of the results is shown in Table 1 below.

The normalized noise (noise power at 1 Hz × volume^2/current^2) varies over five orders of magnitude from a high−strength fiber (modulus of 230 GPa) to a chemical-vapor-deposited one (modulus in excess of 700 GPa). It is this observation that suggests that electrical noise is a sensitive probe of defects and may prove of interest in probing fracture processes. Since noise has been shown to distinguish fibers of different mechanical properties, the next obvious phase of the program was to determine the temperature dependence of the noise in their fibers. Temperature profile often reveals considerable detailed information on the electronic scattering mechanisms and their parameters relating material properties.

IV. LOW TEMPERATURE DEPENDENT NOISE IN CARBON FIBERS

1. Results

Typical results of the noise power, S_N, as a function of frequency are plotted in Fig. 3. Each plot has three curves at 130, 230, and 290 K showing that the magnitude and slopes of the curves are fluctuations of temperature. The three figures are for representative fiber types: (1) Celion 3000, a high−strength, low modulus, ex−PAN fiber, (2) Union Carbide P−100, a pitch−based fiber of high modulus, (3) VC, a catalytic−chemical vapor−deposited fiber annealed to 3000°C of high modulus. (See Table 1 and ref. [2] for details of fiber parameters.)

Table 1. Summary of the fibers studied, their size, Young's modulus, E_y, electrical resistivity, and normalized noise power (at 1 Hz). $S_R = S_v(\text{volume})/I^2(V^2m^3/HzA^2)$.

Fiber Type	Diameter(μm)	E_y (GPa)	Electrical Resistivity($\mu\Omega$ m)	S_R
Celion 3000	7.0	220	19.0	18.3
GY-70	7.0	480	5.0	1.62
GY-70$^+$	7.0	690	3.7	5.1×10^{-2}
P-25	9.5	550	4.2	1.9×10^{-2}
P-100	9.0	690	2.88	9.9×10^{-3}
P130X	9.1	890	1.09	3.0×10^{-3}
P-100B	8.6	690	2.4	5.5×10^{-3}
CCVD	30.2	800	0.95	3.6×10^{-6}

The noise level recorded at 290 K was in good agreement with those in I, with two exceptions. The absolute values of noise in the Celion 3000 and GY−70 samples were inconsistent with I. There was no attempt made to obtain the absolute noise but rather to profile a relative temperature dependence between the fibers.

The slope (α) of the temperature noise profile is an important parameter. Figure 4 shows the experimental data for Celion 3000 low modulus ex−PAN fiber. The parameter α was determined at each temperature using the following expression

$$\alpha = 1 - \frac{1}{\ln(\omega\tau_0)}\left(\frac{\partial \ln(S)}{\partial \ln T} - 1\right) \tag{3}$$

where ω and τ_0 are frequency parameter and thermal activation time constant. The figure clearly shows a temperature dependent constant α. Figure 5 shows the negative slope of the noise−frequency profiles at different temperature for three of the fibers. All fibers exhibit minima in $\alpha(T)$ at ~230 K. It is possible that a maxima occurs at higher temperature (see, for example, the curve for Celion 3000) and an extension of the measurements to temperature above 300 K is necessary especially since considerable interest is now focused on enhancing the high

temperature resistance to oxidation of carbon−carbon composite.

The temperature dependence of the noise power at 22 Hz is given in Fig. 6 for three samples. This frequency was chosen to minimize instrumental factors, and where the noise level is approximately stable. The curves in Fig. 6 are for different sample current levels, but all results are similar, showing a low temperature region of constant noise, an increase above ~200 K, and either saturation or a maximum at 300 K. Further measurements are needed at higher temperature to establish definitively the maximum.

2. Discussion

Although the noise levels of the different fibers vary over orders of magnitude, the behaviors of α(T) and S_v(22 Hz)(T) are surprisingly similar, suggesting a common cause for the phenomena. Some similarities with the data of Fleetwood et al.,[4] on carbon resistors are noted, although the correspondence is not close. Their curves of α(T) show a sinusoidal variation similar to ours, but the noise reaches a minimum of ~300 K and a maximum at ~200 K.

The origin of excess noise is still not well understood. One approach which attempts to give a semi−empirical explanation of the $1/f^{\alpha}$ spectrum starts with the concept of constraining a 1/f spectrum from random events[3]. If the characteristic time is τ, the resulting noise spectral density has a Lorentzian shape [4]

$$S_v \sim \frac{\tau}{1 + \omega^2\tau^2} \tag{5}$$

where $\omega = 2\pi f$. If the noise process involves a distribution of relaxation times $D(\tau) \sim 1/\tau$ for $\tau_1 < \tau < \tau_2$, then

$$Sv \sim \int_{\tau_1}^{\tau_2} \frac{\tau D(\tau)}{1 + \omega^2\tau^2}\, d\tau = \int_{\tau_1}^{\tau_2} \frac{dt}{1 + \omega^2\tau^2} \quad . \tag{6}$$

At high frequency $S_v \propto 1/f^2$, at low frequency it is independent of f, and in the intermediate region $\propto 1/f$. The temperature dependence might be controlled by a thermal activation process, with a characteristic attempt time, τ_0, then

$$\tau = \tau_0 \exp \Delta E/kT \quad . \tag{7}$$

where ΔE is the activation energy. Attempts to fit such an activation energy to the present case was unsuccessful. Noise is generated at inter−particle-contacts in the fiber, this is analogous to inter−ribbon contacts via filaments. Further work on modeling our low temperature noise is required to obtain an acceptable explanation of the results. Such a model will require electrons that are specific to carbon (anisotropic semimetal). High magnetic field studies will enhance this modeling of noise effects in carbon fibers.

V. STRESS DEPENDENT NOISE IN CARBON FIBERS

1. Results from Tensile Tests

In a convenient manner data were stored as normalized relative noise power $\Delta S_v/S_v$, with a frequency span of 10−60 Hz, in carbon fibers as they were stressed to fracture. $\Delta S_v/S_v$ is defined as

$$\Delta S_v/S_v = (L_2/L_1)[S_v(\sigma, f) - S_v(0, f)]/S_v(0, f) \tag{8}$$

where L_2/L_1 is the ratio of fiber length under stress and the distance between the noise probes and σ is the applied stress in GPa. This factor is the result of removing any stress transmitted to the noise contacts which may otherwise cause anomalous result.

a. Low modulus PAN fiber

Typical $\Delta S_v/S_v$ frequency spectrum is shown in Fig. 7 for a low modulus PAN carbon fiber at different stresses. A least square's fit to the data is indicated by the solid line. For clarity only the fit to the data is shown for some of the other stresses. There is a clear change in the noise power with stress. Also there is a distinct change in the slope of the curves in the figure. This slope is the familiar constant α in Eq. 2 which is typically equal to unity at zero stress.

Using Eq. 2

$$S \sim 1/Nf^{\alpha}$$

Now with stress the relative change is the noise power can be rewritten as

$$\Delta S/S = N_0 f^{\alpha_0}/N_0 f^{\alpha} - 1$$

or

$$\log[1 + \Delta S/S] = \log[N_0/N_\sigma] + (\alpha_0 - \alpha)\log(f) \quad (4)$$

where N and α are stress dependent with N_0 and α_0 are the zero stress values. Results in Fig. 7 can now be understood qualitatively. The increase in the slope of the log(1 + ΔS/S) against log(f) corresponds to the constant α which is no longer constant but dependent upon stress. The number of carriers N_σ is also decreasing as a consequence of the change in the intercept.

At a frequency of 35 Hz, $\Delta S_v/S_v$ is plotted as a function of stress, σ(GPa), in Fig. 8 for a low modulus (220 GPa) PAN fiber. This result shows that at low stress values the noise power decreases by a small amount. This is consistent with our low stress noise power results in other samples. After a minimum in the noise power, gradual increase in the signal is observed at higher stresses until the fiber breaks. The increase in noise power at fiber breakage can be as high as 30% in low moduli PAN fibers.

b. High modulus ex-PAN fiber

The noise power (at 35 Hz) with stress for a relatively high modulus (480 GPa) ex−PAN is shown in Fig. 8 also. This result is similar to the low modulus fiber. The main difference is in the magnitude of the noise power at higher stresses. In this fiber there is a 15% increase in the noise power at 0.6 GPa. This compares to 30% at ~5 GPa stress for the low modulus fiber. It is important to point out that from piezoresistance measurements, on these two fibers[6] it was shown that the resistance of the low modulus fiber increased with stress, however, in the higher modulus fiber the resistance decreased with stress. Therefore the two experiments, which are similar in set up, show results which are originating from different mechanisms involving the effect of time constants, carrier type, and carrier concentrations.

C. CCVD fibers

Stress dependent electrical noise power in as−grown and annealed CCVD fibers are shown in Fig. 9. Although there is relatively more scatter in the as−grown data compared to the annealed fiber, the least squares fit solid line show the same trend with those results above. The scatter in the data is reflecting the weak interplaner type contact which are severed upon increasing axial stress. Table 2 shows that the ratio $(\Delta S/S)/\sigma$ is about one−half that of the annealed sample. This value quantifies the degree of ordering between the as−grown and annealed CCVD fibers. Also it is shown that the annealed sample is almost featureless compared to the as−grown sample. The annealed sample is well behaved in terms of the scatter in the data. This is indicative of the more ordered material. These observations are quite important since we show for the first time that noise is a very good tool to determine the degree of ordering in different carbon fibers.

Table 2. Size, Young's modulus, and noise power at maxumum applied stress for a cross section of samples studied.

Fiber Type	Diameter (μm)	Young's Modulus (GPa)	$[S(\sigma_{max})-S(0)]/S(0)$ x$1/\sigma_{max}$
Celion 3000	7.0	220	0.07
GY-70 (PAN)	7.0	480	0.02
CCVD (as-grown)	6.5	-	0.04
CCVD (annealed)	8.0	-	0.01

2. Discussion (Tensile)

It was stated by us[1] that noise would decrease in fibers placed under tension with improved interlayer contact. Also stated in the same article was the comment that noise would be significantly lower for the CCVD fibers. The former speculation was somewhat true in practice. Here we found only a small decrease in noise for small stress due to the fibril-fibril contract. However, considerable increase in the noise was measured for the higher stress due to the fracture and severing of filamentary connections between fibrils as they are put under increasing tension. The second speculation has been shown to be a fact. CCVD fibers do show lower noise due to their better ordered microstructure compared to the low moduli PAN fibers. In fact we showed that the annealed fibers were very well ordered and that high temperature treatment of CCVD fibers can be effectively tested using this technique.

The low modulus ex−PAN fiber show the highest increase in the noise power with stress since the low modulus ex−PAN fiber is more turbostratic compared to the rest of the fibers under investigation. Comparison of the noise power−stress spectra between low modulus (220 GPa) and higher modulus (480 GPa) ex−PAN fiber show that the noise power show a smaller dependence on stress for the higher moduli fibers. This is consistent if the degree of change in the noise power with stress is related to the alignment of the microstructure in these carbon fibers. The ratio of $\Delta S/S$ to the highest stress is a qualitative measure of the degree of order in fibers. From this one can see that the CCVD fibers are more ordered than the lower moduli ex−PAN fibers. The annealed fibers show even lower noise power with stress which corresponds to well aligned system.

The speculation regarding bursts of noise upon fiber breakage may be present to some degree in the amount of scatter in the data. One expects small bursts of noise when interlayer connections are severed. And, if one draws a higher order polynomial fit to the as−grown CCVD fiber data, one observes maxima which corresponds to this point. However, without further data with smaller stress increments no firm conclusions can be drawn

regarding this point at this stage.

Good fit to the noise power spectra can be obtained by employing empirical relation such as

$$a/N_a(\sigma) + b/N_b(\sigma)$$

where a and b are constants with N_a and N_b being positive and negative stress dependent terms respectively. For the ex−PAN (220 GPa) fiber the values are a = 0.9, b = 2.9, $N_a = 0.1 + \sigma 7\times10^{-5}$, and $N_b = 0.27 - \sigma 1.2\times10^{-4}$. This type of behavior is indicative of a two−band model where the applied uniaxial stress separates the two bands in opposite directions[7]. At higher stresses the carriers will be resident in the higher effective mass band, therefore increasing electronic scattering. Physically one may view the low modulus PAN fibers as those depicted in Fig. 6.16a−c (Johnson, 1987 [8]) with a high degree of misorientation of crystallites. Under applied axial stress one expects the fiber to initially become better aligned as the porosity is improved and increased fibril−fibril contact. However, at higher stresses the weaker linkage between fibrils will fracture and then rupture. These dangling fibrils can then act as electronic scattering sites. This is a plausible cause of the observed increase in noise in carbon fibers under applied stress as reported in this work. Further studies are planned on carbon fibers and composites which have been heat treated by different amounts. It has been shown[9] that the heat treatment of carbon fibers leads to increased order from turbostratic to two−dimensional and eventually to three−dimensional ordering as higher graphitic characteristics are obtained. A systematic comparison between the noise power and heat treatment will lead to refined model and a quantification of the degree of ordering/alignment in carbon fibers. This work will further establish noise measurements as a powerful tool in examining these technological important materials.

3. Results and Discussion of Compressive Test

We have, for the first time, carried out electrical noise in a low modulus ex−PAN fiber with applied compressive force via a loop test. Special sample preparation was necessary. A schematic drawing of the set up is shown in Fig. 10 which employs a set up similar to those described in the mechanical characterization chapter. A thin piece of insulator mica was inserted in the loop to avoid an electrical short. The Young's modulus of a fiber can be determined by monitoring the applied force and the loop diameter (see mechanical properties section).

Figure 11 shows the $\Delta S/S_0 - \sigma$ result with a fitted line. In a loop test, a compressive stress is exerted on the inner portion of the loop. The increase in the noise is consistent with a gradual compressive failure of the fibers with a buckling effect. The fact that a variation in the noise is observed with stress in a loop test indicates that considerable structural change occurs during this Sinclair loop test. A comparison of the noise result with the tensile strain data shown in Fig. 8 for the ex−PAN fibers show some interesting observations. Increasing noise with stress

is seen in both, consistent with increasing microstructural failure. There are three orders of magnitude reduction in $\Delta S/S_0$ for the compressed sample compared to the tensile strained one. The insert in Fig. 11 shows the stresses involved in a Sinclair loop test. The compressive stress, σ_c, in the inner portion of the fiber is contributing to the catastrophic failure of the fiber. Since the ex−PAN fiber has a turbostratic microstructure compared to the tree ring morphology of the vapor grown fibers, it is important to repeat this experiment on a CCVD fiber. The layered structure may show a burst of noise as the rings fracture.

VI. CONCLUSION

A low frequency electrical noise in carbon fiber research project has been initiated by this group. It has been shown by a set of experiments that this technique is an extremely useful and powerful tool to examine and diagnose carbon fibers. Manifestation of a conductivity fluctuation, noise was found to have a strong dependence on the degree of crystallinity of carbon fibers. A strong temperature dependent noise in these fibers is indicative of combination of different electronic type mechanisms. The mechanical properties of these fibers have been coupled to the noise data to show a direct correlation. Further work is planned. A diagnosis of the high temperature oxidation problem in carbon−carbon composite using electrical noise.

VII. PROSPECTS FOR THE APPLICATION OF ELECTRICAL NOISE TO CARBON-CARBON COMPOSITES

The success of this noise technique in carbon fibers needs to be fully exploited. Electrical noise in all carbon fibers employed in composites is required. Correlation of the results to mechanical properties are important to establish unusual trends. The effect of high heat treatment on carbon fibers was shown to improve the microstructure of carbon fibers, noise can now be used as an independent technique to serve this need. The effect of coatings on carbon fibers, for composite applications, can be readily examined by noise since interfacial type details are obtained by noise.

REFERENCES

1. M. S. Dresselhaus, G. Dresselhaus, K. Sugihara, I. L. Spain, and H. G. Goldberg, (1988) *Graphite Fibers and Filaments*, Vol. 5 in Springer Series in Materials Science (Springer, Berlin, 1988).
2. R. O. Dillon, R. D. Kirby, and I. L. Spain, Journal of Applied Physics 66, 4284−87 (1989).
3. M. J. Kirton et al., Adv. Phys. 38, 367 (1989).
4. D. M. Fleetwood, T. Postal, and N. Girdano, J. Appl. Phys. 56, 3528 (1984).
5. J. W. Eberhand and P. M. Horn, Phys. Rev. B18, 6681 (1978).
6. H. A. Goldberg et al., submitted to J. Appl. Phys. (1990).
7. R. L. Fagerquist et al., Phys. Rev. B39, 5139 (1989-I).
8. D. J. Johnson, J. Phys. D: Appl. Phys. 20, 286 (1987).
9. T. C. Chien et al., Phys. Rev. B20, 5867 (1982).

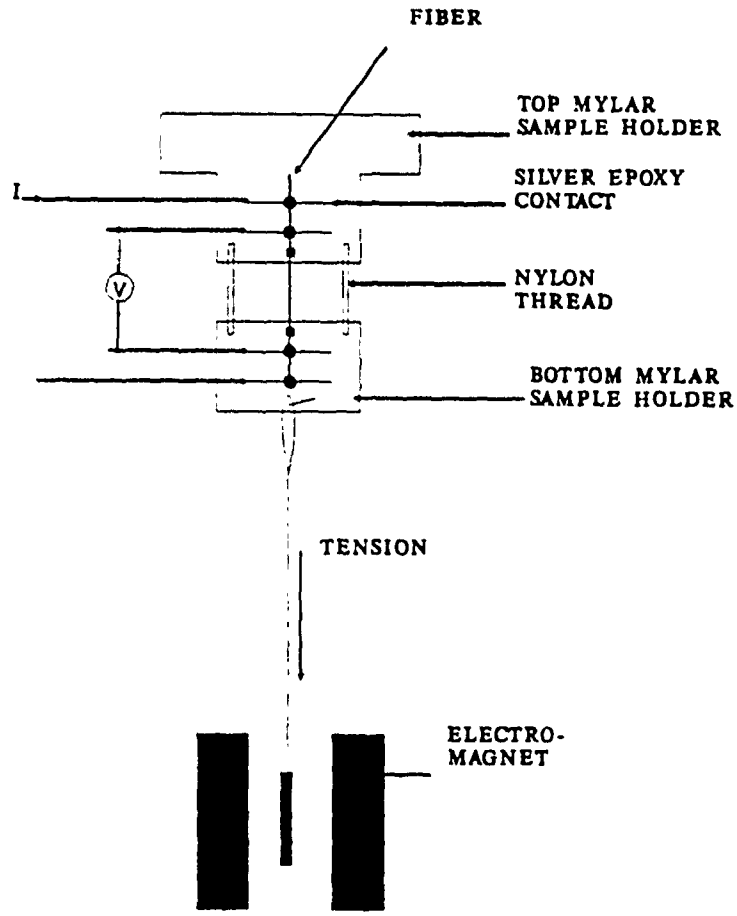

Fig. 1 A schematic diagram of a mono-filament fiber mount for four point electrical measurements with simultaneous application of tensile stress. The nylon is severed by hot soldering iron prior to measurements.

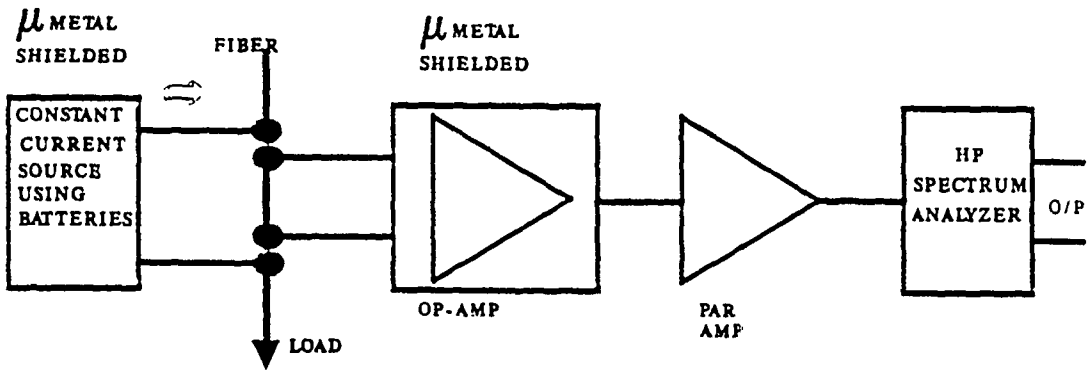

Fig. 2 A block diagram for stress dependent 1/f noise measurements in carbon fibers.

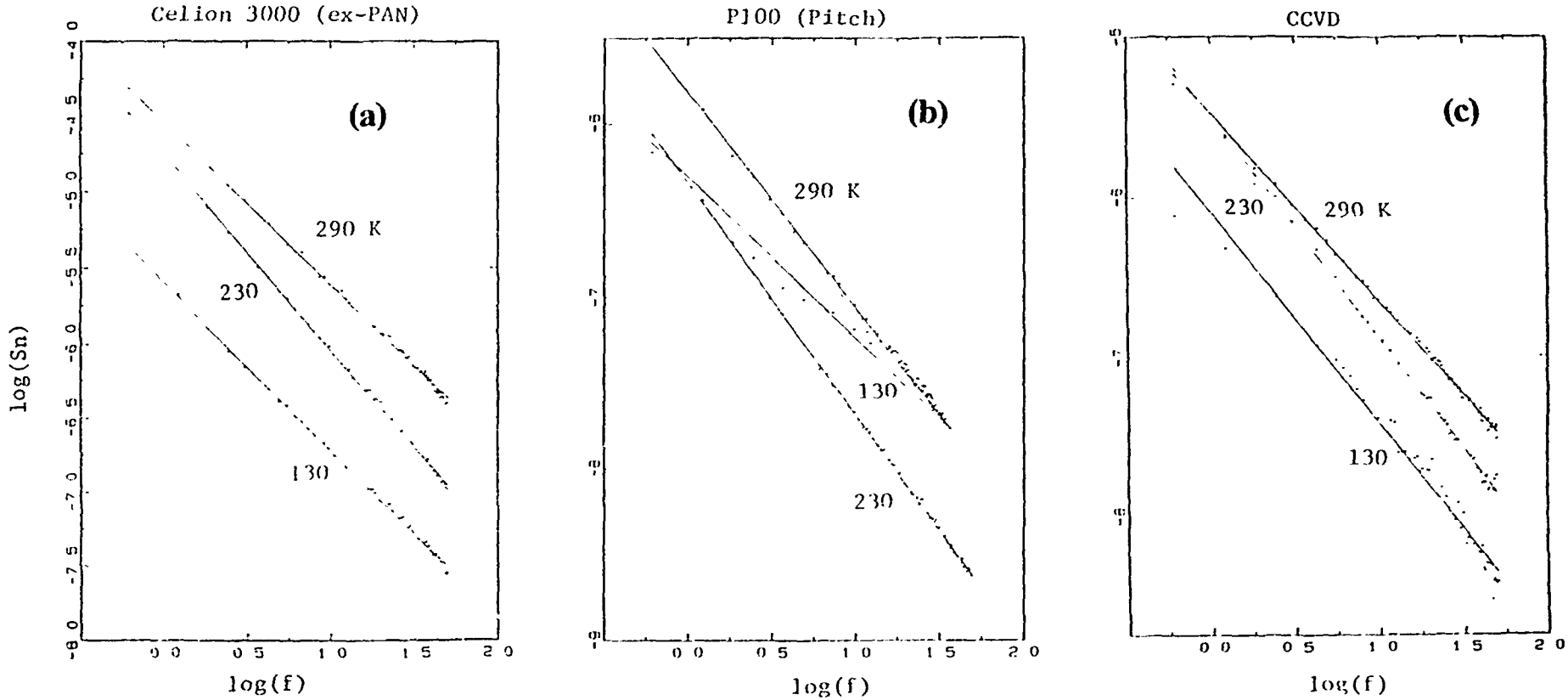

Fig. 3 Typical 1/f noise spectra at different temperatures for three fibers. (a) Low modulus ex-PAN, (b) pitch P100, and (c) vapor grown fiber.

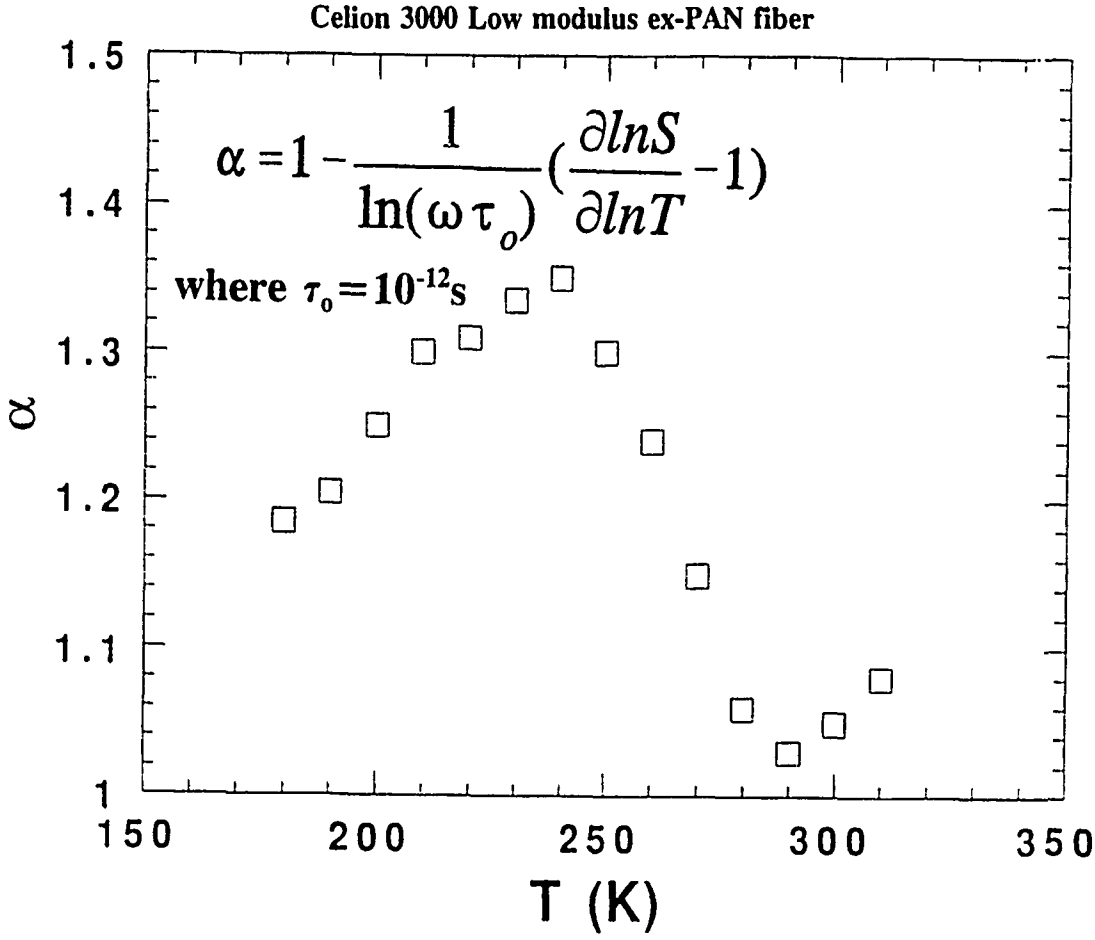

Fig. 4 Determination of the temperature dependent α for low modulus ex-PAN(Celion 3000) fiber.

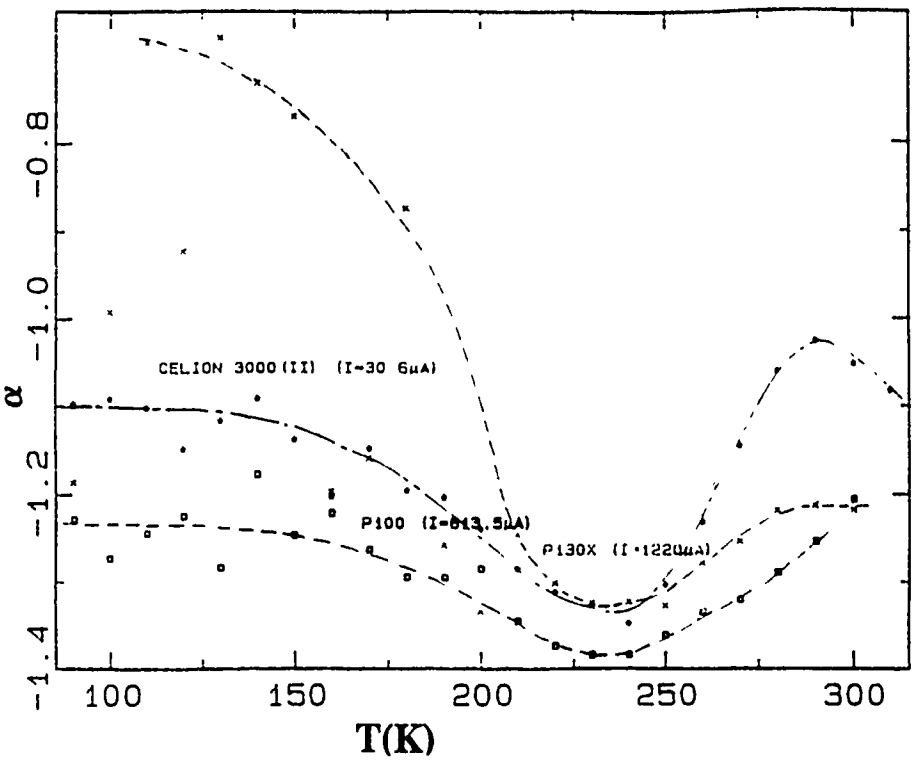

Fig. 5 Measured slope of noise-frequency spectra with temperature for the samples.

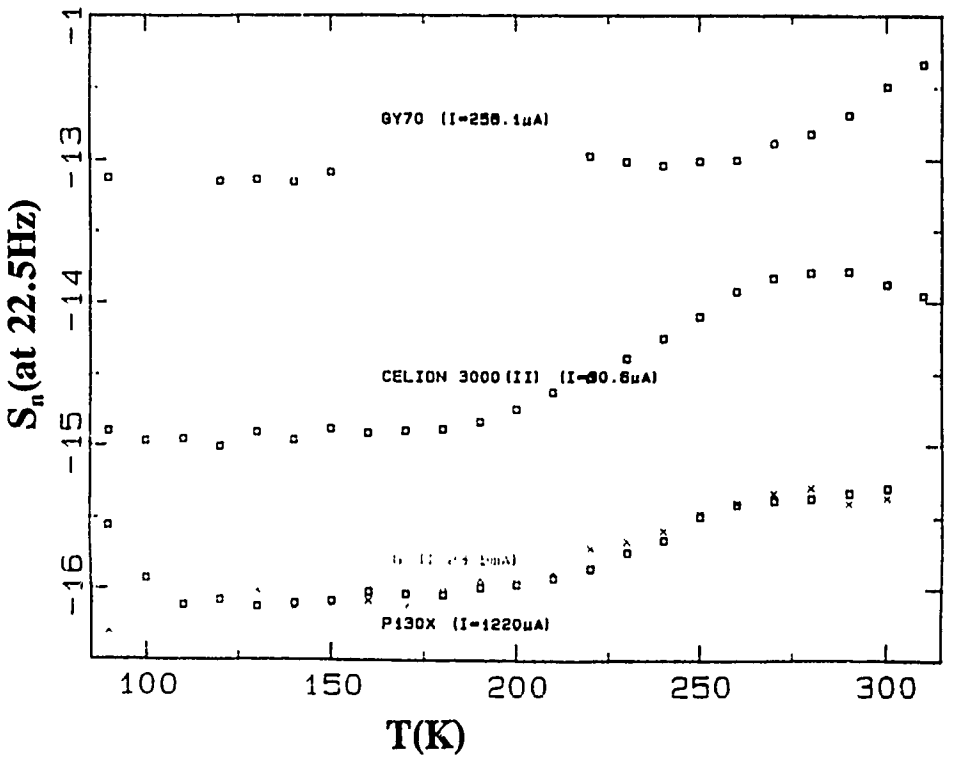

Fig. 6 Noise at 22.5 Hz for three samples at varying temperatures.

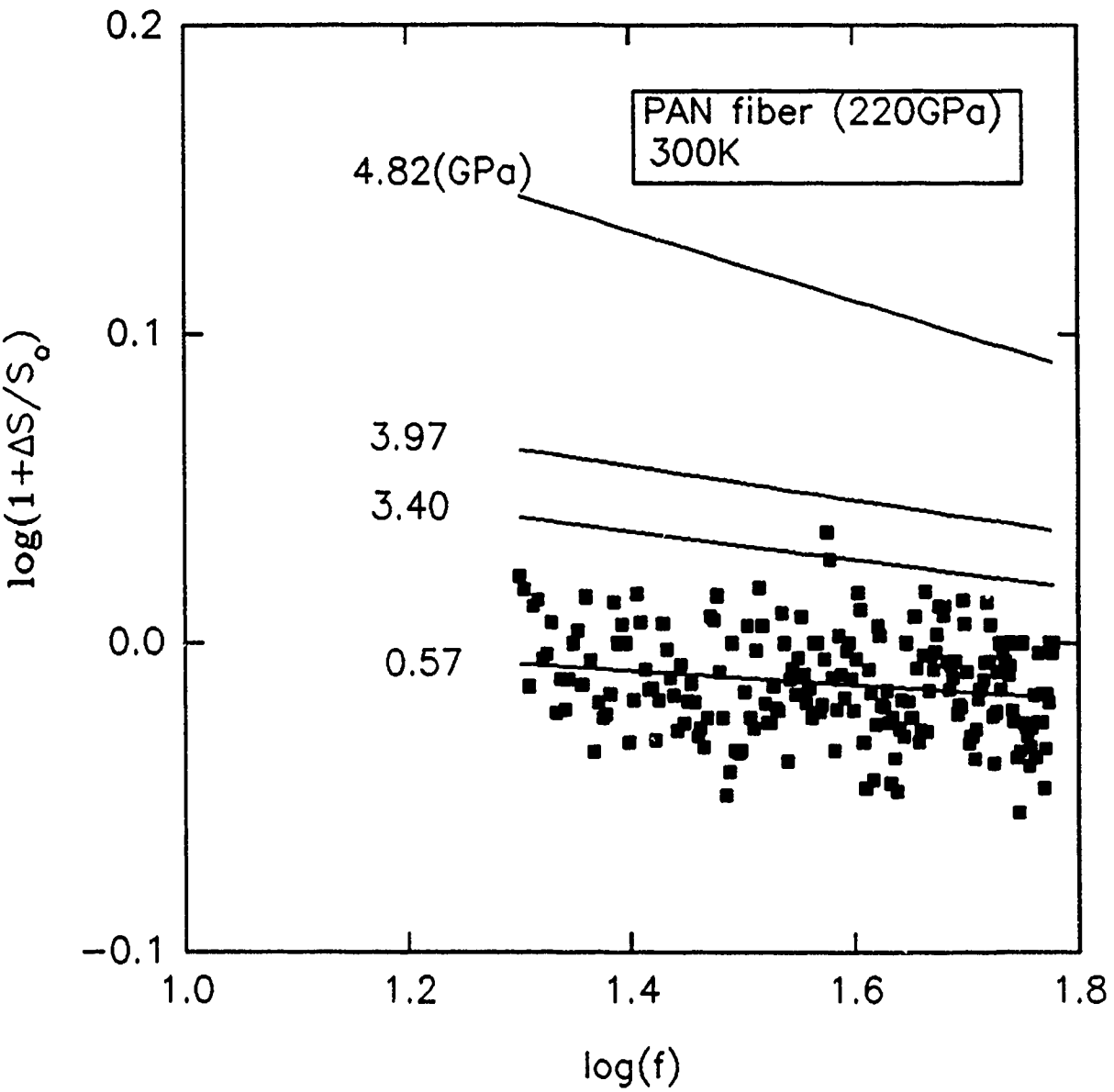

Fig. 7 log(1+ΔS/S) vs. log(f) for Celion 3000 PAN fiber at different stresses. The solid lines are least square's fit to the data.

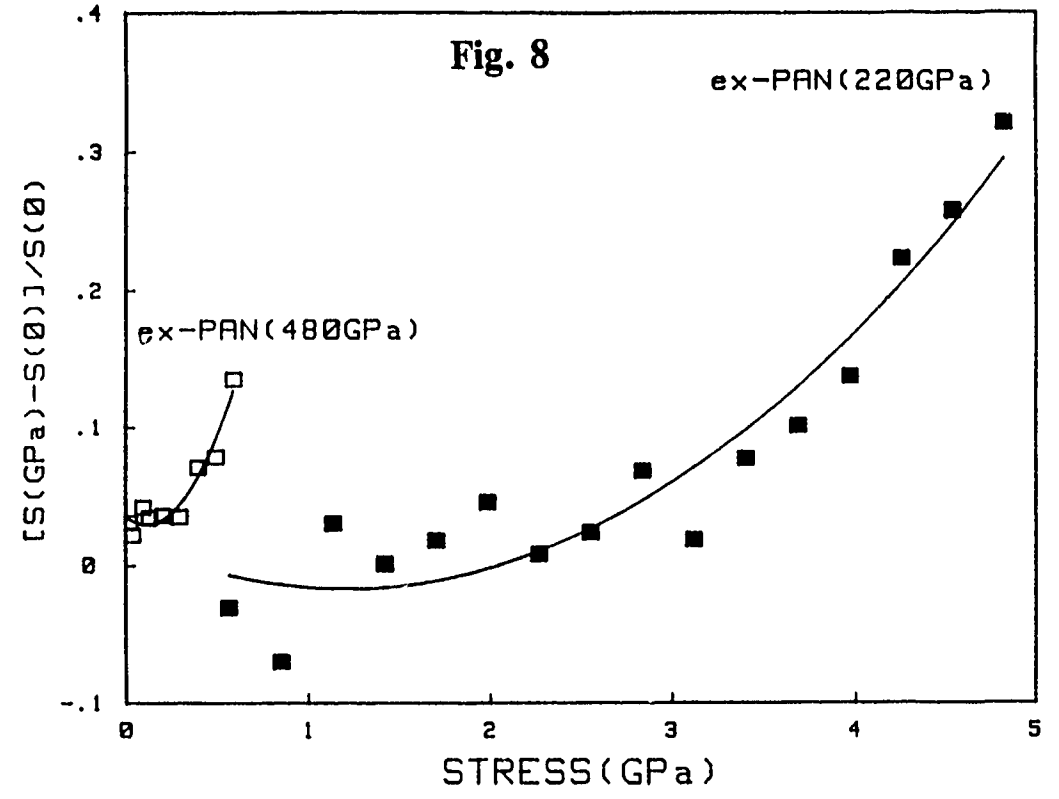

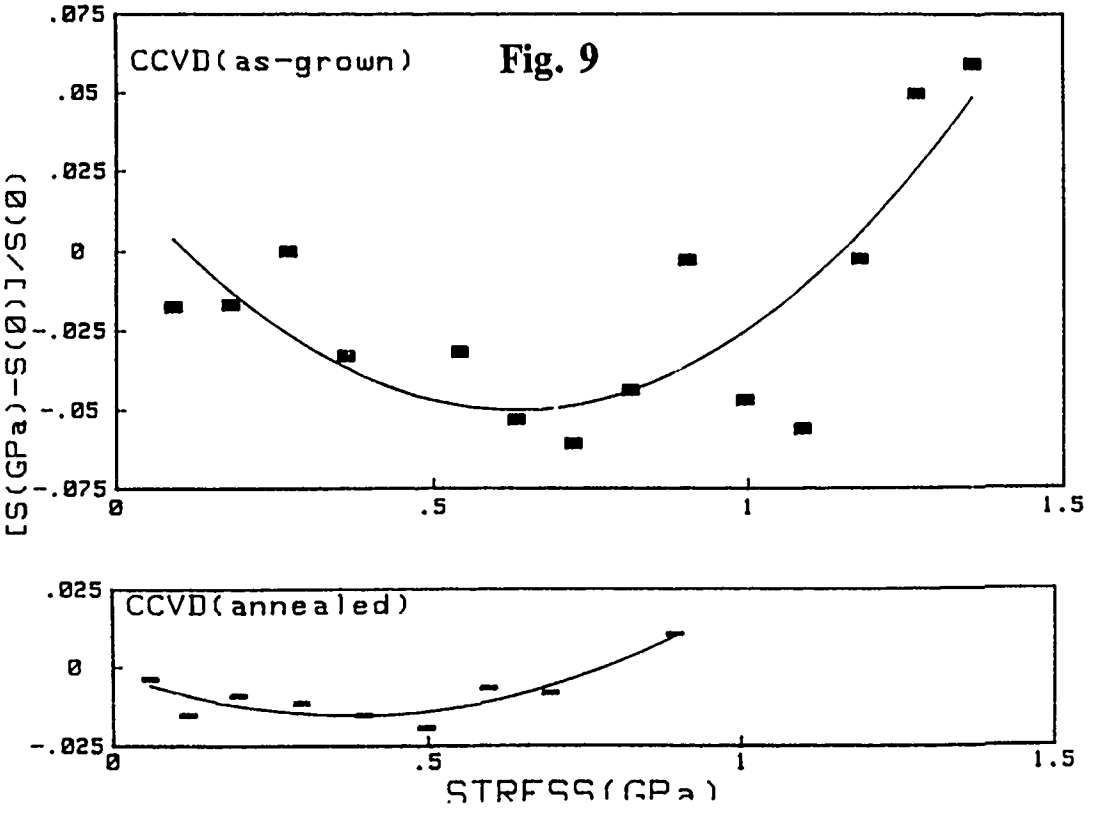

Fig. 8 Stress dependent noise (at 35Hz) change in low and high modulus ex-PAN fiber.

Fig. 9 Stress dependent noise (at 35Hz) change in as-grown and annealed CCVD fibers.

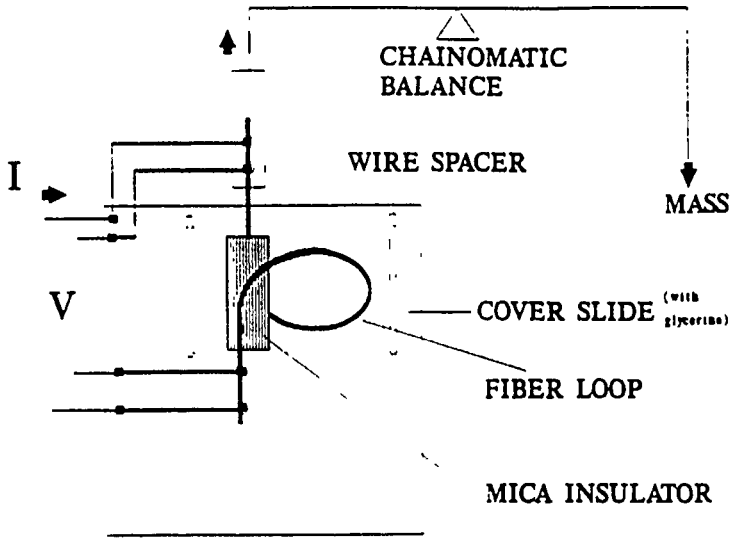

Fig. 10 Sample holder for a Sinclair loop compressive test of a mono filament with the capability of detecting electrical noise using four point probe.

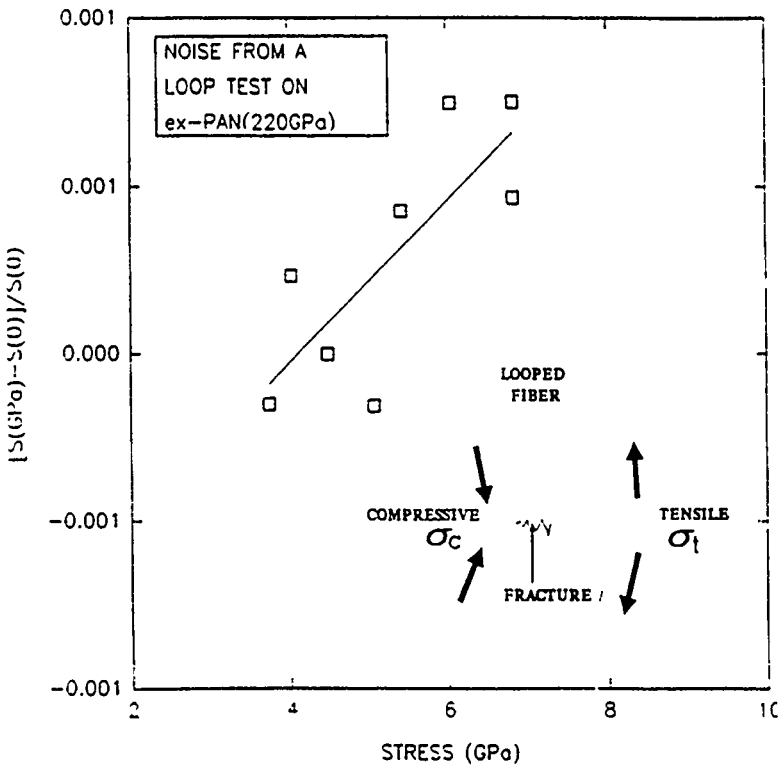

Fig. 11 ΔS/S vs. stress for Celion 3000 low modulus ex-PAN fiber obtained during a loop test. The insert shows the fracture and stresses involved in a loop test of a carbon fiber.

2. MECHANICAL PROPERTIES

A. Diameter dependent E_y of vapor grown carbon fiber from tensile test

B. Loop testing of vapor deposited carbon fibers

C. Torsional modulus of Vapor-grown fibers

D. New Piezoresistance of Carbon fibers

A. DIAMETER DEPENDENT Ey OF VAPOR GROWN CARBON FIBER FROM TENSILE TEST

One of the most important parameters in characterizing a fiber is it's Young's modulus. In this report, a simple yet accurate tensile test has been developed specifically for single fiber stress-strain profiling of vapor grown carbon fibers. The set up allows for repeated stress-strain profiling on a single fiber. A diameter dependent Young's modulus of these CVD fibers is presented. Our results have been compared to those reported elsewhere[1].

I. Experimental

Our apparatus is an inexpensive yet sensitive instrument for quantitative measurement of small linear displacement. The heart of the instrument is a Linear Variable Differential Transformer (LVDT) carrying a resolution of 2 microns. Such a resolution was achieved by lock-in amplifier techniques. Details of the vapor grown carbon fibers can be found elsewhere[2]. Direct fiber handling was minimized by using small pieces of sticky tape to extract a fiber from the tow. The fiber was mounted on an insulating mylar sample holder shown in Fig. 1. Adhesion of the fiber to the sample holder was a two-stage process. Firstly, a drop of silver epoxy was applied to each end of the sample holder; the fiber was then laid in. After five minutes of curing at a temperature of 150 °C, one drop of standard 5-minute epoxy was applied additionally over the silver epoxy at each fiber end and allowed to cure. This two stage process ensures that the fiber was mechanically bound to the sample holder without any adverse effect on the fiber which may result in cases where clamping techniques are used to hold the fibers.

The lower end of the fiber is fixed to a "floating" stage of the sample holder. This floating stage is temporarily secured by two nylon wires parallel to the fiber. Prior to measurements the nylon wires were severed by a soldering iron. A hook system was employed to attach the LVDT element to the lower portion of the sample holder. Measurement of initial fiber length was made, using a travelling microscope, to an accuracy of $\pm$ 0.1 mm. Tensile stress was applied electromagnetically, also sown in Fig.1. Calibration of the electromagnet was obtained on a Chainomatic balance with the LVDT attached to simulate the measuring condition. In lieu of a cross-head-speed parameter so often referred to with the celebrated Instron instrument, we used a ramp generator which linearly increased the current to the solenoid, thus increasing the load to the fiber at a consistent rate.

Vertical displacement of the fiber was monitored by measuring the induced voltage across the LVDT

windings with a lock-in type detection. A second LVDT can be inserted on to the top portion of the mount enabling a differential lock-in analysis and also removing any drifts due to the fixed portion of the sample holder. Automatic data acquisition was employed to collect and analyze the Young's modulus value. A block diagram of the set up is shown in Fig. 2. Calibration of the instrument was carried out using a low modulus (~225 GPa) Celion 3000 ex-PAN fiber.

II. Results and Discussion

Typical stress-strain data for three as-grown CCVD carbon fibers are shown in Fig.3. All the measurements were made at room temperature. Measurements were carried out on as-grown samples of different diameters. The insert in the figure shows the stress-strain curve for Celion 3000 ex-PAN fiber. In agreement with other reports, a linear stress-strain relation was observed for the PAN fiber. The value of Young's modulus determined for such a curve was 225 ± 15 GPa.

Results of the diameter dependent Young's modulus of vapor grown carbon fibers is shown in Fig.4. For comparison, the Young's modulus measured for the low modulus ex-PAN fiber is also shown. The shaded region represents the range of values obtained by Tibbets. This shows that a fairly large variation in the Young's modulus is possible for a given size fiber. The results obtained here are in good agreement for smaller diameter fibers. However, a somewhat smaller Young's modulus was measured for the larger fibers. This is possible from the fact that our moduli were determined from low stress data. The general trend of decreasing Young's moduli with increasing diameter was attributed to less developed layers. This is related directly to the growth parameters of the fibers, specifically a higher growth rate leading to less developed layers. The decreasing tensile strength in these fibers is dependent on the probability of finding a critical flaw, which increases with size/volume of the fiber.

Vapor grown carbon fibers have a common microstructure that can be described by a tree ring morphology since concentric graphene layers parallel to the fiber axis make up the fiber. In contrast to the PAN fibers, the central core of the CCVD fiber can be hollow[3]. The as-grown CCVD fibers appear to have a compact, cohesive structure with $\sim 1\mu$m thick rings. It has been reported that[2] multiple fiber microstructure are possible on what appears to be a single fiber along the length of the fiber. However, without SEM micrographs, it is difficult from optical microscopy alone to successfully isolate a perfectly single fiber.

Two models have been discussed elsewhere[1] to account for the diameter dependent Young's modulus of vapor grown carbon fibers. A uniform stress model involving elastic compliance of single graphite crystal and the azimuthal half-width of the (002) x-ray diffraction peak. An increasing dispersion is shown[1] for increasing diameters, however, in the range of interest here, there is no change in the dispersion from x-ray diffraction. An elastic unwrinkling model involving x-ray diffraction parameters and weighted misorientation of basal planes is more realistic in attempting to quantitatively explain the size dependent Young's modulus of CCVD fibers. However, without structural information in situ to tensile testing no firm conclusion can be made in distinguishing the models for the range of diameters of fibers studied here.

Heat treatment of CCVD carbon fibers has profound effects on their properties[4]. In fact one of the attractions

of CCVD fibers is their ability to almost completely be graphitized by high temperature annealing. It has been shown[2] that annealing temperatures of about 2900°C will crack and separate some of the rings of the CCVD fibers, however, the fiber is highly graphitic, as shown by x-ray diffraction. This separation of the rings can act as different entities in a fiber. A typical result of a tensile test on an annealed CCVD fiber is shown in Fig. 5. It is apparent, from the stair like behavior of the spectrum, that annealing has in fact effectively separated the rings. The positive slopes are seen to increase with applied stress indicative of smaller diameter fibers. The first step in the spectrum represents the outer group or groups of rings; the second step represents the next innermost rings, and so on. The negative slope is indicative of recoil effects in the fiber. Whenever an outer ring or set of rings fail, the inner portion of the fiber elastically recoils. A careful study of this behavior may lead to the determination of the separation ratio for a given diameter of annealed CCVD fiber. Also a study of annealed fibers with known numbers of rings may lead to a better correlation between the Young's modulus of the steps and of the whole fiber. From this result, it is difficult to ascertain an average Young's modulus of the whole annealed fiber.

The above result of stair step σ-ϵ behavior is different to that described[5] as a "sword-in-sheath" effect. In the latter case it was postulated that a surface crack propagates inward before circumferential fracturing of the ring. The large stress is suddenly transferred to an effectively thinner fiber resulting in a different slope of σ-ϵ curve. Further stress will repeat the process of cracking and fracturing at some small distance away from the first failure.

REFERENCES

1 G. G. Tibbets et al, J. Phys: D, Appl. Phys...292, (1987).

2 K. K. Brito et al 34th Int. SAMPE Symposium, 190, (1989).

3 W. KrÖner et al, J. Am. Ceramic. Soc., 73, 1189 (1990).

4 M.S. Dresselhaus, G. Dresselhaus, K. Sugihara, I.L. Spain, and H.A. Goldberg, *Graphite Fibers and Filaments* (Springer, Berlin, 1988), Vol. 5.

5 C. G. Tibbets, C. P. Beetz, Jr., and C. H. Olk, Research Publication, GMR-5624, (1986).

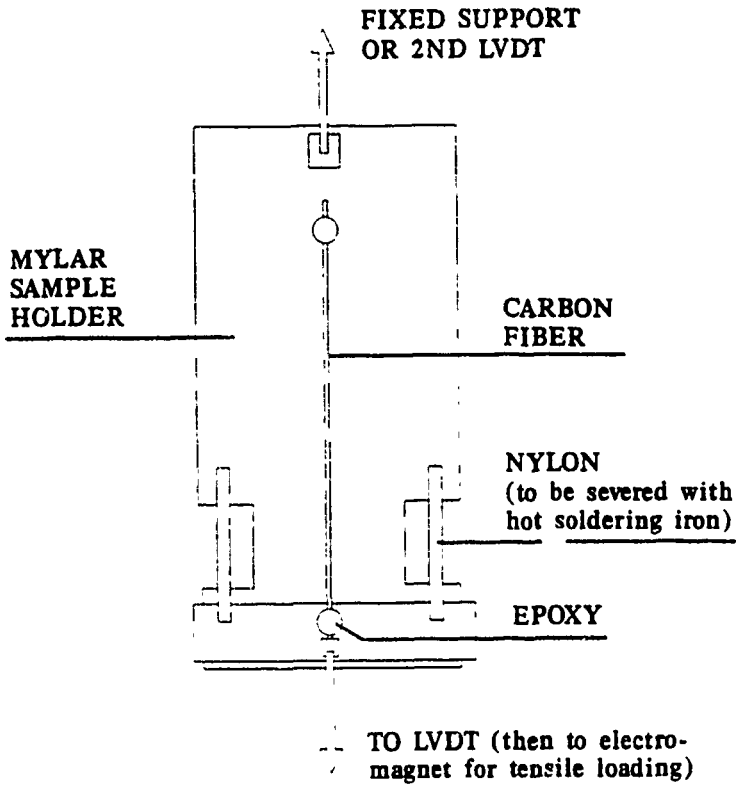

Fig. 1 A schematic representation of the sample holder designed for determining stress-strain profiling of mono-filament of carbon.

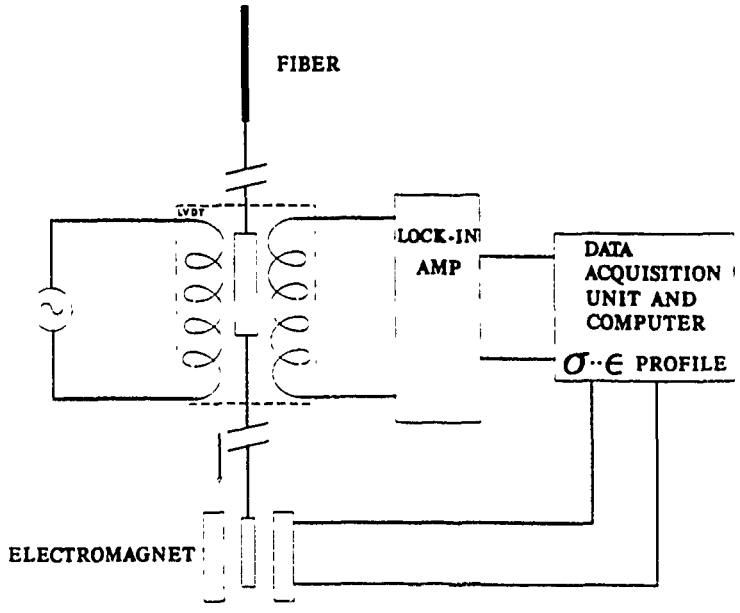

Fig. 2 A block diagram of the Young's modulus apparatus utilizing LVDT. The tensile loading is achieved through an electromagnet.

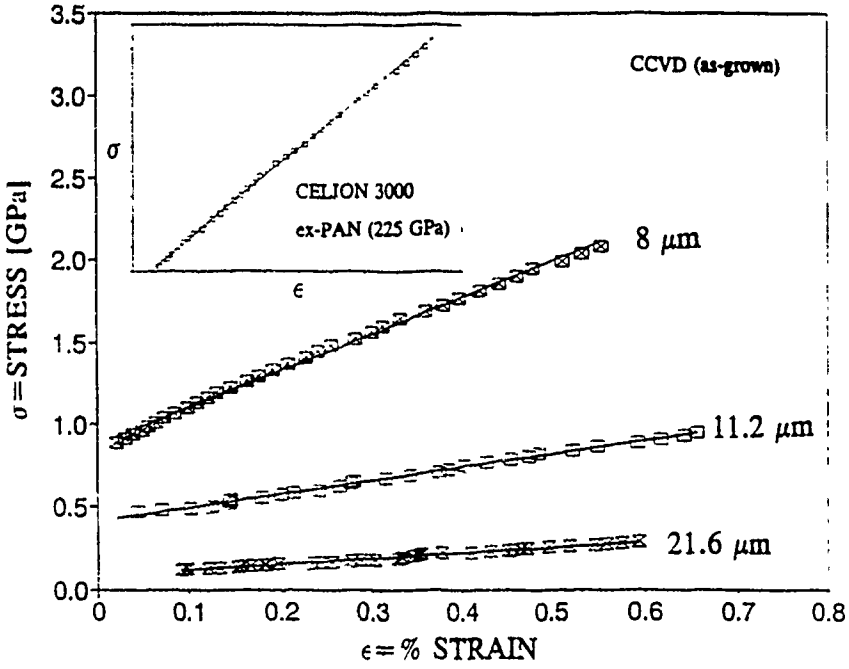

Fig. 3 Typical stress-strain profiles of three different diameter CCVD as-grown carbon fibers. The inset shows the linear profile of a low modulus (Celion 3000) ex-PAN fiber.

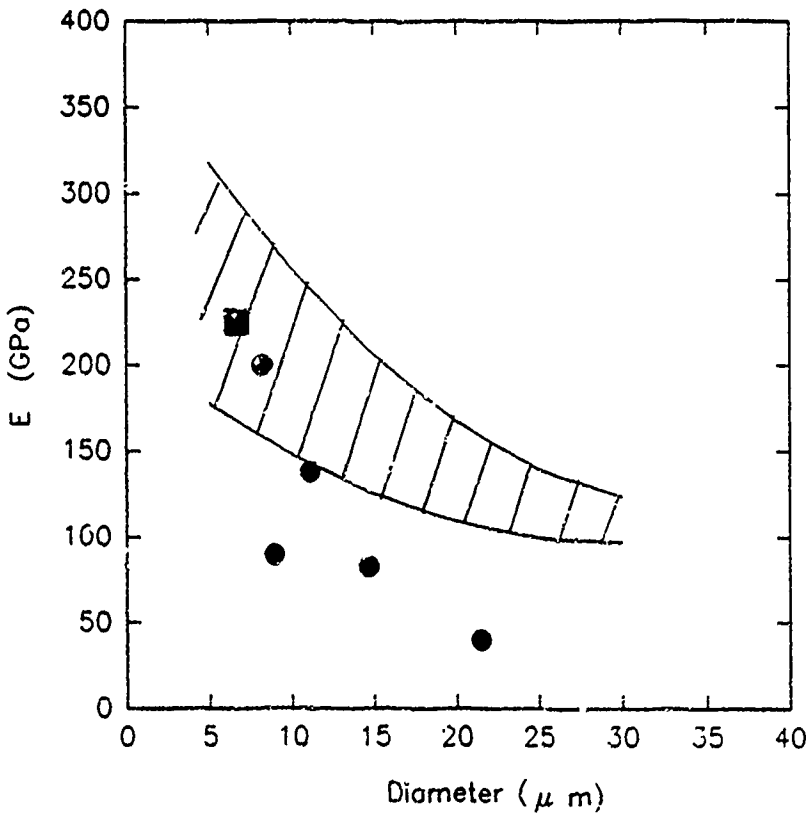

Fig. 4 Diameter dependent Young's modulus, E_y, for CCVD carbon fibers (as-grown). The shaded region represents Tibbet et al [1987] results. The measured E_y for the ex-PAN fiber is shown by ■ for comparison.

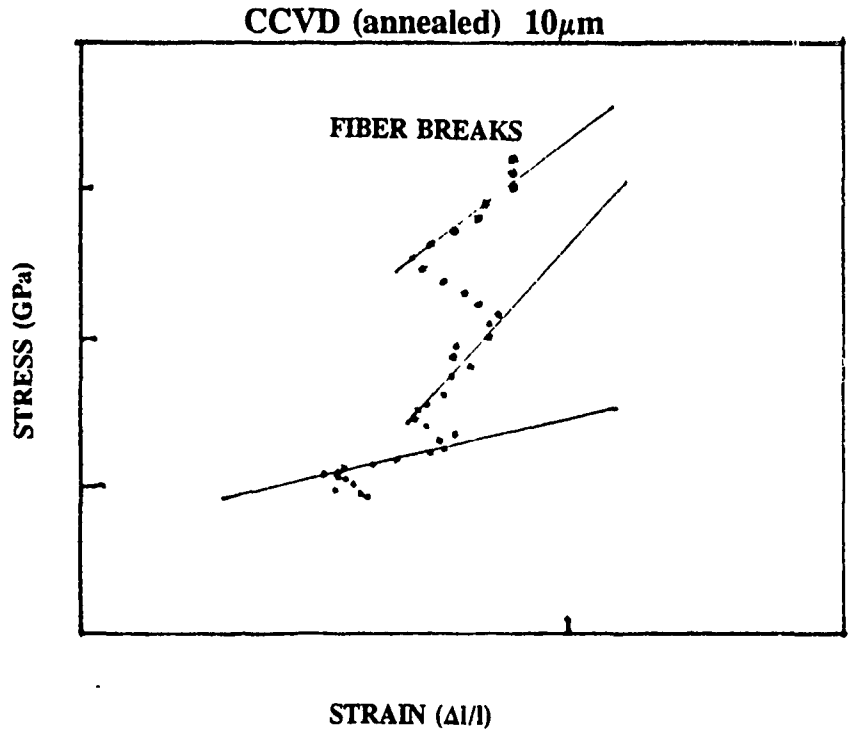

Fig. 5 Typical stress-strain profile of an annealed CCVD carbon fibers obtained on a continuous loading. The stair-step like behavior is due to the annular morphology (see text).

B. LOOP TESTING OF VAPOR DEPOSITED CARBON FIBERS

Background

There appears to be no diameter dependent tensile testing of the vapor grown carbon fibers (CCVD) using a loop (or Sinclair) test. Whereas a conventional stress-strain profiling is determined via instron type set up, the loop test is an important technique for the CCVD fibers because of the different microstructure of these fiber. CCVD fibers have an annular structure (like a series of expanding concentric tree-rings) which provides them with greater normal axial strength than other pitch-type fibers[1]. In fact Tibbet et al.,[1] noted that this graphitic structure is now superior to any other fibers known.

It is widely accepted from tensile tests that both Young's modulus (E_y) and the fiber's tensile strength are diameter dependent (i.e as fiber's diameter increases, both E_y and tensile strength decreases). Several mechanisms have been proposed to explain this relationship; for example, Wicks et al., [2] suggested that layer misorientation increases as diameter increases, Tibbet et al.,[3] believed that this dependence is due to non-uniform carbon deposition rates along the fiber length, and Yetter et al.,[4] discussed the increased crystallite misalignment due to greater pyrolytic deposit disorder which occurs at higher diameters, as well as noted that a larger cross-sectional area can also contain a greater number of strength limiting flaws. Bennett et al.,[5] reported that the gauge-length is related to both E_y and tensile strength since the number of flaws increases with length. Finally, much has also been written about differences in mechanical properties between fibers coming from a given batch[4] and especially about the much wider differences in fiber properties coming from different batches of otherwise similar fabricated fibers[6].

In this experiment we wish to determine E_y as a function of fiber diameter (d) for CCVD as-grown fibers; additionally, we wish to minimize any effects the above variables would introduce to our results, therefore, we only tested fibers that came from a single batch to remove the variability that is inherent of testing fibers coming from different batches. We also removed the fiber gauge-length dependency by applying compressive stress to a small portion of the fiber rather than subjecting the entire fiber to a tensile test. We did this by testing our samples using Sinclair's loop test[7]. Since this test only measures E_y for small portions of the fiber, it greatly lowers the probability of measuring an artificially lowered E_y due to significant flaws within the fibers total length[7]. Thorne [8] noted that the loop test is insensitive to well-spaced but severe flaws; therefore, it provides an idea of the intrinsic breaking strain between severe stress-raising discontinuities.

Experimental

CCVD fibers ($\sim$6-18μm) were tested using a modified version of a Sinclair's loop technique[7]. The apparatus used to apply force was a Chainomatic balance and test weights applied were one mg increments with the

scale being rebalanced after each increment. All loop diameters (D) were taken with a traveling microscope which had an accuracy of $\pm 5\mu$m. Each sample was mounted following a procedure similar to William's[9]. Fig. 1 shows the sample configuration. One sample end was glued (with 5min epoxy) to a small hook assembly. The loop was then formed between a glass slide and a cover slide, and the other end was similarly glued, beneath the loop, to the slide. The cover slide kept the fiber from flipping up as it attempted to uncoil as noted by Torne[8]. A 50μm wire was placed on each side of the loop, between the slide and cover slide, to reduce any friction between the fiber and glass thus ensuring the fiber's free movement during testing. Using capillary action, glycerol was also allowed to seep between the slides to aid in fiber lubrication. Two nylon threads were also initially attached between the slide and hook assembly to provide support to the sample while it was being loaded into the Chinomatic balance, these were then cut with a hot soldering iron immediately prior to testing.

Loop formation initially proved to be quite difficult; either the loop would flip up or the fiber simply broke. A successful technique was found that involved the formation of the fiber loop around a small cylinder or pin that could be held down by a magnet. After the loop was made and secured, the pin was carefully removed while the cover slide was placed over the loop. The inset in Fig. 1 shows our technique of employing a small pin to assist in the fiber loop formation.

Important Results and Discussion

The Young's modulus can be determined from a stress-strain profile. In a single fiber loop test the stress(σ) and strain (ϵ) are given [7] by .

$$\sigma = \frac{16W(3.75D)}{\pi d^3} \qquad \epsilon = \frac{4d}{(3.75D)}$$

where W, D, and d are applied force, loop diameter, and the fiber diameter respectively. Typical stress-strain profile is shown in Fig. 2 for a CCVD fiber with 16.8μm diameter. The elastic range is usually a small linear portion of the curve while the in-elastic behavior is normally seen as a bowing leading to fiber failure. The Young's modulus was determined from the linear portion of the curve for fibers with varying diameters. We must state that these fibers were chosen from a single batch only.

The diameter dependent Young's modulus data for CCVD carbon fibers is shown in Fig. 3. Our results are shown by the data points while the shaded region represents typical results reported by others[3,4,10]. We notice a seemingly underlying order to the pattern of our data. A sawtooth-type pattern of first decreasing and then small increasing E_y values were found to exist. E_y was seen to decrease for $5 < d < 10\mu$m and increase for $10 < d < 20\mu$m fibers. Due to the increasingly brittle nature of the thicker($> 18\ \mu$m) CCVD fibers, we were unable to make a loop in the thicker CCVD fibers without breaking. However, tensile testing by Tibbet's et al., [10]

showed data for fibers in excess of 30μm. We believe that their data not only shows our single tooth's wave but possibly two other waves additionally. Therefore, our study for the first time, on a single batch of fibers ranging from 5 to 20μm, has shown a detailed behavior previously unseen or masked by large numbers of measurements.

A Matthiessen's type of relation may explain the diameter dependent E_y seen in the CCVD carbon fibers. $\{E_y = 1/(\sum y\alpha_i/E_i)\}$ where α_i would most likely converge to give the general dependence reported. It is generally accepted that increasing fiber size leads to an increased probability of detecting a flaw (causing reduced fiber strength). However, this argument can not hold for the observed decrease in E_y with fiber size. A deterioration of the outer layers of the CCVD fiber would cause a decrease in E_y. This is directly related to the growth or deposition rate. A test of this would be to control the growth rate that follows the dE_y/dd curve, and then re-examine the diameter dependent E_y. This may lead to a more uniform deposition of fibers.

Our results also imply that separating entities may exist within the larger CCVD fibers. Such range or number of entities can be determined from the steps in the E_y-d behavior. This, to some degree, has been suggested where at low stresses the fiber bends like a single fiber however, at higher stress (for thicker fibers) there is a separation of the layers, and non-uniform fracture leads to buckling. Scanning Electron Micrographs of the fibers were examined. A typical fracture is shown in Fig. 4. In agreement with other reports[11], the tensile side is rough while the smooth side corresponds to the compressive portion of the looped fiber. It is the tensile stress that leads to fiber failure in these bending tests.

Flexural properties were also determined from the loop tests. Fig. 5 summarizes the results. Critical condition is defined as when the fiber breaks. (a) A decrease in the critical or tensile strength of the CCVD fibers with increasing diameter is agreement with tensile test results, (b) no obvious trend in the breaking or critical strain, is noted as fiber size increases but (c) there is an increase in the critical loop diameter as the fiber size increases.

REFERENCES

1. G. G. Tibbets, M. Endo, and C. P. Beetz, Jr., SAMPE Journal, V22-5, (1986).
2. B. J. Wicks and R. A. Coyle, J. Material Science, 11, 376 (1976).
3. G. G. Tibbets, C. P. Beetz, Jr., Research publication of General Motor Corporation, GMR 5550 (1986).
4. W. E. Yetter, C. P. Bettz, Jr., and G. W. Budd, Research publication of General Motor Corporation, GMR 4759 ((1984).
5. C. C. Bennett and D. J. Johnson, J. Material Science, 18, 3337 (1983).
6. J. D. H. Hughes, J. Phys: D Appl. Phys., 20, 276 (1987).
7. D. Sinclair, J. Appl. Phys. V21, 380 (1950).
8. D. J. Thorne, Nature, Vol 248, 754 (1974).
9. W. S. Williams, D. A. Steffens, R. Bacon, J. Appl. Phys. Vol 41, 4893 (1970).
10. G. G. Tibbets, and C. P. Beetz, Jr., J. Phys. D: Appl. Phys. 20, 292 (1987).
11. (see for example) J. L. P. Da Silva and D. J. Jihnson, J. Material Science, 19 3201 (1984).

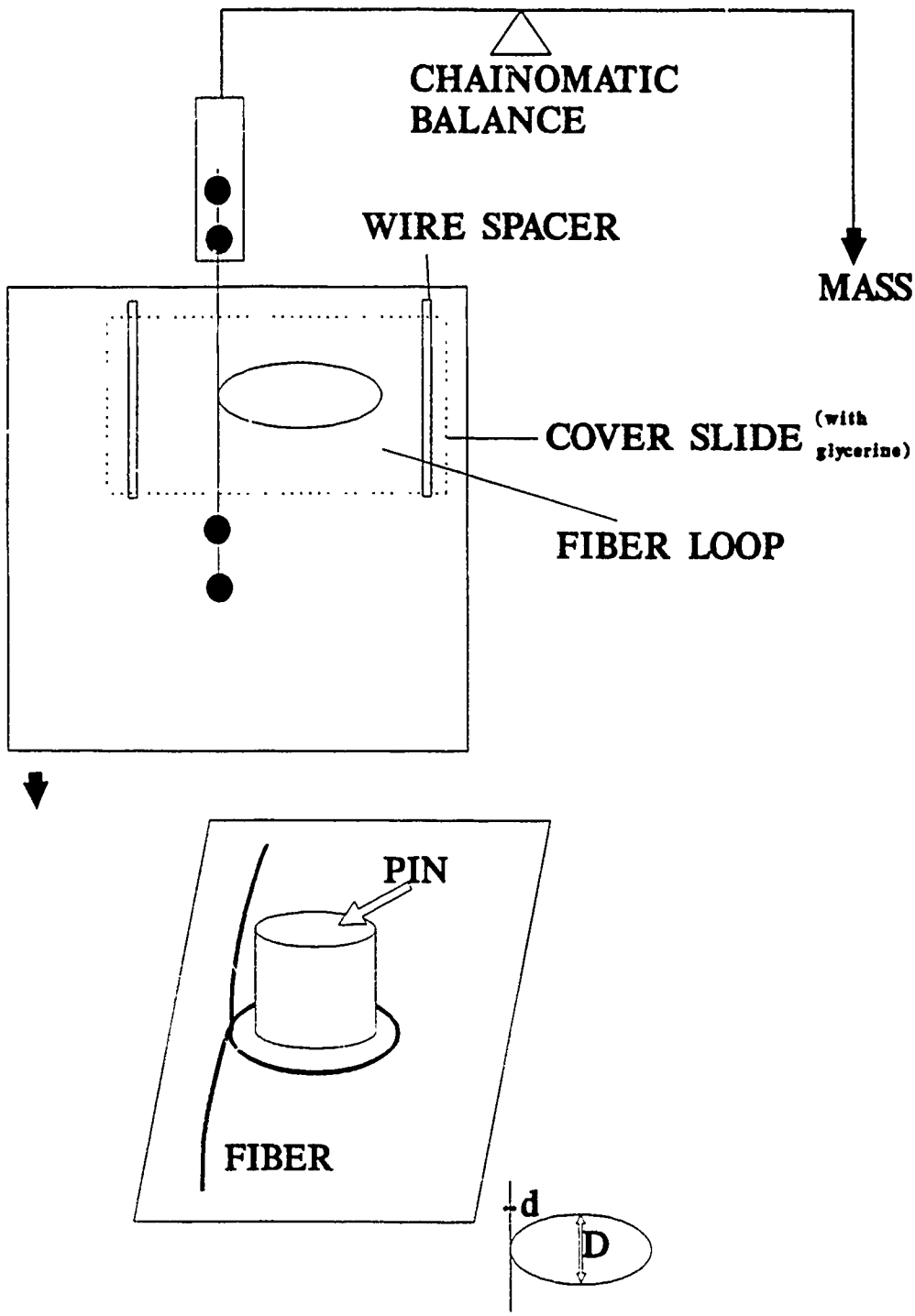

Fig. 1 Sinclair loop lest sample mount for single carbon filament. The inset shows our design to assist in the loop formation.

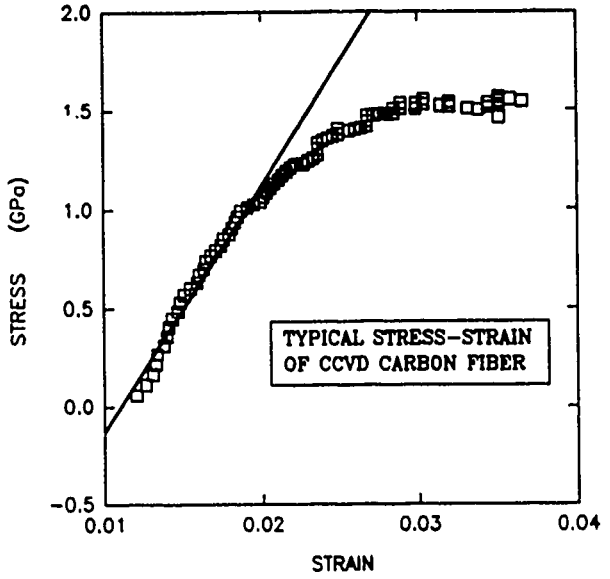

Fig. 2 Typical stress-strain curve for one CCVD sample of 16.8μm diameter.

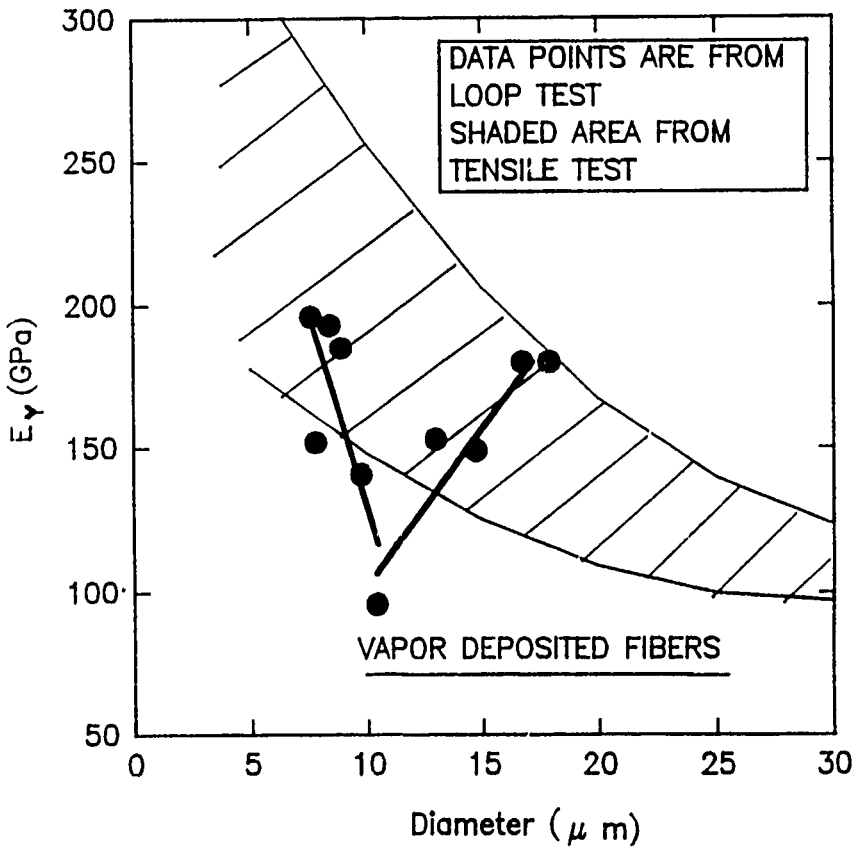

Fig. 3 Diameter dependent Young's modulus for CCVD (as-grown) carbon fibers. The shaded region represents other reported results. The linear fits to our data were obtained by least square's fit.

Fig. 4 A typical SEM micrograph of a CCVD fiber undergone a loop test failure.

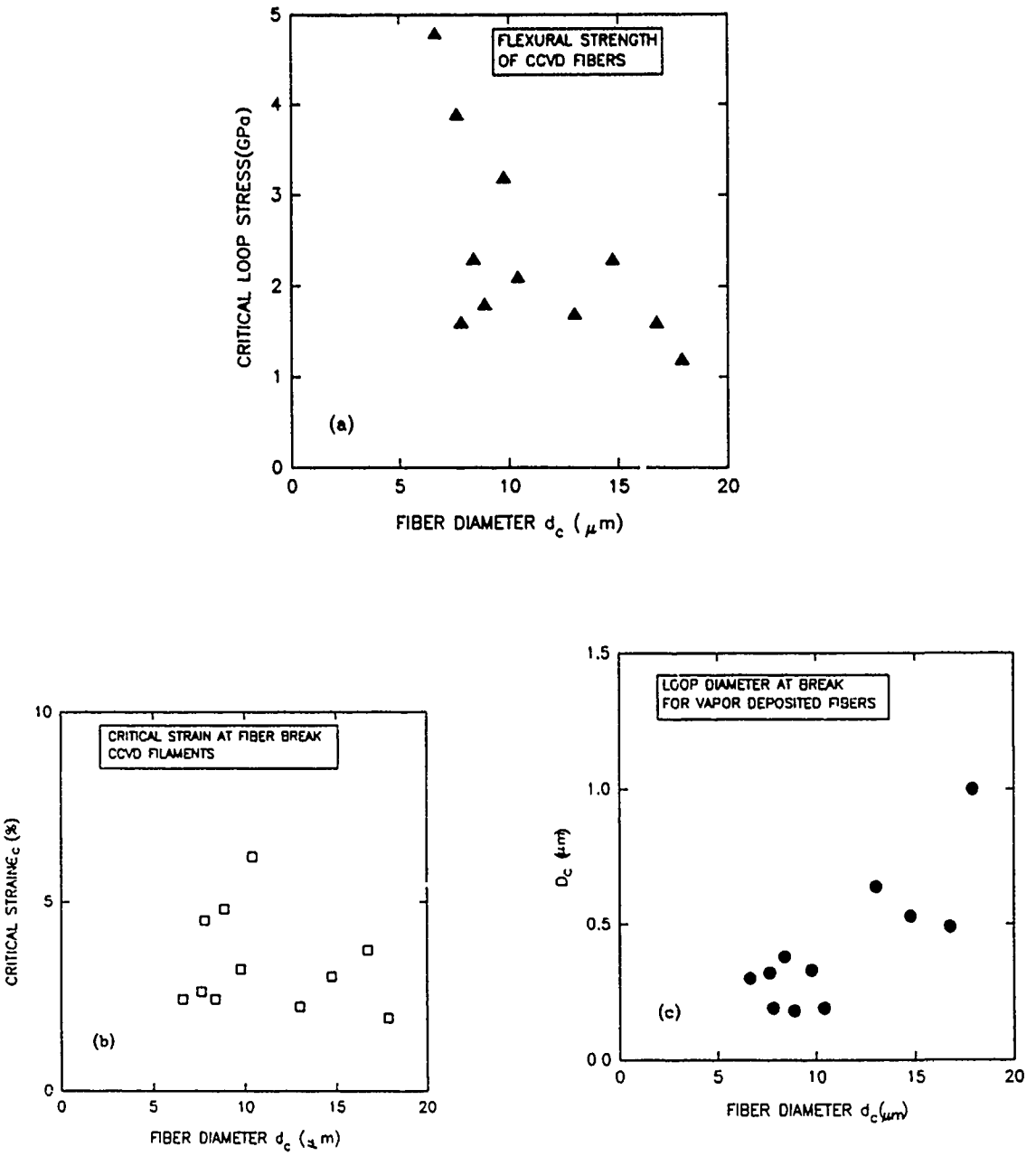

Fig. 5 Critical parameters determined during loop testing of CCVD carbon fibers, (a) loop diameter, (b) maximum strain, and (c) tensile strength.

C. TORSIONAL MODULUS OF VAPOR GROWN CARBON FIBERS

Torsional modulus (G) is more complex because of its dependence on the azimuthal arrangement of graphene planes as well as the misorientation along the fiber axis. To date, no theoretical model has been proposed on the calculation of the torsional modulus of carbon fibers. However, there is some speculation that $G = C_{44} \sim 4$ GPa for fiber with radial structure and $G = (C_{11} - C_{12})/2 \sim 440$ GPa[1] for highly ordered CCVD fibers with perfectly faceted morphology. Measured values of G vary from 17 to 28 GPa for ex-PAN fibers[2], between 10 and 15 GPa for ex-rayon fibers[3], and from 9 to 13 GPa for ex-mesophase pitch fibers[4].

In this report, we report the first experimental results of torsional modulus of both as-grown and annealed CCVD fibers measured using a torsion pendulum. Measurements on fibers with different diameter and under varying stress were conducted. It is found that G is both stress and size dependent. The zero-stress value of G is 105 ± 5 for the smallest available (diameter ~ 5.4 μm) as-grown fiber and only 36 ± 3 GPa for 16.2 μm diameter fiber. For annealed CCVD fibers, it is 200 ± 10 for 8.4 μm to 105 ± 5 GPa for 14.4 μm. These values are significantly higher than those of other types of fibers. They are believed to be the results of the unique morphology and the relatively higher degree of graphitization in CCVD fibers.

I. Experiment

The torsion pendulum, illustrated in Fig. 1, consists of the suspended carbon fiber and a brass disk attached to the middle. The disk provides the momentum of inertia for torsional oscillation and also serves as an electrode for the electrostatic driving system. The excitation vanes are a pair of copper sheets. The electrical circuitry is also shown in Fig. 1. When voltage is applied between the disk and the vanes, the electrostatic force produces the necessary torque to initiate the torsional oscillation. Conducting silver epoxy was used because it is adhesive and can provide electrical contact between the carbon fiber and the brass disk. It was also employed to attach the fiber to the two glass slides. Stress was applied attaching weights to the lower glass slid via h

The oscillation period was measured by reflecting a very low power laser beam off the brass disk. To minimize the air damping, the pendulum was kept in vacuum of typically 10^{-3} torr.

The torsional modulus G of a piece of fiber with radius a and length L is related to the oscillation period T by:

$$G = \frac{2\pi IL}{a^4 T^2}$$

where $I = Mr^2/4$ is the momentum of inertia of the brass disc with mass M and radius r.

The oscillation period was measured for each fiber under varying stress. Extreme care was taken to avoid external vibrations that might affect the measurements.

II. Results and Discussion

The stress dependent torsional moduli are shown in Fig.2. In all the samples, linear relationship was observed within the limit of error. The torsional modulus of an ex-PAN (celion 3000) was also measured and plotted in Fig.2 for comparison. The most important difference is that the G values of CCVD fibers are much higher than that of ex-PAN fiber. As-grown CCVD fibers have torsional moduli ranging from 36 to 105 GPa while ex-PAN has G of 22 GPa (in good agreement with values reported elsewhere of ex-PAN fibers[2]). Annealed CCVD fibers have even higher torsional moduli ranging from 105 to 200 GPa.

These unusually high values of torsional modulus of CCVD fibers are not totally surprising. As discussed by Dresselhaus et al[5], G depends on the azimuthal arrangement of the carbon ribbons. In CCVD fibers, the carbon ribbons are arranged in a circular fashion[6] as a result of growth process. In this scroll-type structure, the strong in-layer c-c bond is responsible for this high torsional modulus of CCVD fibers. It ensembles the shear modulus of an individual layer of graphite where $G = (C_{11} - C_{12})/2 = 440$ GPa[7]. Obviously, CCVD as-grown fibers are not close to complete graphitization. Their elastic stiffness constants are probably smaller than those of graphite. Besides, the misorientation of the graphene planes with the fiber axis also has effect on the torsional modulus. Taking into consideration the factors mentioned above, the torsional moduli of as-grown CCVD fibers are therefore smaller than 440 GPa of graphite. On the other hand, the annealed CCVD fibers have even higher torsional moduli than those of the as-grown fibers because heat treatment (above 3000 °C) improves the inter-layer correlation and increases graphitization of the fibers. The increased crystallite ordering due to annealing probably also increases the elastic stiffness constants.

G also exhibits stronger stress dependence for CCVD fibers, shown in Fig.2. Variations of more than 70% for annealed fibers and more than 100% for as-grown fibers are observed compared to only about 20% for the ex-PAN fiber. The increase of torsional modulus with stress is probably due to the improvement of preferred orientation of graphene planes in the fibers by the increase of strain as suggested by Curtis et al[8]. A similar strong "strain stiffening" phenomenon was also observed in Young's modulus measurement of CCVD fibers by Tibbetts et al[9],[10].

Another feature is the size dependence of G for CCVD fibers. Shown in Fig.3 is the extrapolated zero-stress G values of as-grown and annealed fibers versus fiber diameter. The thinner fibers have higher values of torsional modulus. G is 105 $\pm$ 5 GPa for the smallest diameter available ($\sim$ 5.4 μm) as-grown fiber. It reduces to 36 $\pm$ 3 GPa for 16.2 μm diameter fiber. For annealed CCVD fibers, G reduces from 200 $\pm$ 10 to 105 $\pm$ 5 GPa for diameter increasing from 8.4 to 14.4 μm. This reduction of G with increasing fiber diameter is related to the degree of graphitization of different diameter fibers as the results of different deposition rates. X-ray diffraction revealed that thinner fibers have higher graphitic ordering and better preferred orientation[9]. This also explains why the "strain stiffening" phenomenon is less profound for thinner fibers as seen in Fig.2.

References

1. Same as ref. 5, page 95. There is a misprinting: it sLould read $(C_{11}-C_{12})/2 \sim 440$ GPa. See page 86 for C_{ij} values.
2. S. Srinivasagopalan, Ph.D. Thesis, University of Washington, Seattle, 1979
3. D.B. Fischbach, and S. Srinivasagopalan, 5th Conf. Industrial Carbons and Graphite, London (Society of Chemical Industries, London), p.389
4. R.E. Smith, J. Appl. Phys.43, 255(1972)
5. M.S. Dresselhaus. G. Dresselhaus, K. Sugihara, I.L. Spain, and H.A. Goldberg, "Graphite Fibers and Filaments", Springer-Verlag, Berlin Heidelberg, 1988, p.92
6. A. Yoshida, Y. Hishiyama, and M. Endo, in Extended Abstracts of the 17th Biennial Conference on Carbon, Lexington, KY (American Carbon Society, University Park, PA), p.297 (1985)
7. B.T. Kelly, "Physics of Graphite", Applied Science Publisher, London and New Jersey, 1981, p.66
8. G.J. Curtis, J.M. Milne, and W.N. Reynolds, Nature 220, 1024(1968)
9. G.G. Tibbetts, and C.P. Beetz Jr., J. Phys. D: Appl. Phys. 20, 292(1987)
10. D. Church, D. Patel, and I.L. Spain, (in preparation)

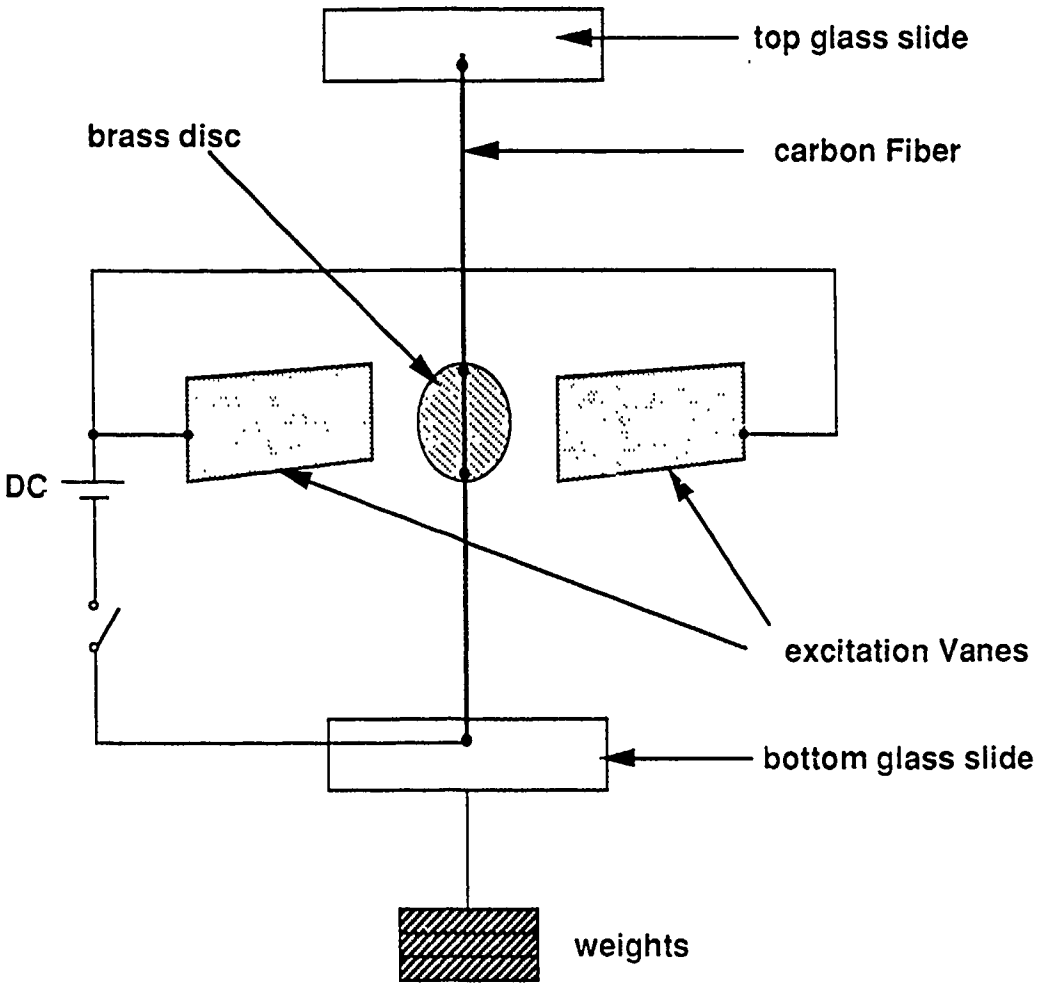

Fig. 1 A schematic diagram of a torsional modulus, G, apparatus for mono filament of carbon. The torque is applied electrostatically. The pendulum is maintained at 10^{-3}torr vacuum for G measurement. The fiber can be tensile strained simultaneously.

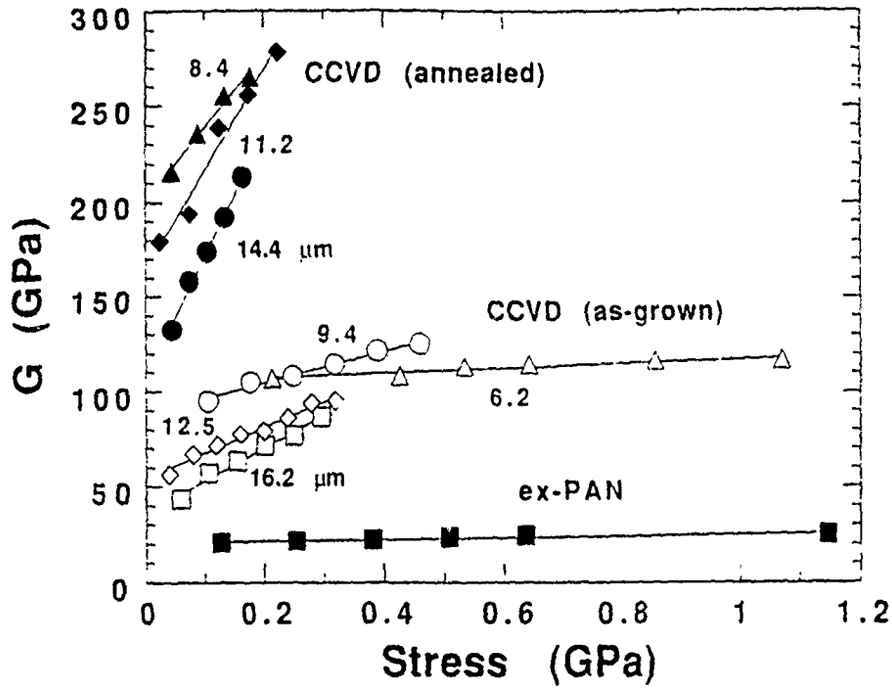

Fig. 2 Stress dependent torsional modulus of as-grown and annealed(>2500°C) CCVD fibers of different diameters. Results of measurements on a low modulus ex-PAN fiber is shown for comparison, The lines are least square's fitted.

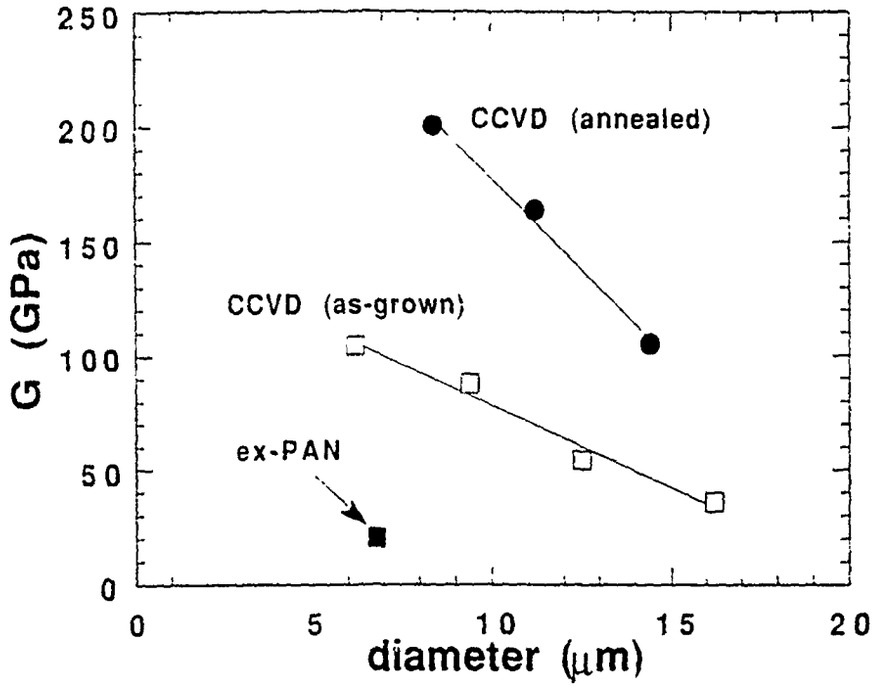

Fig. 3 Diameter dependent torsional modulus, G, of CCVD as-grown and annealed fibers. As with Young's modulus, G also decreases with fiber diameter. The dependence is higher for the annealed/graphitized fibers. These values of G are larger than any previously reported for these CCVD samples.

D. PIEZORESISTANCE OF CARBON FIBERS

I. Piezoresistance of Different Carbon Fibers

Professor Ian L. Spain in-conjunction with Celanese research company performed electromechanical tests on a number of carbon fibers. This work has been submitted and reviewed for publication, however, the death of Professor Spain has rather slowed the process of publication of this manuscript. This work will be published.

It is important to give an account of the above research since the present study is directly related. A copy of the manuscript can be found in the first annual report (1989) for the present contract. This yet unpublished work will be denoted as PR1.

The piezoresistance(PR) of several ex-PAN and ex-pitch carbon fibers was obtained at a temperature of 300K. The piezoresistance is defined as the change in resistance which occur when the fiber is strained longitudinally. The PR is positive for poorly graphitized fibers with low Young's modulus, and falls to increasingly negative values as the graphitization index and Young's modulus increases. A model which qualitatively explains the observed trends is presented, based on geometrical and electronic contribution to PR.

Typical curves of PR for ex-PAN fibers are shown in Fig. 1 where both positive and negative PR behavior are observed. Experimental results show that the PR only tends to be positive for low modulus fibers, and is negative for those with high modulus. This is the case for ex-PAN and ex-mesophase pitch and CCVD fibers (Endo and Koyama, 1979, 1980). These effects are reversible for moderate loadings, and this is the range of interest for the present study.

At a glance only the positive PR can be explained in terms of geometrical effects. Other explanations for the change in the resistance can be related to the inter-particle contacts(Fishbach et al., 1980), changes of the orientation of the fibers under stress (curtis et al., 1968), or electronic effects (Goldberg, 1985). In order to separate these effects it is necessary to consider the structure of the fibers, the relationship of the structure to the elastic behavior, and then calculate the PR using model. This was basically the approach adopted in the paper. X-ray data were presented first, allowing the orientation distribution function and the graphitization of the carbon ribbons to be determined. Since the elastic moduli of the fibers examined by us vary over a wide range, our data allowed a much more detailed examination to be made of the relationship between Young's modulus and elastic/structural parameters than has been done before. Finally, the PR data were presented and compared to models using structural and mechanical data.

Detailed discussion of the results on the structural analysis of carbon fibers using x-ray diffraction can be found in PR1. Experimental results showed a decreasing misorientation angle $<\phi>$ with increasing Young's modulus, E_y. Both the x-ray data and the mechanical properties were interpreted by modifying the Uniform Stress model. Using this model,

$$1/E_y = S_{11} + (2S_{13} + S_{44} - 2S_{11}) \langle \sin^2\phi \rangle$$

$$+ (S_{11} + S_{13} - 2S_{13} - S_{44}) \langle \sin^4\phi \rangle$$

where S_{ij} are elastic compliences (see Kelly, 1981). As an example, for a perfectly aligned crystallites (ϕ=0 degree)

$$E_y = S_{11}^{-1} \ldots\ldots\ldots 1020 GPa.$$

In the calculations, single crystal values of S_{11}, S_{12}, S_{33}, and the Gaussion form for $P(\psi)$ were used(see PR1). The calculated limits of E_y were compared with the measured modulus which were corrected for porosity and apparatus compliance.

The change in the resistance can be written as

$$\delta R/R_o = \delta L/L_o + \delta A/A_o + \delta \rho/\rho_o$$

where L is the length, A the area, and ρ the resistivity. Using the notation in PR1, this can be written:

$$\delta R/R_o = \epsilon_{2'2'} - \nu\epsilon_{2'2'} + \delta\rho/\rho_o.$$

Dividing by $\epsilon_{2'2'}$ gives the PR/strain:

$$\frac{PR}{\epsilon} = \frac{1}{\epsilon_{2'2'}} = (1-\gamma) + \frac{1}{\epsilon 2'2'}\frac{\delta\rho}{\rho_o}$$

Results of the PR on low modulus fibers showing positive behavior can be explained generally by the change in the geometry of the fiber. As the modulus increases the PR shows a negative behavior. Since geometrical effects can not explain these negative PR results, other effects are required. Models involving the unwrinkling of the ribbons, inter-particle contact, and boundary scattering may lead to small refinement of the positive PR, but they are insufficient to explain the experimental PR results.

For these reasons Goldberg[1985] proposed that the resistivity changes in the PR could be understood in terms of electron density changes. The electron density changes occur because, as is well known, straining the fiber pushes the graphite basal planes closer together, so that the carrier density increases. For this effect to be applicable, it is necessary for the fiber to have 3D ordered graphite and not be completely turbostratic. The increase

in 3D ordering has been shown by Stamatoff et al., [1983] to occur gradually with increasing modulus. Thus the trend towards more negative PR with increasing modulus has a natural qualitative explanation when this model is used. In order to quantitatively understand the data, one can write an expression for the change in resistivity with strain as follows:

$$\frac{\Delta\rho}{\rho}\frac{1}{\epsilon_{2'2'}} = 7q\frac{\epsilon_{33}}{\epsilon_{2'2'}}$$

where the notation and further definitions can be found in PR1 and Kelly (1981). q is a dimensional parameter which depends on the degree of 3D order in the fiber. It is expected that in turbostratic carbon, the electron density will not depend on the c-axis strain , and thus q goes from 0(no 3D order) to 1(complete 3D order).

The average compression of the basal planes of the crystallites can be evaluated using the uniform stress model, following the same technique as described in [6] to yield

$$\frac{\epsilon_{33}}{\epsilon_{2'2'}} = E_y[S_{13} + (S_{33} - S_{13})\langle\sin^2\phi\rangle$$

Following this type of analysis, a plot of the PR per unit strain is shown vs Young's modulus E_y in Fig. 2 along with the two theoretical limits q=0 (indicated by 2D) and q=1 (indicated by 3D). The experimental results lie between the 2D and 3D curves when S_{13} is chosen to be -1.8×10^{-12}/Pa.

An important point needs to be addressed. If electronic mechanism plays a dominating role in PR of high modulus fibers, then the PR should be extremely sensitive to temperature. Therefore, low temperature PR of carbon fibers with different Young's modulus was carried out.

II New Low Temperature PR in Carbon Fibers

1. Experimentation

New apparatus for monitoring the PR of carbon fibers at low temperature was designed and constructed here at CSU. Measurements were performed on a number ex-PAN fibers, pitch fibers, and CCVD fibers. Fig. 3 shows a schematic of the set up. Briefly a sample was attached to the cold finger of a close cycle He refrigerator capable of 10-300K. Isolated by two shields and a heat retarding fins, an electromagnet was also installed in the cryostat to apply the tensile load to the sample at low temperature. PR measurements were performed first at 300K and then at 11K.

2. Results

2A. Ex-PAN and Pitch Fibers

The results of the temperature dependent PR with stress in ex-PAN and pitch fibers have been shown in Fig. 4. As expected, fibers which showed positive PR were temperature independent since the PR in these fibers were caused by geometrical effects alone. However, high modulus fibers such as GY70 and GR21 ex-PAN fibers which showed negative PR at 300K, were different at 11K. At this low temperature the PR becomes less negative in both samples. P100 pitch sample showed the negative PR at 300K consistent with Goldberg et al.,[4] but attempts to measure PR at 11K was unsuccessful because of non-ohmic behavior. Table 1 shows the types of fibers, their diameter, Young's modulus, and resistivities ratio.

T A B L E 1

Sample and their parameters used in the piezoresistance measurements.

SAMPLE	DIAMETER(μm)	$E_{y(GPa)}$	ρ(11/300K)
ex-PAN			
Celion 3000	6.7	230	1.1
GY-70	9	520	1.3
GR 21	11.8	690	1.7
ex-pitch			
P50	10	380	1.2
P75	10.8	500	1.1
P100	9.1	690	#
CCVD			
as-grown	8.4	~250	1.0
annealed	6.3	+	1.5

\+ unable to determine because of step like stress-strain behavior

\# non-ohmic behavior at low temperature

2B. CCVD Fibers

Measurements on the as-grown fiber showed positive PR that was temperature independent (data not shown). This as-grown CCVD fiber had a relatively low Young's modulus and temperature insensitive resistivity. In contrast the annealed CCVD fiber has a large Young's modulus and showed a large increase in resistivity at 11K (see Table 1). Room temperature PR was positive, consistent with Endo et al., [1980]. A remarkable result is shown in Fig. 5 where the positive PR of the annealed fiber at 300K makes a large transition to a negative PR at 11K. This to our knowledge has never been observed before.

3. Discussion

It was stated earlier that the resistance can be written as

$$\frac{\Delta R}{R} = \frac{\Delta L}{L} + \frac{\Delta A}{A} + \frac{\Delta \rho}{\rho}$$

where L, A, and ρ are length, area and resistivity. The positive PR observed for the ex-PAN and pitch fibers can be explained by the geometrical terms alone. This of course leads to the temperature insensitivity positive PR.

Goldberg [4] showed that the most probable explanation for the negative PR was the variation of electron density when the basal planes were pushed together by the applied tensile stress. This was possible if there was some degree of 3D ordering. From the above discussion in I the change in resistance can be re-written as

$$q\epsilon_{zz} = \frac{\sigma}{7E}\left[\frac{\Delta R(\sigma)}{R}\frac{E}{\sigma} - 1 - 2\nu\right]$$

Since all the parameters on the right-hand side are known we can determine $q\epsilon_{zz}$ $q\epsilon_{zz}$ is the parameter representing the change in the basal plane separation, therefore, for a temperature sensitive PR, q must change. Since q accounts for the change in the carrier density, it must decrease in order to explain the temperature behavior of our results on the ex-PAN fibers. Room temperature value of -5.7×10^{-4} was obtained for $q\epsilon_{zz}$ compared to -4.37×10^{-4} at 11K. This reduction in the electron density parameter can be via carrier freezout at low temperature.

The temperature sensitivity PR of the annealed CCVD fiber is an opposite effect compared to the ex-PAN fibers. These annealed fibers have high E_y therefore, a negative PR should be observed at 300K. However, the positive result shows that there is considerable 3D ordering present in these fibers. The transition to a negative PR at 11K need to be explained qualitatively by the high degree of graphitization and the tree ring morphology of these fibers. The microstructural factor may not be critical since the as-grown fibers showed no temperature dependence. The annealed sample, however, may be dominated by ionized impurity scattering which is a major parameter at low temperature. Models for our new results are being developed with H. Goldberg at Celanese Research Company.

III. References

1. M. Endo and T. Koyama, IEE of Japan, 100A, 633 (1980) (in Japanese).
2. D. B. Fischbach, K. Komaki, and S. Srinivasagopalan, (1980): Technical Report to US Army Research office (Grant No. DAAG29-76-G-0169)(unpublished).
3. G. J. Curtis, J. M. Milne, W. N. Reynolds, (1968): Nature (London) 220, 1024.
4. H. A. Goldberg (1985): Final Report to US Army Research Office, Contract No. DAAE29-81-C-0016 (unpublished).
5. B. T. Kelly, (1981): *Physics of Graphite* (applied Science, London).
6. M. S. Dresselhaus, G. Dresselhaus, K. Sugihara, I. L. Spain, and H. G. Goldberg, (1988) *Graphite Fibers and Filaments*, Vol. 5 in Springer Series in Materials Science (Springer, Berlin, 1988).

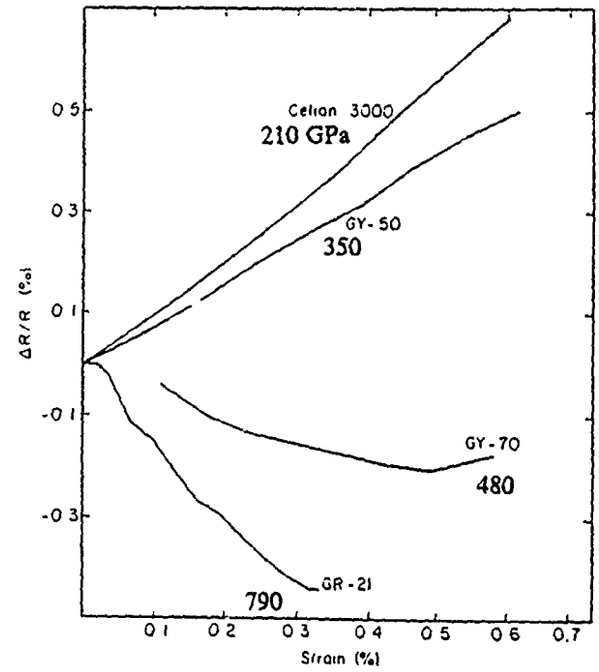

Fig. 1 Measured piezoresistance(PR) of ex-PAN fibers at 300K. The Young's modulus(in GPa) of the fibers are shown besides the curves. Decreasing PR is observed for higher modulus fibers.

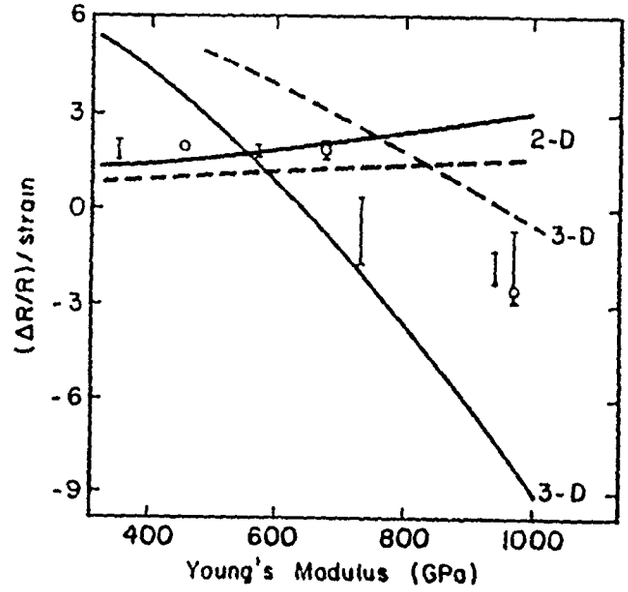

Fig. 2 Young's modulus dependent piezoresistance/strain of carbon fibers. The solid lines are calculated using the uniform stress model with S_{44} and S_{13} as variables. The positive slopes represents 2D whereas the negative slopes 3D.

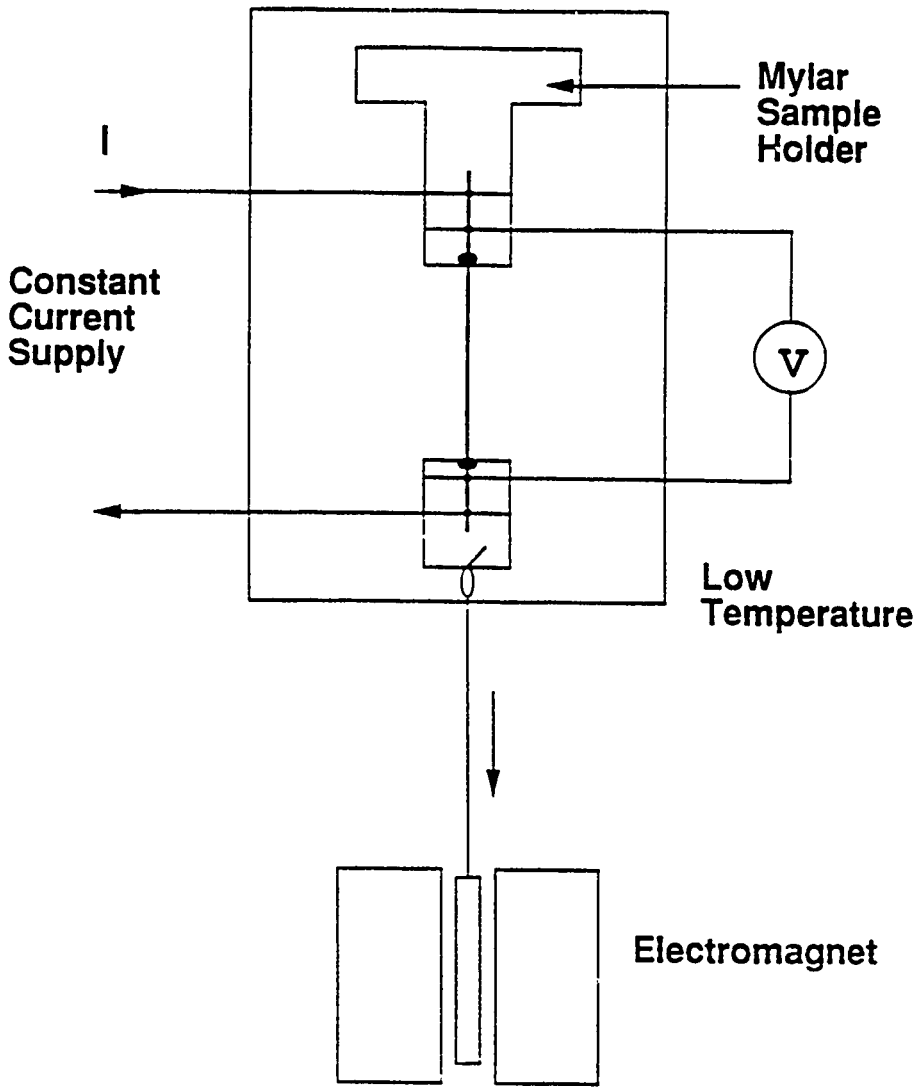

Fig. 3 A schematic diagram of the set up used in observing the piezoresistance of carbon fibers at low temperature. A close cycle He refrigerator was employed for the low temperature (300-10K) system.

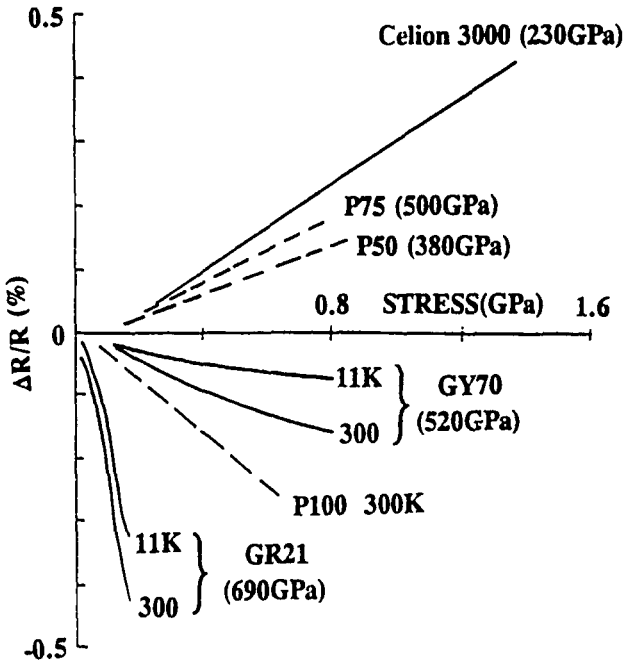

Fig. 4 Piezoresistance(PR) vs. stress(GPa) of ex-PAN (solid curves) and pitch (broken curves) fibers performed at 300K and 11K. No temperature dependence was observed for low modulus fibers that showed positive PR at 300K. However, higher moduli fibers with negative PR at 300K showed less negative PR at 11K. The high modulus P100 pitch fiber, which showed negative PR at 300K, became non-ohmic at 11K for meaningful PR measurement.

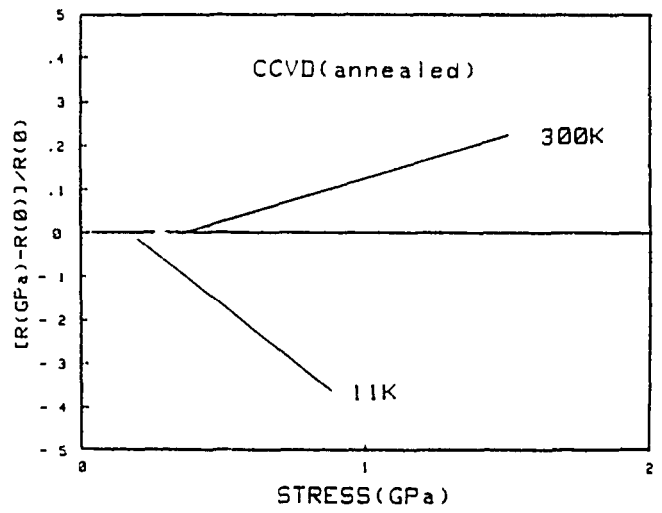

Fig. 5 Temperature sensitivity of the piezoresistance(PR) in annealed (>2500°C) CCVD carbon fibers. This highly graphitic fiber show a positive PR at 300K. Surprisingly, a much more negative PR is seen at 11K. The PR of the as-grown fiber (not shown) showed no temperature dependence.

3. ELECTRICAL & MAGNETIC PROPERTIES OF THICKENED ex-PAN & CCVD CARBON FIBERS

ABSTRACT

Electrical characterization of thickened ex−PAN and chemical vapor−deposition of carbon fibers (CCVDF) have been carried out. Four−point resistivities measured between 10 and 300 K have been compared with other commercially available fibers. The magnetoresistance of these fibers was also obtained at 4.2 K with fields up to 15 Tesla at The National Magnetic Facility. The magnetoresistance curves were fitted with Bright's [A. A. Bright, Phys. Rev. B20, 5142 (1979).] theory with the addition of ionized impurity scattering for electronic parameters such as electronic mobility and carrier concentration.

Ex−PAN carbon fibers were thickened to varying degrees by CVD of hydrogen/acetylene gaseous mixtures. The pyrolysis of the hydrogen/acetylene mixture can produce two distinct forms of carbon: (1) vitreous pyrolytic carbon and (2) colloidal soot. The production of vitreous pyrolytic carbon is favored when the partial pressure of acetylene is low. The reaction conditions (partial pressure of acetylene, total gas flow, and time) were varied to optimize the thickening rate and minimize nonuniform thickening along the length of the fiber. The reaction mechanism controlling the thickening of CCVD filaments appears to control the CVD thickening of ex−PAN carbon fibers. Both are composed of concentric rings of pyrolytic carbon.

I. INTRODUCTION

Catalytic chemical vapor deposited (CCVD) filaments have superior structural characteristics relative to polymer−based (e.g., PAN) carbon fibers [1]. They can, however, only be produced in finite lengths whereas polymer−based carbon fibers can be produced in continuous lengths. This limitation on the length of the CCVD filament restricts its utilization in a variety of applications.

Recently, workers such as Matsumura et al. [2] and Shioya et al. [3] have produced composite carbon fibers (i.e., a polymer−based carbon fibre coated with pyrolytic carbon) by CVD and plasma−assisted CVD respectively. The carbon is deposited from a gaseous reaction mixture of hydrogen and hydrocarbon (e.g., benzene and cyanoacetylene). The pyrolytic carbon is deposited in concentric rings around the polymer−based carbon fibre. The rate of deposition is primarily controlled by the partial pressure of the hydrocarbon, the ratio between the surface area of the carbon fibers and the volume occupied by the pyrolyzing gas, and by the overall gas flow.

The pyrolysis of a hydrogen/hydrocarbon gaseous mixture results in a complex series of chemical reactions (dehydrogenation, condensation, and aromatization) which, depending on the reaction conditions, can produce two distinct forms of carbon, vitreous pyrolytic carbon and colloidal soot. During the CVD process an entire series of molecular species are generated ranging in size through aromatics to complex transitional molecules of low hydrogen content and high molecular weight [4]. Colloidal soot is formed when the pyrolyzing atmosphere becomes supersaturated with high molecular weight macromolecular species which homogeneously nucleate to produce gas−born carbon particles. The vitreous pyrolytic carbon is formed when the carbon macromolecular species condense directly onto the deposition surface, in this case, ex−PAN carbon fibers.

Koyama and Endo [5] state that the development of CCVD filaments occurs in two distinct phases:

(1) an initial growth stage which produces thin filaments, and

(2) a thickening stage where the filaments thicken due to pyrolytic carbon deposition on the filament sides.

There is a critical temperature, 1040°C, above which the thickening process is dominant and below which the growth of the filament is favored [6]. However, Oberlin et al. [7] believe that it is impossible to separate both stages in the development of CCVD filaments because they are statistically concomitant, though successive for a given part of the filament. It seems conceivable that the secondary stage can be utilized in the CVD thickening of ex−PAN carbon fibers. Consequently, the heat treatment temperature (HTT) for the CVD process during this work was set at 1100°C, which is above the temperature at which thickening starts to dominate in CCVD.

Electrical and magnetic characterization can be employed to distinguish between fibers of different origin. The electrical resistivity of graphite shows values of about 10^{-5} Ωcm at room temperature and decreases at lower temperatures. The resistivity behavior of graphite is quite different at low temperatures. This decrease in resistivity for $T < 100$ K is most prominent in single crystal fibers [1]. The highly graphitized carbon fibers are usually heat treated [9] to >2500°C. At lower heat treatment temperature of ~1500°C, the fibers have less graphitic character and fibers heat treated at about 1000°C exhibit [8] almost amorphous characteristics. Report [8] also indicate that

carbon fibers with small diameters have superior properties.

In carbon fibers where graphitization is incomplete, drastic changes in the electrical properties may be produced [10] by a small quantity of impurities or defects causing shift in the Fermi level. It has been reported [10] that quantitative parameters are difficult to ascertain from electrical resistivity measurements. However, good approximations can be obtained. Tahar et al. [11] reported a study of the electrical properties of different sizes of graphite fibers. In their study the temperature dependence of the electrical resistivity were fitted with two band model to obtain carrier concentration and mobility due to possible carrier scattering mechanisms in graphite fibers.

Magnetoresistance in carbon fibers (pre−graphitic) was given by Bright [12]. Magnetoresistance measurements on graphite fibers by Rahim et al. [13] extended Bright's approach to include change in mobility at high field to quantitatively explain the experimental results for fields up to 5 Tesla. The change in the mobility factor has to be taken into account because of ionized impurity scattering. Magnetoresistance measurements shows negative values for the heat treated fibers above 1300°C temperature [14,15]. This behavior is believed to be due to the two−dimensional graphitic order in fibers. Initial increase in the heat treatment temperatures above 1300°C results in reduced 2−D plane order and a reduction in the amount of negative magnetoresistance. However, as the heat treatment temperature is increased to values above 1700°C, there is a transition from amorphous to 2−D in plane ordering to 3−D ordering which leads to increase in the magnetoresistance for $T > 2100°C$. Therefore one can take the sign of the magnetoresistivity as an indication of the degree of graphitization in carbon fibers.

During this work, single ex−PAN fibers were coated to varying thicknesses with pyrolytic carbon by CVD of hydrogen/acetylene mixtures. The reaction conditions such as the partial pressure of acetylene, the overall gas flow, and the reaction time were varied in order to optimize the production and deposition of pyrolytic carbon. Characterization included temperature dependent resistivity of the thickened ex−PAN fibers produced by chemical vapor deposition technique, and catalytic CVD straight and thin fibers. Magnetoresistance measurements were also made at 4.2 K temperature in fields up to 15 Tesla. The results are compared with other carbon and graphite fibers with different degrees of graphitization.

II. EXPERIMENTAL DETAILS

Single ex−PAN carbon fibers were fixed with a colloidal graphite adhesive (LADD colloidal graphite) to a graphite (nuclear grade) substrate. The fibers were heat treated in a resistance furnace in a steady stream of hydrogen gas (99.999%) to 1100°C at a heating rate of 1°C sec^{-1}. At 1100°C a known quantity of acetylene gas (99.7%) was allowed to flow into the system, mixing with the hydrogen to form the gaseous reaction mixture. The flow rates of hydrogen and acetylene were controlled by individually calibrated Cole--Palmer flowmeters. The temperature of the furnace was controlled by a Leeds Northrup temperature controller. The CVD was carried out at atmospheric pressure (~632 torr in Colorado) and for periods of time ranging from 60−180 minutes.

Scanning Electron Microscopic (SEM) observations were carried out using a Philips series 505 SEM system, typically operating at an acceleration voltage of 20 eV. The thickened fibers were gold coated (plasma

deposited) prior to SEM analysis.

Straight carbon fibers with dimensions of few microns and submicrons have been grown using CCVD method involving the decomposition of acetylene over iron catalyst on Highly Oriented Pyrolytic Graphite (HOPG) substrate. Iron was deposited on HOPG substrates by two methods: electroplating using $FeCl_2$, HCl, and KCl, and by dipping the graphite substrate into supersaturated solution of $FeCl_2-H_2O$. Straight micron and submicron filaments were successfully grown at a deposition temperature of 1000°C. The success of this technique has been limited because of the difficulties with: types of substrates whether graphite or quartz or silicon wafer, types of catalyst employed such as Ni or Fe. Details of the CCVD growth parameters will be reported separately.

Four-point resistivity method was employed. Electrical contacts to the fibers were made using silver epoxy and 18 μm gold wires. The fibers were laid on four gold wires. Our techniques of laying down electrical contacts to microstructures with 100 μm dimensions allowed us to lay down four leads to a submicron fiber with a total length of about 300 μm. The diameter of the fibers were obtained from SEM cross-section while the distance between the potential contacts were measured with a traveling microscope. Considerable care had to be taken to avoid unwanted stress in the thin fibers. Fiber with electrical leads were assembled on a thin microscope slide suitable for loading into a cryogenic dewar. Currents were kept small to avoid unnecessary heating. Resistivity measurements were made in a close-cycle He refrigerator capable of scanning between 10 and 300K. Magnetoresistance measurements were made at 4.2 K temperature and fields up to 15 Tesla. These field dependent resistance measurements were carried out at the National Magnetic Laboratories at MIT.

III. RESULTS AND DISCUSSION

1. Thickened Fiber

According to Koyama et al. [18] the optimum partial pressure of the hydrocarbon (benzene) for the development of CCVD filaments is 180 torr. Therefore the partial pressure of acetylene in the first two runs was set at approximately 180 torr (see Table 1 for exact partial pressures). At this partial pressure the pyrolyzing atmosphere became supersaturated with carbon macromolecular species which nucleated to form soot so that the ex-PAN carbon fibers in Runs 1 and 2 were coated with colloidal soot and vitreous pyrolytic carbon (Fig. 1).

In the next series of runs (3, 4, and 5) the partial pressure of the acetylene was reduced approximately by half to avoid the supersaturation of carbon macromolecular species in the pyrolyzing atmosphere. This reduction in the partial pressure of acetylene eliminated the production of soot and enhanced the deposition of pyrolytic carbon (Figs. 2, 3, and 4). The reaction conditions in Runs 3-5 were kept constant except for the reaction time which ranged from 60 minutes in Run 3 to 180 minutes in Run 5. In all of the runs the CVD process was dominated by the production and deposition of pyrolytic carbon.

From detailed SEM observations of the thickened fibers from Runs 3, 4, and 5 it appears that there is nonuniform deposition of pyrolytic carbon along the length of the fibers. The nonuniform deposition is due to a concentration of gradient of pyrolysis products in the reaction chamber, the pyrolysis products being more

concentrated at the gas inlet portion of the reaction chamber. By increasing the overall gas flow, this concentration gradient can be considerably reduced and hence the CVD, along the length of the ex−PAN carbon fibers, more uniform. Therefore, in the next series of runs (6, 7, and 8) the overall gas flow was increased. All other reaction conditions were approximately the same as those in Runs 3, 4, and 5. The increased gas flow did reduce the nonuniform thickening along the length of the fibers. It also increased the rate of thickening substantially (Table 1).

The surface texture of the thickened fiber can be altered by increasing the partial pressure of hydrocarbon or by increasing the total flow rate of gas. At lower partial pressures of hydrocarbon or low flow rates, the CVD carbon surface is smooth and essentially featureless. As the partial pressure of hydrocarbon or the total flow rate of gas is increased the CVD carbon surface becomes roughened and the surface of the thickened ex−PAN carbon fiber takes on a granular appearance (see Figs. 5 and 6). This is potentially a very useful feature if the thickened ex−PAN carbon fibers were to be used in composites. The surface irregularity increases the surface area available for wetting, thereby enhancing the mechanical bonding between the fiber and the matrix material.

As the structural order of carbon materials improves, so does the oxidation resistance [17]. This is simply due to the reduced number of exposed prismatic edges and other active sites (e.g., structural imperfections in the graphite lattice) present in the more ordered carbon materials. The prismatic edges are orders of magnitude more reactive to oxygen than the basal planes. Therefore if the pyrolytic carbon coating surrounding the ex−PAN carbon fiber is more ordered than the outer layers of carbon in the ex−PAN carbon fiber, there will be a consequent improvement in oxidation resistance. Another reason for an improvement in the oxidation resistance of thickened ex−PAN carbon fibers is that the pyrolytic carbon does not contain the trace transition element impurities inherent in ex−PAN (and pitch) carbon fibers. It is well known that trace transition element impurities act as catalysts in the oxidation of carbonaceous materials [18,19]. Since the pyrolytic carbon can be produced with virtually no trace elements present, it acts as a protective shield against catalytic oxidation. It must be stressed, however, that pyrolytic carbon coating is not a solution to high temperature (>2000°C) oxidation resistance. Other coatings such as SiC and BN have been developed for such purposes.

2. CCVD of Thin Carbon Films

A program was established for CCVD of filaments from acetylene or benzene with Fe and Ni catalysts. Details are given separately.

3. Resistivity of Thickened ex−PAN and Ni CCVD Fibers

The temperature dependent resistivity of pristine ex−PAN fiber and the thickened ex−PAN fibers are shown in Fig. 7. for all the fibers, resistivity shows a small drop with increasing temperature, consistent with non−graphitic carbon. Figure 8a shows the temperature dependence of resistivity for various carbons such as the single crystal graphite and glassy carbon. The results of our measurements on the thickened CVD fibers shown again in Fig. 8b are similar to the pyrolytic carbon and petroleum coke carbon with typical resistivity of

$\sim 10^{-3}$ Ωcm. It is difficult to obtain a clear dependence of resistivity on the fiber diameter on these thickened fibers. There is a small trend in decreasing resistivity with increasing fiber diameter, however, on a realistic scale, such as the one used in Fig. 8b there is relatively no correlation between the resistivity and the fiber diameter for our thickened fibers. Thickened ex−PAN fibers were obtained with different H_2 to C_2H_2 gas flow rates, pressure, and growth time. The temperature dependent resistivity of the fibers do not indicate any correlation or show any graphitization.

In carbon fibers, heat treatment temperature is important in controlling the graphitic character of the fiber. Specifically, fibers grown at lower temperatures are more amorphous than highly oriented fibers treated at much higher temperatures. It seems plausible that by using a known core, like the ex−PAN fibers, and depositing pyrolytic carbon on it that a well ordered structure would result when using a lower growth/treatment temperature. Our temperature dependence of resistivity in thickened ex−PAN fibers do not indicate .. y substantial increase in ordering.

Typical temperature (10−300 K) dependent resistivity for two CCVD straight−thin samples are shown in Fig. 9. Most of these fibers were 5 lm in diameter. The CCVD fibers were intentionally grown with these small diameters and relatively straight for the purposes of obscuration application.

Our resistivity values of $\sim 10^{-3}$ Ωcm contradicts the above discussion which suggested that graphite fiber with lower resistivity would be possible for small diameter fibers. Also the spectra in Fig. 9 show relatively insensitive temperature dependence of resistivity with 10^{-3} Ωcm, compared to 10^{-5} Ωcm for the graphitic fibers shown in Fig. 8a. All the fibers differ by growth parameters. The fibers were derived from iron catalyst on highly oriented pyrolytic graphite substrates, with some fibers derived by decomposition of acetylene, instead of benzene. It is surprising, perhaps, that the temperature dependence of the CCVD thin fibers are similar to the CVD thickened ex−PAN fibers since iron catalyst was used in growing the CCVD fibers. The growth plays a dominant role in determining the fiber resistivity behavior with temperature.

The diameter dependent room temperature resistivity of all the fibers of interest here are shown at the top of Fig. 10. Familiar decrease in resistivity with diameter is observed in the thickened ex−PAN fibers. Data for the CCVD fibers are also shown. For comparison results of vapor grown brominated samples show a similar behavior, but a lower magnitude of resistivity. Since the temperature dependence of the thickened ex−PAN and thin CCVD fibers are similar, different electronic scattering mechanisms between the fibers are unlikely. The size dependent resistivity is due to the crystallite boundary scattering.

4. Magnetoresistance

Measurements at 4.2 K and for fields up to 15 Tesla showed negative magnetoresistance in the thickened ex−PAN and CCVD thin−straight carbon fibers. Previous magnetoresistance were reported for up to 5 T only. Figure 11 shows the magnetoresistivity spectra for all the ex−PAN thickened CVD fibers and Ni−CCVD on HOPG fibers. The spectra are labelled with the sample numbers. Comparing the thickened fiber, the magnitude of the

magnetoresistivity is smaller than the pristine ex−PAN fiber. The thickened fiber show lower magnetoresistivity than the pristine ex−PAN fiber, with the exception of Sample 7. The high magnetoresistivity of Sample 7 is attributed as an anomalous result. The general result of reduced signal for the thickened fibers compared with the pristine ex−PAN fiber resembles a trend shown in Fig. 12. This trend shows that in carbon fibers the negative magnetoresistivity becomes a positive one for fibers exposed to higher heat treatment temperatures. One can, perhaps, also deduce from Fig. 11 with reduced magnetoresistivity with respect to ex−PAN fibers, that the thickened fiber behave as though they become more ordered though well short of being graphitic since their resistivities are relatively higher, Fig. 8. However, because of the relatively higher resistivities and their temperature insensitivity, the carbon fibers are more likely amorphous than graphitic.

The results of magnetoresistivity measurements on the CCVD grown straight−thin carbon fibers from catalyzed highly oriented pyrolytic graphite substrate are also included in Fig. 11. These spectra are very similar to those obtained for the thickened ex−PAN fibers. Although Sample D8 shows a large negative magnetoresistivity, the signal from the two remaining samples show small magnetoresistivity at 15 Tesla.

These samples show negative magnetoresistivity even up to 15 Tesla. Bright's [12] theory of increased density of states and carrier concentration with field can explain the results for low fields. In Bright's explanation of negative magnetoresistivity, a saturation of signal occurs at about 1.4 Tesla. The inclusion of ionized impurity scattering [13] improves the quantitative description of the negative magnetoresistivity in carbon/graphite fibers at higher fields (>1 Tesla). Our results show no saturation up to the highest field of 15 Tesla.

IV. CONCLUSION

Ex−PAN carbon fibers can be uniformly thickened by CVD from a gaseous reaction mixture of hydrogen/acetylene. The rate of thickening can be enhanced by increasing the partial pressure of the acetylene and the flow rate of the gaseous reaction mixture. Growth parameters for optimum thickening of ex−PAN fibers were emphasized. Ni−CCVD carbon fibers on HOPG have been grown with less than 5 μm diameter. SEM micrographs of the thickened ex−PAN fibers show annular or tree ring morphology similar to CCVD grown fibers. Electrical resistivity of these fibers are relatively insensitive to temperature (10−300 K). Their magnitudes are higher than those of well graphitized fibers. The familiar decrease in resistivity with diameter was observed for the thickened ex−PAN fibers. Magnetoresistance measurements at 4.2 K and magnetic fields as high as 15 Tesla corroborated the resistivity data, that no graphitic character existed in these thickened nor the Ni−CCVD fibers grown on HOPG. Although these electrical and magnetic properties shown enhanced properties of the thickened CVD ex−PAN fibers. It is anticipated that the mechanical properties of the thickened fibers will be superior to the PAN fibers because of the annular macrostructure of the vapor thickened fiber.

V. POSSIBLE APPLICATION OF THICKENED ex-PAN CARBON FIBERS

(1) As a reinforcement material in composites, and

(2) as a host for intercalation.

Assuming that the cost of producing pyrolytic carbon pound for pound is less than ex−PAN carbon fibers (since pyrolytic carbon can be produced from virtually any gaseous hydrocarbon including industrial waste), the logical step would be to reduce the amount of ex−PAN carbon fiber used in the composites and replace it with pyrolytic carbon.

In any carbon fiber composite there is a particular volume fraction of fibers with respect to matrix material that gives the composite the optimum mechanical strength. The fibers dissipate the energy when a carbon fiber composite is placed under stress. It is therefore important that when using thickened fibers one must still incorporate a certain amount of fibers so that the stress that each fiber experiences is not so great as to cause failure. If the number of fibers in a composite were to be considerably reduced by using the same volume of reinforcement material (thickened fibers) but a reduced number of fibers, a reduction in the mechanical properties of the composite is likely. Hence, the need to find the minimum number of fibers needed in a particular composite to avoid any significant reduction in mechanical properties.

High modulus pitch carbon fibers are often used for intercalation due to their high degree of structural order. They are, however, not as widely used as ex−PAN carbon fibers because of their reduced mechanical properties as compared to ex−PAN carbon fibers. If, as in this case, the ex−PAN carbon fiber was coated with a highly ordered carbon deposit, one would have a "composite fiber" with the advantageous properties of both ex−PAN and pitch carbon fibers; the strength of the ex−PAN carbon fiber and the structural order of pitch carbon fibers. Consequently, the thickened ex−PAN carbon fibers would be suitable for intercalation. There are many useful properties of an intercalated thickened ex−PAN carbon fiber as a conductor as opposed to conventional conductors such as copper in that, it is a fiber and as such can be wound, weaved, or easily incorporated into a thermoplastic matrix. The thickened fiber has most of the desirable properties of other carbon fibers, chemically inert, low weight, heat resistant. Although the heat resistance of intercalated carbon fibers will be much less than that of pristine carbon fibers.

There is still, however, a great deal of work to be carried out on the thickened ex−PAN carbon fibers before any firm conclusions can be drawn about the potential applications mentioned above.

REFERENCES

1. M. S. Dresselhaus, G. Dresselhaus, K. Sugihara, I. L. Spain, and H. Goldberg, "Carbon fibres and filaments," Springer Verlag, Berlin (1988).
2. K. Matsumura, A. Takahashi, and J. Tsukamoto, Synthetic Metals 11, 9 (1985).
3. J. Shioya, H. Matsubara, and S. Murakami, Synthetic Metals 14, 113 (1986).
4. K. Bokros, in Chemistry and Physics of Carbon 5.

5. T. Koyama and M. Endo, Jap. J. Appl. Phys. 13, 1175 (1974).
6. M. Endo and T. Koyama, Katai Butrui (Japan) 12, 1 (1977) (in Japanese).
7. A. Oberlin, M. Endo, and T. Koyama, J. Cryst. Growth 32, 335 (1976).
8. J. D. H. Hughes, J. Phys. D: Appl. Phys. 20, 276 (1987).
9. G. Dorey, J. Phys. D: Appl. Phys. xx, 245 (1987).
10. J.-P. Issi, B. Nysten, and L. Piraux, J. Phys. D: Appl. Phys. xx, 257 (1987).
11. M. Z. Tahar, M. S. Dresselhaus, and M. Endo, Carbon 24, 67 (1986).
12. A. A. Bright, Phys. Rev. B20, 5142 (1979).
13. I. Rahim, K. Sugihara, M. S. Dresselhaus, and J. Hermemau, Carbon 24, 663 (1986).
14. M. Endo, Y. Hishiyama, and T. Koyama, J. Phys. D: Appl. Phys. 15, 353 (1982).
15. A. A. Bright and L. S. Singer, Carbon 17, 55 (1977).
16. T. Koyama, M. Endo, and Y. Onuma, Jap. J. Appl. Phys. 11, 445 (1972).
17. D. W. McKee and V. J. Mimeault, in: Chemistry and Physics of Carbon 8 (1973).
18. D. W. McKee, Carbon 8, 131 (1970a).
19. D. W. McKee, Carbon 8, 623 (1970b).

Table 1. CVD thickening of ex-PAN carbon fibers.

	Runs							
	1	2	3	4	5	6	7	8
Gases Used	H_2 C_2H_2	H_2 C_2H_2	H_2 C_2H_2	H_2 C_2H_2	H_2 C_2H_2	H_2 C_2H_2	H_2 C_2H_2	H_2 C_2H_2
% Gas Mixture								
H_2	71	71	89.8	89.8	89.8	89.4	89.4	89.4
C_2H_2	29	10.2	10.2	10.2	10.2	10.6	10.6	10.6
Partial Pressure (torr)								
H_2	451.6	450.8	566.6	563.9	569.3	570.4	569.5	564.0
C_2H_2	184.4	184.2	64.4	64.1	64.7	67.6	67.5	67
Gas Flow cm^3 min^{-1}								
H_2	120	120	120	120	120	228	228	228
C_2H_2	49	49	49	13.6	13.6	27	27	27
Pressure (torr)*	636	635	631	628	634	638	637	637
HTT (°C)	1100	1100	1100	1100	1100	1100	1100	1100
Run Time (min)	60	120	60	120	180	60	120	180
Type of Carbon Deposited	soot P.C. ***	soot P.C.	P.C.	P.C.	P.C.	P.C.	P.C.	P.C.
Amount of Thickening (μm)**	n/a	n/a	1	4.0	4.8	15	22	---

*Atmospheric pressure (~632 torr in Colorado).

**Determined from detailed SEM observations.

*** P.C. = Pyrolytic Carbons.

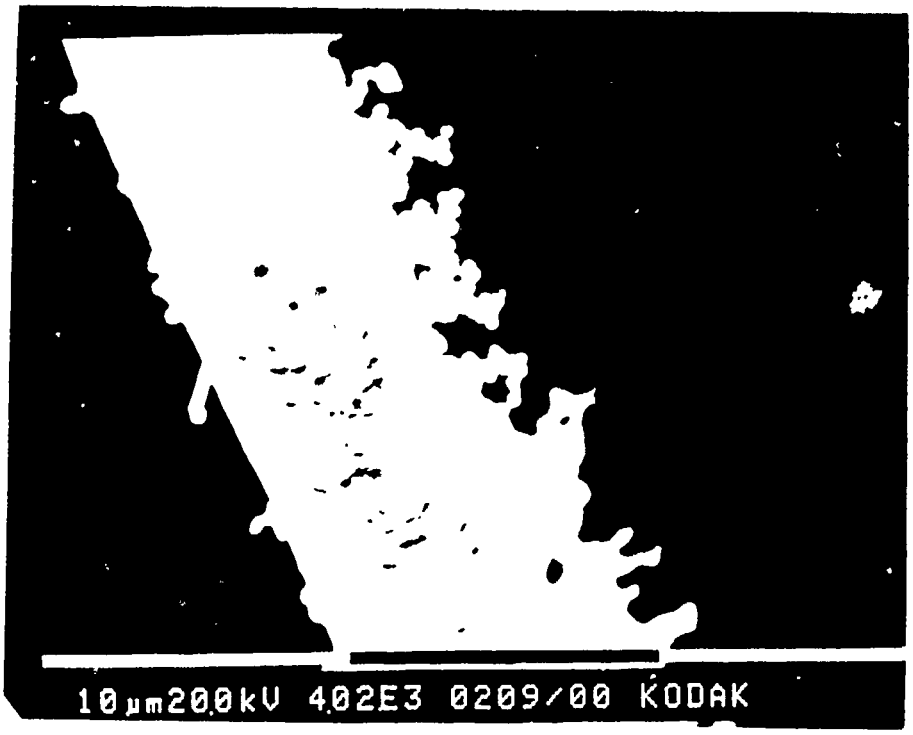

Figure 1.

Shows an ex-PAN carbon fibre coated with colloidal soot. There is also a thin veneer of pyrolytic carbon surrounding the fibre.

Figure 2.

Shows two ex-PAN carbon fibres thickened by a vitreous pyrolytic carbon deposit.

Figure 3.

Shows a single ex-PAN carbon fibre thickened by concentric rings of pyrolytic carbon. Note the 'droplets' on the surface of the pyrolytic carbon. These droplets appear to represent the intermediate stage between direct deposition of pyrolytic carbon and the formation of soot.

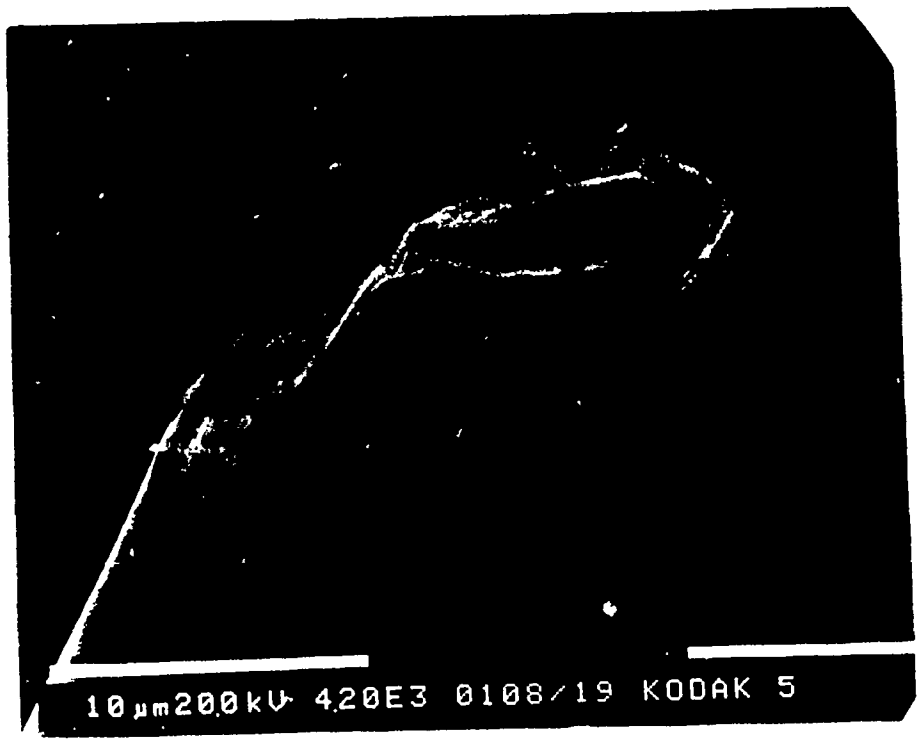

Figure 4.

The concentric rings of pyrolytic carbons surrounding the ex-PAN carbon fibre are obvious in this photomicrograph.

Figure 5.

Thickened ex-PAN carbon fibre from Run 5. (See Table 1 for reaction conditions). The surface of the pyrolytic carbon deposit is smooth and essentially featureless.

Figure 6.

Thickened ex-PAN carbon fibre from Run 6 (see Table 1 for reaction conditions). The surface of the pyrolytic carbon deposit is roughened.

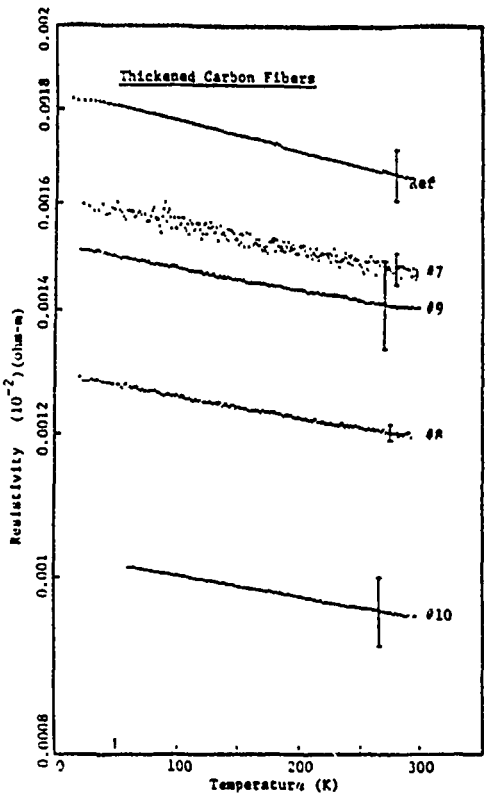

Fig. 7 dρ/dT of thickened ex-PAN fibers.

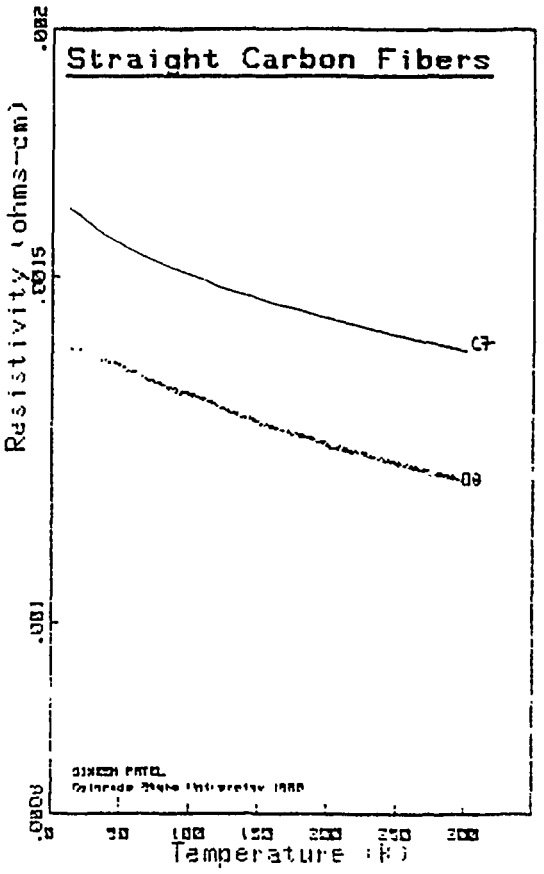

Fig. 9 dρ/dT of Fe-CCVD fibers.

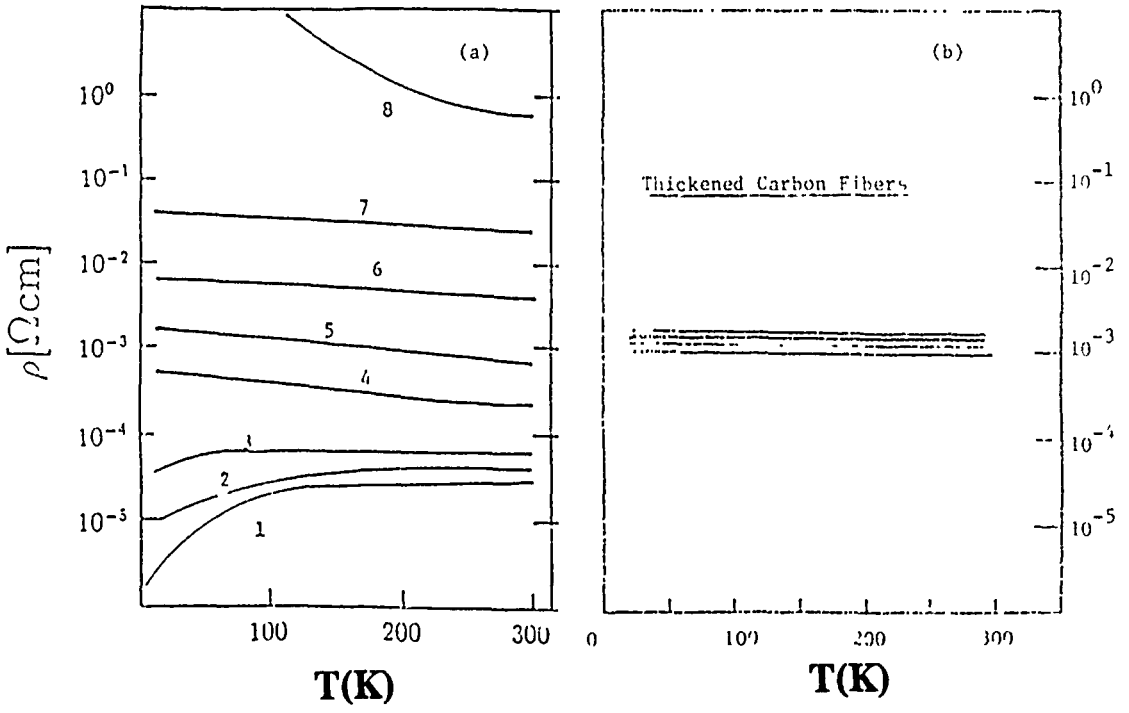

Fig. 8 (a) Resistivities of various carbon and boronated carbon-vs-temperature: 1)single crystal graphite, 2) HOPG, 3) graphite whisker, 4)pyrolytic carbon, 5)petroleum coke carbon, 6)lampblack base carbon, 7)glassy carbon, 8)carbon film-electron beam evaporated. b) resistivities of thickened carbon fibers.

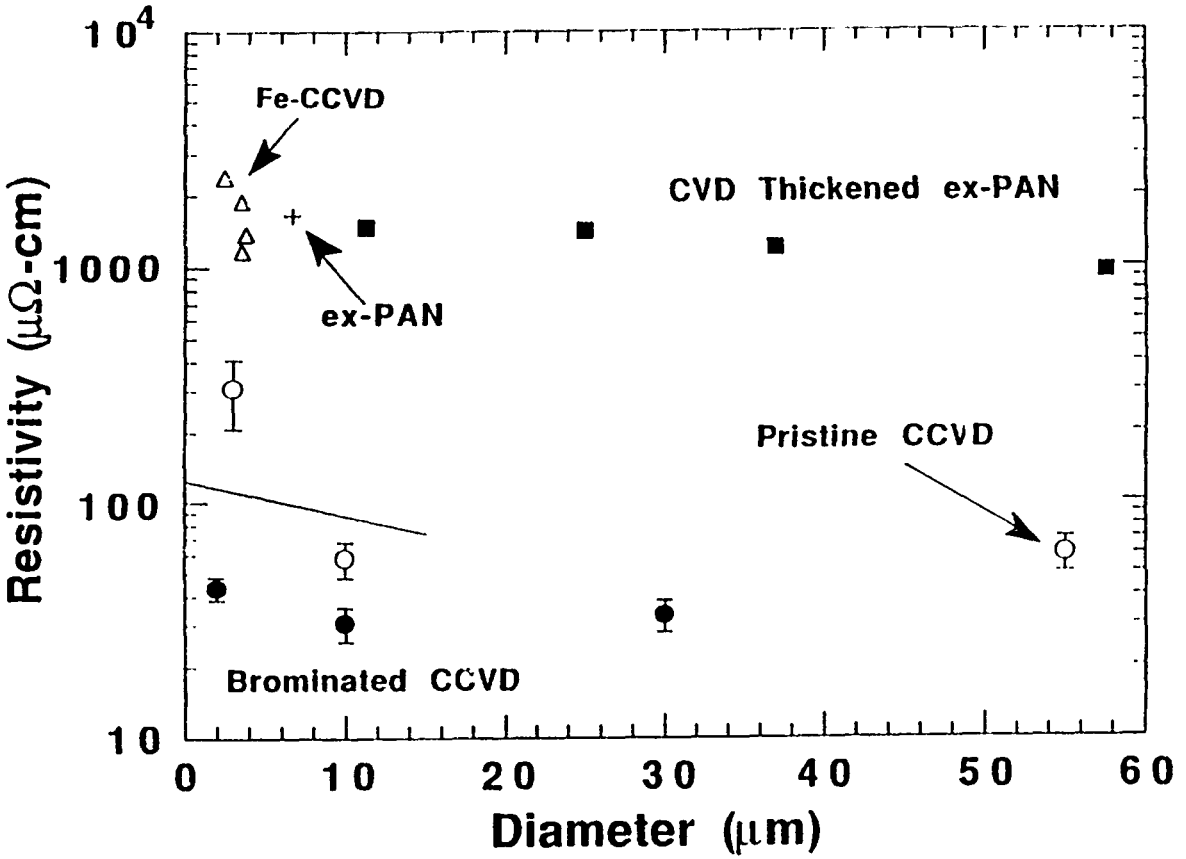

Fig. 10 Diameter dependent resistivity at 300K of; ■ CVD thickened ex-PAN fibers, + Celion 3000 ex-PAN, △ Fe-CCVD, ○ pristine CCVD and ● Brominated CCVD carbon fibers. The solid line represents results of Tahar et al 1986.

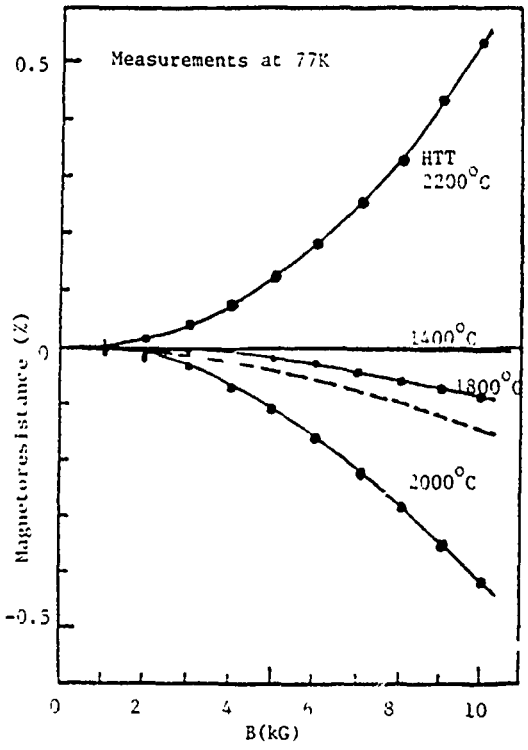

Fig. 12 Transverse magnetoresistance of vapor grown carbon fibers heat treated between 1400°C and 2200°C, plotted as a function of magnetic field. Measurements were carried out at 77K. The dotted curve is for PAN-based fibers heat treated at 2800°C[Endo et al. 1982].

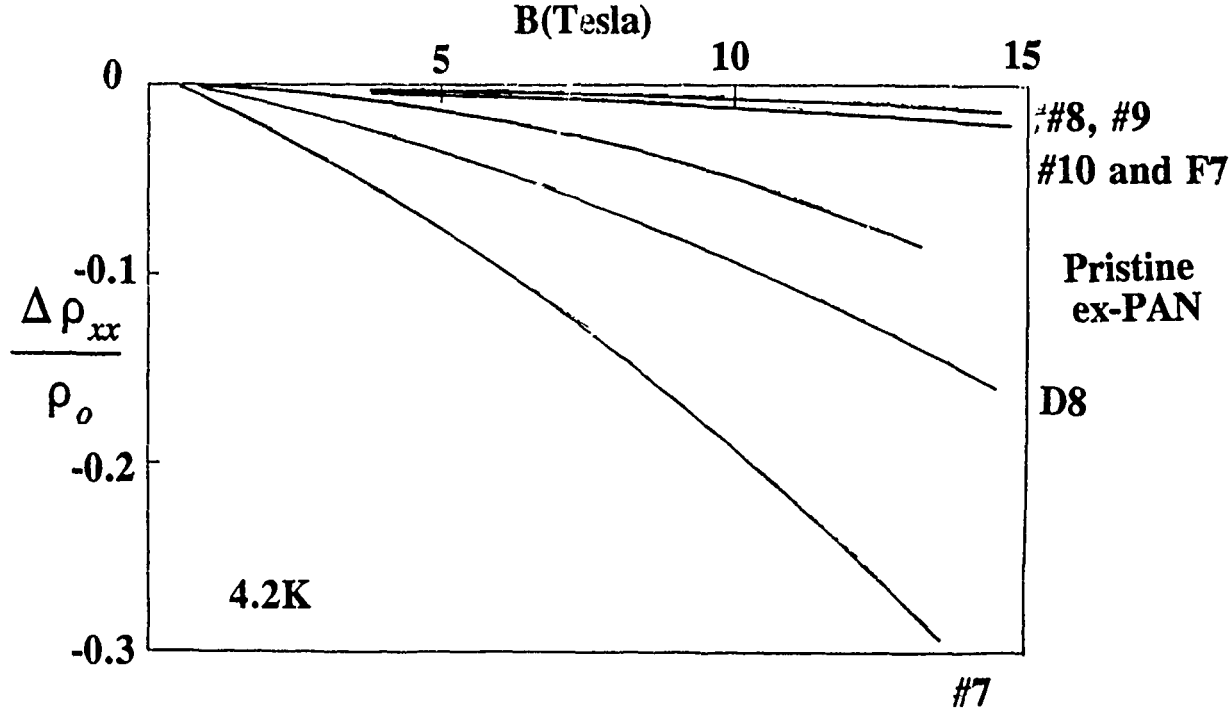

Fig. 11 Megneto-resistance (4.2K) up to 15 Tesla of thickened ex-PAN and Fe-CCVD fibers.

4. CCVD OF THIN FIBERS

1. CCVD of carbon filaments from acetylene as catalyzed by Iron and Nickel
2. Growth and structure of vapor-deposited filaments on graphite and silicon substrates
3. Growth of carbon filaments from Ferrocene based Iron catalyzed decomposition of Benzene
4. Effects of catalyst, additives, and substrate on the iron catalyzed decomposition of benzene
5. Effects of partial pressures and growth times on catalytic chemical vapor deposited (CCVD) benzene derived carbon filaments
6. Electron microscope studies of carbon filaments
7. Carbon Fiber Project report: Summary of work by D. Udpa

CHEMICAL VAPOR DEPOSITION OF CARBON FILAMENTS FROM ACETYLENE AS CATALYZED BY IRON AND NICKEL

Christina C. Schmitt and Carol M. McConica
Department of Chemical Engineering
Colorado State University
Fort Collins, Colorado 80523

ABSTRACT

Carbon filaments have been grown by catalytic chemical vapor deposition (CCVD) on both iron and nickel catalysts in a high vacuum differential reactor. Nickel catalysts were prepared by evaporation and electrochemical deposition onto highly oriented pyrolytic graphite (HOPG) substrates. Iron catalysts were prepared by electroplating and immersing HOPG substrates into iron chloride solutions. For the temperature range 873-1273 K, acetylene decomposition on nickel produced non-uniform twisted submicron filaments. Straight submicron diameter filaments with aspect ratios in excess of 1000 result from the decomposition of acetylene over iron. Filament diameters are dependent upon the iron chloride solution concentration, deposition time and the partial pressure of acetylene.

INTRODUCTION

Carbon filaments are a unique form of carbon deposited on many types of surfaces during certain high temperature reactions. The first initiatives for research on CCVD carbon filaments were guided towards the prevention of their formation. In various applications, catalyst deactivation, decreases in heat transfer efficiencies and corrosion can all be attributed to carbon deposition on metals. Eventually, studies migrated towards the potential uses of the filaments, most obviously as a highly attractive replacement for carbon fibers prepared from organic precursors. These play a key role in the development of stronger, lighter, and more heat-resistant materials. Perhaps the biggest limitation on organic fibers is that they do not have an appreciable amount of crystallite orientation, deeming them unsuitable for meeting today's standards for many physical and optical properties in materials. Filaments grown by CCVD however, have been found to posses excellent structural and optical characteristics, and can be easily modified by chemical means to suit them to specific applications.[1]

The specific goal of this carbon filament research was to produce straight filaments with submicron diameters and high aspect ratios. Filaments of these dimensions are desired for their optical properties, more specifically, to examine theoretical models on obscuration. Straight filaments are not requisite for optical applications, but they are necessary for meaningful interpretation of obscuration measurements, such as scattering and absorption cross-sections, which can be compared to theories based on straight filaments of the same size order.

The method chosen for growing carbon filaments involves a gas-solid reaction. A hydrocarbon is decomposed over a metal catalyst at high temperatures. Hydrogen is used to aid the reaction as a diluent and to prevent the accumulation of amorphous carbon deposits by inhibiting the dehydrogenation reactions. Many elements in these reactions are unknown and there is much controversy as to the mechanisms involved in filament growth. It is not in the scope of this research to determine mechanisms, but instead to prepare a method by which carbon filaments of the desired dimensions can be produced. Details of proposed mechanisms for a variety of filament types are discussed in the literature. [1,2,3]

APPARATUS

A differential high vacuum system has been constructed to allow the growth and in-situ characterization of CCVD carbon filaments in a clean environment (Fig. 1). The pumping station is a turbo-molecular pumping unit, having a nitrogen volume flow rate capacity of 170 l/s, and an operating pressure range from 5×10^{-8} torr to 760 torr. All plumbing in the system prior to the heated zone of the reactor is Pyrex. The 2.6 cm diameter reactor is quartz and is attached to the system by socket joints. A Varian 524-2 cold cathode ionization gauge was used to determine the system pressure during the sample evacuation. The system could be evacuated to the pressure regulators on the gas cylinders.

Gas flow rates are controlled by MKS type 1259B flow controllers. The hydrogen and helium flows range from 0-200 sccm and the hydrocarbon flow controllers have ranges of 0-20 and 0-200 sccm. Accuracy is 0.5% of full scale. An Omega CN-2010 programmable temperature controller and SSR 240 A45 solid state relay are used to power and control the resistance oven. The PID control loop gives and overshoot of less than 10^{o} C at 1000^{o} C and controls within 1^{o} C after 5 minutes of stabilization.

All gases used in CCVD filament growth experiments are of high purity: hydrogen (99.9998%), helium (99.998%), argon (99.999%), and acetylene (grade 2.6). Breathing quality air was used for baking out the system after the completion of a run.

EXPERIMENTAL PROCEDURES

Substrates were cleaned with organic solvents, rinsed in deionized water and baked in a convection oven at 333 K. The source for the evaporated nickel catalysts was 99.999% pure nickel powder. Nickel was electroplated from a Watts nickel solution comprised of $NiSO_4$, $NiCl_2$ and boric acid at a local printed circuit board manufacturing company. Iron was deposited on HOPG substrates by two methods: electroplating using $FeCl_2$, HCl and KCl, and by dipping the graphite into supersaturated solutions of $FeCl_2*H_2O$. For the electroplated samples, the time of plating was varied, and for the dipped substrates both solution concentration and time of dipping were varied. After they were seeded with catalyst, the substrates were stored in a dessicator until the time of the deposition.

The reactor system was closed off to the atmosphere and evacuated continuously when no depositions were taking place. The reactor, with substrates inside, was attached to the rest of the system prior to a run and was then also evacuated. All lines, from the source gases to be used, were evacuated at room temperature and then filled with their respective gases up to the mass flow controllers. The evacuated system was then shut off from the pump station. The system was filled with inert gas until the capacitance manometer read above atmospheric pressure (630-640 torr), and then an exit line was opened, bringing the pressure back down to atmospheric pressure. At this time the temperature programming began. Pressure and temperature were monitored closely. When the reactor was up to the run temperature, hydrogen replaced the inert for a reduction period. Directly following the reduction period there was either the actual run (hydrogen and hydrocarbon) or a hydrocarbon saturation period (inert and hydrocarbon) followed by the CCVD run. In either case the total flow was kept constant by adjusting the hydrogen or inert flow rate. All runs were at constant temperature throughout the duration of the deposition. When the deposition was complete, the oven input was turned to zero, and the reactor cooled by natural convection. Only inert flowed through the system during cooling. The inert was left flowing until the reactor and substrate were below 600K. When the inert flow was shut off, air could enter the system, so the substrate was cooled enough to assure that there would be no oxidation of the filaments.

When runs were complete, substrates were removed and placed in a dessicator until ready for analysis. The reactor was baked at 1123 K in air flowing at 100 sccm to burn off carbon deposited on the walls. The reactors were periodically cleaned in aqua regia to remove metal deposits which may cause extraneous reactions.

A scanning electron microscope (SEM) was used to observe the substrates for filament growth. Substrates were glued onto SEM stubs with graphitic paint and baked in a vacuum oven. The following conditions were found to work the best for the carbon filament samples in the Philips 505 SEM: Accelerating Voltage (A.V.) at 25-30 keV, filament current at 30 μA, bias voltage at 150 eV, and a spot size of 20 nm. For Energy Dispersive X-ray analysis (EDAX), a lower A.V. and larger spot size were used: approximately 20 keV and 50 nm respectively. EDAX was done to check for impurities on the substrate which may be a source of filament growth. Larger A.V.'s were used to penetrate the carbon o the sample surface to identify impurities and catalysts. Lower values were used to identify the filaments as being carbon.

EXPERIMENTAL RESULTS

Twelve runs were made using a variety of nickel catalysts. See Table 1 for a description of substrates, run conditions, and results. Using nickel catalysts it was possible to grow filaments with diameters as small as 20 nm, about twice the lowest possible limit of carbon filaments which 9 nm.[4] Filament diameters were not uniform on each substrate, and filaments were usually indistinguishable from each other because they were very tangled. Some SEM micrographs are shown in Figures 2-5 as examples of these filaments.

Substrates prepared by evaporation of nickel powder produced more consistent results. A matrix of experiments was run around a variety of conditions using this type of substrate. The matrix was determined by the method of Self-Directing Optimization[5] in order to isolate the ideal conditions for growing straight, submicron filaments. Table 2 shows all of these runs. The results of these experiments showed that the best filaments that could be grown on this substrate were grown at the lower temperatures (600°C) and longer run times (30 minut
All other variables seemed to have little or no effect on improving the growth. Higher temperatures were examined in the attempt to produce straighter, more ordered filaments. These runs are listed in Table 3. Very few filaments were

produced at the higher temperatures. It was concluded that it is not possible to grow the desired filaments using nickel catalysts.

Iron was deposited on HOPG substrates to examine the possibility of growing straight, submicron filaments using this catalyst. Filaments of the desired dimensions were grown, and the results were repeated a number of times (Table 4). Although the substrates used in each run were not identical, filaments of the same dimensions could be produced by altering the run conditions. SEM micrographs of some of these filaments are shown in Figures 6-9.

Straight submicron filaments with aspect ratios of 1000 were successfully grown under the following conditions: acetylene:hydrogen = 5:1, total flow = 40 sccm, heating rate of 10° C/min, deposition T = 1000° C, reduction time = 10 min, hydrocarbon saturation time = 1 min, and a deposition time of 60 min. This experiment was reproduced several times. The D-Runs were set up in the optimization matrix form similar to the A-Runs with nickel. This matrix directed the optimization to the conditions stated above. While straight filaments were grown, the overall density of filaments was found to be much less than for the nickel catalyzed filament growth.

DISCUSSION

It has not been possible to grow long, straight filaments using substrates seeded with nickel. Iron, on the other hand, which is similarly structured transition metal, and which possesses many of the same catalytic properties, catalyzes the growth of long, straight filaments using identical run conditions.

Experiments with both iron and nickel catalysts were run below the melting temperatures of the metals. The melting point of iron is 1538° C, and for nickel it is 1453° C. At run conditions, both of these pure metals have front centered cubic structures. It is assumed that run temperatures were well enough below the melting points that even if the melting points were lowered due to the small particle sizes, the metals were still in the solid phase. It is difficult to interpret nickel-carbide and iron-carbide phase diagrams correctly because of the many unknowns involved in filament growth. Some of these unknowns are: the actual temperature of the catalyst pellets, property changes due to the small particle size, and carbide concentrations within the metal.

A critical difference between iron and nickel is that acetylene adsorption is dependent upon the plane of nickel on which it chemisorbs. The {100} and {111}

surfaces more readily adsorb acetylene and break the C-C bonds than does the (110) surface. There are none of these surface dependencies with iron.[6] If the catalyst particles are faceted solid clusters then there would be non-uniform growth off of nickel because of the differential reaction rates on each exposed crystal face. Iron would give straight filaments under similar growth conditions due to the facile nature of acetylene decomposition on iron.

Catalyst particles have been observed as fragments along the filament when nickel is used. The direction of growth changes and branches sometimes exist where particles are observed. Both of these phenomena could be due to new nickel faces becoming exposed during the catalyst fragmentation.

In general, the iron/HOPG substrates appear to be less active than the nickel substrates, producing fewer filaments and only small amounts of flocculent on the HOPG regions without filaments. The tangled matted growth observed with nickel could also be due to the amount of carbon being deposited and interference between adjacent filaments. If the catalyst is on the surface and the filament is extruded, then this surface carbiding would quickly render the catalyst inaccessible by reactants and result in short filaments. When isolated filaments were found growing from the nickel surface, they were never straight.

On many of the runs where long, straight filaments grew from iron, much of the growth was observed to originate from areas of the substrate where defects occurred. These defects were parts of the graphite that had peeled back due to cutting of the substrate prior to catalyst seeding. Boundaries may be exposed, giving the iron a different type of surface to deposit on. This type of deposit may be characterized by a unique support/catalyst interaction and thus promote growth in some way. These areas may also be contaminated by handling of the substrates, resulting in a co-catalyst effect.

CONCLUSIONS

Straight filaments with aspect ratios in excess of 1000 have been grown from iron catalysts supported by highly oriented pyrolytic graphite. Filament diameters can be controlled by varying deposition time and the hydrocarbon to hydrogen ratio during deposition. While iron was found to grow straight filaments, the catalyst utilization was small. Either most of the catalyst particles were not active or the iron diffused into the graphite during the heat cycle. Nickel catalysts never

gave straight filaments even though the density of filament growth was very high on nickel. This difference in filament structure is attributed to the structure sensitivity of acetylene decomposition on nickel and it facile nature on iron.

REFERENCES

1 R.T.K. Baker and P.S. Harris, *Chem. and Phys. of Carbon*, 14, 1978, p. 83.

2 P.K. deBokx, A.J.H.M. Kock, E. Boellaard, W. Klop, and J.W. Geus, *J. Catalysis*. 96, 1985, p.454.

3 A. Sacco Jr. and J.C. Caulmare, Coke Formation on Metal Surfaces, Albright and Baker, eds., 1982, p. 177

4 G.G. Tibbetts, *J. Crystal Growth*, 66, 1984, p. 632

5 C.D. Hendrix, *Chemtech*, August 1980, p. 488

6 J.C. Bertolini and J. Massardier, The Chemical Physics of Solid Surfaces and Heterogeneous Catalysis, D.A. King and D.dP. Woodruff eds., Vol. 3, 1984, p.107.

7 J.D. Bracey and R. Burch, *J. Catalysis*. 86, 1984, p. 384.

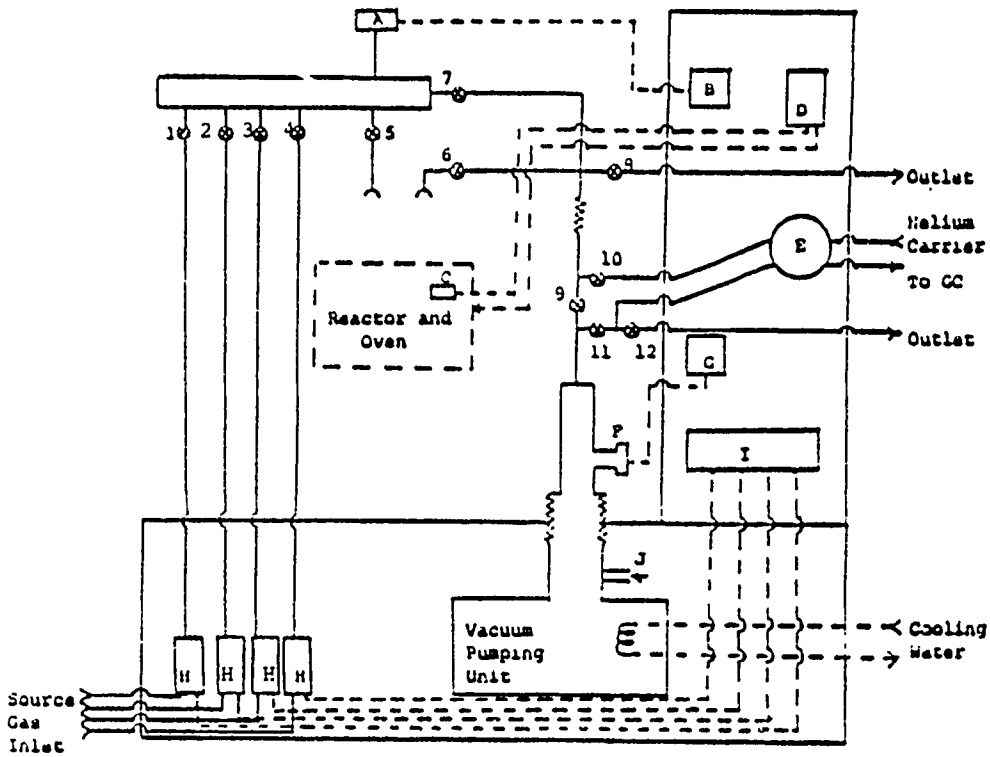

A- Capacitance Manometer
B- Manifold Pressure Readout
C- Thermocouple
D- Temperature Programmer and Controller
E- Six-Way GC Valve
F- Cold-Cathode Ion Gauge
G- Ion Gauge Readout
H- Mass Flow Controllers
I- Flow Controller Readout
J- Emergency Vent Valve

Valves #1-8: High Vacuum Glass Stopcocks
Valves #9-12: Stainless Nupro (SS-4H)

Figure 1 Schematic of High Vacuum CCVD System

Figure 2 Nickel Catalyzed Carbon Filaments (Run CS#2)

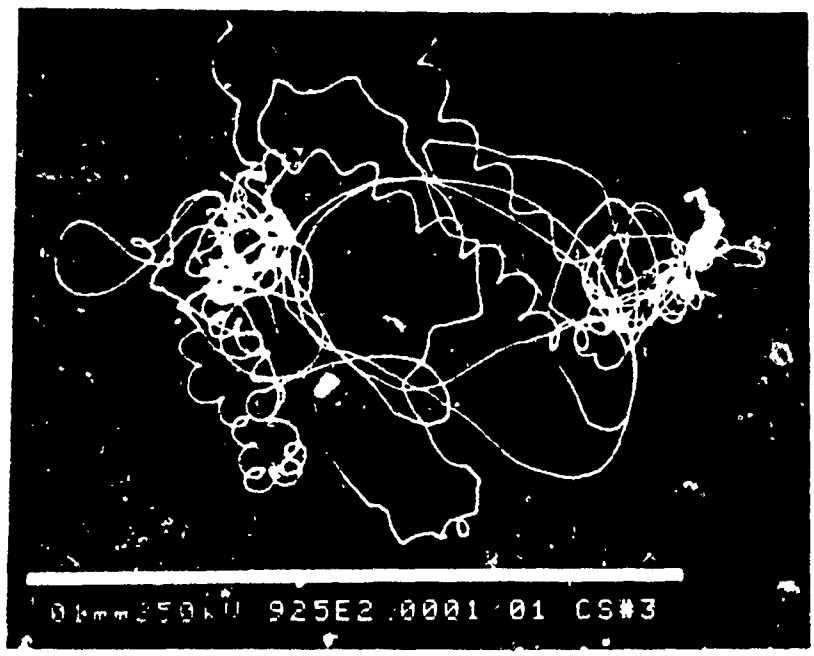

Figure 3 Nickel Catalyzed Carbon Filaments (Run CS#3)

Figure 4 Nickel Catalyzed Carbon Filaments (Run CS#3)

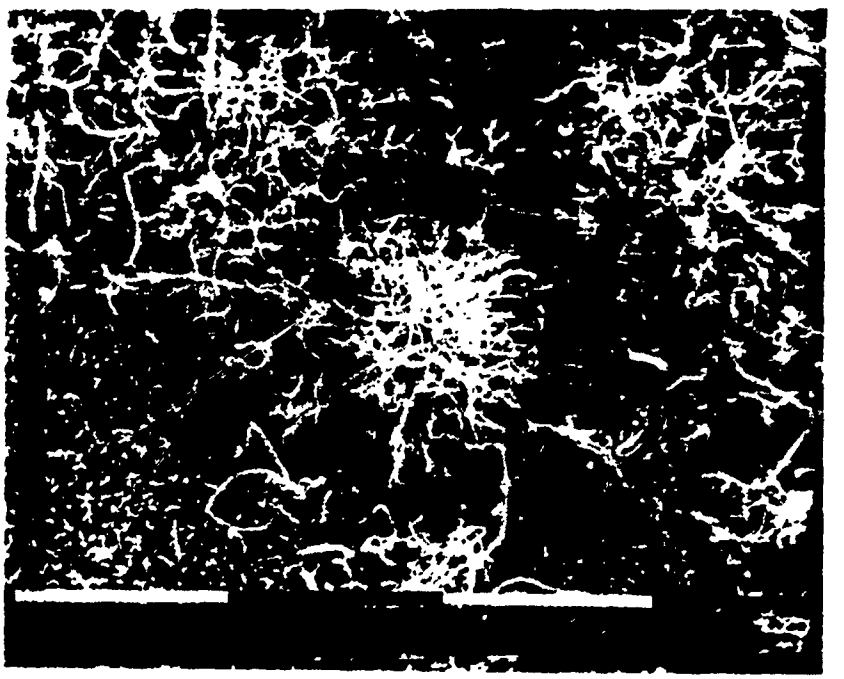

Figure 5 Nickel Catalyzed Carbon Filaments (Run PCB1)

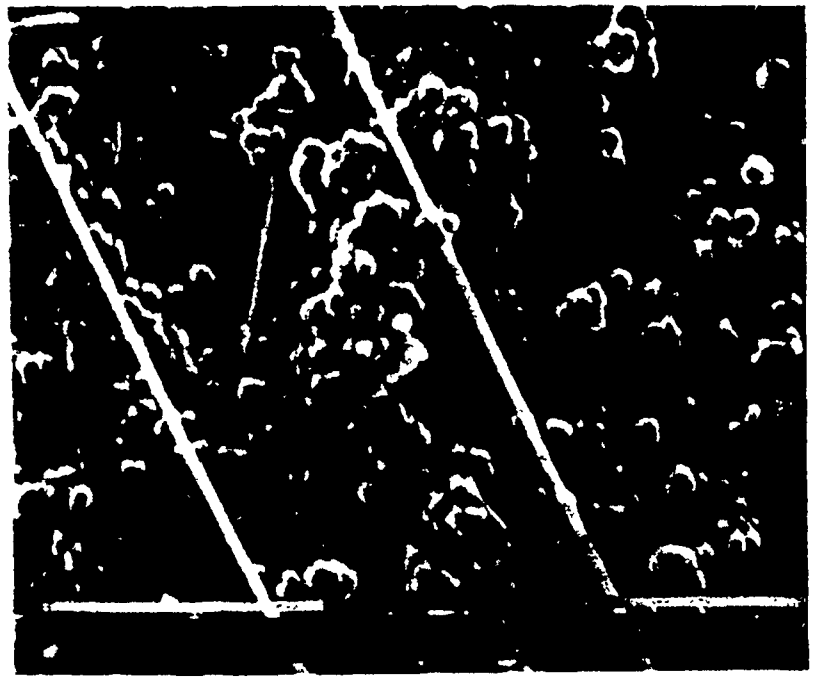

Figure 6 Iron Catalyzed Carbon Filaments (Run C3)

Figure 7 Iron Catalyzed Carbon Filaments (Run C7)

Figure 8 Iron Catalyzed Carbon Filaments (Run C7)

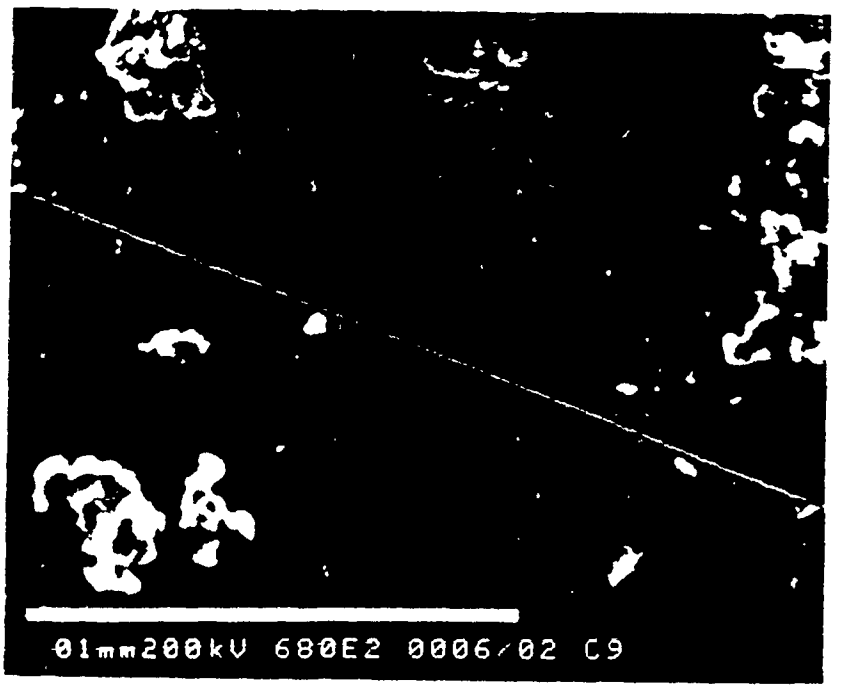

Figure 9 Iron Catalyzed Carbon Filaments (Run C9)

TABLE 1 MISCELLANEOUS NICKEL RUNS

RUN	SUBSTRATE	NI DEP. (Å)	RAMP (°C/min)	RUN T °C)	RUN t (min)	TOT. FLOW (sccm)	H_2:C_2H_2	COOL. GAS	COMMENTS
CS#1	Poco	500	10	700	15	203	50:1	H_2	Twisted, d=.2-.4μm, l<20μm.
CS#2	Poco	500	13.3	850	15	209	20:1	H_2	Smokey, d=.1μm, AR=100.
CS#3	Poco	500	13.3	850	15	198	10:1	H_2	Helix,curls, d=.4-1.0μm.
CS#4	2.73%Ni/Si	---	13.3	850	15	100	10:1	H_2	No filaments found.
PCB1	Poco	Plated	5	600	30	203	50:1	H_2	Octopussy, d=.1-.5μm.
PCB2	Poco	Plated	13.3	750	15	200	10:1	H_2	D=.15-1.0μm, AR<100.
A3LP	Poco	25	15	600	10	53	50:3	H_2	D=.1-1.0μm, Run P=10-100
3I	Poco	25	13.3	850	10	100	10:1	He	Tangled, d=.02-.05μm.
Si-1	Si	500	15	850	10	50	4:1	He	No filaments found.
4I	2.73%Ni/Si	---	13.3	850	15	100	10:1	He	No filaments found.
IX-1	SiO_2	?	20	1000	10	60	5:1	He	No analysis.
IX-2	SiO_2	?	10	1000	30	50	4:1	He	No analysis.

TABLE 2 A-RUNS (NICKEL)

RUN	SUBSTRATE	NI DEP. (Å)	RAMP (°C/min)	RUN T (°C)	RUN t (min)	TOT. FLOW (sccm)	H_2:C_2H_2	COOL. GAS	COMMENTS
A1	Poco	25	5	600	5	204	50:1	H_2	D=.06μm, l=.4μm.
A2	Poco	25	25	1000	2.5	200	1:1	H_2	No filaments found.
A3	Poco	25	25	600	30	53	50:3	H_2	Smokey, d=.05-.4μm,AR=100.
A4	Poco	25	5	1000	10	40	5:1	H_2	D=.4μm, short, few.
A5	Poco	100	5	1000	5	40	40:1	He	No filaments found.
A6	Poco	100	5	600	30	200	3:1	H_2	Tangled.d=.15-1μm, l=10μm.
A7	Poco	100	25	600	5	40	3:1	He	Tangled, d=.15-1μm.
A8	Poco	100	25	1000	30	200	50:1	He	Curly, d=.4μm, l=50μm.
A9	Poco	100	4	360	37	76	61:1	H_2	No filaments found.
A10	Poco	100	20	360	10	20(	57:1	H_2	No filaments found.
A11	Poco	100	4	360	35	147	12:1	H_2	One filament found, d<.01μm

TABLE 3 B-RUNS (NICKEL)

RUN	SUBST.	NI DEP. (Å)	RUN T (°C)	RUN t (min)	TOT.FLOW (sccm)	H_2:C_2H_2	RED.t (min)	HC SAT.t (min)	COMMENTS
B1	Poco	100	1000	60	40	5:1	10	0.5	Straight,d=5-6μm,AR<50.
B2	SiO_2	?	1000	50	40	5:1	10	1.0	No analysis.
B3	Poco	Plated	1000	60	40	5:1	10	0.5	One filament,d=.6μm,AR<20.
B4	Poco	100	1000	60	40	5:1	10	1.0	Same as B1.
B5	Poco	100	1000	60	40	5:1	10	0	Same as B1.
B6	HOPG	50	1000	60	40	5:1	10	0.75	Octopussy,d=.2-.5μm,AR<100.
B10	HOPG	100	1000	60	126.5	10:1	10	1.0	No filaments found.
B11	HOPG	100	1000	15	126.5	10:1	10	1.0	No filaments found.
B12	HOPG	100	1000	60	126.5	10:1	10	1.0	No filaments found.
B14	HOPG	100	1000	60	126.5	10:1	10	1.0	No filaments found.
B15	HOPG	100	850	60	126.5	10:1	10	1.0	Bundles,d=.2μm, long.

TABLE 4 MISCELLANEOUS C, D, and E-Runs (IRON)

RUN	RUN T (°C)	RUN t (min)	RED.t (min)	TOT. FLOW (sccm)	H_2:C_2H_2	COMMENTS
C2	750	30	10	126.5	10:1	No filaments found.
C3	1000	60	10	40	5:1	Straight, d=1μm, l>1mm.
C4	850	60	10	40	5:1	No filaments found.
C7	1000	60	10	40	5:1	Same as C3.
C9	1000	60	10	40	5:1	Same as C3.
C12	1000	30	10	40	5:1	D=1μm, l<.2mm.
D2	1000	60	10	40	5:1	Straight, d=2-5μm, AR=500.
D4	1000	60	10	40	5:1	Straight, d=1μm, l=100μm.
D5	1000	60	5	100	10:1	Straight, d<1μm, l<1mm.
D6	1000	60	5	100	3:1	Straight, d=10μm, AR<50.
D7	1000	60	15	100	10:1	No filaments found.
D8	1000	60	15	20	3:1	Many filaments, d=10μm, l<1mm, Cl found.
D9	1000	60	5	20	10:1	No filaments found.
D10	1000	60	5	20	3:1	No filaments found.
E1	1000	60	10	40	5:1	Straight, d=5μm, l<1mm.
E2	1000	60	10	40	5:1	Same as E1.
E3	1000	60	10	40	8:1	Straight, d=.75μm, l=1mm.

GROWTH AND STRUCTURE OF VAPOR-DEPOSITED FILAMENTS ON GRAPHITE AND SILICON SUBSTRATES

C. W. Bowers and I. L. Spain
Department of Physics
Colorado State University
and
C. M. McConica
Department of Chemical Engineering
Colorado State University

ABSTRACT

Filaments have been grown by catalytic-chemical-vapor-deposition techniques on graphite and silicon substrates at temperatures from 700- 1000°C. Nickel catalyst and acetylene/hydrogen reaction- gas mixtures were used for all experiments. X-ray diffraction examination of the filaments indicated that those grown on graphite substrates were disordered, and those on silicon between 700-800°C were partially graphitic. Silicon carbide was formed on the silicon substrates between 900-1000°C but was probably not filamentary. The results are discussed in terms of a model for the growth process.

INTRODUCTION

In a previous paper (1) the growth of partially graphitic filaments was reported on silicon surfaces from acetylene at 850°C. The silicon surfaces were coated with a thin layer of Ni to provide a catalyst for th@ growth. The catalyst film forms small spherules on the surface when the temperature rises to that of the reaction. These spherules then act as surfaces for the decomposition of the hydrocarbon, and thedeposited carbon deposits under the spherule, pushing it forward. The filament then grows outwards from the surface with the catalyst particle at its end (for a review, see Ref. 2).

The results reported in (1) suggested that the degree of graphitization of the filament was increased when growth occurred on silicon surfaces. X-ray diffraction patterns obtained on filaments grown on graphite substrates under the same conditions showed no evidence of graphene planes (i.e., (002) reflections were so broad that the structure was close to amorphous). On the other hand, those grown on silicon substrates showed well developed (002) reflections, with interlayer spacing characteristic of a graphitization index (3) of about 0.5. This is similar to the graphitization achieved by heat-treating an organic precursor such as anthracene to a temperature of about 2200°C.

This result is of possible technological significance, since it may allow high strength carbon filaments to be grown by the catalytic chemical-vapor-deposition technique (CCVD) at significantly lower temperatures than those used presently (1100-1200°C) (4). The present study was carried out to investigate the temperature dependence of the graphitization index of the filaments.

The present report is provisional, of work that is not yet complete.

Experimental Details

Filaments were grown by the methods described in Ref. 1. Substrates were either a fine-grain nuclear graphite or single-crystal silicon. Table 1 lists the runs that were carried out. Nickel was used as the catalyst in all cases, 5:1 hydrogen:acetylene for the reaction gas.

After growth the filaments were studied using x-ray diffractometer techniques. The surfaces were also studied in a Phillips 505 scanningelectron microscope to verify that filaments had grown. Efforts are being made to obtain diffraction patterns using transmission-electron microscopy, but this study is not complete.

Experimental Results

Filaments were grown successfully on graphite substrates from 700-1000°C. Diffractometer traces of the filaments did not reveal (002) diffraction lines consistent with earlier findings (1).

Filaments grew on silicon substrates between 700-800°C. The diffractometer traces of these filaments showed well-developed (002) lines, whereas those grown at 850°C did not. The diffractometer traces of filaments grown at 900°C could be

indexed on the basis of SiC (5). No filament growth occurred at 950c

C or 1000°C, but a thin film of SiC was formed on the substrate. Preliminary results using electron diffraction suggest that the 900°C filaments are not SiC, but further results are necessary to establish this definitively.

Discussion of Results

The present results suggest that graphitic filaments can be grown on silicon substrates over a limited range of temperature (-700-800°C). One possible model for their growth is postulated by us as follows:

1. Graphitic filaments grown on graphite substrates at temperature >1150°C- are associated with liquid catalyst particles. Carbontransition metal eutectics are above this temperature (7), so that either impurities or the effect of small particle size must be responsible for depressing the eutectic temperature below its normal value. (Alternatively, the dehydrogenation reaction heats up the catalyst particle, but this coul only bege temperature rise is too small (8).) These filaments aretubular in structure with a hollow core (9,10).

2. Filaments grown on graphite substrates below about 1100°C have solid catalyst particles. The facets of the catalyst particles favoring growth inhibit the formation of graphene layer tubes. A herringbone structure results (see discussion in Section 4) consistent with electron diffraction examination (11). The small dimensions of the graphene layers prevent the development of strong (002) x-ray diffractions.

3. The growth of partially graphitic filaments at relatively low temperature on silicon substrates is related to the depression of the catalyst particle eutectic below the reaction temperature, so that it is in a liquid-like state. The eutectic may again be depressed below its normal, bulk, value by the small particle size and by the presence of both carbon and silicon in the metal.

4.The formation of silicon carbide inhibits the growth of carbon filaments from liquid-like catalyst particles at higher temperature.

Several experiments can be carried out to test these hypotheses. The most valuable would be to carry out structural investigations at the temperature of the reaction, but this may not be possible. A more accessible experiment would be to utilize transition metal alloys as catalysts and to investigate the structural evolution of filaments at room temperature as a function of the reaction temperature. A systematic study of this kind could find a direct correlation between the eutectics (bulk) and the reaction thresholds for production of graphitic filaments. One interesting possibility mentioned above is that the small particle size lowers the eutectic temperature. it would be interesting to investigate this experimentally. This may be done using magnetic measurements. Also, models of the melting could be developed as a function of particle size.

Finally, it may be possible to check the ideas proposed here using computer simulation techniques. These simulations are planned for the future.

References

1. Y. X. Zhao, C. W. Bowers, and I. L. Spain, accepted by Carbon (see also Final Report to AFOSR, 1986,

Grant No. F49620-84-K-0006).

2. R. T. K. Baker and P. S. Harris, Chem. Phys. Carbon 14, 83 (1978).
3. J. Maire and J. Mering, Proc. 4th Int. Conf. Carbon, p. 345 (1960).
4. T. Koyama, Carbon 10, 757 (1972).
5. ASTM Card File.
6. M. Endo, T. Koyama, and Y. Hishiyama, Japan. J. Appl. Phys. 11, 2073 (1976).
7. M. Hansen and K. Anderko, "Constitution of Binary Alloys" (McGraw Hill, 1958).
8. See Section 4 of the present report.
9. M. Endo, A. Oberlin, and T. Koyama, Japan. J. Appl. Phys. 15, 1519 (1977).
10. G. G. Tibbets, J. Cryst. Growth 66, 632 (1984).
11. E. Boelland, P. K. DeBokx, A. J. H. M. Kock, and J. W. Gues, J. Catalysis 96, 481 (1988).

Table 1.

Experimental details of runs.

Catalyst:Nickel, evaporated onto substrates to thickness of 0.2 mm

Reaction gas: 5:1,H2/acetylene

Graphite substrate:	Poco ZXF-50
	silicon; (100) orientation from Monsanto; p-doped with boron; resistivity 3Opm (Lot #9808 SN 190.063312)
Furnace purge gas:	Ar/H2 see Ref. 1)
Furnace profile:	See Ref. 1
Reaction temperature:	700, 750, 800, 850, 900, 950, 1000, ±5 K

Growth of Carbon Filaments from Ferrocene Based Iron Catalyzed Decomposition of Benzene

K. Baughman[1], C. McConica[2], I.L. Spain[3], and S.R.D. Udpa[2]

[1]Department of Mechanical Engineering

[2]Department of Agricultural and Chemical Engineering

[3]Department of Physics

Colorado State University, Fort Collins, Colorado 80523, USA

ABSTRACT

Transmission Electron Microscopy (TEM) has been used to study carbon filaments grown from ferrocene based iron catalyzed decomposition of benzene. Ferrocene was introduced into a Catalytic Chemical Vapor Deposition (CCVD) reactor by sublimation in a hydrogen carrier gas. Vaporized benzene was admitted to the CCVD reactor also in a hydrogen carrier gas concurrent with the ferrocene.

Carbon filaments grown by this method had the desired length and width characteristics for obscuration research. However, their structure was poorly organized with inclusions of many iron catalyst particles and filament branching.

INTRODUCTION

The use of vaporizable organometallic substances as precursors of metallic catalysts has been recognized by various researchers for some time.[1,2,3,4,5,6,7] The advantage of catalysts derived from organometallic compounds is the small diameter of catalytic particles obtained. These small diameter catalytic particles in turn catalyze the formation of small diameter carbon filaments.

The objective of our research was to grow straight, submicron carbon filaments with aspect (length to width) ratios > 1000. Previous work by Schmitt[8] found filament morphology to be dependent upon choice of catalyst. Iron catalysts gave straight filaments, while the use of nickel and other catalysts resulted in a variety of vermicular forms of filaments. Ferrocene, $(C_5H_5)_2Fe$, was chosen as the catalyst precursor because its sublimation around 100°C provided a convenient method of introducing iron into the CCVD reactor.

Filaments grown by Schmitt on iron by the catalytic decomposition of acetylene had diameters of several micrometers and aspect ratios of ~100. To obtain submicron filaments it was necessary to not only change catalyst precursors but also hydrocarbons. Baker and Harris[9] determined that as hydrocarbon saturation increased, filament diameter decreased. Benzene produced filaments with the desired diameters in several studies, including a process described by Hatano et. al.[5], and therefore was selected to replace acetylene as the process hydrocarbon.

A discussion of experimental methods and results of structural studies using TEM is presented for carbon filaments grown from the catalytic chemical vapor deposition of benzene on iron catalyst derived from ferrocene.

EXPERIMENTAL

The CCVD reactor used to perform the experiments was essentially the same as described by Schmitt[8]. Modifications included the addition of a bubbler for the vaporization of benzene, a new inlet cap which minimized the distance from the ferrocene source to the reactor tube to prevent solidification of the ferrocene in inlet lines, and new reactor tubes and end caps. Figure 1 shows the schematic representation of the complete CCVD reactor system.

Materials

All process gases were manufactured by General Air. The process gases used and their purities were: hydrogen (99.9998%, 4.5 um prepurified), helium (99.998%), and air (breathing quality). Fisher Scientific spectroscopic grade benzene provided the hydrocarbon source. Aldrich Chemical ferrocene functioned as the organometallic catalyst precursor.

Procedure

Both the benzene bubbler and flask containing ferrocene were weighed before beginning the experiment. All connections to the system were made, isolating the entire system from the atmosphere. Bypass valves were opened on the ferrocene flask and benzene bubbler. The gas manifold, reactor tube, and connecting lines were then

evacuated to a pressure of $< 10^{-2}$ Torr as measured by an ion gauge at the inlet of the turbo pump. The reactor tube was subsequently isolated from the system. The bypass valves on the ferrocene flask and benzene bubbler were opened and both vessels were brought to atmospheric pressure in helium. The bypass valves were again closed and the lines evacuated to a pressure of $< 10^{-5}$ Torr. This procedure was repeated several times to completely purge the system of oxygen and other contaminants. The system was pressurized to above local atmospheric pressure (~630 Torr) in helium, then vented to the atmosphere. The reactor tube was heated to 1000°C by the furnace. This temperature was monitored by a thermocouple placed at the furnace center, between the heating element and reactor tube. The thermocouple provided feedback to the programmable temperature controller. The benzene bubbler was maintained at 30°C in a water bath of sufficient volume to minimize temperature transients. The ferrocene flask was heated to 150°C with a heating mantle controlled by a variac. When the reactor reached 1000°C, hydrogen was admitted to the benzene bubbler and ferrocene flask at 20 sccm. These conditions were sustained for 1 hour. The reactor tube was cooled to room temperature in helium. The ferrocene flask and benzene bubbler were weighed and usage of ferrocene and benzene was calculated. Typical usage of ferrocene was 0.1 grams with 0.8 grams of benzene expended.

RESULTS

The observation of the inside of the reactor tube after a run showed three distinct regions of carbon deposits. Filamentous carbon grew in dense mats from the inlet side of the heated zone for approximately 2 inches. The middle 4 inches of the heated zone was coated with a shiny layer of graphitic carbon. The third region mirrored the inlet and occurred for 2 inches before the outlet of the heated zone of the reactor tube. Samples were removed from the reactor tube by moistening the deposits with absolute ethanol followed by scraping. The samples were suspended in absolute ethanol and applied dropwise to Formvar coated copper TEM grids.

Figures 3 - 6 depict carbon filaments typical of the process. The micrographs were taken on a Philips EM 400T Transmission Electron Microscope used for the structural analysis of the carbon filaments. Average width of the filaments is 0.07 um. Due to the extreme amount of filament intertwining exhibited an estimation of length is difficult. Also, since the aspect ratio is high and the diameters small, a micrograph could not be made in which individual filaments were distinct. However, several shorter distinct filaments were measured with lengths of approximately 50 um. This yields a lower bound of 700:1 for the aspect ratio of the carbon filaments.

CONCLUSIONS

The three regions of carbon deposition in the reactor tube can be explained by figure 2. The reactor temperature profile shows that filament growth occurred in regions of the reactor tube that were between ~800 - 950°C. Graphitic carbon growth proceeded in the middle of the reactor tube, at temperatures of ~950 - 1000°C.

Figure 3 shows the intertwining nature of the filaments as grown. Clumps of polycrystalline graphite are also visible in the micrograph. These polycrystalline masses, as well as amorphous carbon, are found

simultaneously in the sample of carbon filaments.

Figure 4 depicts similar carbon filaments at an higher magnification. Dark specks are visible, imbedded within the filaments. Figure 5 is a carbon filament with these darker areas more clearly illustrated. These areas are either graphitic inclusions, somewhat rectangular appearing, or iron catalyst particles, which are more round. When catalyst particles are embedded within filaments several types of behavior can occur. Most commonly observed is a change in the direction of filament growth. This is seen in figure 5. Branching of filaments is also frequently seen. Multiple catalyst particles are often found in carbon filaments as evidenced by figure 6.

Based on the structure of the filaments, including many catalytic particle inclusions and the mycelium-like growth, it can be concluded that carbon filaments grown by this method are inferior to catalytic particle seeded substrate derived carbon filaments for obscuration research.

RECOMMENDATIONS

Although carbon filaments grown by the discussed method are unsuitable for obscuration there may be many applications for such filaments. The filaments high aspect ratios and small diameters make them attractive for numerous services. Carbon-resin and carbon-carbon composites are two examples of possible applications. Electromagnetic radiation shielding and heat transfer mediums are further suggestions for continued research.

REFERENCES

1) A. Oberlin, M. Endo and T. Koyama, J. Crystal Growth, 32, 1976, p.335

2) H.G. Tennent, U.S. Patent 4,663,230, May 5, 1987.

3) K. Arakawa, U.S. Patent 4,640,830, Feb. 3, 1987.

4) K. Arakawa, U.S. Patent 4,572,813, Feb. 25, 1986.

5) M. Hatano, T. Ohsaki, and K. Arakawa, 30th National SAMPE Symposium, March 19-21, 1985.

6) T. Koyama and M. Endo, Japan. J. Appl. Phys., 13, 1974, 1175.

7) T. Koyama and M. Endo, Oyo Buturi, 42, 1973, p.690.

8) C.C. Schmitt, Thesis, "Chemical Vapor Deposition of Carbon Filaments From Acetylene as Catalyzed by Iron and Nickel", Colorado State University, Fort Collins, Colorado, U.S.A., 1988.

9) R.T.K. Baker and P.S. Harris, "The Formation of Filamentous Carbon", Chem. and Phys. of Carbon, 14, 1978, p.83.

FIGURE CAPTIONS

Fig. 1. Reactor Schematic.

Fig. 2. Reactor Temperature Profile. Negative position indicates reactor tube inlet, positive position indicates reactor tube outlet.

Fig. 3. Carbon filaments and polycrystalline graphite deposits. 13,000x, 80 kV

Fig. 4. Carbon filaments with common inclusions. 28,000x, 80 kV

Fig. 6. Carbon filament with graphitic inclusions (darker rectangles) and catalytic iron particle (dark oval). Note the change in the direction of growth at the catalytic particle. 220,000x, 80 kV

Fig. 7. Carbon filament showing fine structure and embedded multiple iron particles. 410,000x, 80 kV

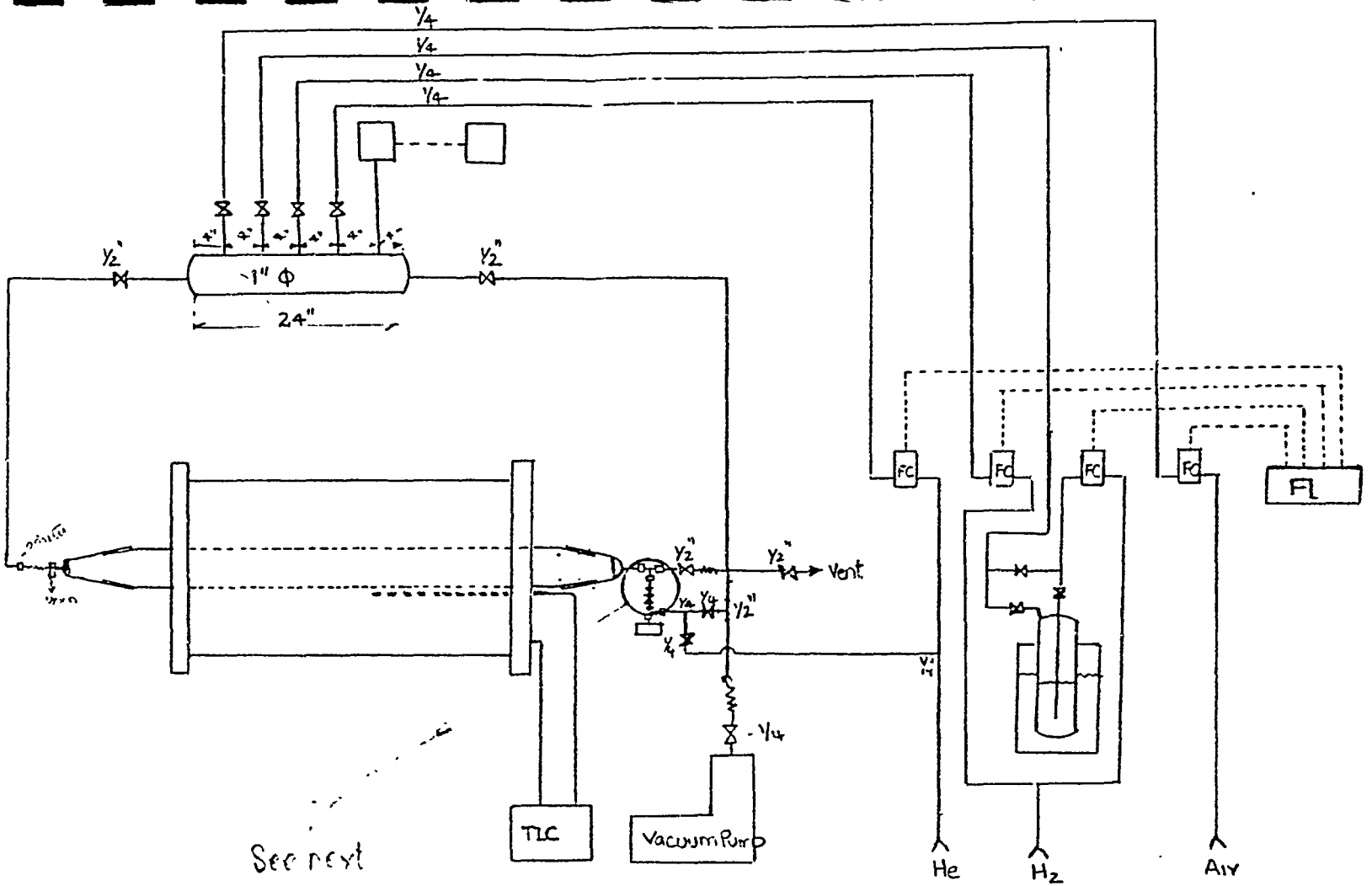

See next page

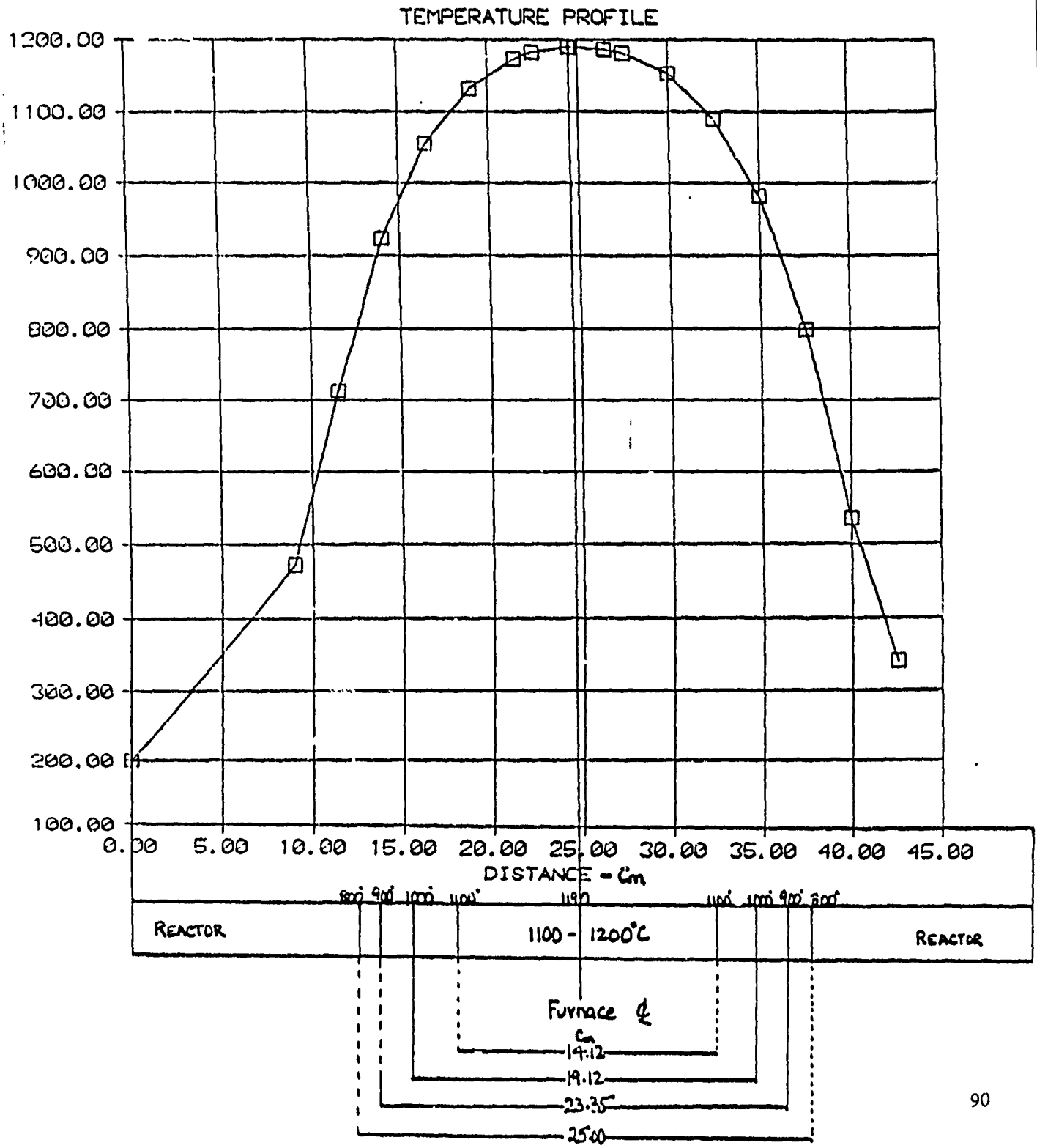
TEMPERATURE PROFILE
1200.00
1100.00
1000.00
900.00
800.00
700.00
600.00
500.00
400.00
300.00
200.00
100.00
0.00
5.00
10.00
15.00
20.00
25.00
30.00
35.00
40.00
45.00
DISTANCE - Cm
REACTOR
1100 - 1200°C
REACTOR
Furnace ℄
19.12
19.12
23.35
25.00

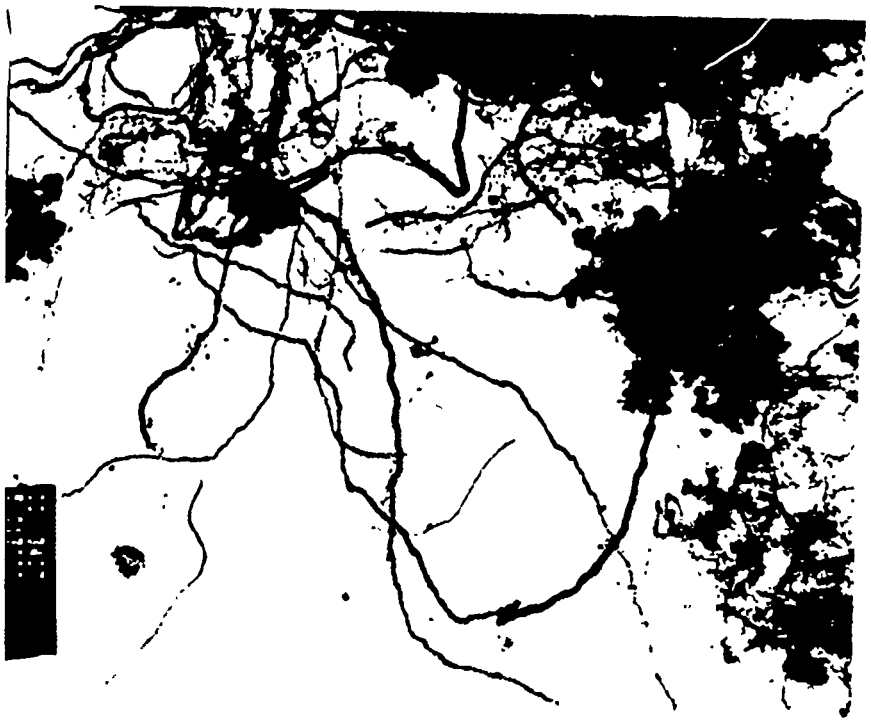

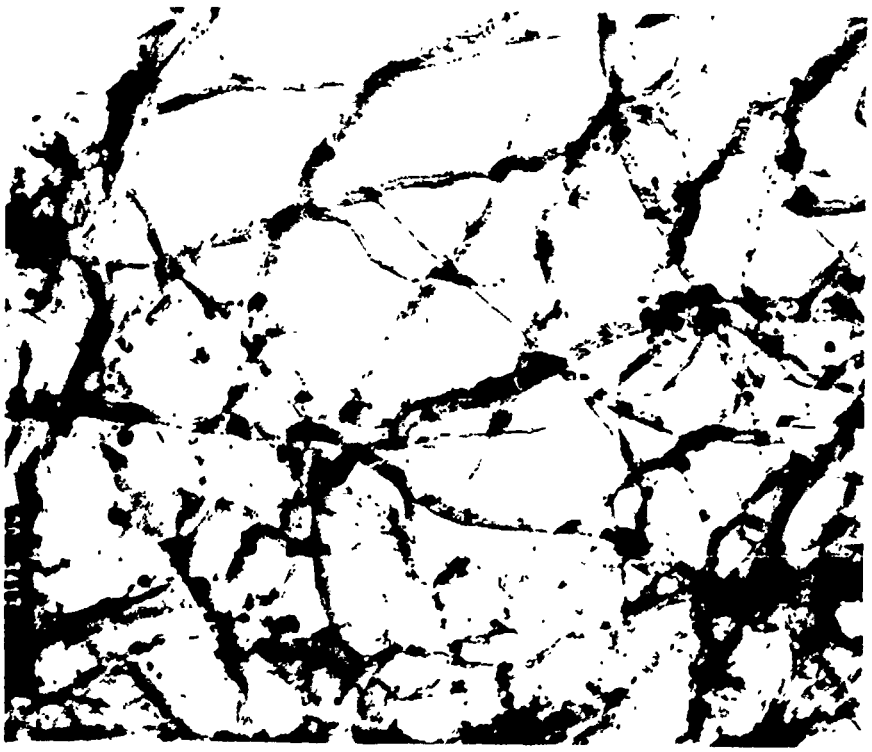

Effects of Catalyst, Additives, and Substrate on the Iron Catalyzed Decomposition of Benzene

K. Baughman[1], C. McConica[2], I.L. Spain[3], and S.R.D. Udpa[2]

[1]Department of Mechanical Engineering

[2]Department of Agricultural and Chemical Engineering

[3]Department of Physics

Colorado State University, Fort Collins, Colorado 80523, USA

ABSTRACT

Scanning Electron Microscopy (SEM) and Energy Dispersive X-Ray Spectroscopy (EDS) have been used to study carbon filaments grown from different iron salts by Catalytic Chemical Vapor Deposition (CCVD). The effects upon linear growth of an additive, calcium, and several substrates was also investigated.

The morphology of the carbon filaments was found to be dependent on all three items - catalyst salt, the addition of calcium, and substrate choice.

INTRODUCTION

Although an immense amount of research has focused on the growth of carbon filaments, little has been done to study the effects of catalyst starting materials or substrate/catalyst/carbon filament interactions. The objectives of this study were to obtain straight, submicroncarbon filaments with length to diameter ratios greater than 1000 and to obtain sufficient quantities to allow physical characterization of the filaments.

Work by Schmitt[1] on the iron/acetylene system, using highly oriented pyrolytic graphite (HOPG) as substrates to support the catalyzed filament growth, yielded desirable filaments. These filaments were on the average 5 um in diameter and had aspect ratios of less than 100. Although the filaments were very straight it would be necessary to decrease the diameter and increase the aspect ratio of the filaments. Additionally, the density of the filaments per substrate required an increase over the average 10 filaments per cm^2 observed to meet the stated goals.

A discussion of experimental methods and the results of experiments to determine the effects of catalyst, the addition of calcium, and choice of substrate is presented with analyses of the carbon filaments by SEM and EDS.

EXPERIMENTAL

Equipment

Preliminary experiments were performed on the CCVD system described by Schmitt[1]. The remainder of the experiments were carried out on the modified CCVD reactor described previously[2].

Materials

All process gases were manufactured by General Air. The process gases used and their purities were: hydrogen (99.9998%, 4.5 um prepurified), helium (99.998%), acetylene (grade 2.6), and air (breathing quality). Fisher spectroscopic grade benzene provided another hydrocarbon source. Mallinckrodt Chemical Works $FeSO_4 7H_2O$ and Fisher Scientific $CaCl_2 2H_2O$ were used to prepare substrates.

Procedure

The procedure for the preliminary experiments was the same as that used by Schmitt in growing filaments from the iron/acetylene system on HOPG[1]. The procedure consisted of inserting one to three substrates into the reactor tube and pumping the system down to less than 10^{-5} torr, then bringing the system to atmospheric pressure with He and heating the system to 1000°C in He. H_2 replaced the He for a 10 minute reduction period, after which C_2H_2 was admitted to the reactor. The H_2 and C_2H_2 flows were maintained for 1 hour, then they were replaced with He and the system cooled to room temperature. Other experiments utilizing benzene as the hydrocarbon use a

procedure similar to the above. With the addition of a bubbler for benzene it was necessary to purge the bubbler to remove any dissolved atmospheric gases. This was accomplished by repeatedly pumping on the bubbler to a pressure of less than 10^{-2} torr and re-pressurizing the bubbler to local atmospheric pressure with H_2.

HOPG substrates were seeded by dipping them into a supersaturated $FeCl_2 \cdot xH_2O$ solution by Schmitt. Additional substrates were prepared by spraying a solution of $FeSO_4 7H_2O$ and $CaCl_2 \cdot 2H_2O$ onto heated HOPG and quartz substrates. The substrates were stored in a desiccator until used.

Scanning Electron Microscopy was performed on a Philips 505 SEM equipped with a Kevex x-ray analysis unit and EDAX polymer windowed x-ray detector.

RESULTS

The substrates used by Schmitt were dipped in a solution containing $FeCl_2 \cdot xH_2O$ as the iron salt. Research by Egashira et al.[3,4] has shown that halogens inhibit the growth of carbon filaments, while sulfur or sulfur compounds enhance filament growth. In an effort to increase the aspect ratio of the filaments $FeSO_4 \cdot 7H_2O$ replaced $FeCl_2 \cdot xH_2O$ during substrate preparation. The first substrates prepared from a supersaturated solution of $FeSO_4 \cdot 7H_2O$ yielded such dense growth that filaments were indistinguishable from one another. Ensuing substrates were prepared using an 2.9×10^{-3} molar solution (0.8 g/l) of $FeSO_4 \cdot 7H_2O$ applied by spraying onto the substrates. Examples of the resulting filaments are illustrated in figures 1 - 3. A higher density of filaments in range of 0.1 to 6.5 mm long and 5 um in diameter was obtained with the new seeding method. If the catalyst solution is not used immediately, a precipitate forms upon cooling. To prevent the precipitate, 2.72 ml concentrated HNO_3 was added to the solution.

Figures 4 - 7 show a serendipitous finding. Figures 4 and 5 are micrographs of two iron catalyst particles separated by ~25 um. Figure 6 is an EDS spectrum of the catalyst particle in figure 4, with the cross-hairs indicating the region from which the spectrum arises. The large escape peak indicates the sample is composed mostly of carbon, from the graphite substrate, plus iron. Figure 7 is an EDS spectrum of the catalyst particle in figure 5 which has a 5 um diameter by 6.5 mm long filament growing from it. This spectrum indicates the presence of carbon, aluminum (from the aluminum stub on which the sample is glued), iron, and calcium. Filaments of such length were seen to always emanate from catalyst particles containing calcium whereas pure iron catalyst particles grew shorter or no filaments. This occurred on many samples. Calcium was not found in the chemical analysis of the $FeSO_4 \cdot 7H_2O$ nor was it present during any other phase of preparation in materials or apparatus. Calcium containing samples were found to have been prepared without gloves and calcium containing catalyst particles were most frequently found about the periphery of the substrates. The source of calcium was hypothesized to be the finger tips of the substrate preparer, although this was not substantiated.

To increase the percentage of longer filaments calcium was added to the catalyst solution at the rate of 0.08 g $CaCl_2 \cdot 2H_2O$ per liter H_2O along with the 0.8 g $FeSO_4 \cdot 7H_2O$.

To grow filaments of smaller diameters it was necessary to change the hydrocarbon source. Baker and

Harris[5] and Hatano et al.[6] found benzene to grow filaments with diameters in the desired submicron range. Following their lead acetylene was replaced by benzene as hydrocarbon source. Figures 8 and 9 are typical of filaments grown from the iron catalyzed decomposition of benzene on HOPG. Typical diameters were 0.33 um and lengths of greater than 0.15 mm were common, giving aspect ratios greater than 500.

Observation of catalyst seeded HOPG substrates by SEM, before and after reduction in H_2 at 1000°C for 10 min., indicated that the iron catalyst was disappearing from the surface of the substrate. This disappearance was thought to be caused by the diffusion of iron into the HOPG and the formation of iron carbides. The lack of a large amount of active iron catalyst on the surface of the HOPG precludes the growth of carbon filaments in sufficient numbers to make HOPG a suitable substrate.

Quartz was chosen as a substrate material because it is fairly inert and could withstand growth temperatures. Density of filaments on quartz substrates was much higher than on HOPG substrates as shown in figure 10. The catalyst solution application rate on quartz was half that of HOPG. This was necessary to permit SEM analysis of the carbon filaments. Figure 10 also illustrates a morphological difference between carbon filaments grown on HOPG and quartz substrates: quartz based filaments are not as straight as ones grown on HOPG. Filament diameters are approximately equal on both substrates. Lengths are shorter, but more uniform, on quartz. Figures 11 through 14 are the results of an experiment on the effect of Ca to Fe ratio on filament length. Table 1 gives the ratio of Ca to Fe and filament lengths obtained.

Table 1

T = 1000°C, T C_6H_6 = 30°C, P ~ 630 torr, run time = 1 hr.
substrate = quartz

Run	$FeSO4{\cdot}7H_2O/CaCl_2{\cdot}2H_2O$ (wt/wt)	C_6H_6 (g/hr)	H_2 (sccm)	L (um)	D (um)
CA1	5:1	0.9	40	6.5	0.24
CA2	2.5:1	0.8	40	21.7	0.43
CA3	1.67:1	1.1	40	40.9	0.45
CA4	1.25:1	0.8	40	43.5	0.45

CONCLUSIONS

Carbon filaments of submicron diameters and high aspect ratios can be grown from the benzene/iron/quartz system. Reasons why submicron diameters are obtained from benzene and not acetylene may be the gas phase polymerization of acetylene at growth temperatures, the difference in rates of formation of critical precursors, or a combination of the two. Baker and Harris[5] present evidence from literature and research to support stepwise decomposition of hydrocarbons. They also mention that no conclusive studies have been made to identify the precursor responsible for filament growth. The rate of precursor formation by stepwise decomposition of acetylene would be higher since the molecule is smaller than the benzene molecule. Since this is an uncatalyzed decomposition the filament diameter is also higher with acetylene than with benzene. Identification of specific

precursors would be beneficial in that linear filament growth, which is catalytic, and the increase in diameter, which is pyrolytic, may be caused by two different precursors. Controlling the ratio of these precursors would allow precise control of filament dimensions.

The increase in density of filaments on HOPG substrates by using $FeSO_4 \cdot 7H_2O$ instead of $FeCl_2 \cdot xH_2O$ is believed to be due to the difference in the method of catalyst solution application, rather than a fundamental difference in catalyst salt chemistry.

Denser growth of filaments on quartz occurs since more catalytic iron particles remain on the surface of the quartz. Simple diffusion of iron into the grain boundaries of HOPG may not adequately explain the loss of iron observed from HOPG substrates. The mechanism of iron loss is discussed in section ? of this report.

The difference in filament morphology on the two substrates may be due to differences in the layer of carbon that forms on quartz HOPG substrates. Carbon filaments grow by extrusion from catalytic particles which remain on the surface of the substrate. This mode of growth was verified by EDS and TEM of filament tips, which were shown to contain no iron. Comparing catalyst particles in figures 1 - 5 to figure 15 this layer can be seen. The quartz, with its higher surface density of iron catalyst, appear to more rapidly deposite non-filamentous carbon. As the layer builds up on the catalyst particle the diffusion of reactants to the surface may become limited preferentially such that one side of the filament grows more quickly, hence curved filaments. Finally the layer thickness becomes great enough to extinguish filament growth. Calcium caused a liquid interface between the iron catalyst particle and carbon deposits that eventually terminate filament growth. By floating off these deposits calcium extends the growth time and therefore the length of the carbon filaments.

RECOMENDATIONS

A detailed study to identify the precursors responsible for filament lengthening and diameter increase may provide key information for the controlled growth of CCVD filaments.

The identification of the mechanism by which calcium increases filament length should be made. In addition, other compounds with properties similar to calcium should be sought.

REFERENCES

1) C.C. Schmitt, Thesis, "Chemical Vapor Deposition of Carbon Filaments From Acetylene as Catalyzed by Iron and Nickel", Colorado State University, Fort Collins, Colorado, U.S.A., 1988.

2) K. Baughman, C. McConica, I.L. Spain, and S.R.D. Udpa, "Growth of Carbon Filaments from Ferrocene Based Iron Catalyzed Decomposition of Benzene", this report.

3) M. Egashira, H. Katsuki, Y. Uchikawa, and S. Kawasumi, "Inhibition of Carbon Fiber Growth from Naphthalene with Halogens", Carbon 20, 283 (1982).

4) M. Egashira, H. Katsuki, Y. Ogawa, and S. Kawasumi, "Whiskerization of Carbon Beads by Vapor Phase Growth of Carbon Fibers to Obtain Sea Urchin-Type Particles", Carbon 21, 89 (1983).

5) R.T.K. Baker and P.S. Harris, "The Formation of Filamentous Carbon", Chem. and Phys. of Carbon, 14, 1978, p.83.

6) M. Hatano, T. Ohsaki, and K. Arakawa, 30th National SAMPE Symposium, March 19-21, 1985.

FIGURE CAPTIONS

Fig. 1. SEM of RUN FS4. Carbon filaments on HOPG substrate from C_2H_2/Fe. T= 1000°C, t = 1 hr, H_2 = 33.3 sccm, C_2H_2 = 6.7 sccm, P = 630.3 torr, catalyst = $FeSO_4 \cdot 7H_2O$.

Fig. 2. SEM of RUN FS3. Carbon filament and iron catalyst particles. T= 1000°C, t = 1 hr, H_2 = 33.3 sccm, C_2H_2 = 6.7 sccm, P = 630.3 torr, catalyst = $FeSO_4 \cdot 7H_2O$, HOPG substrate.

Fig. 3. SEM of RUN FS3. Higher magnification view of filament and catalyst particle in figure 2.

Fig. 4. SEM of RUN FS4. Two iron catalyst particles, one growing a filament 6.5 mm by 5 um. Cross-hairs indicate location of EDS analysis.

Fig. 5. SEM of RUN FS4. The same filament and catalyst particle pictured in figure 4, with cross-hairs showing the location of EDS analysis.

Fig. 6. X-ray spectrum of the catalyst particle in figure 4.

Fig. 7. X-ray spectrum of the catalyst particle with filament in figure 5.

Fig. 8. SEM of RUN B4. Benzene derived filament (BDF). T = 1000°C, T C_6H_6 = 30°C, t = 1 hr, H_2 = 40 sccm, C_6H_6 = 0.8 g, P = 629.8 torr, catalyst = $FeSO_4 \cdot 7H_2O$, HOPG substrate.

Fig. 9. SEM of RUN B4. Lower magnification view of the filament pictured in figure 8.

Fig. 10. SEM of RUN B17. Morphology and density of filaments on quartz substrate. T = 1000°C, T C_6H_6 = 30°C, t = 2.5 hr, H_2 = 40 sccm, C_6H_6 = 0.72 g/hr, P = 633.3 torr, catalyst = $FeSO_4 \cdot 7H_2O$.

Fig. 11.SEM of RUN CA1. $FeSO_4 \cdot 7H_2O$ to $CaCl_2 \cdot 2H_2O$ = 5:1, T = 1000°C, T C_6H_6 = 30°C, t = 1 hr, H_2 = 40 sccm, C_6H_6 = 0.9 g/hr, P = 630.1 torr, quartz substrate.

Fig. 12.SEM of RUN CA2. $FeSO_4 \cdot 7H_2O$ to $CaCl_2 \cdot 2H_2O$ = 2.5:1, T = 1000°C, T C_6H_6 = 30°C, t = 1 hr, H_2 = 40 sccm, C_6H_6 = 0.8 g/hr, P = 630.1 torr, quartz substrate.

Fig. 13.SEM of RUN CA3. $FeSO_4 \cdot 7H_2O$ to $CaCl_2 \cdot 2H_2O$ = 1.67:1, T = 1000°C, T C_6H_6 = 30°C, t = 1 hr, H_2 = 40 sccm, C_6H_6 = 1.1 g/hr, P = 627.4 torr, quartz substrate.

Fig. 14. SEM of RUN CA4. $FeSO_4 \cdot 7H_2O$ to $CaCl_2 \cdot 2H_2O$ = 1.25:1, T = 1000°C, T C_6H_6 = 30°C, t = 1 hr, H_2 = 40 sccm, C_6H_6 = 0.8 g/hr, P = 632.8 torr, quartz substrate.

Fig. 15. SEM of RUN B18. Micrograph of a BDF and iron catalyst particle showing carbon coating of quartz substrate. T = 1000°C, T C_6H_6 = 30°C, t = 0.5 hr, H_2 = 40 sccm, C_6H_6 = 1.0 g/hr, P = 633.7 torr.

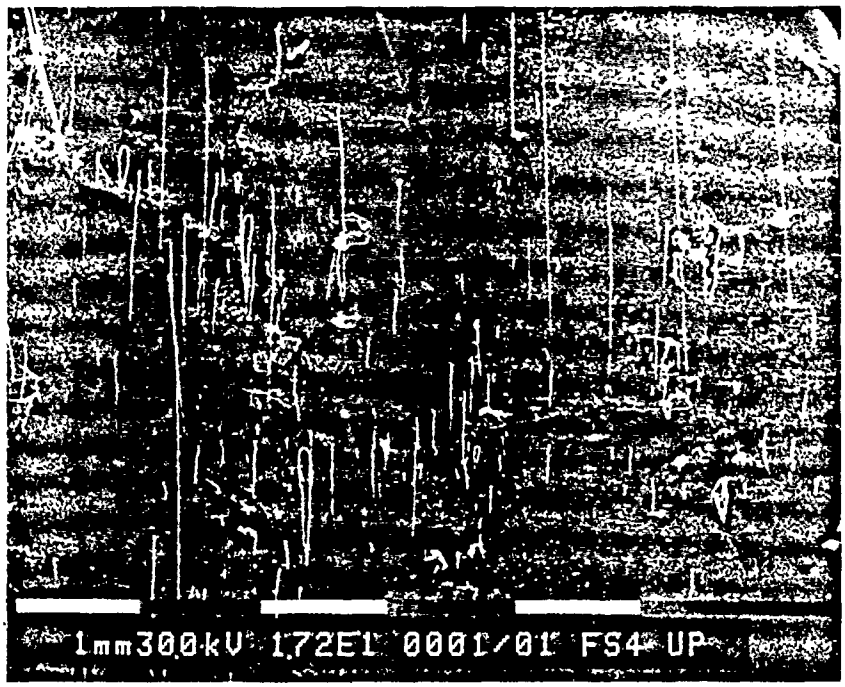
1mm30.0kV 1.72E1 0001/01 FS4 UP

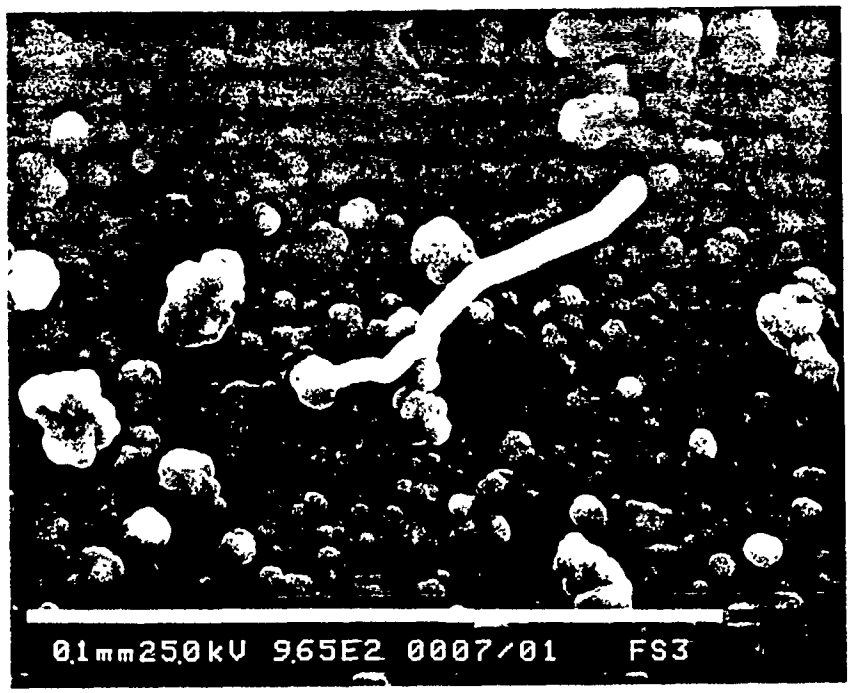
0.1mm25.0kV 9.65E2 0007/01 FS3

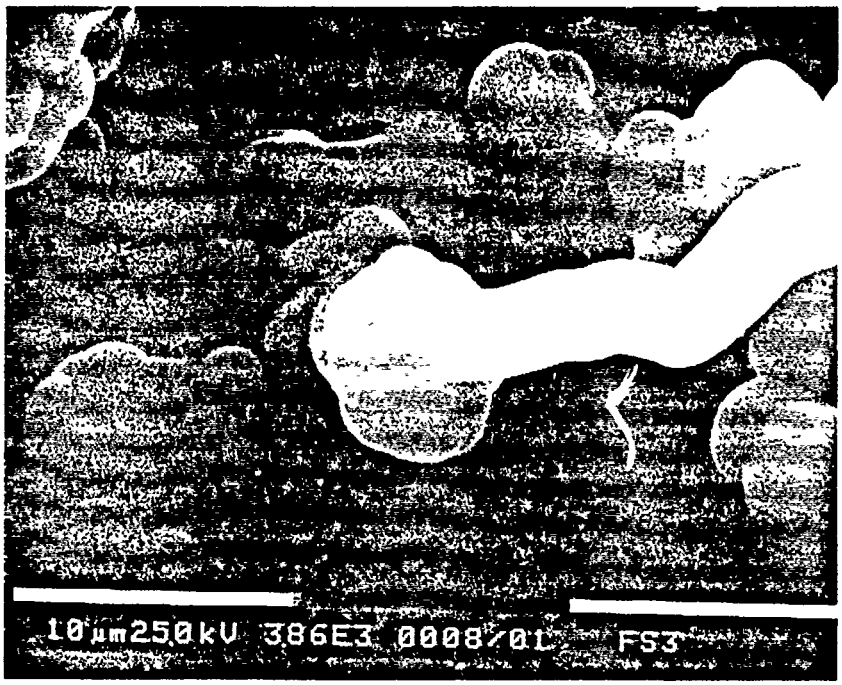
10µm250kV 3.86E3 0008/01 FS3

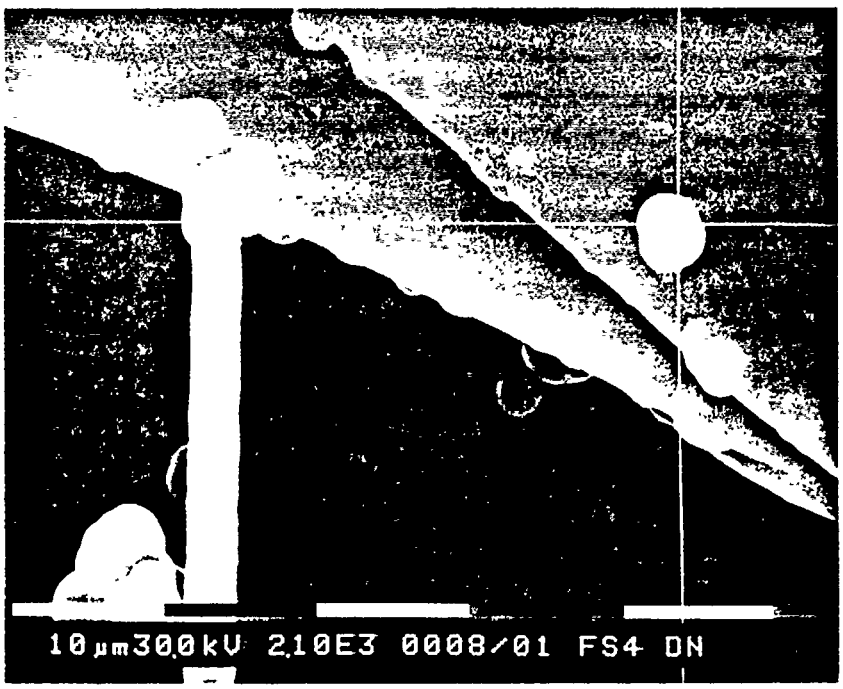
10µm30.0kV 2.10E3 0008/01 FS4 DN

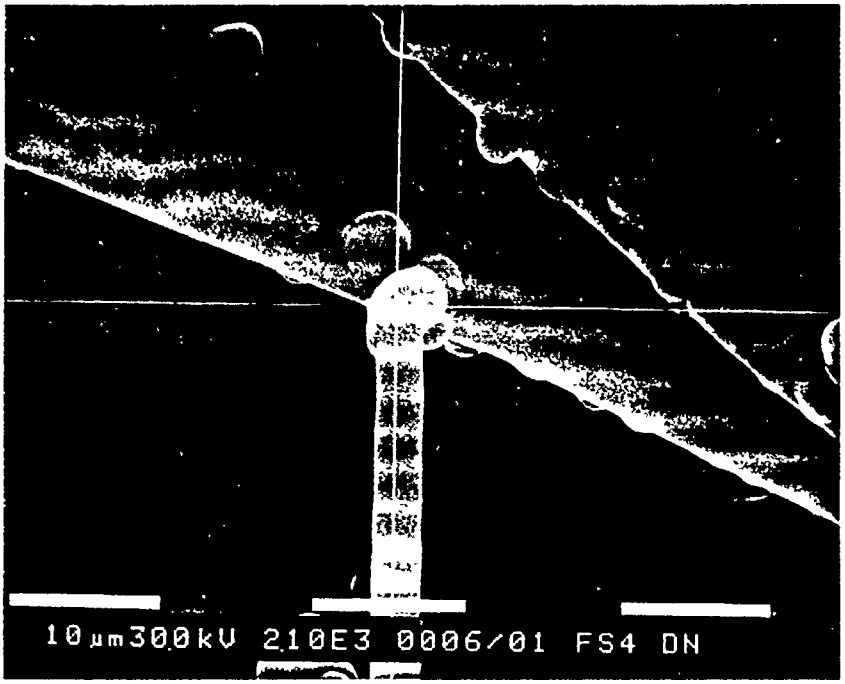
10µm30.0kV 2.10E3 0006/01 FS4 DN

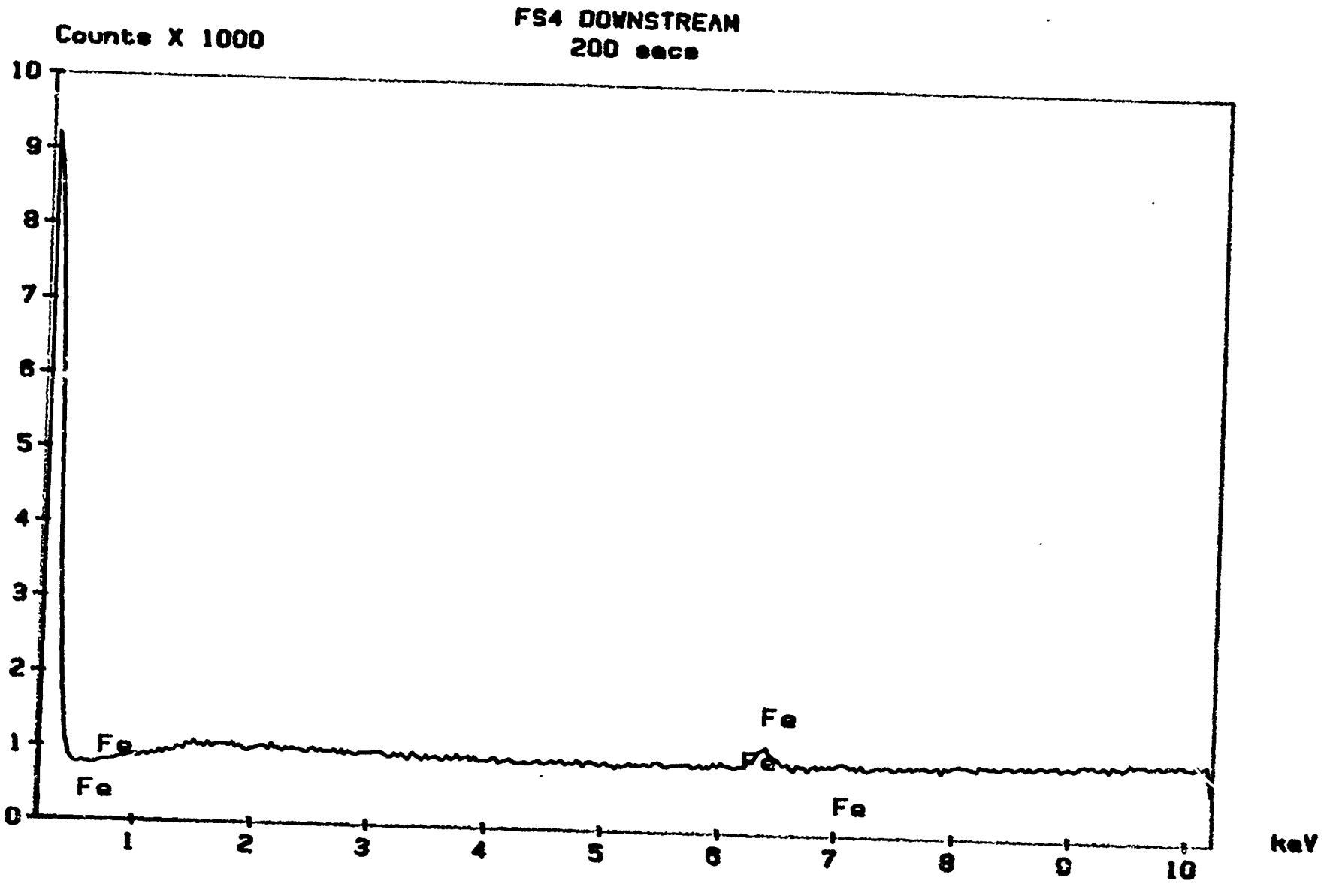
FS4 DOWNSTREAM
200 secs
Counts X 1000
10
9
8
7
6
5
4
3
2
1
0
Fe
Fe
Fe
Fe
Fe
1
2
3
4
5
6
7
8
9
10
keV

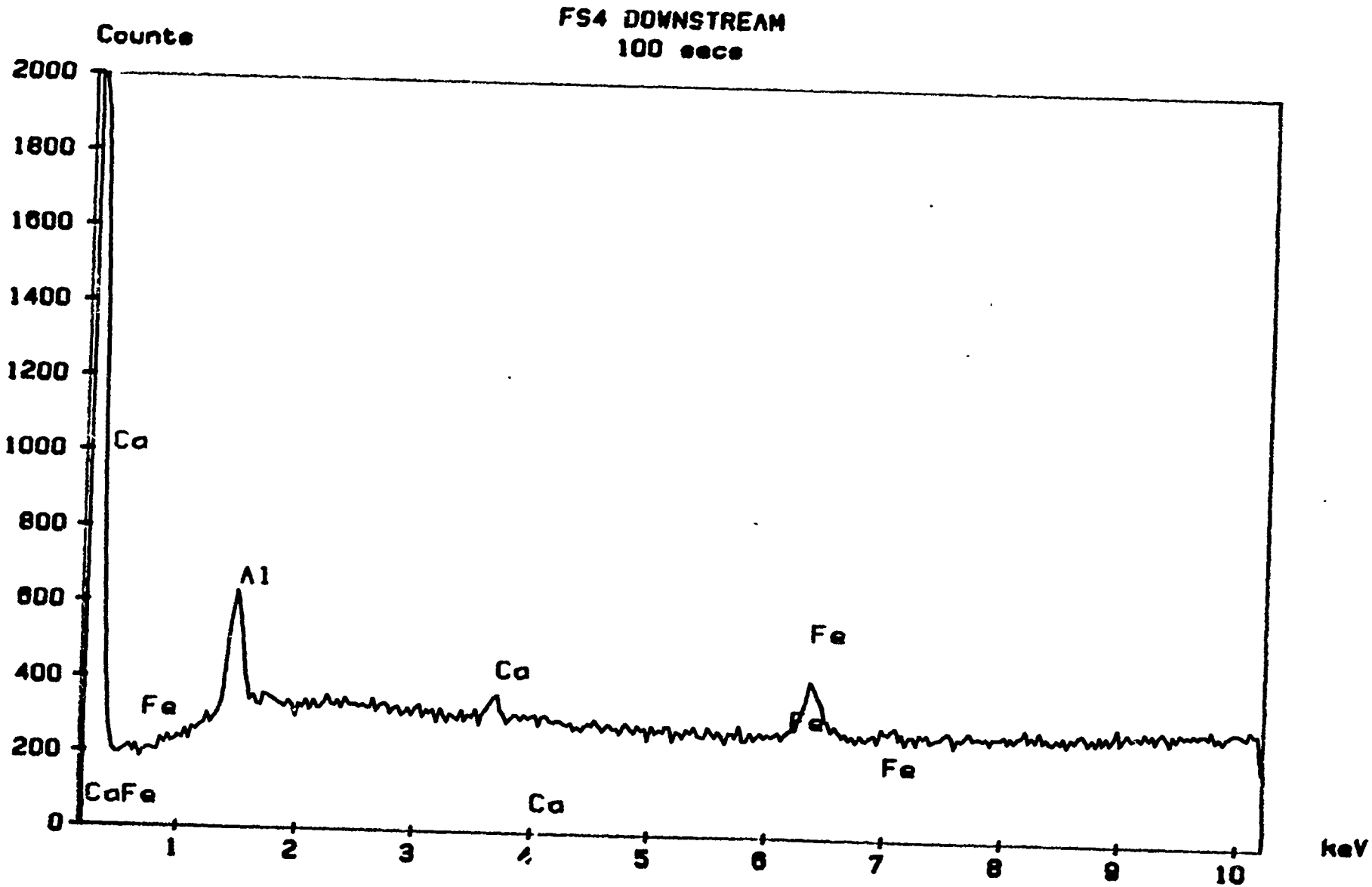
FS4 DOWNSTREAM
100 secs
Counts
2000
1800
1600
1400
1200
1000
800
600
400
200
0
Ca
Al
Fe
Ca
Fe
Fe
CaFe
Ca
1
2
3
4
5
6
7
8
9
10
keV

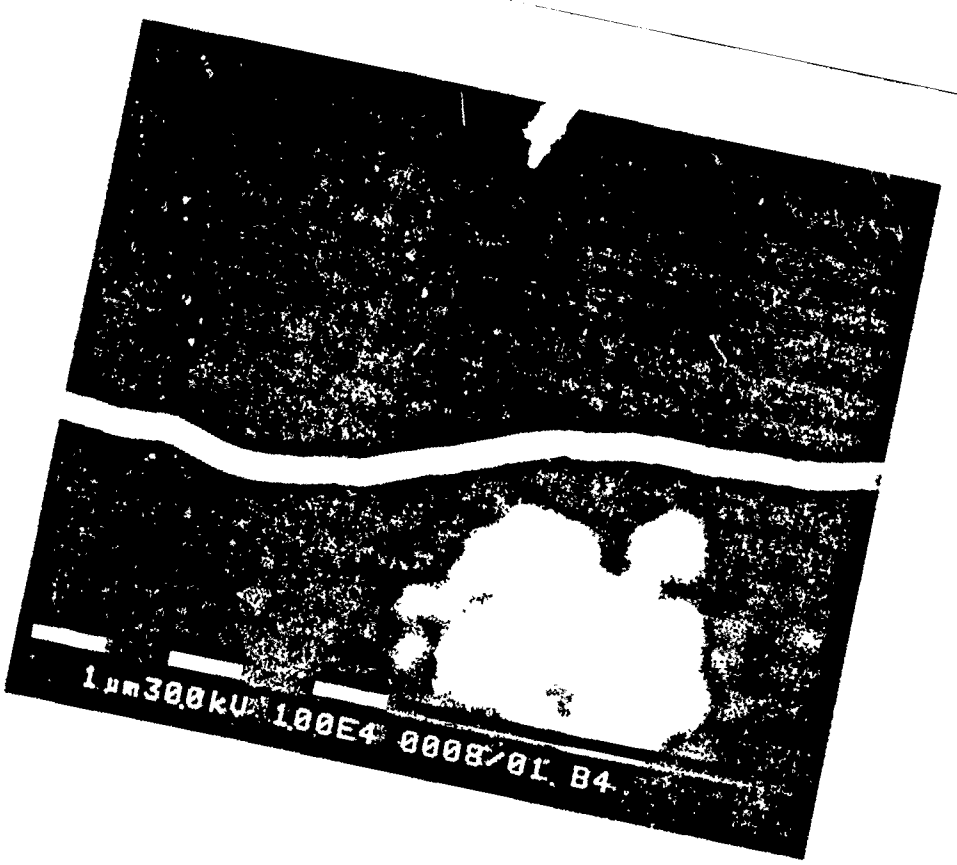
1µm30.0kV 100E4 0008/01 B4


0.1mm30.0kV 625E2 0007/01 B4

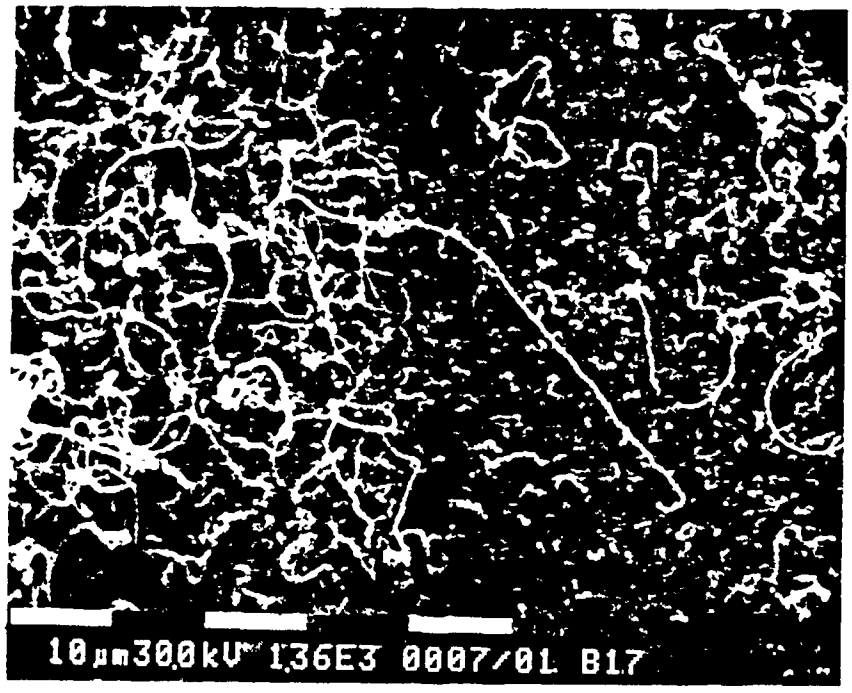
10µm30.0kV 1.36E3 0007/01 B17

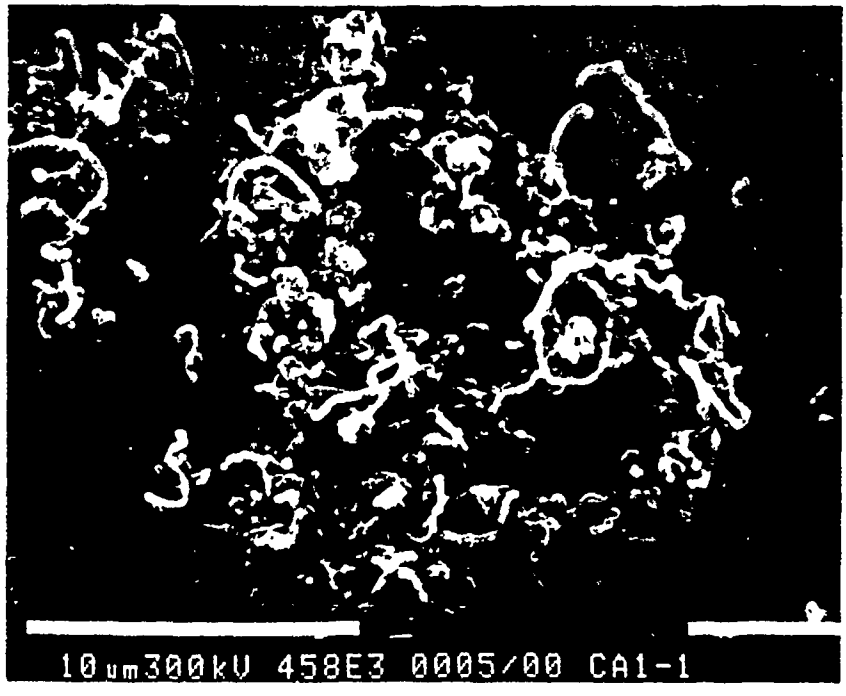
10µm300kV 458E3 0005/00 CA1-1


10µm30.0kV 230E3 0010/00 CA2-1


10µm30.0kV 115E3 0013/00 CA3-1

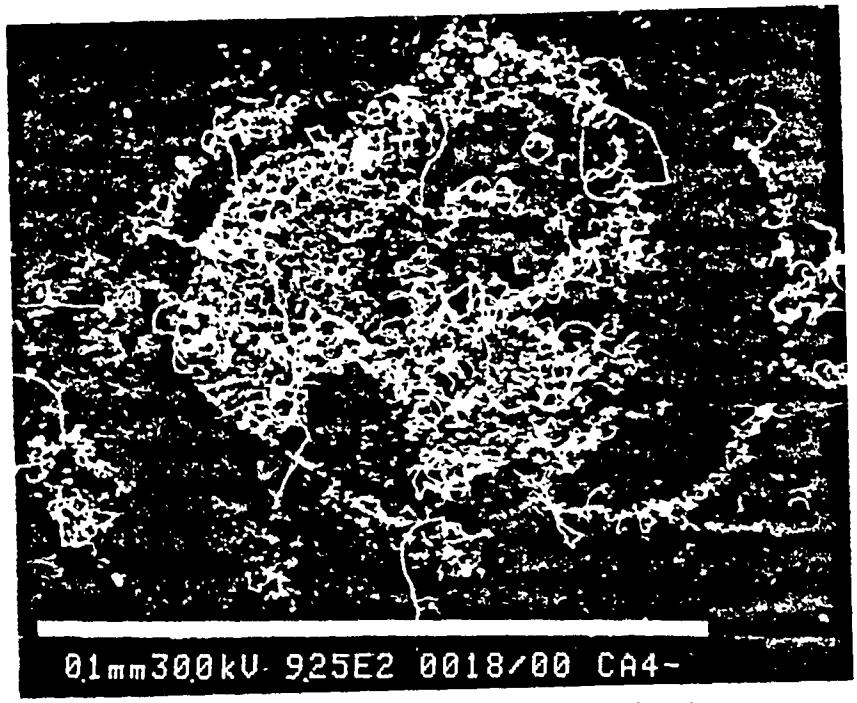

CA4-2

Effects of Partial Pressures and Growth Times on Catalytic Chemical Vapor Deposited (CCVD) Benzene Derived Carbon Filaments

K. Baughman[1], C. McConica[2], I.L. Spain[3], and S.R.D. Udpa[2]

[1]Department of Mechanical Engineering

[2]Department of Agricultural and Chemical Engineering, 3Department of Physics

Colorado State University, Fort Collins, Colorado 80523, USA

ABSTRACT

A matrix of growth times and partial pressures of reactants was used to optimize the length to diameter ratio of benzene derived carbon filaments grown on quartz substrates and iron catalyst. Filaments were grown in a CCVD reactor from benzene and hydrogen at 1000°C. Filament diameters increased with time and increasing partial pressure of benzene. Filament length also increased with growth time, but went through a local minimum then a local maximum as the partial pressure of benzene increased. A theory for the role of hydrogen in the catalytic chemical vapor deposition of carbon filaments is presented along with a theory for the vermicular growth of filaments on quartz substrates.

INTRODUCTION

In order to achieve the objectives of the project, to grow straight submicron diameter carbon filaments diameter ratios greater than 1000 and to obtain sufficient quantities to allow physical characterization of the filaments, any catalysts,reactants, and substrates were investigated [1,2,3].

The system showing results most consistent with the stated objectives was found to be the following:

Reactants - Hydrogen and benzene

Catalyst - $FeSO_4.7H_2O$ and $CaCl_2$ $2H_2O$

Substrate -Quartz= Reaction Temperature - 1000°C

An experimental matrix was designed, using this system, to optimize carbon filament characteristics. Results of the matrix gave filaments with diameters as small as 0.12 μm and aspect ratios of up to 416 with growth times of one hour.

The experimental details of the matrix and results are discussed, also theories for the role of hydrogen and the vermicular growth of filaments on quartz are presented.

EXPERIMENTAL

Equipment

The experiments were carried out in the modified CCVD reactor described, in detail, previously[2]. The system was comprised of a quartz reactor tube, a resistance furnace, a gas mixing manifold, a temperature controlled benzene bubbler, mass flow controllers, a temperature controller, and a turbo pump. Materials

All process gases were manufactured by General Air. The process gases used and their purities were: hydrogen (99.9998%, 4.5μm prepurified), helium (99.998%), and air (breathing quality). Fisher spectroscopic grade benzene provided the hydrocarbon source. Mallinckrodt Chemical Works $FeSO_4.7H_20$ and Fisher Scientific $CaCl_2.2H_2O$ were used as catalysts. Substrates were quartz glass broken into pieces with an area of 2 approximately 1 cm2.

Procedure

The procedure for the experiments consisted of inserting three substrates into the reactor tube and pumping the system down to less than 10-5 torr. The benzene bubbler was repeatedly pumped down to a pressure of less than 10^{-2} torr and repressurized to local atmospheric pressure with H_2 to remove any dissolved atmospheric gases in the bubbler. The system was brought to atmospheric with He and then heated to 1000°C in He. H_2 replaced the He for a 10 minute reduction period, after which C_6H_6 was admitted to the reactor. The H_2 and C_6H_6 flows were maintained for 1 hour, then they were replaced with He and the system cooled to room temperature.

Substrates were prepared with catalyst by spraying a solution of $FeSO_4.7H_20$ and $CaCl_2.2H_2O$ onto eated quartz substrates. The substrates were stored in a desiccator until used.

Scanning Electron Microscopy was performed on a Philips 505 SEM equipped with a Kevex x-ray analysis unit and EDAX polymer windowed x-ray detector. Transmission Electron Microscopy was carried out on a Philips 400T TEM.

RESULTS

Table 1 shows the results of the experiments. The lengths and diameters are averages for the particular substrate. Position in the reactor is delineated by a -1, -2, or -3 after the run number with -1 indicating 2 inches upstream of center, -2 being the center of the reactor, and -3 signifying 2 inches downstream of center. No number after the run number indicates that the substrate was placed in the center of the reactor.

Figures 1 and 2 display the effect of time on the diameter and length of the carbon filaments- Figures 3 and 4 are graphs of the diameter and length of the carbon filaments with the change in partial pressure of C_6H_6. Figures 5 - 13 are photomicrographs representative of each of the experimental runs made. Figures 14 and 15 are a comparison of highly oriented pyrolytic graphite (HOPG) and quartz substrates.

DISCUSSION

The calculated rate of reaction from figure 1 is, on the average, approximately 55 times slower than the reaction rate calculated from figure 2. The difference in reaction rates can be attributed to the different growth mechanisms involved.

The change in diameter of a filament with time is due to the pyrolytic deposition of carbon about the filament, giving rise to the observed tree ring structure of filament cross sections. The change in filament length with time is enhanced through the catalytic action of the iron and calcium.

Figures 3 and 4 show the effect of increasing the partial pressure of benzene. Both filament width (figure 3) and length (figure 4) show a high degree of dependence upon the C_6H_6 partial pressure. Previous experimental data indicated that increasing the partial pressure of the benzene above the limits used in the matrix caused catalyst fouling by carbon and no filament growth. Figure 4 further indicates that between C_6H_6 partial pressures of 30 - 70 torr there exists a residence time effect on the lengthening of carbon filaments.

The difference in reaction rates between filament diameter increase and lengthening and the residence time effect on filament lengthening point to the existence of different hydrocarbon species being accountable for the filament diameter and the filament length reactions. The step wise dehydrogenation of the hydrocarbon has been proposed to be the mechanism for carbon filament growth by many researchers. At the temperatures studied, a wide distribution of hydrocarbon fragments is to be expected. Our hypothesis is that there is a very narrow range of these fragments that is responsible for the catalytic lengthening of carbon filaments. The remaining majority of the hydrocarbons are responsible for the pyrolytic thickening of filaments and the deactivation of catalytic sites.

The exact mechanism of carbon filament formation on catalysts has not yet been determined. Evidence exists for both of the two most popular theories - that the carbonaceous species move through the catalyst particle under a concentration or temperature gradient, or the carbon moves across the surface of the catalyst particle and

forms filaments at energetically favorable surfaces. In either case the ultimate length and thickness of the filaments is highly dependent upon the degree of saturation of the starting hydrocarbon[4,5]. The filament diameter decreases with increasing degree of saturation, since the reaction rate for thickening decreases as the degree of saturation increases. Additionally, saturated hydrocarbons produced filaments with a higher degree of graphitization and well defined outer sheaths. Further evidence for the hypothesis comes from catalyst deactivation studies. At higher temperatures the catalyst is deactivated by the formation of graphitic layers. Lower temperatures enhance the formation of flocculent amorphous carbon from the gas phase polymerization of the hydrocarbon gas that render the catalyst inactive[6,7]. Therefore temperature, as well as the starting hydrocarbon, has major effects on the growth of carbon filaments through the hypothesized growth mechanism.

Another vital link in the hypothesis is the composition of the process gases. A mixture of 90% H2 10% C_2H_2 had filament formation rates 20 times higher than a 90% N_2, 10% C_2H_2 mixture [4]. Other research has shown reduced or under identical conditions. no filament growth in hydrocarbon/carrier gas systems with N_2 [4,8,9]. Hydrogen has also been shown to reactivate catalyst particles that were deactivated by carbon formation[4,8,9,10,11,12] Oxygen will also reactivate catalysts, however oxygen also thins the carbon filaments which does not occur with hydrogen.

The foregoing discussion provides the background for the hypothesis that hydrogen is a reactant required for carbon filament growth and not just a carrier gas. Thermodynamics of the reaction between diatomic and monoatomic hydrogen and a range of hydrocarbons, such as might be present during filament growth, indicate that reactions of the form

$$C_x + H_z \rightarrow C_x H_{1+z} \ldots\ldots\ldots\ldots with_z = 1,2$$

do not occur at the temperatures utilized to grow carbon filaments. However, reactions of the form

$$C_x H_y + H^* > X_x H_{y+1}$$

(where H* is a chemisorbed H atom on the catalyst surface)
can take place[13]. This is most probably why carbon filaments are not thinned by hydrogen at reaction temperatures - catalytic sites are not available along the length of the carbon filament. Reactions between oxygen and carbon or hydrocarbons are favorable at reaction temperatures in the absence of catalysts, which is why the carbon filaments are thinned in the presence of oxygen.

With the two hypotheses presented thus far it is possible to discuss a final hypothesis for the vermicular growth of carbon filaments on quartz substrates. Figure 14 is a SEM of a HOPG substrate showing the catalyst particle. Figure 15 is a SEM of a catalyst particle on a quartz substrate. The surface of the quartz and the catalyst

particle is obscured by a layer of graphitic carbon. This layer is not present on HOPG substrates as it can diffuse into the substrate. This is not possible on quartz substrates, so the carbon layer grows up onto the catalyst particle, eventually deactivating the catalyst particle and ceasing filament growth. Due to differences in the topography or energy of the catalytic site it is hypothesized that this carbon layer is nonuniform, forcing the filament to grow more slowly on part of its circumference because of the imposed diffusion limitations. This gives rise to vermicular filaments that are observed on quartz but not HOPG substrates.

This hypothesis can be expanded to other substrates and catalysts. For example, many catalysts such as nickel and platinum support vermicular carbon filament growth - even on carbon or graphite substrates. Both are known for their high catalytic activity. Sites on these catalysts that have a lower rate of formation of chemisorbed hydrogen may become occluded rapidly giving rise to vermicular filaments.

RECOMMENDATIONS

Further work to identify the hydrocarbon species responsible for the pyrolytic thickening and the catalytic lengthening of carbon filaments would prove extremely valuable. Through control of the process variables the optimal conditions could be maintained to achieve carbon filaments with the desired properties. More precise methods for fragmenting the hydrocarbon, such as plasma enhanced CCVD, should also be investigated.

REFERENCES

1) C.C. Schmitt, Thesis, "Chemical Vapor Deposition of Carbon Filaments From Acetylene as Catalyzed by Iron and Nickel", Colorado State University, Fort Collins, Colorado, U.S.A., 1988.

2) K. Baughman, C. McConica, I.L. Spain, and S.R.D. Udpa, "Growth of Carbon Filaments from Ferrocene Based Iron Catalyzed Decomposition of Benzene", 1988 AFOSR report.

3) K. Baughman, C. McConica, I.L. Spain, and S.R.D. Udpa, "Effects of Catalyst, Additives, and Substrate on the Iron Catalyzed Decomposition of Benzene", 1988 AFOSR report.

4) R.T.K. Baker and P.S. Harris, in "Chemistry and Physics of Carbon", P.L. Walker, Jr. and P.A. Thrower, eds.,14, 1978, P- 83.

5) T. Baird, J.R. Fryer, and B. Grant, Carbon, 12, 1974, P- 591.

6) R.T.K. Baker, D.J.C. Yates, and J.A. Dumesic, in "Coke Formation on Metal Surfaces", L.F. Albright and R.T.K. Baker, eds., ACS Symposium Series 202, 1982, p. 1.

7) R.T.K. Baker, P.S. Harris, R.B. Thomas, and R.J. Waite, J. Catal., 30, 1973, p. 86.

8) H.G. Tennent, U.S. Patent 4,663,230, May 1987.

9) T. Koyama, M. Endo, and Y. Onuma, Jpn. J. Appl. Phys., 11 (4), 1972, p. 445.

10) R.T.K. Baker and R.J. Waite, J. Catal., 37, 1975, p. 101.

11) M. Egashira, H. Katsuki, Y. Uchikawa, and S. Kawasumi, Carbon, 20 (4), 1982, p. 283.

12) R.T.K. Baker, M.A. Barber, P.S. Harris, F.S. Feates, and R.J. Waite, J. Catal., 26, 1972, p. 51.

13) M.W. Chase, Jr., C.A. Davies, J.R. Downey, Jr., D.J. Frurip, R.A. McDonald, and A.N. Syverud, eds., JANAF Thermochemical Tables, Third Edition, J. Phys. and Chem. Ref. Data, 1985.

TABLE 1.

EXPERIMENTAL RUN CONDITIONS AND RESULTS

RUN #	RUN TIME (hr)	AVERAGE L (um)	AVERAGE D (um)	P H_2 (torr)	P C_6H_6 (torr)
B18	0.50	4.50	0.14	566.0	67.7
B14	1.00	10.00	0.26	579.2	55.4
B16	1.50	17.00	0.41	585.0	51.1
B21	2.00	20.00	0.45	584.1	52.4
B17	2.50	18.00	0.45	583.1	50.2
B19-1	1.00	20.00	0.33	546.9	85.0
B19-2		20.00	1.00		
B19-3		20.00	0.77		
B20-1	1.00	30.00	0.27	553.1	79.3
B20-2		30.00	1.00		
B20-3		30.00	0.73		
B23-1	1.00	5.00	0.24	566.1	67.7
B23-2		10.00	0.52		
B23-3		10.00	0.50		
B24-1	1.00	15.00	0.14	593.4	42.6
B24-2		7.00	0.27		
B24-3		5.00	0.16		
B25-1	1.00	10.00	0.14	607.4	29.1
B25-2		15.00	0.18		
B25-3		8.00	0.12		

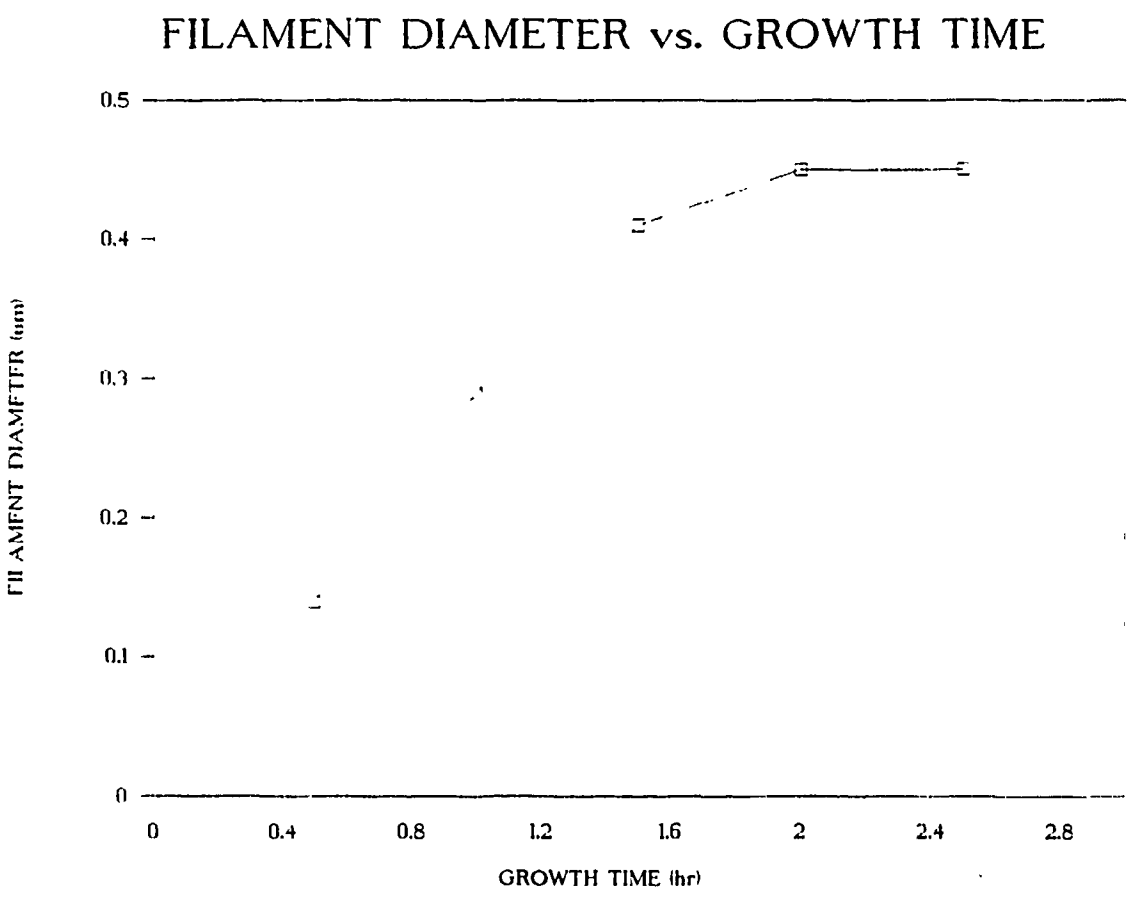

Fig. 1. Filament diameter versus time.

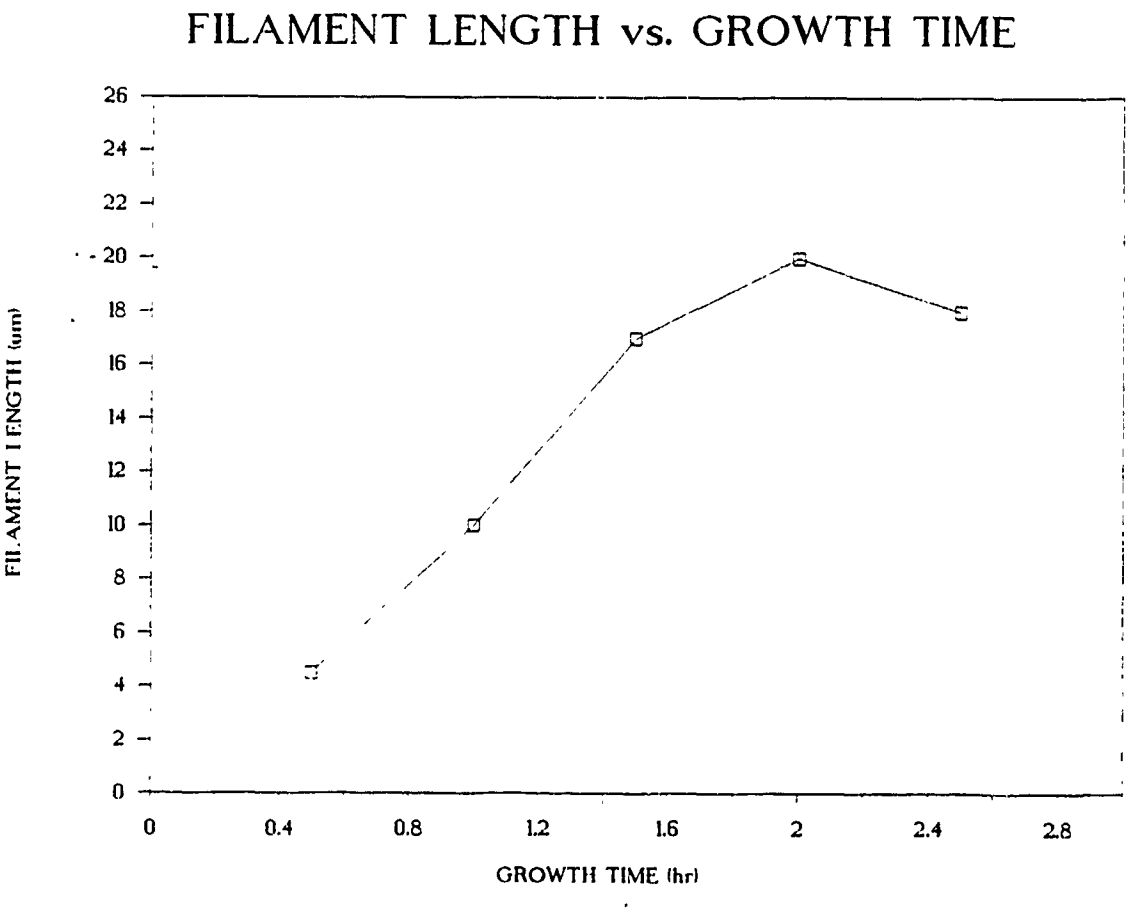

Fig. 2. Filament length versus time.

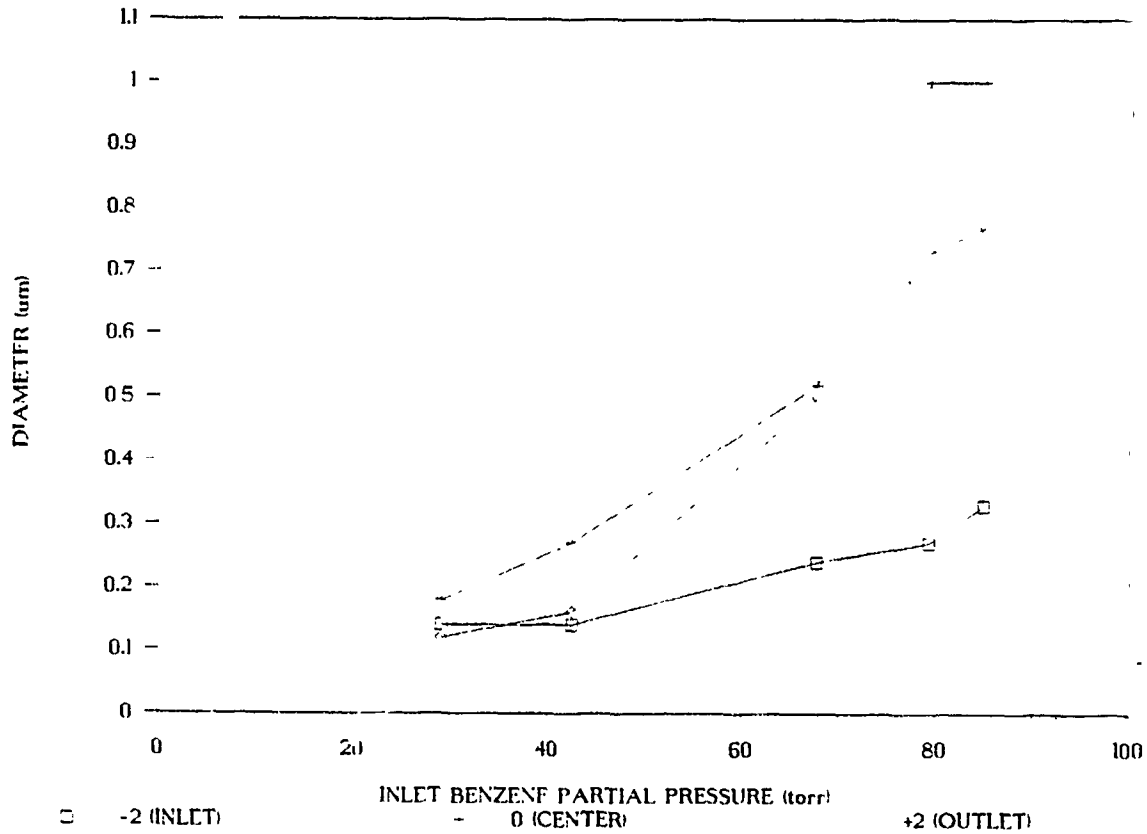

Fig. 3. Filament diameter as a function of substrate position and benzene partial pressure.

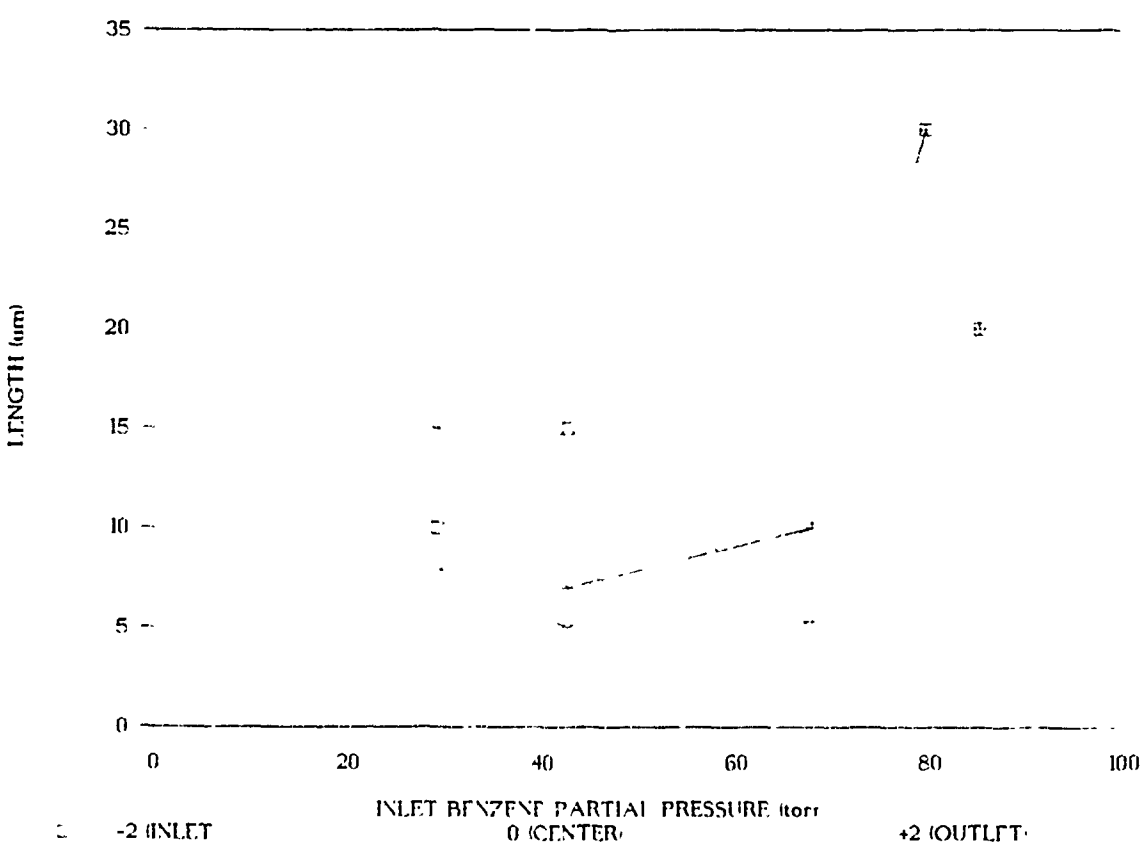

Fig. 4. Filament length as a function of substrate position and benzene partial pressure.

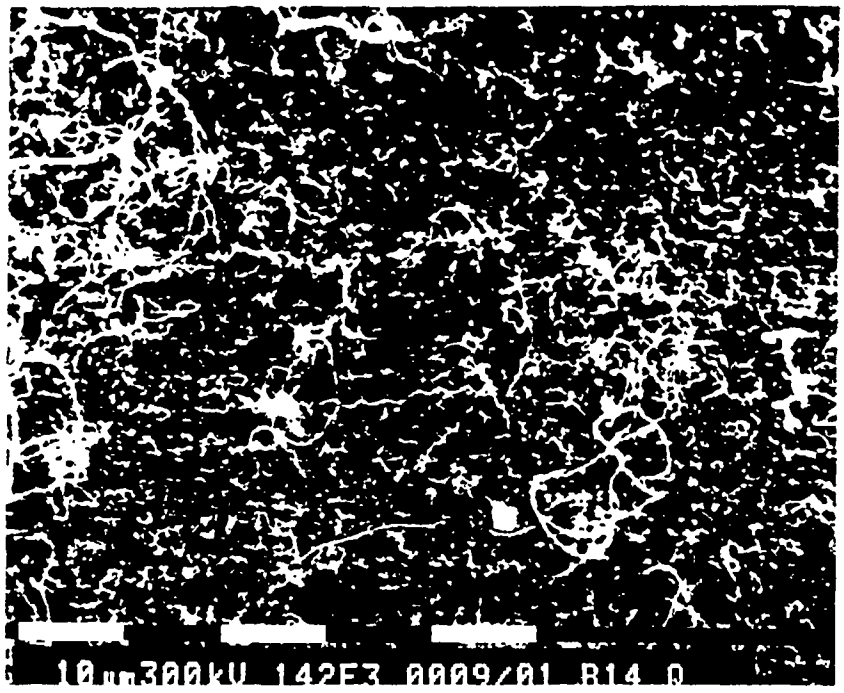

Fig. 5. SEM of run B14.

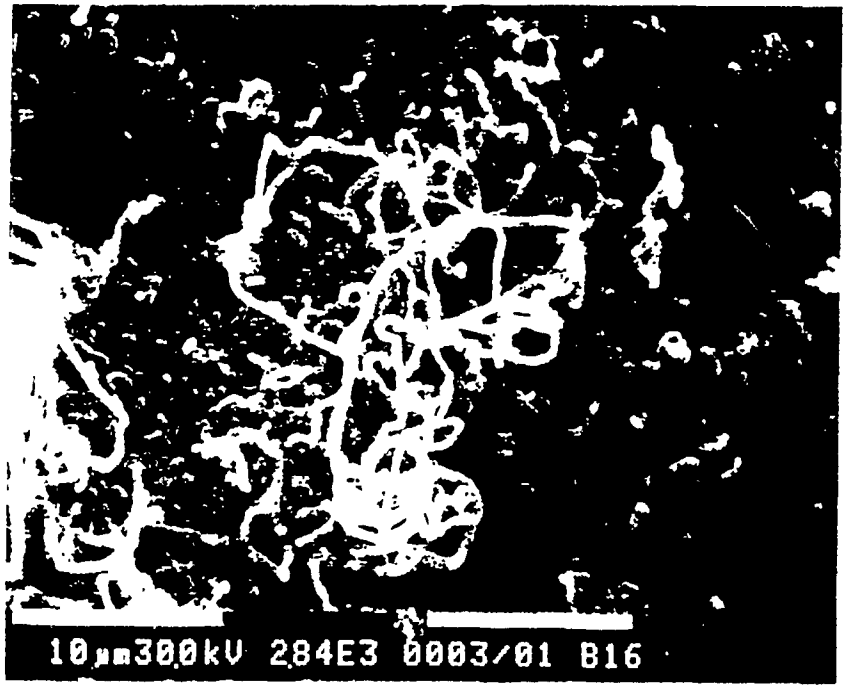

Fig. 6. SEM of run B16.

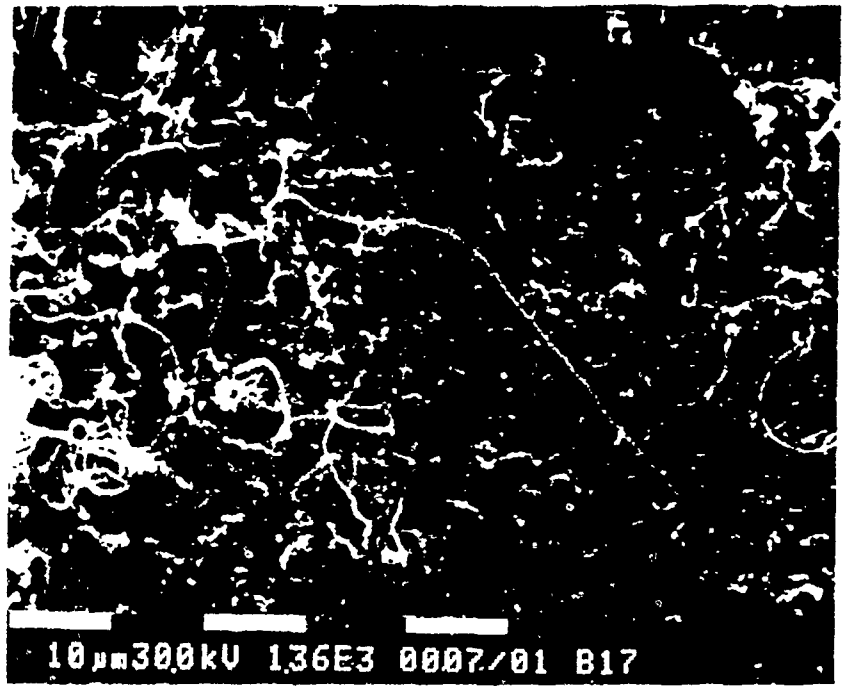

Fig. 7. SEM of run B17.

Fig. 8. SEM of run B18

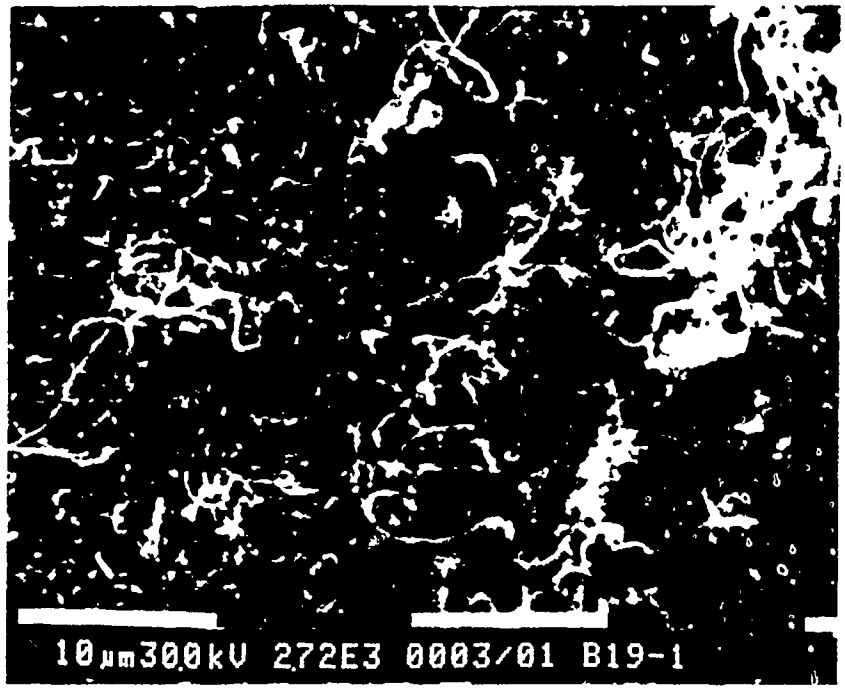

Fig. 9. SEM of run B19-1.

Fig. 10. SEM of run B20-1.

Fig. 11. SEM of run B23-3.

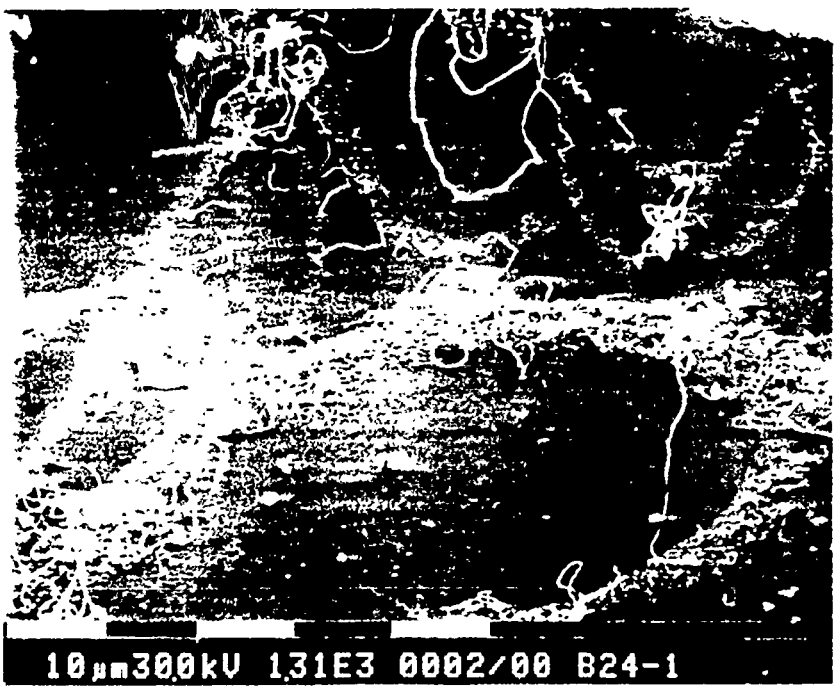

Fig. 12. SEM of run B24-1.

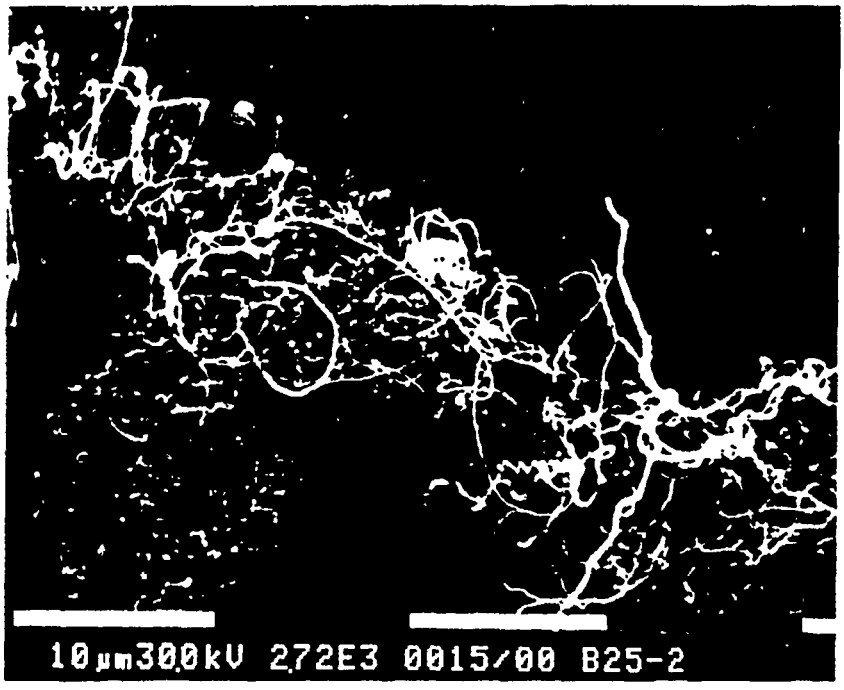

Fig. 13. SEM of run B25-2.

Fig. 13. SEM of a catalyst particle, with filament, on a highly oriented pyrolytic graphite (HOPG) substrate.

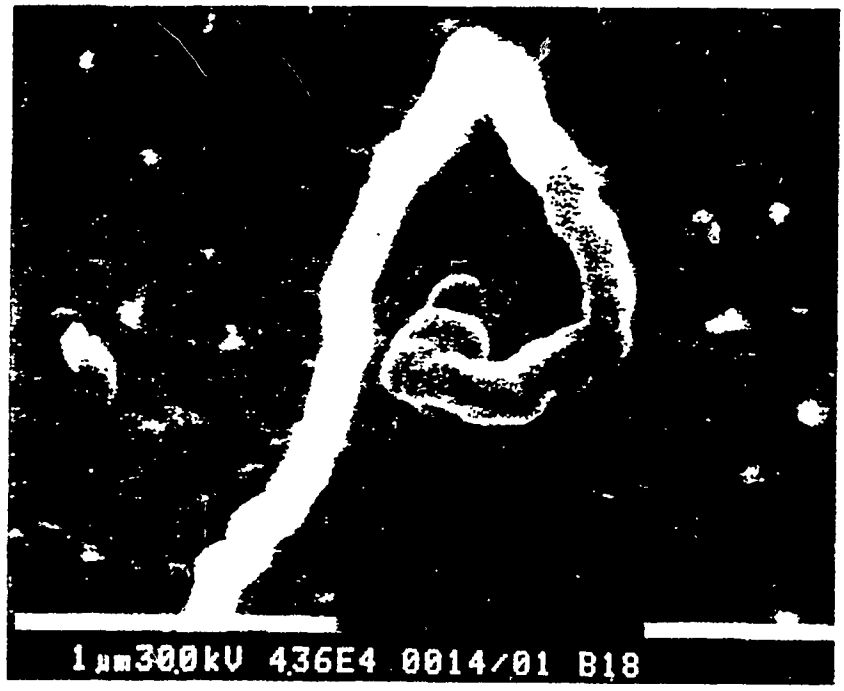

Fig. 14. SEM of a catalyst particle, with filament, on a quartz substrate. Note graphitic carbon layer covering substrate and particle.

ELECTRON MICROSCOPE STUDIES OF CARBON FIIAMENTS

K. Baughman, T. McCormick, C. M. McConica and
I. L. Spain

Abstract

A program of study is underway to obtain structural information on CCVD carbon filaments. Experimental methods include scanning electron microscopy, energy-dispersive x-ray spectrometry, high-resolution transmission electron microscopy, electron diffraction in both selectedarea and convergent-beam modes, and lattice-fringe imaging. This preliminary report discusses techniques and some results on filaments grown at 700 and 850°C.

I. INTRODUCTION

A number of different morphologies of carbon fibers have been described in the literature (e.g., Baird et al, 1971, Endo et al., 1977, Boellaard et al., 1985), and several different mechanisms of growth have been proposed. It is clear that structure is strongly controlled by growth conditions including catalyst particle, substrate, temperature, gas composition, flow rate, etc. A discussion and some results were given in the previous AFOSR Report (Spain, 1986). It is of interest to determine the relationship between structure of the carbon fibers and their growth conditions. It was decided to study the structure of the fibers in finer detail than can be seen in the scanning electron microscope (SEM) to compare different fibers grown under different known growth conditions.

The present report is of work in progress. One of the objectives was to train a graduate student (Kit Baughman) in techniques of transmission electron microscopy (TEM) and electron diffraction. This report outlines the steps we have taken to meet these objectives, the types of equipment and techniques employed, and some preliminary results.

II. EXPERIMENTAL TECHNIQUES

Structural characterization was undertaken using both scanning and transmission electron microscopy. The SEM used was a Philips 505, fitted with secondary and backscattered electron detectors and a Kevex Quantum (thin polymer window) solid state detector and Kevex 8000 multichannel analyzer for energy-dispersive x-ray spectrometry (EDS). Substrates upon which fibers were grown were generally mounted on aluminum stubs and sputter-coated with gold for optimum imaging resolution. Most of the photomicrographs were taken using accelerating voltages of 25 kV and filament current of 0.03 mA. SEM was used primarily to determine the size characteristics of fibers after specific growth experiments and results are described by Schmitt et al. elsewhere in this report.

The TEM used was a Philips 400T fitted with a scanning transmission (STEM) attachment and an EDAX solid state detector and Kevex 8000 multichannel analyzer for EDS. Most of the studies were undertaken with a 100 kV accelerating voltage. Images were recorded using low- and high-magnification modes, and high-resolution TEM (HRTEM) was performed to obtain structural information by lattice-fringe imaging. Electron diffraction patterns were obtained both in selected-area (SAED) and convergent-beam (CBED) modes. Selected-area diffraction employs parallel illumination and an aperture to eliminate diffracted electrons from outside the area of interest and can typically yield diffraction information from areas of 1 micron or more in diameter. In the CBED mode, a focussed probe was used together with a small condenser aperture to increase the resolution of the diffraction spots. A probe diameter of about 70 nm allowed diffraction patterns to be obtained from areas less than 100 nm across. Dark-field imaging uses one or more diffracted beams to form the @mage and was used to determine the region of the sample contributing to a particular diffraction pattern.

Filaments studied in transmission were prepared as follows: Material grown under known conditions was scraped off the substrate into absolute ethanol and put in an ultrasonic bath for several seconds to several minutes.

A drop of the suspension was then evaporated on a holey carbon support film on a 3-mm-diameter grid for TEM investigation. Five different samples were studied by TEM and descriptions of each of these samples are given in the following section.

III. EXPERIMENTAL RESULTS AND DISCUSSION

III. 1 Standards

A number of standards were studied first to allow training of a graduate student (Kit Baughman) who will continue to work in this area. Polycrystalline aluminum and gold and single crystal graphite were among the materials studied to allow the microscopist to gain familiarity with TEM operation, diffraction techniques and interpretation.

III.2 Fibers on Silicon Substrates

Material grown on silicon substrates at 700 and 860°C (Bowers et al., 1988) were examined by TEM. Much of the material on the substrate after the runs was flocculent material (Fig. 1) that showed diffraction patterns consistent with silicon carbide. Although EDS analysis has not yet been performed on the fibers grown on the silicon substrate, diffraction patterns from the fibers resemble tubostratic carbon and not crystalline silicon carbide. Further investigation of these fibers using EDS analysis and x-ray and electron diffraction is currently underway.

III.3. Fibers on Graphite Substrates: Sample RK #1

Typical distribution of size and morphology of CCVD filaments in this sample are shown in Fig. 2. These were grown previously (Spain, 1986, p. 41) at 850°C on a graphite substrate using a Technical grade acetylene and hydrogen 1:7 mixture for 20 minutes (total flow - 80 cc/min). The presence of acetone impurities in the acetylene may have had an effect on the growth.

In addition to relatively straight, feathery-structured filaments, there are a number of filaments that exhibit helical morphologies. They appear to have a uniform width of approximately 0.2 microns, but some of the fibers are helical along parts of their length and straight along other parts (Fig. 3). It has been summarized that twisting can occur as a result of a tilted, solid, catalyst particle (see Baker and Harris,
1978, for a review). Diffraction patterns showed these fibers to be turbostratic but with no preferred orientation. The feathery-structured fibers in this sample are composed of turbostratic carbon showing strong preferred orientation. Figure 4 shows typical fibers of this type together with microdiffraction patterns (CBED) of either side of the fiber. Analyses of diffraction patterns indicate that graphitic c-axes are oriented more or less parallel to the "branches." These results are consistent with observations of Boellaard et al. (1985). Many of the fibers show V-shaped fractured ends, also observed by Boellaard et al. and interpreted to be (002) cleavage surfaces. Separation of the "branches" is also evident in many of the fibers, particularly at the edges. The fibers also commonly show a core of less dense material, or possibly a hollow core. No catalyst particles were observed in these fibers.

Boellaard et al. (1985) proposed a model for growth of these feathery type of fibers whereby carbon is

excreted at the interface between the fiber and a solid, conical-shaped catalyst particle so that conical graphitic layers are parallel to this interface. Since the growth direction is oblique to the graphite planes, edge dislocations are introduced. Therefore, these areas of well-ordered graphitic carbon may be separated by areas in which there is local structural disorder. The separation of the branches at the edges of the fibers may result from structural weakness in these disordered zones.

III.4 Graphite Substrate: Sample #AI

This sample (see Section II.1 of this report) was prepared by passing a 50:1 hydrogen/acetylene mixture at 600°C over a AYF-5Q graphite substrate. SEM did not reveal any fiber growth, so TEM was used to determine the presence of fibers. Very short fibers were observed in flocculent material on the substrate.

III.5 Silica Substrate: Sample #4

This sample was prepared (see Section II.1 of this report) by passing a 10:1 hydrogen/acetylene mixture over powdered silica with Ni catalyst at 850°C. No fibers were observed in the TEM, and only flocculent material was present.

III.6 Graphite Substrate: Sample #3-I

Fibers were grown on AYF-5Q graphite substrate using Ni as a catalyst (see Section II.1 of this report) by passing a 10:1 hydrogen/acetylene mixture over the substrate at 850°C. Very thin and long fibers are present in this sample (Fig. 5), along with graphitic non-fibrous carbon. The fibers are typically about 25-35 nm wide and appear to have hollow cores 20-30 nm in diameter. The outer parts of the fibers are seen in Fig. 5 to have variable contrast resulting from a range of orientations, the darker parts being in a strong diffraction condition. This suggests that the fibers have crystalline edges with strong preferred orientation. Due to the reduced thickness of these fibers, HRTEM was possible. Graphitic fringes (0.34 nm) are shown in Fig. 6 to be parallel to the length of the fiber. Some of the graphite layers can also be seen peeling away from the wall of the fiber toward the center. These fibers are similar to those described by Baird et al. (1971). No catalyst particles were seen in this sample, although further work is currently in progress.

REFERENCES

Baird, T., J. R. Fryer, and B. Grant (197@) Structure of Fibrous Carbon. Nature, 233, 329-330.

Baker, R. T. K. and P. S. Harris (1978) Chemistry and Physics of Carbon 14, 83.

Boellaard,E., P. K. de Bokx, A. @. H. M. Kock, and J. W. Geus (@985) The Formation of Filamentous Carbon on Iron and Nickel Catalysts-- III. Morphology. J. Catalysis, @@, 481-490.

Endo, M., A. Oberlin, and T. Koyama (1977) High Resolution Electron Microscopy of Graphitization Carbon Fiber Prepared by Benzene Decomposition. Japan. J. Appl. Phys. 1@, 1519.

Spain, I. L. (1986) Final Report to AFOSP., "Carbon Whisker Study" (Contract #F49620-84-K-0006).

Zhao, Y. X., C. W. Bowers, and I. L. Spain (1988) "Graphitic Nature of Chemical Vapor-Deposited Carbon Filaments Grown on S@licon Surfaces from Acetylene" to be published in Carbon (and p. SO in Spain, 1936).

FIGURE CAPTIONS

Fig.1. TEM @mage of flocculent material on silicon substrate. Scale bar - 5000 A.

Fig.2. TEM image showing the range of fiber morphologies grown on graphite substrate. Scale bar - 2 microns.

Fig.3. TEM image of a single straight carbon fiber with helical ends. Scale bar - S microns.

Fig.4. Feathery type of carbon fibers. (a) TEM image showing (002) cleavage on fractured end (upper left) and branching structure of fibers. A paler line running down the center of the fibers suggests a hollow core. Scale bar - 5000 A. (b) Higher magnification TEM image of fiber in (a). Microdiffraction pattern from upper left of the fiber is shown in the upper left corner, microdiffraction from the lower, right side of the fiber is shown in the lower right. Scale bar - 1000 A.

Fig. 5. Thin carbon filaments on graphite substrate together with nonfibrous ¿ .tic carbon. Scale bar 1000 A.

Fig. 6. HRTEM image of carbon filament showing 3.4 A fringes on the edges of the fiber. Scale bar -100 A.

Fig. 1. TEM image of flocculent material on silicon substrate. Scale bar = 5000 Å.

Fig. 2. TEM image showing the range of fiber morphologies grown on graphite substrate. Scale bar = 2 microns.

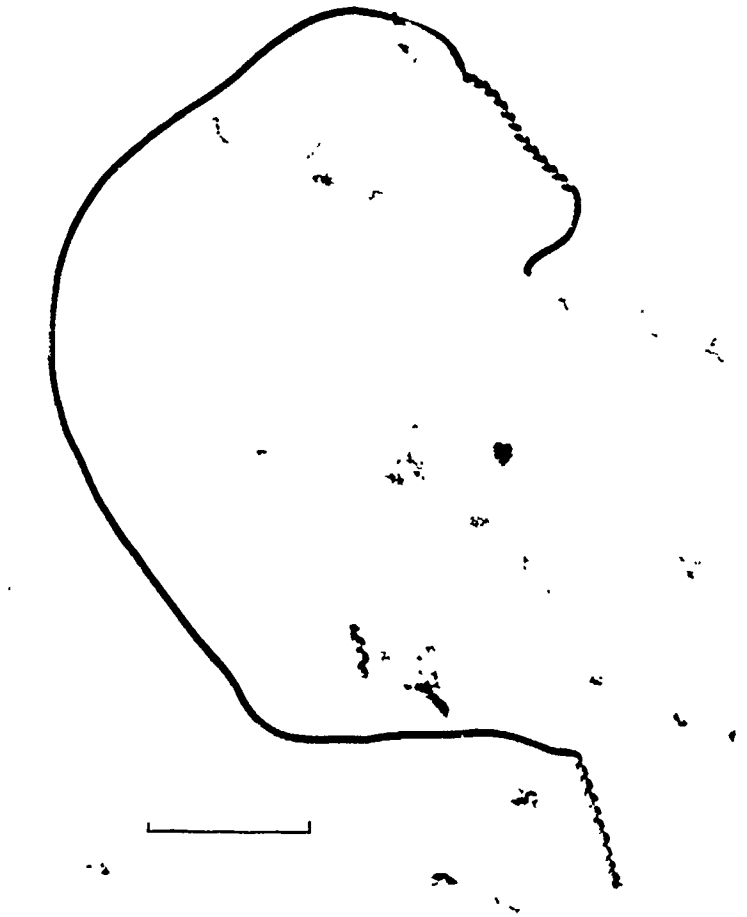

Fig. 3. TEM image of a single straight carbon fiber with helical ends. Scale bar = 5 microns.

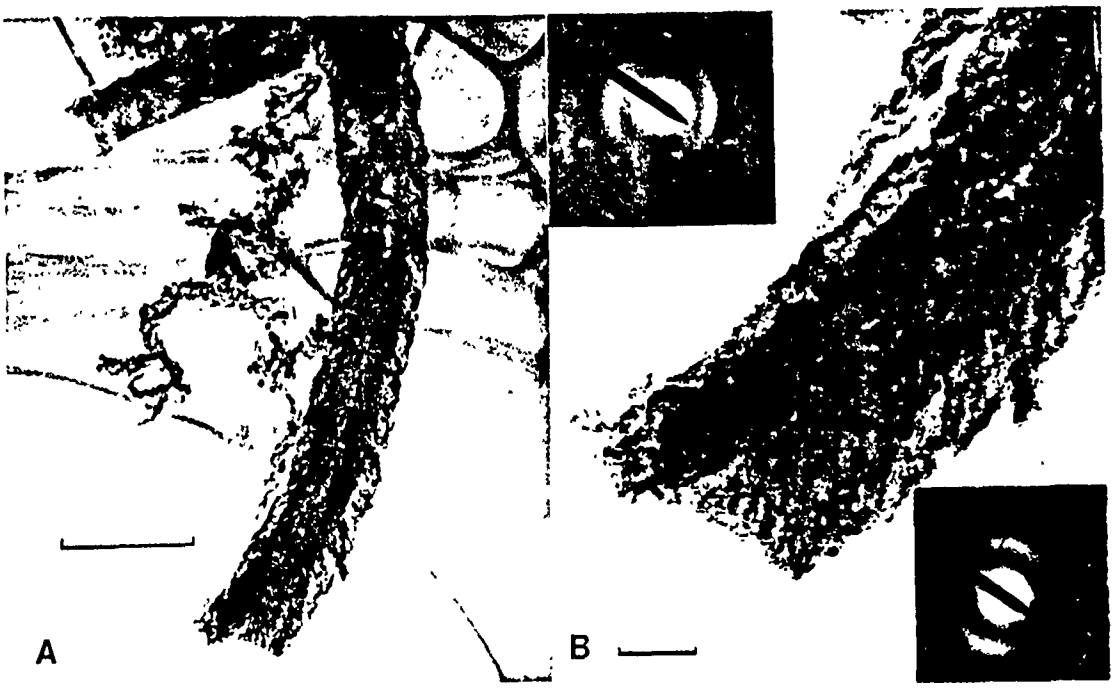

Fig. 4. Feathery type of carbon fibers. (a) TEM image showing (002) cleavage on fractured end (upper left) and branching structure of fibers. A paler line running down the center of the fibers suggests a hollow core. Scale bar = 5000 Å. (b) Higher magnification TEM image of fiber in (a). Microdiffraction pattern from upper left of the fiber is shown in the upper left corner, microdiffraction from the lower, right side of the fiber is shown in the lower right. Scale bar = 1000 Å.

Fig. 5. Thin carbon filaments on graphite substrate together with non-fibrous graphitic carbon. Scale bar = 1000 Å.

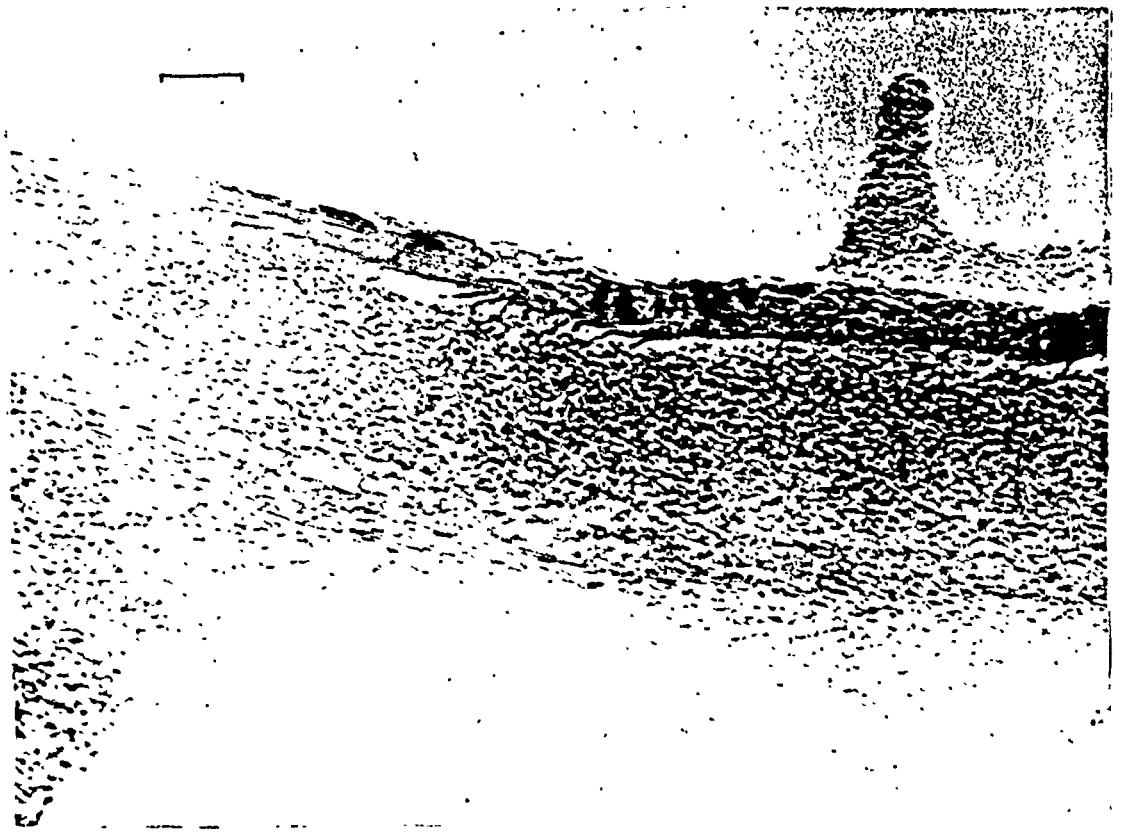

Fig. 6. HRTEM image of carbon filament showing 3.4 Å fringes on the edges of the fiber. Scale bar =100 Å.

CARBON FIBER PROJECT REPORT

SUMMARY OF WORK DONE BY DINESH UDPA AS RESEARCH ASSISTANT

WORK SUMMARY

SUMMARY OF WORK DONE ON CARBON FIBER PROJECT BY DINESH UDPA

The work done by me under this project can be broadly divided into two phases.

Phase-1 : Jcint work with Mr. Kit Baughman.

Phase-2 : Independent work on fiber growth.

PHASE-1 WORK

I Joined the carbon fiber project on July 1, 1988 as Research Assistant and initially was assigned to assist Mr. Kit Baughman in planning and execution of experiments for growing carbon fibers in the existing scheme of experimental set-up.

The split of responsibility between Mr.Kit Baughman and me being that while I planned and ran the experiments, Mr.Baughman would analyze the samples on SEM. The catalyzed substrates were prepared by Mr.Baughman.

The operating conditions for growing carbon fibers on Quartz substrates in a Quartz reactor were fixed at $1000^{0}C$ temperature and atmospheric pressure. The catalyst was deposited on the substrate by spraying a solution of Iron sulphate/ Calcium chloride with a hair spray bottle. The growth characteristics were studied by varying the Operating Temperature, H_2 - C_6H_6 Ratio, Total Flow Rate at constant H_2 - C_6H_6 ratio and the Duration of Reaction and observing their influence on Carbon Fiber Length and Diameter. The charts showing the growth trends are attached herewith. Benzene was used as the source of carbon, Helium was used as the inert purge gas and Hydrogen was used as the carrier gas.

With Mr.Baughman leaving the project in October 1989, I was asked to repeat the experiments to check reproducibility of growth under similar conditions and confirm the findings. To our surprise, I found that the growth characteristics varied even under identical operating conditions. This disturbing finding led us to redefine our research objectives for a more meaningful outcome which is covered under Phase-2 work.

Details of the work done in Phase-1 can be referred to in Mr.Kit Baughman's M.S. Thesis.

OPERATING PROCEDURES

* PROCESS
* SEM

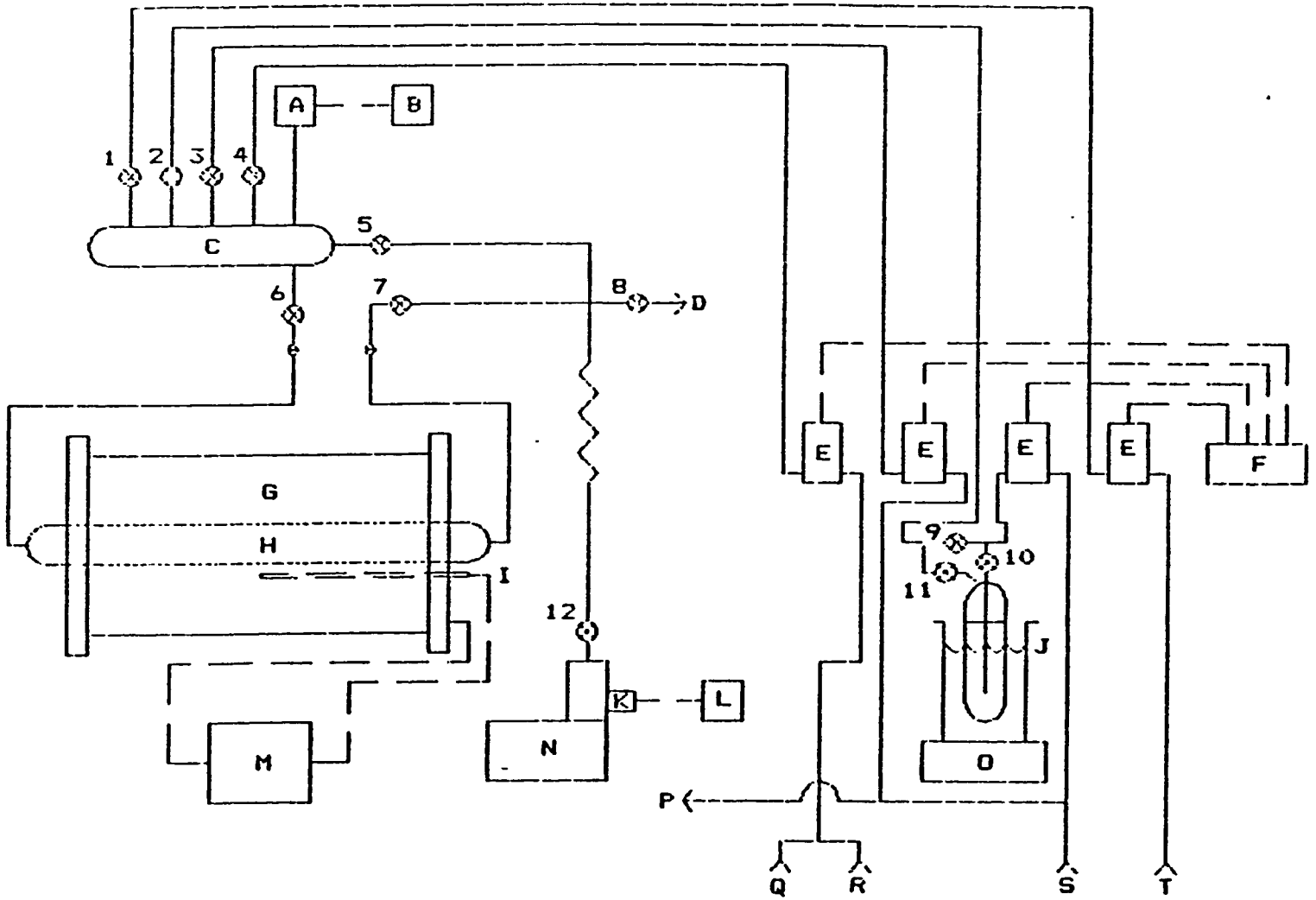

1 - 11: High Vacuum Glass Stopcocks
12 : Stainless Steel Nupro Valve (SS-4H)

A : Capacitance Manometer
B : Manifold Pressure Readout
C : Manifold
D : Exhaust Vent
E : Mass Flow Controllers
F : Flow Controller and Readout
G : Resistance Furnace
H : Reactor Tube
I : Thermocouple
J : Liquid Hydrocarbon Bubbler and Water Bath

K : Cold-Cathode Ion Gauge
L : Ion Gauge Readout
M : Programmable Temperature Controller and Readout
N : Vacuum Pumping Unit
O : Hot Plate
P : Hydrogen Carrier Gas for Organometallics
Q : Compressed Air Inlet
R : Helium Inlet
S : Hydrogen Inlet
T : Hydrocarbon Gas Inlet

OPERATING INSTRUCTIONS

Catalyst Vapor Deposition

1. Weigh the required amount of Ferrocene on the mettler balance. (0.05 g)
2. Place the Ferrocene at the inlet of the reactor.
3. Place the clean, dry substrates at the center of reactor.
4. Wipe the reactor clean with methanol rinsed tissue paper.
5. Place the reactor in the furnace with the center of reactor located nearly at the center of furnace.
6. Grease the reactor ends and place the end connections in position.
7. Place the thermocouple in position. Insulate the exposed portion of the reactor at both ends to seal the gap between the furnace and reactor with asbestos rope.
8. Close all the gas cylinder valves and set the flow controllers to the maximum.
9. Open the manifold valves, reactor inlet and outlet valves.
10. Open the vacuum pump suction valve slowly to avoid tripping of the pump and evacuate the system to eliminate oxygen.
11. Once the pressure gauge reading and flow controller display reads zero, close all the manifold valves and switch off the controllers.
12. Open the valves on Helium and Hydrogen gas bottles and shut off the vacuum pump suction valve.
13. Open the Helium manifold valve and switch on the flow controller # 4 and allow the pressure to reach ~650 mm Hg and then open the vent valve.
14. Reduce the flow to 40 sccm and allow the pressure to stabilize.
15. Set the H_{21} flow to 40 sccm.

16. Set the temperature controller heating cycle as follows:

set point #	set point-^{0}C	time #	time duration-mts
0	150	-	--
1	250	1	10
2	500	2	5
3	700	3	5
4	800	4	10
5	900	5	10
6	1000	6	99
7	1000	7	99
8	1000	8	99

17. Start heating by pressing START/AUTO/YES and simultaneously start the stop clock.
18. Log the temperatures every 10 minutes and when the temperature reaches 1000^{0}C (in about 45 minutes) switch on controller # 3, open H_{21} manifold valve (# 3), close He manifold valve (# 4) and switch off controller # 4.
19. Reduce the catalyst for 15 minutes. Then stop heating and open the furnace cooling air, open the He manifold valve and switch on the flow controller # 4 . Shut off the H_{21} manifold valve and flow controller # 3 .
20. When the temperature falls below 100^{0}C, close the # 4 manifold valve for He and the flow controller # 4 . Close all the gas cylinder valves and furnace cooling air valve.
21. Remove the reactor from the furnace and carefully remove the substrates from the furnace, place them in a petri dish and tag it. Place the petri dish in a desiccator.

Benzene Runs

1. Place the catalyzed substrates at the center of the reactor. Place the reactor in the furnace after wiping clean with methanol. The center of the reactor should approximately match the center of furnace.
2. Grease the reactor ends and place the end connections.
3. Ensure that all gas cylinder valves and furnace cooling air valve is closed.
4. Weigh the benzene bubbler on a single-pan scale and note the weight in the log book.
5. Place the thermocouple in position. Insulate the exposed portion of the reactor at both ends to seal the gap between the furnace and reactor with asbestos rope.
6. Set the flow controllers to the maximum and open all the manifold valves, reactor inlet and outlet valves.
7. Open the vacuum pump suction valve slowly to avoid tripping of the pump and evacuate the system to eliminate oxygen.
8. Once the pressure gauge reading and all flow controller displays reads zero, close all the manifold valves and switch off the controllers.
9. Open the valves on Helium and Hydrogen gas bottles and shut off the vacuum pump suction valve, reactor inlet and outlet valves.
10. Open the H_{22} manifold valve (# 2) and switch on the flow controller # 2 and when the pressure reads about 300 mm Hg, open the benzene bubbler outlet valve, inlet valve and close the by-pass valve in the same order of sequence. This is to eliminate the Oxygen in the benzene.
11. When the pressure reads about 650 mm Hg, shut off the flow controller, H_{22} manifold valve, benzene bubbler inlet and outlet valves and open the bubbler by-pass valve.
12. Open the reactor by-pass valve and the vacuum pump suction valve. Evacuate the system until the pressure reads 0.

13. Close the reactor by-pass valve and the vacuum pump suction valve.
14. Open the He manifold valve and the flow controller # 4.
15. Open the reactor inlet and outlet valves and when the pressure reaches 650 mm Hg open the vent valve.
16. Set the He flow controller to 40 sccm and H_{21} and H_{22} flow controllers at the desired levels.
17. Set the temperature controller heating cycle as follows:

set point #	set point-^{0}C	time #	time duration-mts
0	400	-	--
1	600	1	5
2	800	2	10
3	1000	3	10
4	1150	4	99
5	1150	5	99
6	1150	6	99
7	1150	7	99
8	1150	8	99

17. Start heating by pressing START/AUTO/YES and simultaneously start the stop clock.
18. Start the hot plate heater and manually control the benzene bubbler bath temperature at the required level.
19. Log the temperatures every 10 minutes and when the temperature reaches 1150^{0}C.
20. Once temperature reaches 1000^{0}C switch on flow controller # 3, open H_{21} manifold valve (# 3), close He manifold valve (# 4) and switch off controller # 4.
21. When temperature reaches 1150^{0}C, open H_{22} manifold valve, flow controller # 2, benzene bubbler inlet valve, outlet valve and close the bubbler by-pass valve.
22. Confirm Hydrogen flows at the required levels.
23. Log the temperatures and pressure at every 20 minute intervals.

24. At the end of the reaction time, close the flow controller # 2, H_{22} manifold valve, benzene bubbler inlet and outlet valves, open He flow controller # 4 and He manifold valve and close H_{21} manifold valve and flow controller # 3.
25. Open furnace cooling air.
26. Weigh the benzene bubbler to calculate the amount of benzene consumed.
27. Once the temperature falls below $100^{0}C$, shut off the flow controller # 4, He manifold valve # 4, furnace cooling air valve and all gas cylinder valves.
28. Remove the reactor from the furnace and carefully remove the substrates, place them in a tagged petri dish and place the petri dish in a desiccator.

Reactor Cleaning

1. Place the reactor in the furnace and connect the inlet side of the system to the reactor. The reactor outlet is left open.
2. Start the furnace heating by pressing START/MANUAL/YES and make sure that the display reads MAN, if not press MANUAL again.
3. Open the Compressed air bottle and set the flow controller # 4 to about 100 sccm. Open He manifold valve (# 4) and switch on the flow controller # 4.
4. When the reactor temperature reaches above $800^{0}C$, start moving reactor about two inches at a time and holding the reactor at about $800^{0}C$ for about a minute for burning out the carbon.
5. Stop heating once the entire reactor has been exposed, close the flow controller, manifold valve and gas cylinder valve.
6. If the reactor was used for catalyst deposition, then the reactor need to be immersed in aqua regia for removing iron deposits from the walls for about a day.

PHASE-2 WORK

The first step in the Phase-2 was to identify the goals of the project and adopt the ' Management by Objectives ' technique to achieve the goals. The Objectives of further research work were identified as follows:

1. To Trouble-Shoot the Phase-1 set-up and identify the system bottlenecks that contributed to irregularities in growth characteristics.

2. Modify the system to eliminate the draw-backs in the Phase-1 set-up and ensure reproducibility.

3. Optimize the operating parameters which would enable us to grow long carbon fibers.

4. Test the physical/electrical properties of carbon fibers grown.

5. Identify the precursor which are responsible for the fiber growth through Raman Spectra Analysis of exit gases and suggest a mechanism for carbon fiber growth.

6. In addition, after the recent meeting with the Airforce, it was decided to modify the reactor from Hot-wall to Cold-Wall system to enable insitu Raman Spectra Analysis.

Objective No. 1. - Trouble Shooting

On critical analysis of the Phase-1 system for finding reasons that contributed to the irregular growth characteristics, we found atleast two major factors that influenced the parameters.

The first reason is the lack of control of catalyst density on substrate surface due to highly individualistic method adopted for catalyst deposition on substrate. The method of catalyst deposition using a spray bottle is too individualistic and hence very difficult to reproduce. Some of the factors contributing to the inconsistency in spraying technique are listed below:

1) The pressure on the spray head and the time taken for each squirting varies from person to person.
2) The distance of spray nozzle tip from the substrate surface may vary each time one sprays and also with person.
3) The relative radial location of substrate in the projected spray cone circle contributes to variation of catalyst density.

The second reason is that the Benzene bubbler is located relatively far away from the reactor and there is a significant length of tubing on the downstream side of bubbler which is left exposed to ambient temperature. Hence, even though the bubbler is immersed in a water bath held manually at a constant temperature, the Hydrogen gas saturated with Benzene vapor tends to cool down during it's flow through the bare tubing, causing the Benzene to condense. This causes inconsistent Benzene-Hydrogen ratio in the reactant feed gas mixture, even though the manipulative variables were all held steady. This problem was noticed because the phase-1 experiments were conducted during summer and early autumn while reproducibility runs were made in winter, thereby experiencing wide variation in ambient temperatures.

Besides above, most literature cited good carbon fiber growth above $1000^{0}C$. In the existing set-up, use of Quartz as material of construction for reactor and substrate material limited operating at higher temperatures. Hence, in view of above shortcomings in the present set-up and the need to run experiments at higher temperatures, the experimental set-up needed to be modified.

Objective No. 2. - System Modification

The primary emphasis in achieving this objective was to eliminate or minimize the influence of factors identified in the trouble-shooting which contributed to inconsistent results and poor carbon fiber growth.

Improvement on Catalyst Deposition Technique.

The catalyst deposition method was modified to remove the individualistic factors which introduced inconsistencies in Phase-1 results. The vapor deposition method of catalyst deposition was adopted by placing a fixed amount of Ferrocene at the inlet of reactor and heating under inert atmosphere. Thus, the variables in this method of deposition were identified to be amount of Ferrocene placed at the inlet of reactor, Inert carrier gas flow conditions and furnace heating cycle during deposition. The premise for adopting this technique is that the flow conditions in the reactor during deposition can be held constant by the mass flow meters and the heating cycle can be reproduced through the pre-programed automatic temperature controller. The Ferrocene can be accurately measured up to even fourth decimal place accuracy on the mettler balance. Thus, the vapor deposition method of catalyst deposition offers to be a far superior and reproducible technique compared to the spray technique and is free from human factor as all key variables are controlled accurately.

Ambient Temperature Influence Minimization.

The problem of ambient temperature influence on Benzene consumption was minimized by relocating the benzene bubbler closer to manifold, heat-taping the exposed portion of bubbler and insulating the downstream tubing up to the reactor. This should minimize the Benzene condensation downstream of bubbler and lead to more consistent Hydrogen-Benzene ratio.

Overcoming Operating Temperature Limitations.

In order to operate at higher temperatures, the reactor material of construction was changed to ceramic (Manufactured by Coors) instead of quartz. This ceramic material could withstand up to $1700^{0}C$, However the operating temperature was limited to $1200^{0}C$ only, due to furnace heating limitations.

Initially, Graphite was chosen as the substrate material for carbon growth at higher operating temperatures - since Graphite could withstand the temperature and was stable at proposed operating temperature range in absence of oxygen. However, during test runs, we observed an unusual surface activity on Graphite substrates. After the catalyst was deposited on Graphite, we noticed that the Iron disappeared from the surface of substrate during subsequent heating process for fiber growth. This was noticed from significant difference in carbon fiber growth densities between Graphite and Quartz substrates and later on confirmed through catalyst density measurements on EDX. This led us to change the substrate material for fiber growth studies from Graphite to Ceramic (Similar to reactor material - Manufactured by Coors.). The disappearance was attributed to diffusion of Iron from surface to the bulk of substrate.

A series of experiments were conducted first to test the efficacy of catalyst vapor deposition technique, comparing the growth densities between Graphite, Ceramic and Quartz substrate materials and confirming suitability of Quartz material as substrates.

Objective No. 3. - Operating Parameters Optimization

Prior to starting of the optimization experiments, a detailed work on characterization of ceramic reactor and thermocouples were done, wherein the thermocouple outputs were calibrated with respect to the Automatic Temperature Controller Display and the temperature profile inside the Ceramic reactor was plotted with reference to the controller readout. The results are attached herewith:

This was then followed by optimization of operating parameters to maximize carbon fiber growth in terms of length and diameter through variation of operating temperature, Hydrogen-Benzene ratio, total flow rates and duration of reaction. Each of the parameter was varied one at a time and the effect on the carbon fiber length and diameter was plotted.

The results are summarized in the following tables and graphs.

However, it is sufficient to say that the effect of the modifications made in the Phase-2 on the growth characteristics of carbon fiber has been very significant. The Phase-1 studies had yielded carbon fibers of length of the order of magnitude 40-50 microns and diameters of around a micron. In comparison, the Phase-2 Experiments yielded fibers of length up to 15.0 millimeters and diameters up to 60-90 microns.

SUMMARY

RUN #	REACTION TIME Hrs.	$H_2:C_6H_6$ RATIO	REACTION TEMP. ^oC	TOTAL FLOW SCCM	REMARKS
REACTION TIME EFFECT ON GROWTH					
B-016	1.5	10.26	1000	40	EXPERIMENTS DONE ON
B-017	2.5	10.45	1000	40	QUARTZ SUBSTRATE
B-018	0.5	7.52	1000	40	USING BENZENE AS
B-021	2.0	10.03	1000	40	CARBON SOURCE
B-022	1.0	9.40	1000	40	
$H_2:C_6H_6$ RATIO CHANGE EFFECT ON GROWTH					
B-019	1.0	5.79	1000	40	
B-020	1.0	6.27	1000	40	
B-023	1.0	7.52	1000	40	-DO-
B-024	1.0	12.53	1000	40	
B-025	1.0	18.80	1000	40	
TOTAL FLOW RATE CHANGE EFFECT ON GROWTH					
B-026	1.0	6.27	1000	80	
B-027	1.0	6.48	1000	100	
B-028	1.0	6.64	1000	120	-DO-
B-029	1.0	7.52	1000	140	
TEMPERATURE EFFECT ON GROWTH					
B-030	1.0	6.84	600	80	
B-031	1.0	7.16	700	80	
B-032	1.0	5.79	800	80	-DO-
B-033	0.83	6.84	1000	80	
B-034	1.0	7.16	1000	80	
REPRODUCIBILITY CHECK RUNS					DIAM /LENGTH /RHO
B-037	1.0	5.37	1000	40	8.0μ/ 2.0mm/ SG
B-038	1.0	9.40	1000	40	16.0μ/ 0.7mm/ SG
B-039	1.0	9.40	1000	40	4.4μ/ 2.3mm/ PD
B-040	1.0	8.36	1000	40	1.8μ/ 55.0 μ/ GD
B-041	1.0	6.27	1000	40	1.7μ/ 73.0 μ/ SG
B-042	2.0	7.91	1000	40	5.0μ/ENTAGLD/ GD
B-048	2.0	8.85	1000	40	1.0μ/ 53.0 μ/ GD
B-049	2.0	8.36	1000	40	2.8μ/ENTAGLD/ GD
B-050	2.0	8.36	1000	40	3.3μ/110.0 μ/ FG
B-054	1.0	7.16	1000	80	0.7μ/ 0.16 μ/ GD
B-056	1.0	7.92	1000	80	1.0μ/ENTAGLD/ GD

TUNGSTEN CARBIDE SUBSTRATE RUNS

B-043	1.0	7.52	1000	40	NO GROWTH
B-045	1.0	6.26	1000	80	NO GROWTH
B-051	1.0	7.52	1000	80	NO GROWTH

VAPOR DEPOSITED CATALYST SUBSTRATE RUNS
(GRAPHITE / QUARTZ / CERAMIC SUBSTRATE MATERIALS)

Following experiments were conducted to confirm growth of fibers after vapor deposition and also to confirm disappearance of catalyst on graphite substrate surface as reflected in poor fiber density characteristics in comparison with Quartz substrates.

B-053	1.0	7.52	1000	40	G--L=25.0μ/D=1.2μ/SG Q--L=40.0μ/D=0.92μ/ ENTAGLD/GD
B-061	1.0	8.36	1000	40	G--L=14.0/D=0.29μ/FG Q--L=ENTGLD/D=0.44μ/ GD
B-062	1.0	7.52	1000	40	G-L=37.5μ/D=0.37μ/SG
B-065	1.0	8.36	1000	40	G-L=20.0μ/D=0.45μ/SG
B-067	1.0	7.52	1000	40	G-L=0.13μ/D=0.72μ/SG
B-068	1.0	10.74	1000	40	G-L=44.0μ/D=0.46μ/SG
B-070	1.0	7.52	1000	40	G-L=33.0μ/D=0.28μ/SG Q-L=0.2mm/D=1.00μ/FG
B-072	1.0	6.84	1000	40	G-L=11.0μ/D=0.60μ/SG
B-078	1.0	4.70	1000	40	G-L=21.0U/D=1.00U/SG

Following experiments were conducted to confirm growth of fibers on new ceramic substrates, suitable for high temperature operation, using vapor deposition method of catalyst deposition and compare the density with Quartz substrates.

B-077	1.0	10.74	1000	40	Q-L=ENTGLD/D=0.7μ/GD C-L=ENTGLD/D=0.8μ/GD
B-079	1.0	9.40	1000	40	C-L=33.0μ/D=0.47μ/FG
B-082	1.0	9.40	1000	40	C-L=20.0μ/D=0.38μ/FG Q-L=20.0μ/D=0.42μ/FG
B-083	1.0	9.40	1000	40	C-L=0.2mm/D=0.50μ/FG Q-L=96.0μ/D=0.50μ/FG
B-096	1.0	6.27	1000	40	C-L=30.0μ/D=0.60μ/GD

G=GRAPHITE SUBSTRATE ; Q=QUARTZ SUBSTRATE ; C=CERAMIC SUBSTRATE

Having confirmed the suitability of new ceramic substrate material experiments to optimize the growth conditions were done.

B-097	1.0	8.36	1200	40	DETAILS OF GROWTH
B-099	1.0	25.07	1200	40	GIVEN IN
B-100	1.0	12.53	1200	40	SUBSEQUENT TABLES
B-101	1.0	37.60	1200	40	(AFTER CATALYST
B-102	1.0	25.07	1100	40	DENSITY ANALYSIS
B-104	1.0	25.07	1150	40	TABLES.)
B-105	2.0	21.49	1200	40	
B-106	2.0	25.07	1150	40	
B-108	2.7	23.28	1150	40	
B-109	4.0	28.23	1150	40	
B-110	3.5	27.17	1150	40	
B-112	4.0	22.18	1150	40	
B-114	4.0	18.60	1150	60	
B-115	4.0	25.31	1150	75	
B-117	4.0	20.25	1150	60	
B-119	4.0	21.83	1150	55	
B-121	5.0	25.87	1150	40	
B-122	6.0	21.17	1150	40	

CATALYST VAPOR DEPOSITION RUNS

Following deposition runs were made to confirm relation of catalyst particle density to initial amount of Ferrocene placed on substrate.

B-052	0.100 g FERROCENE AT INLET
B-057	0.100 g FERROCENE AT INLET
B-058	0.050 g FERROCENE AT INLET
B-059	0.025 g FERROCENE AT INLET
B-060	0.050 g FERROCENE AT INLET
B-063	0.025 g FERROCENE AT INLET
B-064	0.025 g FERROCENE AT INLET
B-066	0.035 g FERROCENE AT INLET
B-069	0.050 g FERROCENE AT INLET
B-071	0.035 g FERROCENE AT INLET
B-073	0.050 g FERROCENE AT INLET
B-074	0.050 g FERROCENE AT INLET
B-075	0.025 g FERROCENE AT INLET
B-076	0.035 g FERROCENE AT INLET
B-080	0.050 g FERROCENE AT INLET
B-081	0.025 g FERROCENE AT INLET
B-084	0.035 g FERROCENE AT INLET
B-085	0.040 g FERROCENE AT INLET

Following are the catalyst vapor deposition runs for benzene runs.

B-095	0.050 g FERROCENE AT INLET
B-098	0.050 g FERROCENE AT INLET
B-103	0.050 g FERROCENE AT INLET
B-107	0.050 g FERROCENE AT INLET
B-111	0.050 g FERROCENE AT INLET
B-113	0.055 g FERROCENE AT INLET
B-116	0.055 g FERROCENE AT INLET
B-118	0.050 g FERROCENE AT INLET

VAPOR DEPOSITED CATALYST - DENSITY ANALYSIS

Following deposition runs were made to confirm relation of catalyst particle density to initial amount of Ferrocene placed on substrate.

RUN #	FERROCENE AT INLET gms.	SUBSTRATE MATERIAL	AREA $(\mu M)^2$	NUMBER OF DOTS	DENSITY OF DOTS # / $(\mu M)^2$	
B-052	0.100	QUAR+GRAPH		----TRIAL RUN----		
B-057	0.100	GRAPHITE	702.0	123	0.1750	
B-058	0.050	GRAPHITE	409.0	144	0.3520	2
B-059	0.025	GRAPHITE	370.0	172	0.4656	
B-060	0.050	GRAPHITE	420.0	237	0.5637	
B-063	0.025	GRAPHITE	11687.0	105	0.0090	1
B-064	0.025	GRAPHITE	463.5	221	0.4768	
B-066	0.035	GRAPHITE	360.0	135	0.3750	
B-071	0.035	GRAPHITE	98.5	36	0.3656	
B-073A	0.050	GRAPHITE	351.4	63	0.1793	
B-073B	0.050	GRAPHITE	415.0	86	0.2070	
B-074A	0.050	CERAMIC	166.3	161	0.9684	
B-074B	0.050	CERAMIC	159.3	144	0.9003	
B-075	0.025	CERAMIC	323.0	36	0.1115	
B-076	0.035	CERAMIC	130.4	40	0.3067	
B-081	0.025	CERAMIC	276.0	27	0.0978	
B-085	0.040	CERAMIC	243.4	163	0.6700	

1. Sample was dropped.
2. Higher starting temperature.

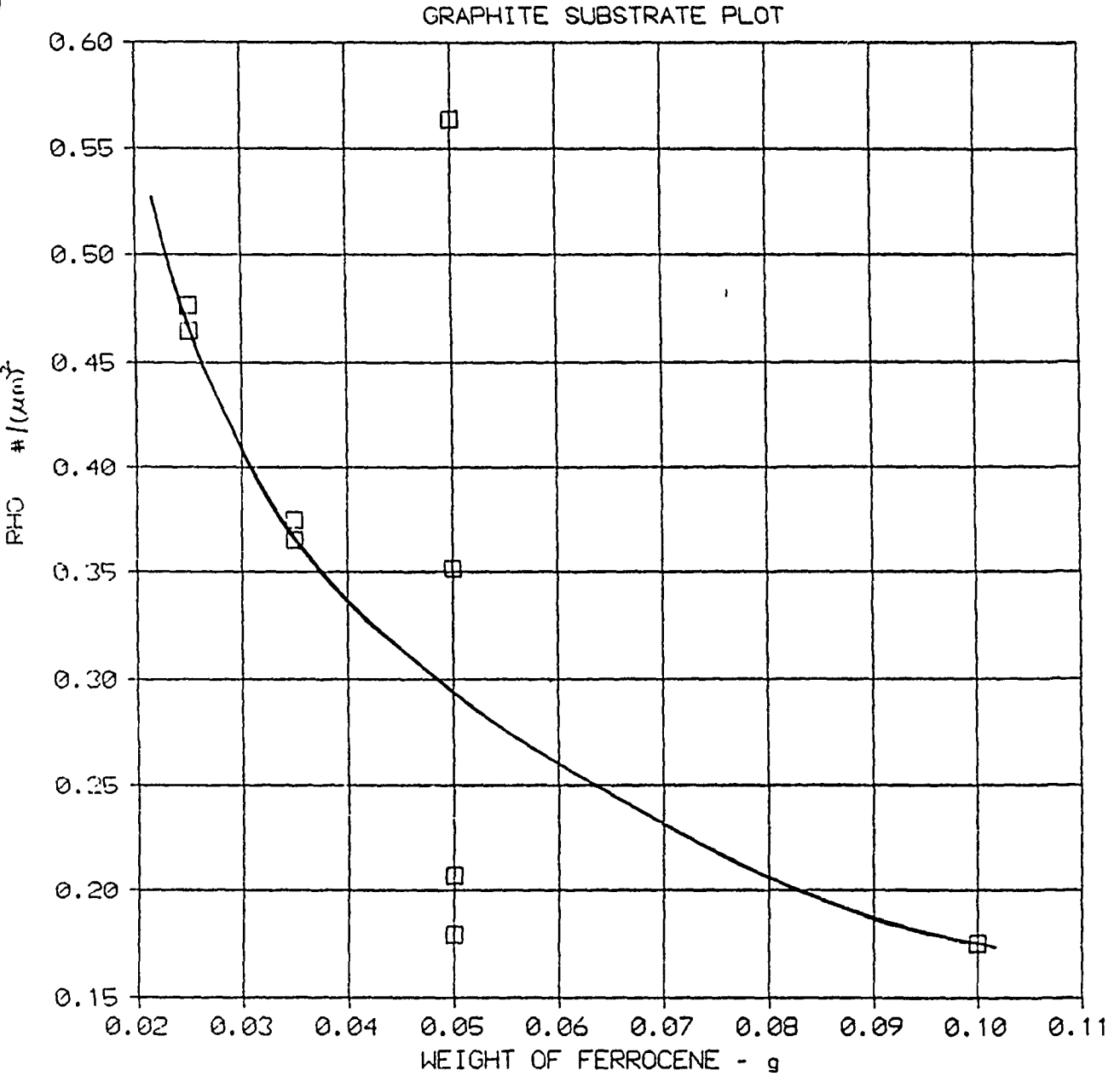
GRAPHITE SUBSTRATE PLOT
0.60
0.55
0.50
0.45
0.40
0.35
0.30
0.25
0.20
0.15
RHO #/(μm)²
0.02
0.03
0.04
0.05
0.06
0.07
0.08
0.09
0.10
0.11
WEIGHT OF FERROCENE - g

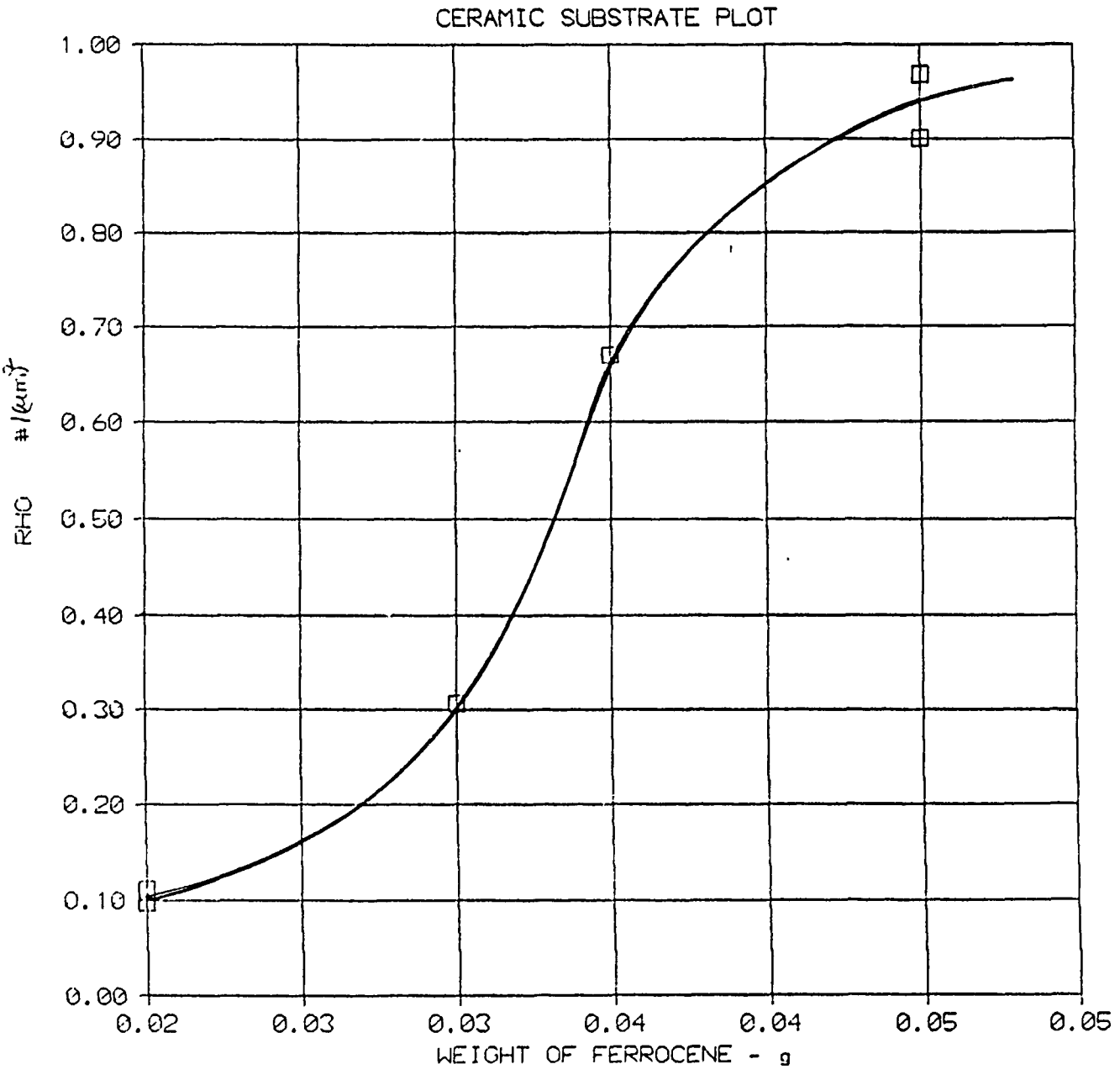
CERAMIC SUBSTRATE PLOT
1.00
0.90
0.80
0.70
0.60
0.50
0.40
0.30
0.20
0.10
0.00
RHO #/(μm)³
0.02
0.03
0.03
0.04
0.04
0.05
0.05
WEIGHT OF FERROCENE - g

REACTOR CHARACTERIZATION

Colorado State University
Fort Collins, Co-80523
Tel: 303-491-1184
FAX: 303-491-2249

REQUEST :

- Confirmation required
  1. Suitable for minimum 1400°C continuous operation
  2. Reactor should be suitable for high vacuum operation (
  3. Reactor tapered ends dimensions compatible with 29x42 size standard taper outer joints (To enable upstream/downstream tubing connections)

- PRICE
- SHIPPING
- Delivery period

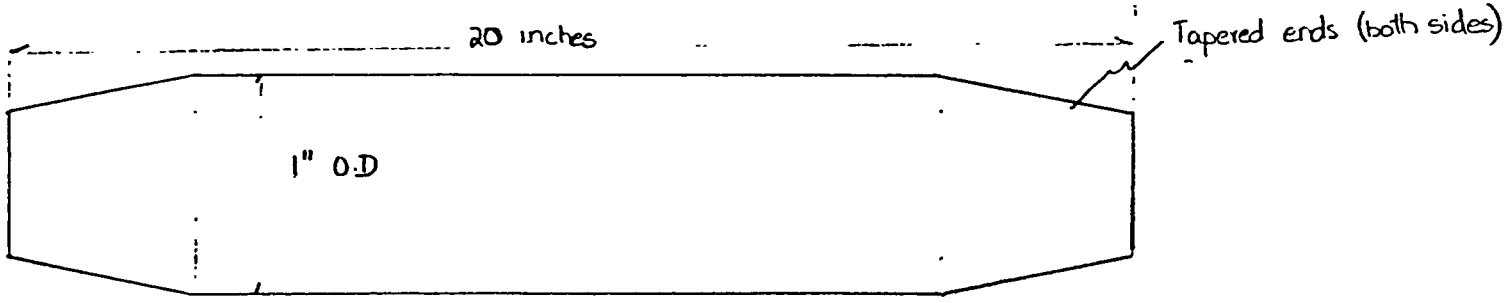

Standard Taper Inner Joints

Provide dependable leakproof connections. Ground inner joints, hand-tooled, interchangeable.

·Ground to AS.m E676 T desig nations indicate largest dia.t.a mm (Corning 6560)

T No.	Tubing O.D.	Total Length	Cat. No.	Price	Case of
10/30	8mm	150mm	11-373-5C	Ea/4 13	12
12/30	10	150	11-373-5D	—	12
14/35	12	150	11-373-5E	Ea/5 30	12
19/38	17	150	11-373-5F	Ea/5 57	12
24/40	22	150	11 373-5G	6/36 43	12
29/42	27	200	11-373-5H	6/40.06	12
34/45	32	200	11-373-5J	—	6
45/50	42	200	11-373-5L	4/51 65	6

mVolts	Temp.
0.149	24
0.230	25
9.982	262
10.154	268
15.435	393
17.654	446
17.790	450
21.130	527
22.270	555
23.420	581
24.510	607
28.300	696
29.180	716
32.425	793
35.160	858
35.910	876
36.975	902
38.080	929
38.850	947
40.010	976
40.790	996
41.060	1000
41.120	1001
41.130	1001

Equation of Line = Temperature = $A + B \times x = T$

where x = mVolts output

A = 25 °C

B = 23.733 °C/mV

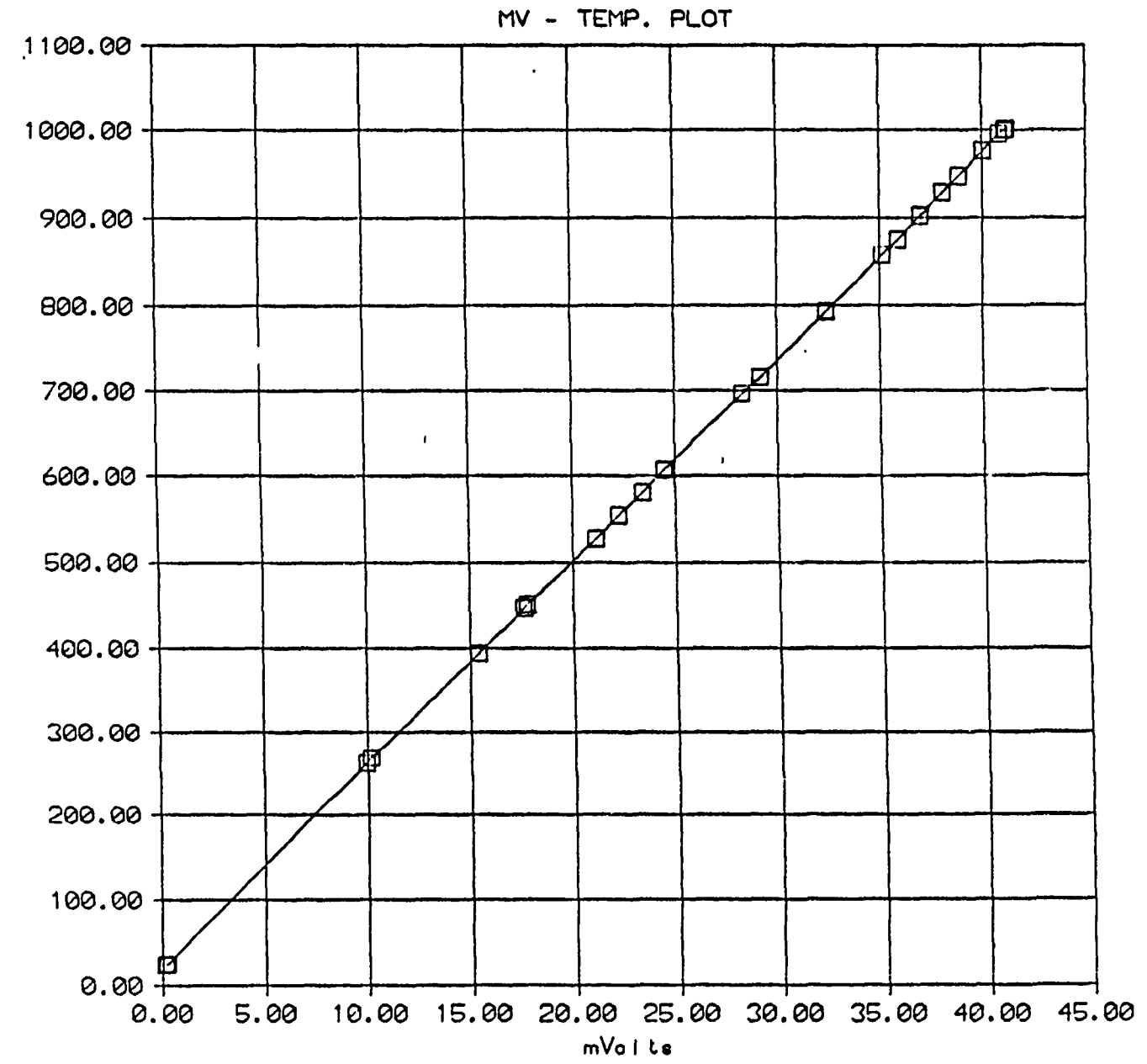

ΔT	T
19.5	0
19.5	25
18.0	268
17.0	450
16.0	581
15.0	696
13.5	793
12.5	858
10.5	902
9.0	947.5
8.0	996
5.0	1000
5.0	1001
4.5	1001

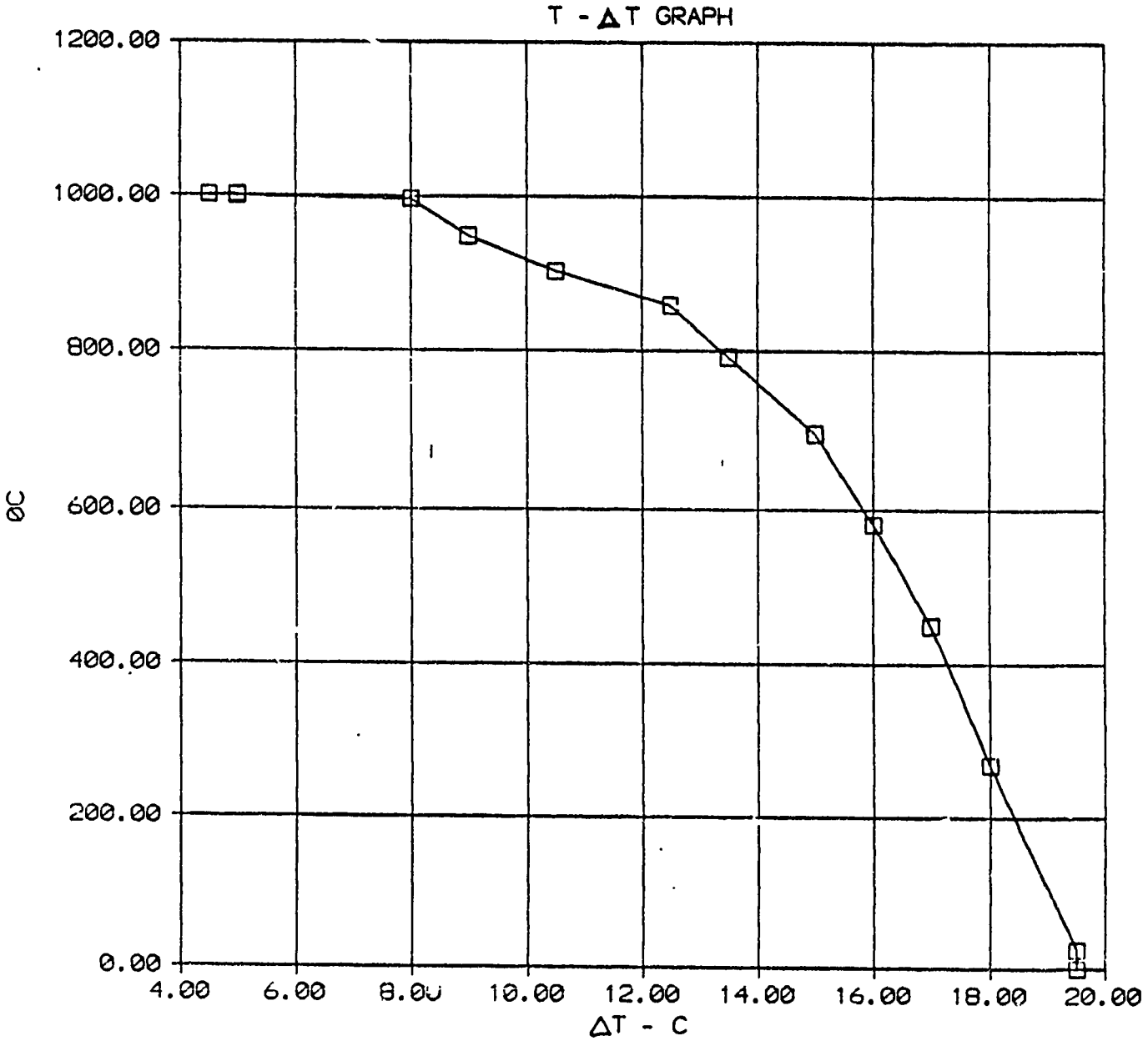
T - ΔT GRAPH
1200.00
1000.00
800.00
600.00
400.00
200.00
0.00
ØC
4.00
6.00
8.00
10.00
12.00
14.00
16.00
18.00
20.00
ΔT - C

DISTANCE Cm	TEMPERATURE ^{O}C
0.00	200
9.00	472
11.50	713
14.00	923
16.50	1055
19.00	1131
21.50	1173
22.50	1182
24.50	1190
24.50	1190
26.50	1186
27.50	1181
30.00	1153
32.50	1089
35.00	982
37.50	799
40.00	535
42.50	341
50.00	100

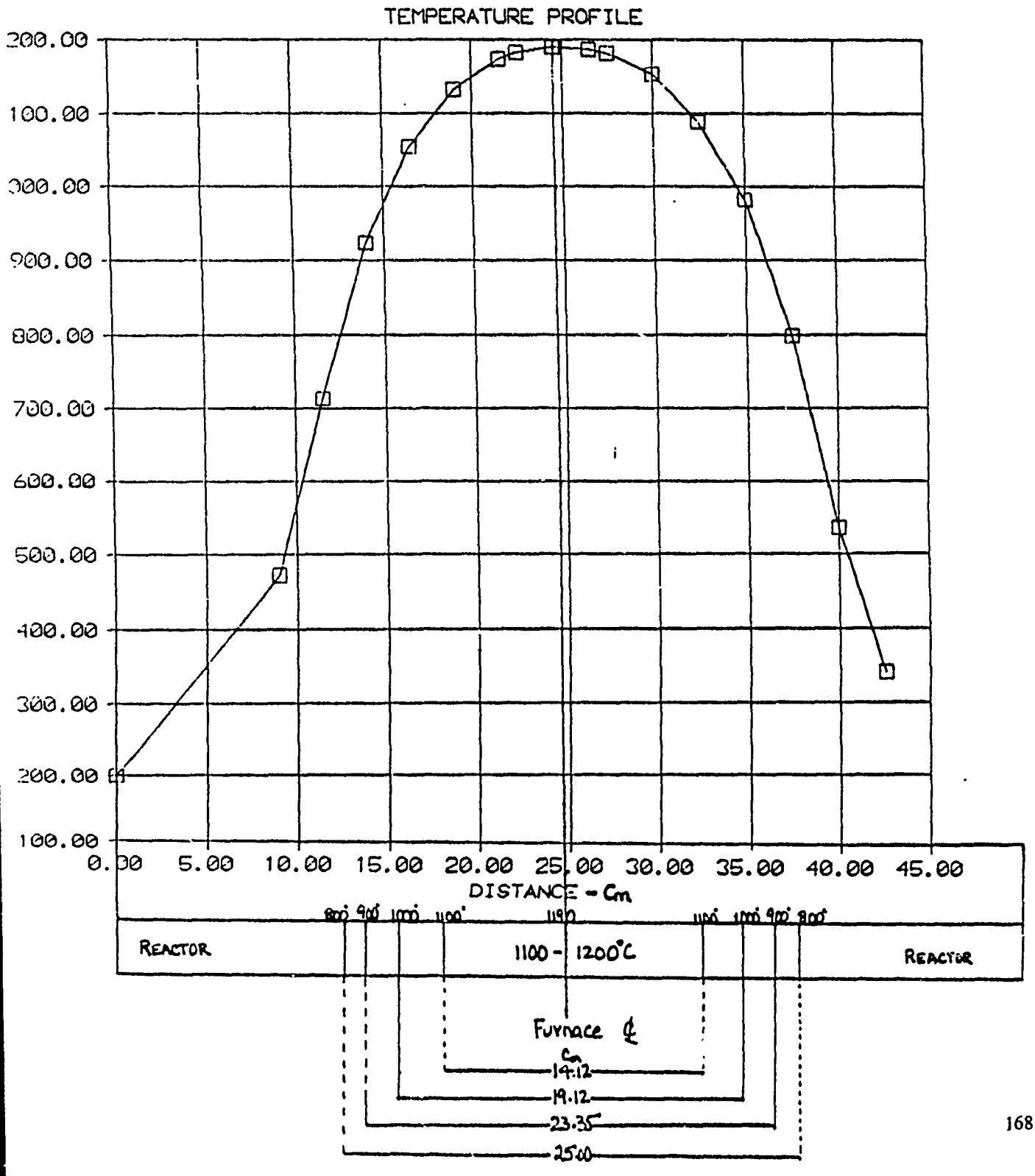
TEMPERATURE PROFILE
200.00
100.00
900.00
800.00
700.00
600.00
500.00
400.00
300.00
200.00
100.00
0.00
5.00
10.00
15.00
20.00
25.00
30.00
35.00
40.00
45.00
DISTANCE - Cm
800 900 1000 1100 1190 1100 1000 900 800
REACTOR
1100 - 1200°C
REACTOR
Furnace ℄
Cm
14.12
19.12
23.35
25.00

BENZENE RUNS

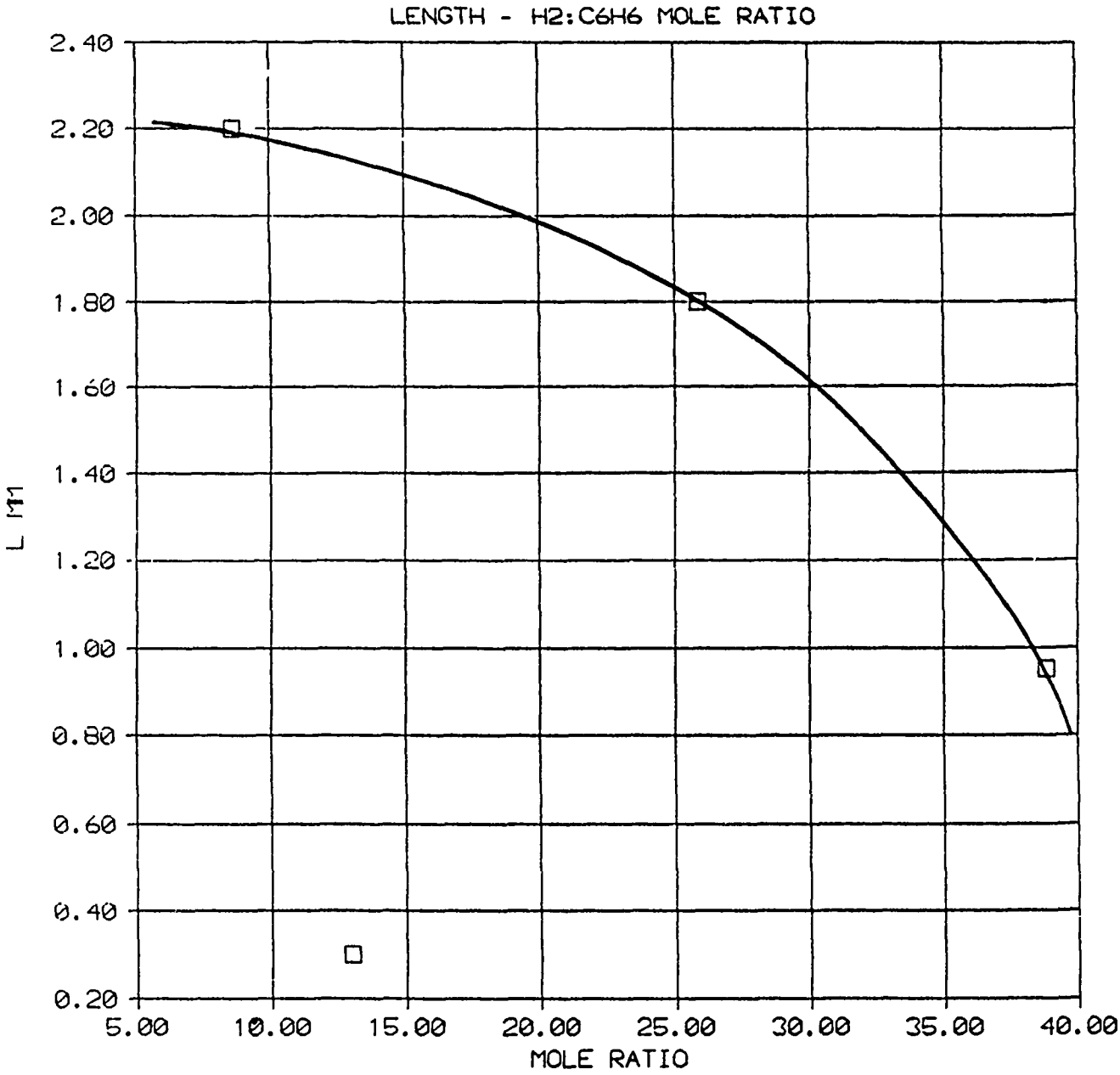
LENGTH - H2:C6H6 MOLE RATIO
2.40
2.20
2.00
1.80
1.60
1.40
1.20
1.00
0.80
0.60
0.40
0.20
L MM
5.00
10.00
15.00
20.00
25.00
30.00
35.00
40.00
MOLE RATIO

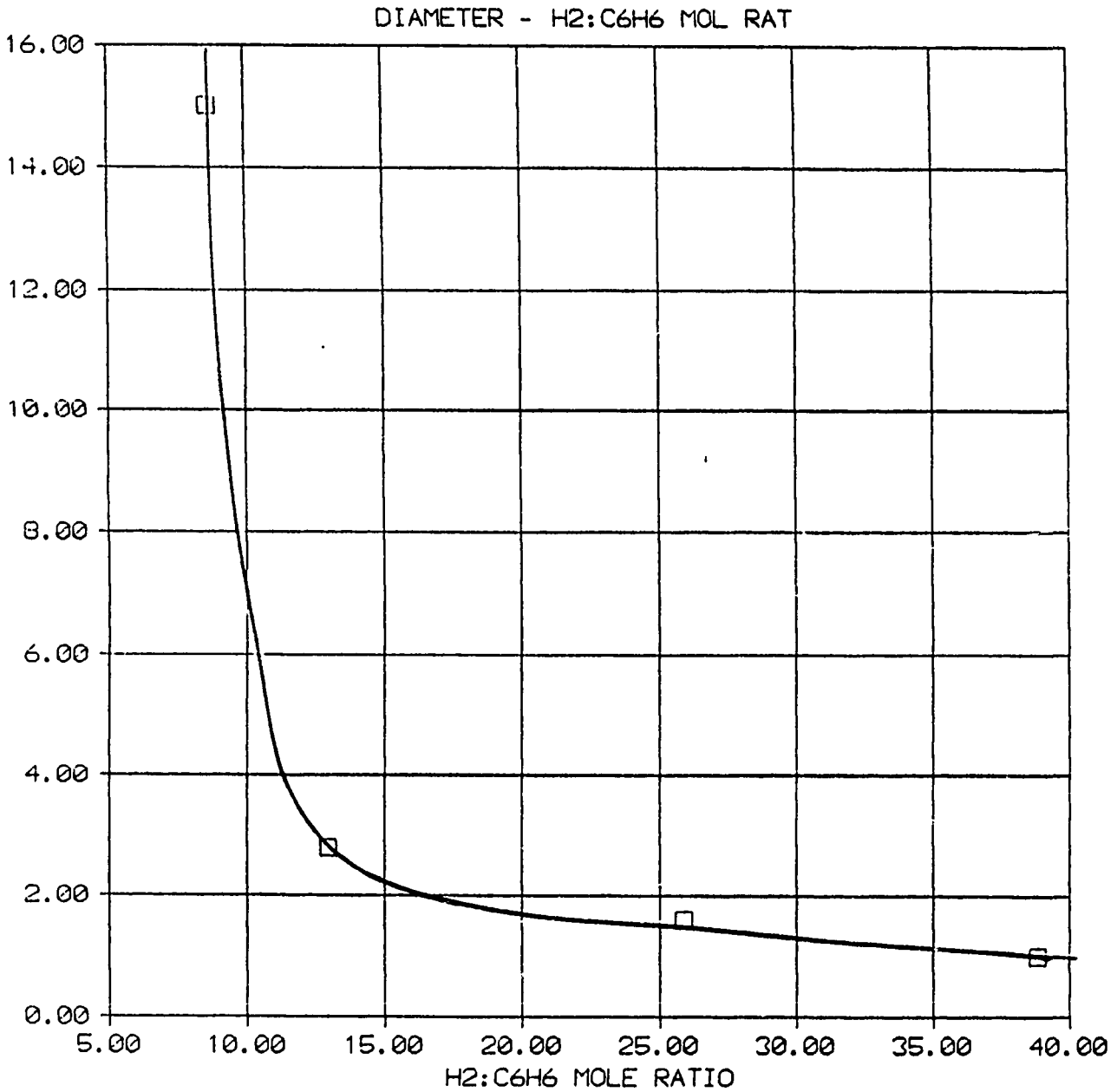
DIAMETER - H2:C6H6 MOL RAT
16.00
14.00
12.00
10.00
8.00
6.00
4.00
2.00
0.00
5.00
10.00
15.00
20.00
25.00
30.00
35.00
40.00
H2:C6H6 MOLE RATIO

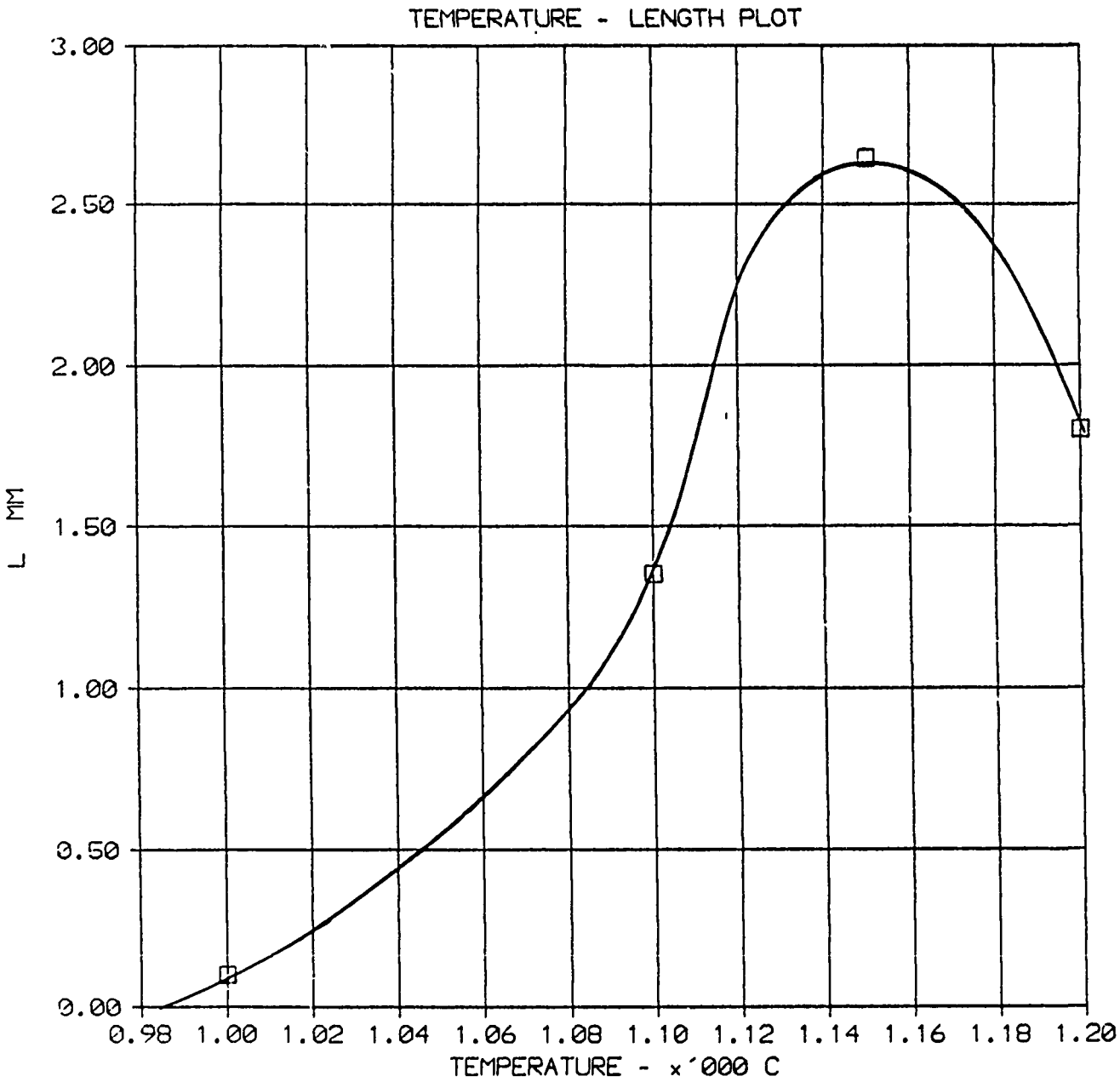
TEMPERATURE - LENGTH PLOT
3.00
2.50
2.00
1.50
1.00
0.50
0.00
L MM
0.98 1.00 1.02 1.04 1.06 1.08 1.10 1.12 1.14 1.16 1.18 1.20
TEMPERATURE - x'000 C

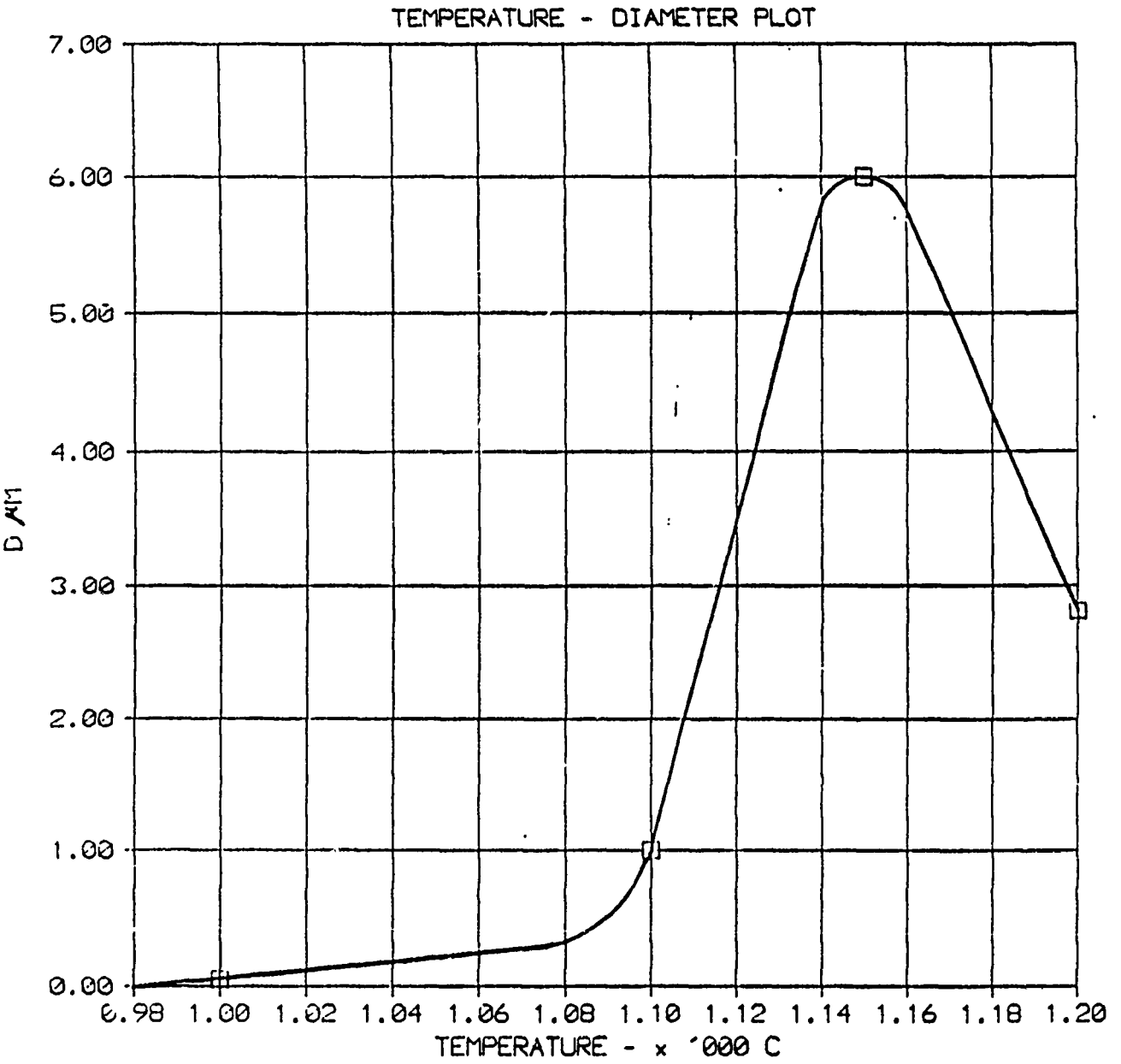
TEMPERATURE - DIAMETER PLOT
7.00
6.00
5.00
4.00
3.00
2.00
1.00
0.00
D MM
0.98 1.00 1.02 1.04 1.06 1.08 1.10 1.12 1.14 1.16 1.18 1.20
TEMPERATURE - x '000 C

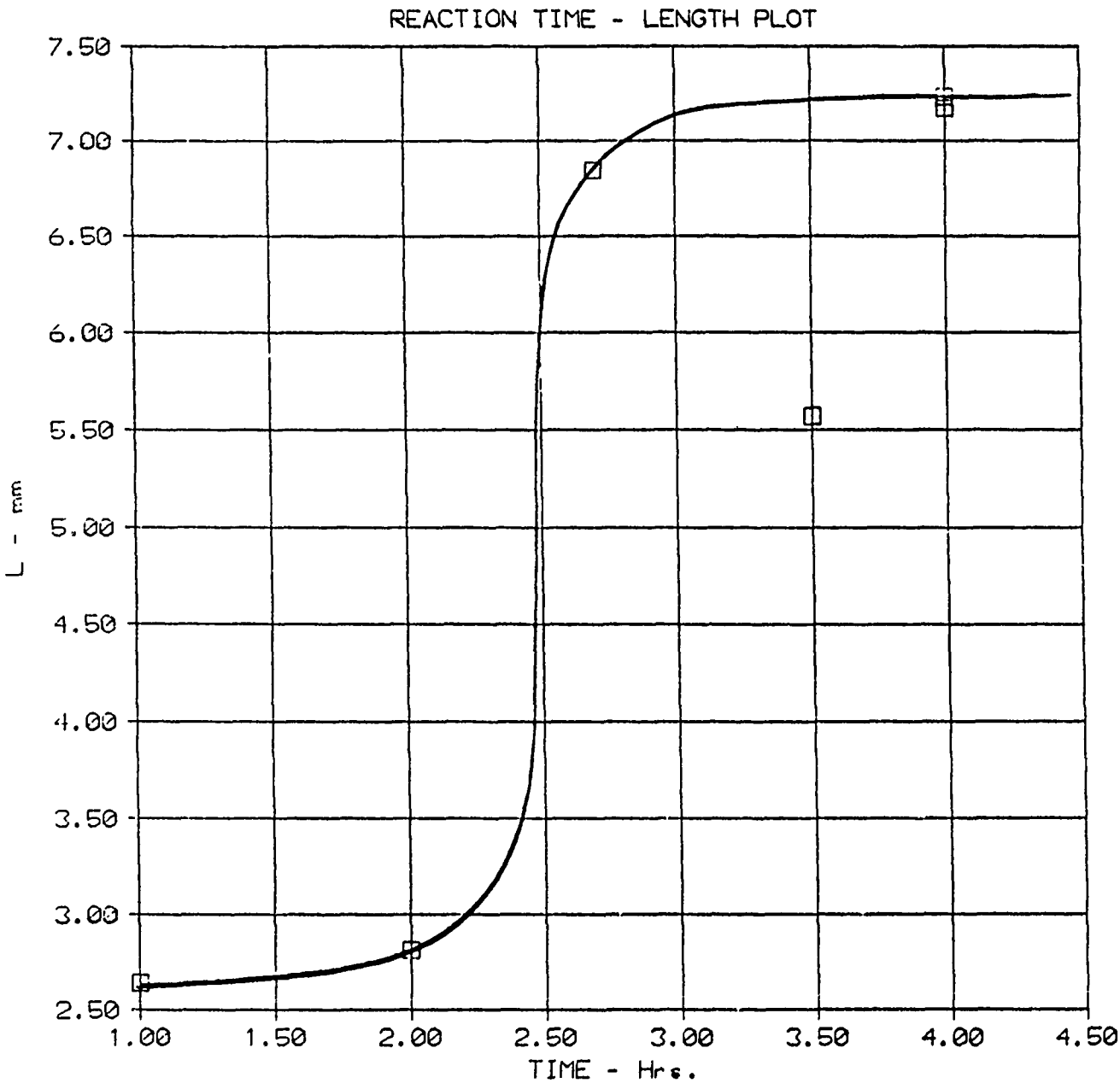
REACTION TIME - LENGTH PLOT
7.50
7.00
6.50
6.00
5.50
5.00
4.50
4.00
3.50
3.00
2.50
L - mm
1.00
1.50
2.00
2.50
3.00
3.50
4.00
4.50
TIME - Hrs.

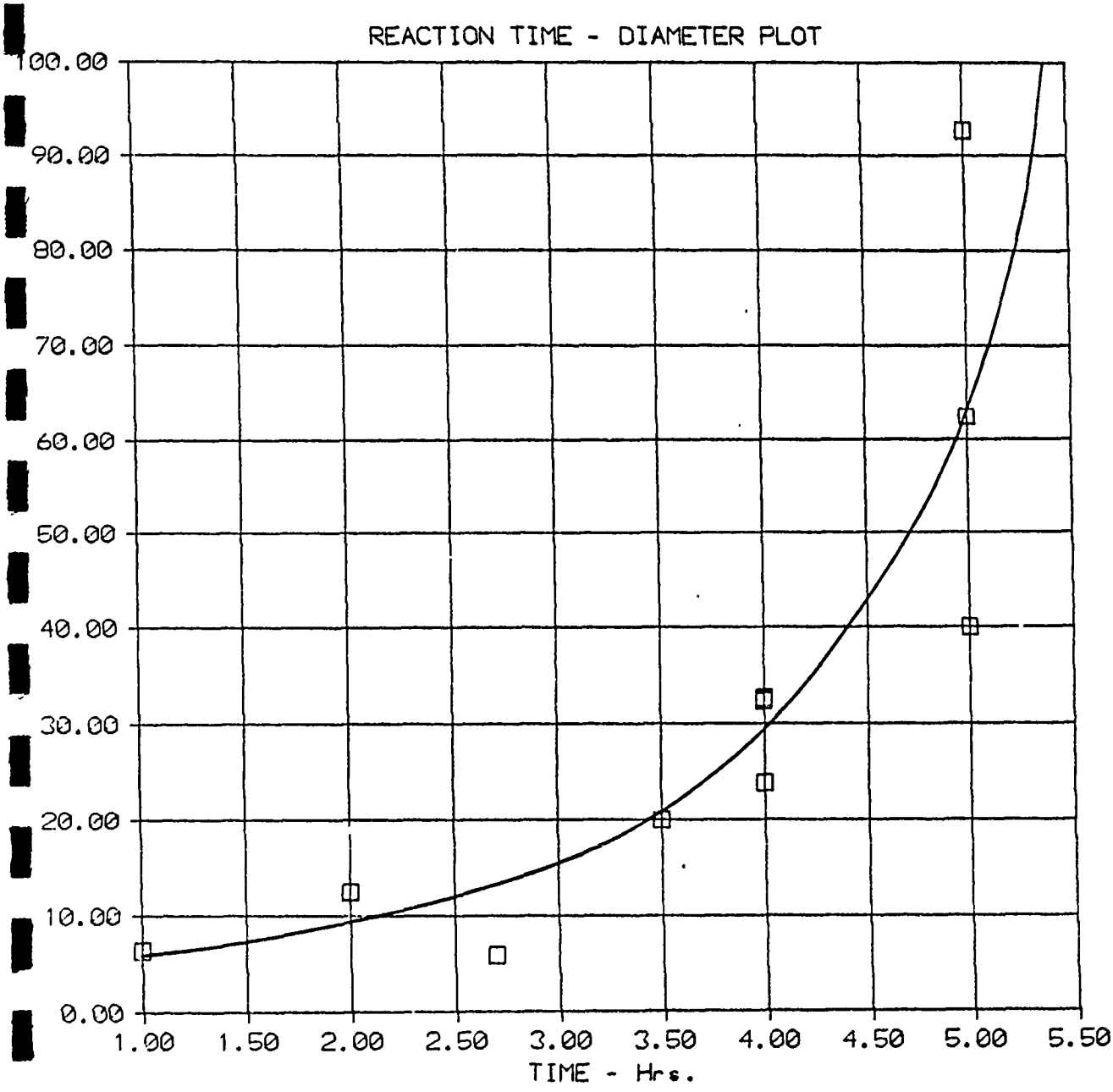
REACTION TIME - DIAMETER PLOT
100.00
90.00
80.00
70.00
60.00
50.00
40.00
30.00
20.00
10.00
0.00
1.00
1.50
2.00
2.50
3.00
3.50
4.00
4.50
5.00
5.50
TIME - Hrs.

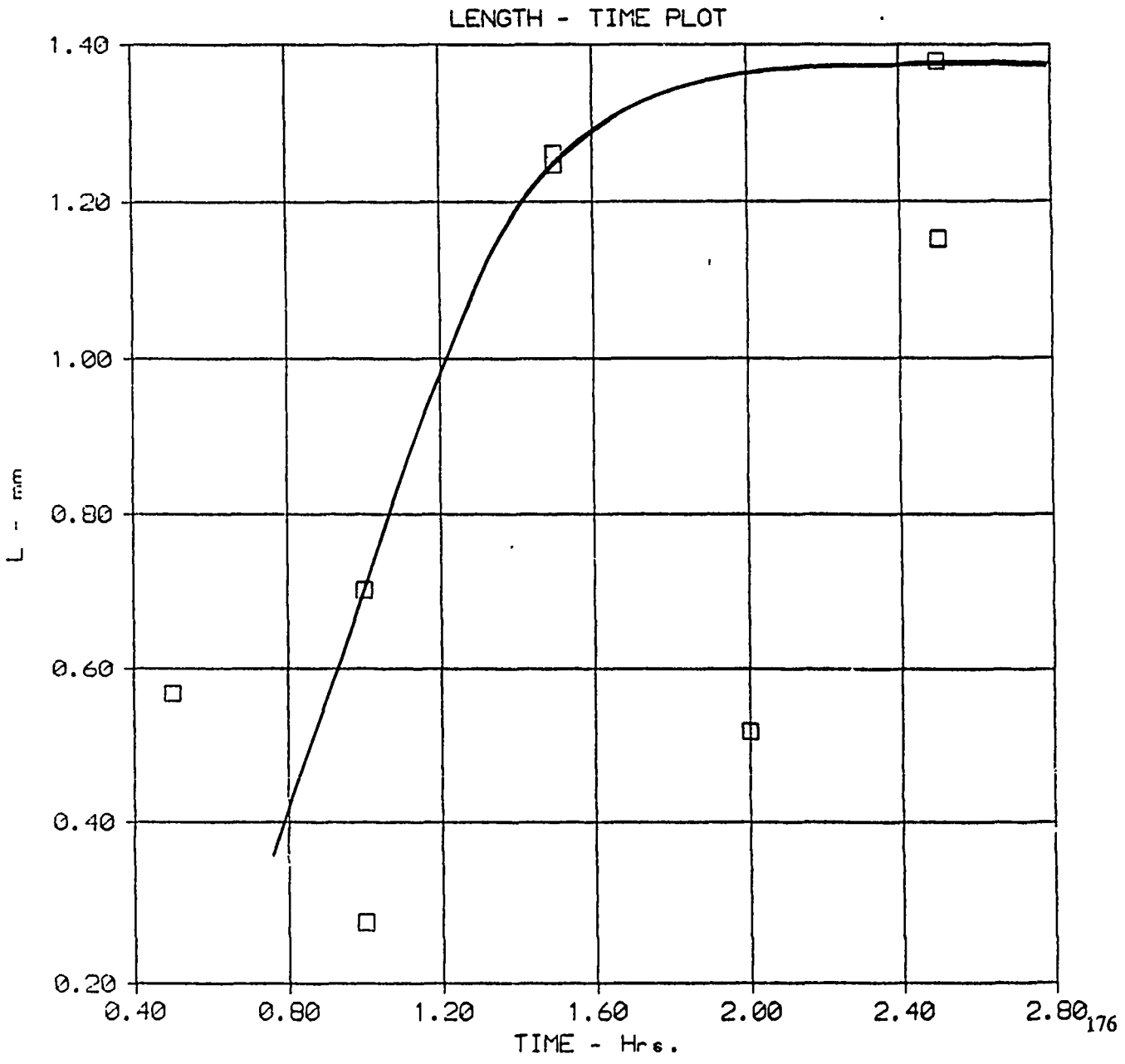
LENGTH - TIME PLOT
1.40
1.20
1.00
0.80
0.60
0.40
0.20
L - mm
0.40
0.80
1.20
1.60
2.00
2.40
2.80
TIME - Hrs.

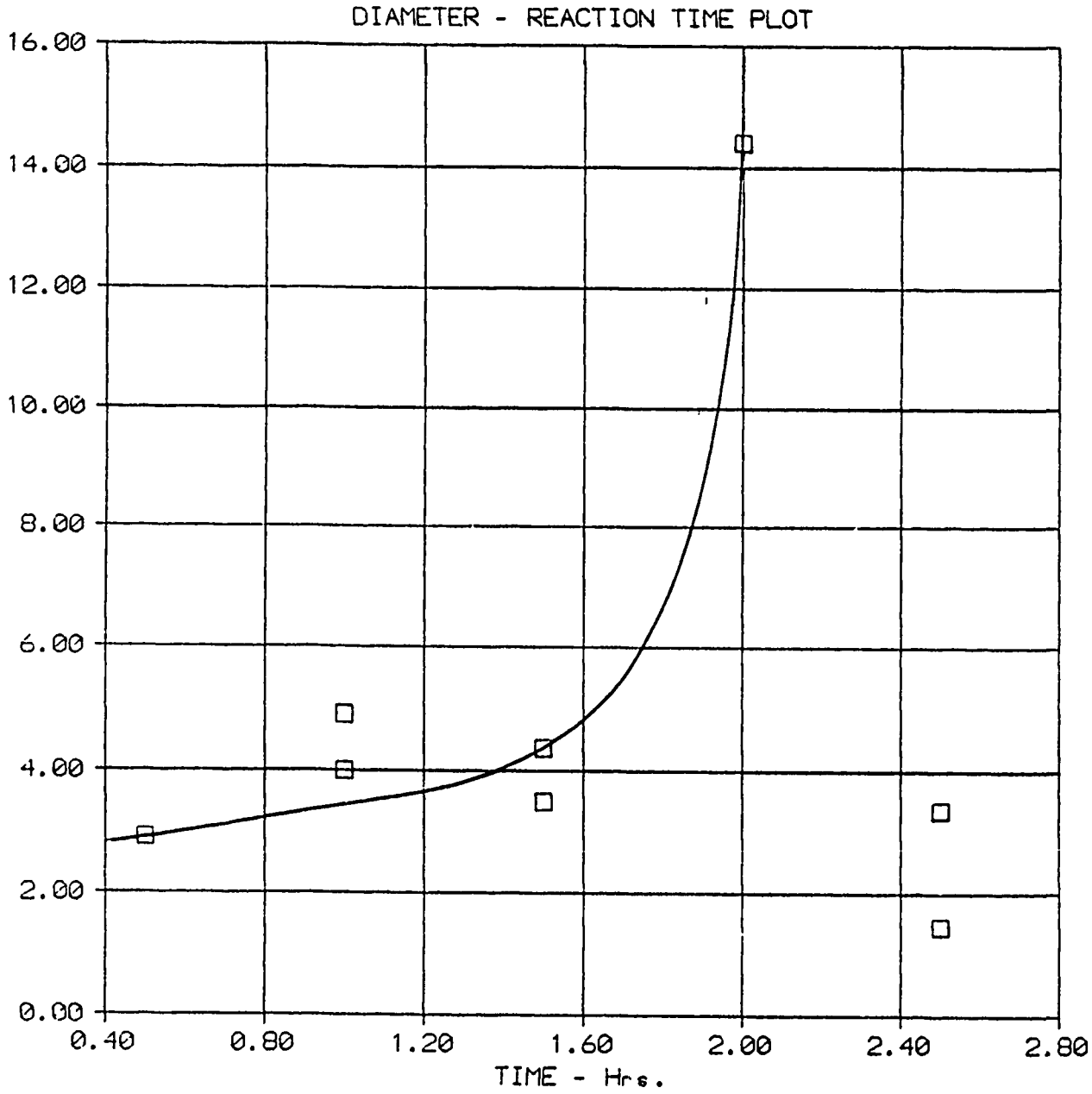
DIAMETER - REACTION TIME PLOT
16.00
14.00
12.00
10.00
8.00
6.00
4.00
2.00
0.00
0.40
0.80
1.20
1.60
2.00
2.40
2.80
TIME - Hrs.

Objective No. 4. - Physical Properties Of Carbon Fiber

The carbon fibers grown were handed over to the Physics Department for testing of mechanical properties.

Surface Activity on Graphite Substrate

The disappearance of Iron catalyst particle from the surface of Graphite substrate as seen from significant difference in fiber growth densities between Graphite and Ceramic or Quartz substrates led us to believe that Iron was diffusing into the bulk of graphite during heating of substrate to $1000^{0}C$ for fiber growth studies. This was also seen from the erratic results obtained for Graphite during catalyst density measurements by EDX to find the effect of variation of amount of Ferrocene at the inlet of Reactor. The phenomena was later confirmed from electrical measurements carried out by physics department. Preliminary measurements showed very encouraging results and the Iron doped graphite substrate material exhibited very low resistivity even at extremely low temperatures($77\ ^{0}K$). The Iron doped Graphite materials also exhibited the uncharacteristic Johnson Oscillations which gave us an added impetus to study further on this unusual behavior of this Iron doped graphite material. The experiments were repeated on two different type of graphite materials, labeled ZYB and ZYC, obtained specifically for this study from Union Carbide. This time the catalyst (Iron) was doped in three different ways, namely : Spraying technique, Vapor deposition and evaporation. The electrical measurements are proposed to be conducted at various temperatures including at much below $77^{0}K$.

TEMPERATURE EFFECT TEST CONDITIONS

S.NO	EXPT NO.	SAMPLE	CAT.DEP.METHOD	TEMP. ^{O}C	SUBS.QTY. BRIDGE	FLAT
1	B-086	ZYC	SPRAYING	1000	1	1
2	B-087	ZYB	SPRAYING	1000	1	1
3	B-088	ZYC	VAPOR DEPOSITION	1000	1	1
4	B-089	ZYB	VAPOR DEPOSITION	1000	1	1
5	B-090	ZYC	SPRAYING	850	1	1
6	B-091	ZYB	SPRAYING	850	1	1
7	B-092	ZYC	VAPOR DEPOSITION	850	1	1
8	B-093	ZYB	VAPOR DEPOSITION	850	1	1
9	B-120A	ZYC	EVAPORATION(400A)	1000	1	-
10	B-120A	ZYB	EVAPORATION(400A)	1000	1	-
11	B-120B	ZYC	EVAPORATION(800A)	1000	1	-
12	B-120B	ZYB	EVAPORATION(800A)	1000	1	-
13	B-120C	ZYC	EVAPORATION(400A)	850	1	-
14	B-120C	ZYB	EVAPORATION(400A)	850	1	-
15	B-120D	ZYC	EVAPORATION(800A)	850	1	-
16	B-120D	ZYB	EVAPORATION(800A)	850	1	-

1. All Samples subjected to 45 minutes heating time followed by holding the samples at required temperature for one hour.
2. Catalyst spraying solution concentration -- 0.2 g $FeSO_4$ in 250 cc DI Water.
3. Catalyst vapor deposition -- 0.05 g Ferrocene at the inlet of reactor. Deposition under 40 sccm Helium flow.

Objective No. 5. - Precursor Identification

A detailed flow scheme was prepared for Raman Spectra Analysis work and is attached herewith.

Specifications for all additional equipment needed within the constraints of budget limitations were drawn and purchase orders placed. The equipment received were shifted to ERC, where the equipment was to be set-up. The equipment ordered include:

- Monochromator and Grating assembly.
- Photomultiplier Tube, Cooled Housing and H V Power Supply Unit.
- Personal Computer.
- Cell.
- Mirrors, Lenses and Mountings.
- Spare Thyratron Switch.
- Spare Laser Gases.
- Stainless Steel Tubing, Valves and Fittings.

The existing XeCl excimer laser in Dr. Rocca's laboratory was to be utilized as light source and the optical table was donated by IBM. The optical table was installed in Room B-310 in ERC after obtaining the equipment layout approval from Dr. Rocca. The location of the optical table was fixed with respect to the location of Laser Beam. The modifications to the room including puncturing of the wall for passing the laser beam were completed.

The stainless steel tubing were fabricated and installed. Leak testing of the system was completed.

A brief report justifying use of Raman Analysis and proposed methodology to be adopted is attached herewith.

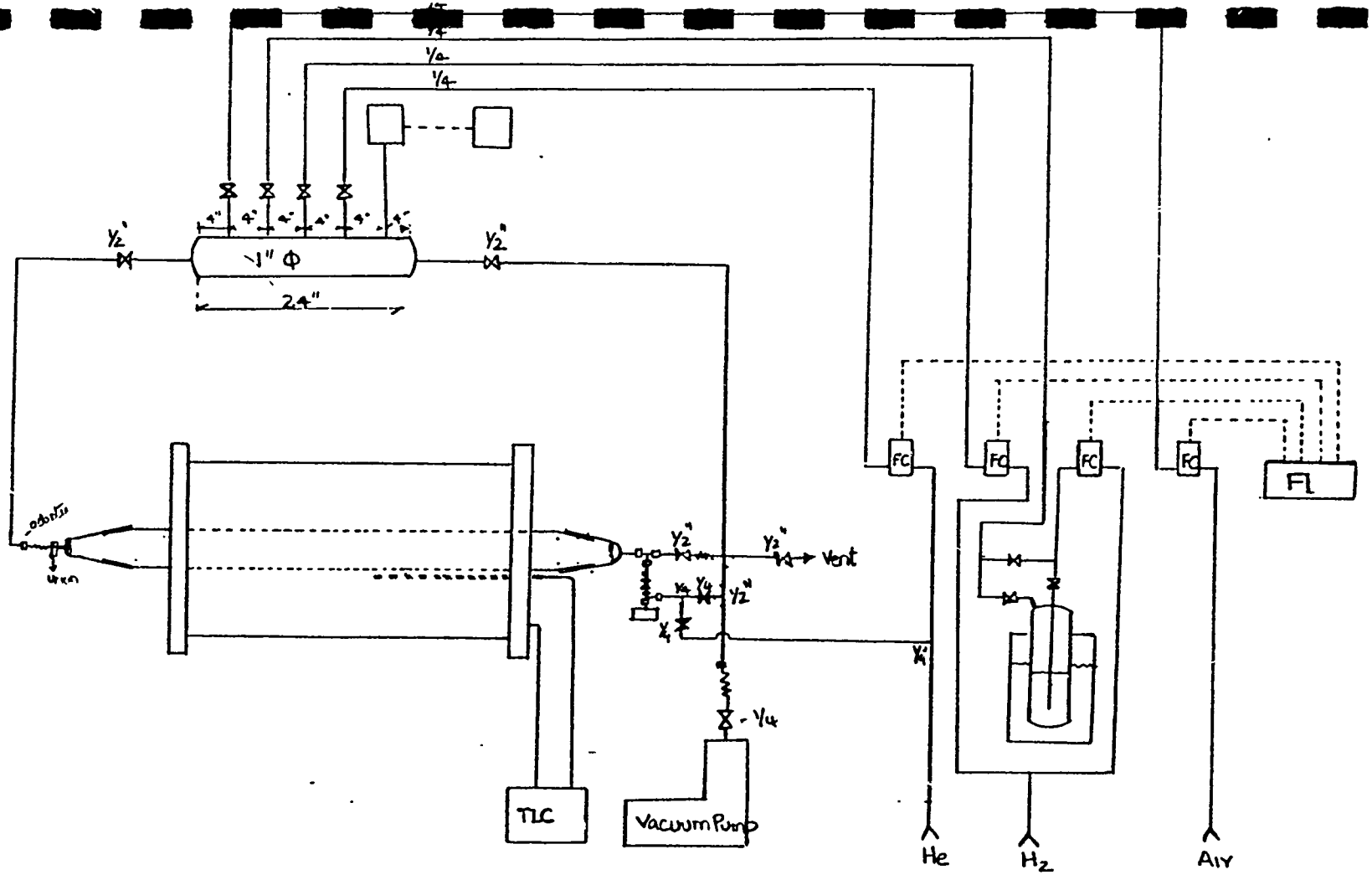

MODIFIED SCHEME FOR RAMAN SPECTRA ANALYSIS OF EXIT GASES.

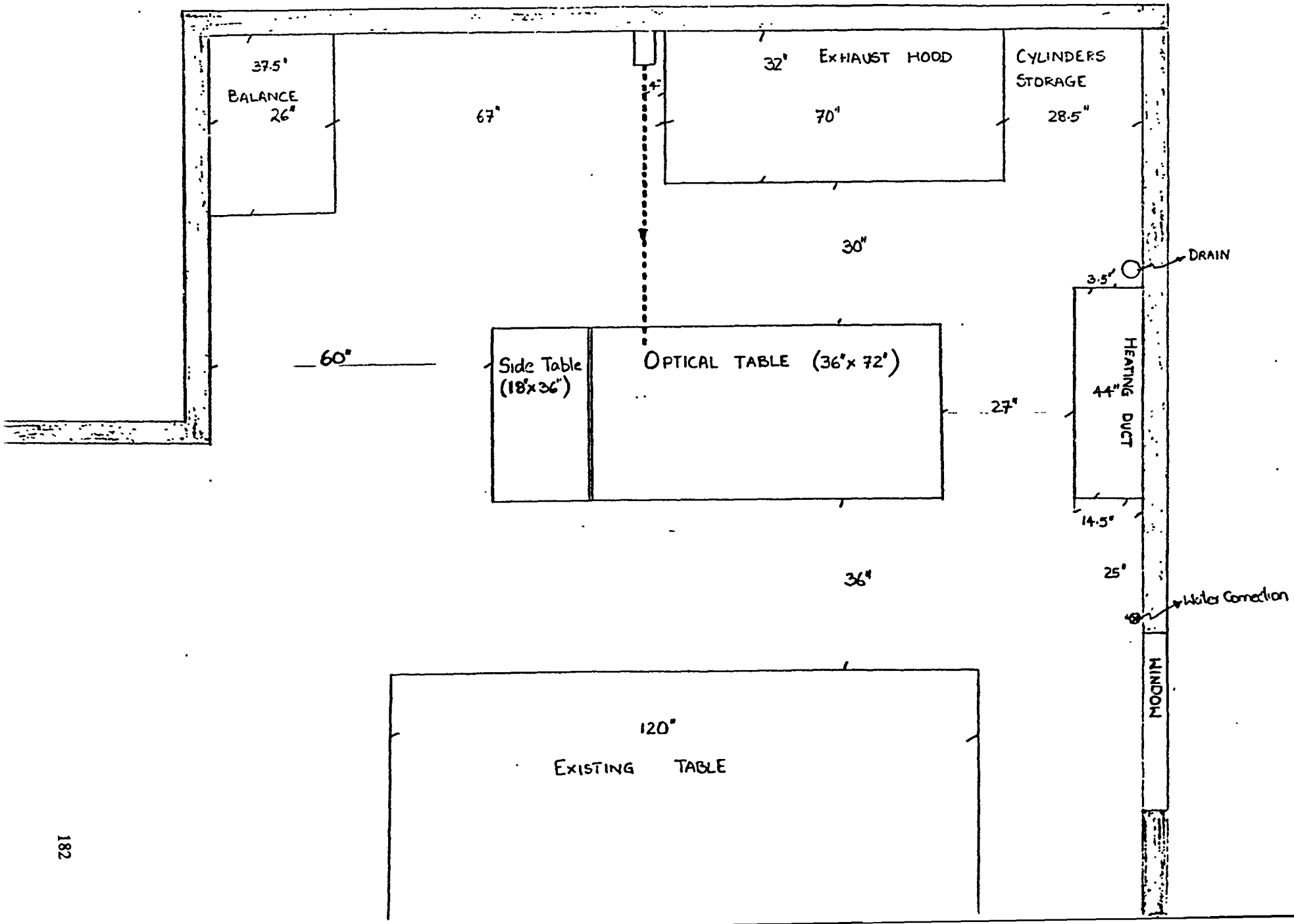
37.5"
BALANCE
26"
67"
32"
EXHAUST HOOD
70"
CYLINDERS
STORAGE
28.5"
30"
DRAIN
3.5"
60"
Side Table
(18"x36")
OPTICAL TABLE (36"x 72")
27"
HEATING DUCT
44"
14.5"
36"
25"
Water Connection
WINDOW
120"
EXISTING TABLE

RAMAN SPECTRA ANALYSIS FOR PRECURSOR IDENTIFICATION

We propose to adopt the technique of insitu pulsed laser Raman spectroscopy to selectively monitor/identify the reactive precursor species/concentrations during Chemical Vapor Deposition method of Carbon for producing fibers using Benzene as the carbon source. The reason for adopting this technique is that it offers a non-intrusive, selective method with high spatial resolution together with the advantages of generality - as virtually all species exhibit Raman spectra.

The procedure for generating the Raman spectrum essentially involves focusing a pulsed laser beam from the laser source into a sample cell. Scattered light collected at right angles to the incident beam is dispersed by a monochromator and detected by a photomultiplier tube. The Raman scattered radiation is viewed at right angles to the direction of excitation in order to ensure that unscattered radiation, which is 10^3 to 10^4 times as intense as Raleigh scattering and 10^7 to 10^8 times as intense as Raman scattering, does not reach the detector and only Raleigh and Raman scattered radiation enters the monochromator and falls on detector. Signals are then processed by a gated integrator interfaced with a computer. Since the Raman spectra is characteristic of each species and the signal is directly proportional to the gas densities or respective partial pressures, the pulsed laser can be used to identify reactive gas species during Chemical Vapor Deposition (CVD).

Reasons for adopting Raman spectra analysis for precursor species identification include :

a) Raman spectra are usually simpler than corresponding Infrared spectra primarily because overtone and combination effects are relatively small compared to principal Raman scattered frequencies.

b) Totally symmetric modes of vibration can be studied via the Raman effect, whereas they are not observed in Infrared spectra.

c) The intensity of a Raman line is directly proportional to concentration whereas there is a logarithmic (Beer's Law) relationship for conventional spectroscopy. Thus quantitative analysis is often more convenient in Raman spectroscopic analysis and sometimes more accurate.

The major disadvantage of this technique is that the excitation of Raman radiation is very inefficient and hence the intensity of Raman scattered radiation is very low making detection a formidable task. This problem can be circumvented to a large extent by using the following techniques:

a) Use of laser as the source of exciting radiation.

The Raman scattering is directly proportional to the intensity of the incident light. Hence higher the power that can be concentrated into a specific volume of sample, the more intense will be the recorded spectrum. Since lasers are a stable, coherent monochromatic source of high intensity radiation, high powered lasers can be used to bring weak spectra, especially those from gases, up to a level where they can be detected.

Further, Raman scattering is proportional to the fourth power of the frequency of the laser line exciting the spectrum. Thus a red laser will be less efficient as a source for Raman spectroscopy than a green laser. Hence it is more advantageous to use a higher frequency exciting laser source for increasing the scattering intensity. Unfortunately, the higher frequency excitation lines tend more to excite fluorescence than do the lower frequency lines and one is often forced to compromise because of this.

b) Stray light minimization

Since the intensity of Raman scattered radiation is low relative to Raleigh scattered radiation, it is essential that stray light in the monochromator be minimized. This calls for a monochromator system with very high discrimination.

The proposed method utilizes pulsed laser as the exciting light source which enables use of gated detection techniques with apertures as short as 4-15 ns pulses. This effectively suppresses the dark current and susceptor black body radiation by several orders of magnitude and greatly improves the signal to noise ratio.

Qualitative Analysis.

The Raman spectrum of a mixture of nonreacting components is the superposition of the Raman spectrum of individual components. With an unknown sample, an identification can be made by a simple matching process if the spectra of possible components of the sample are available. Although Raman spectra of a compound is unique, it must be emphasized that differences between the spectra of homologs may be small.

Quantitative Analysis.

In Raman effect overtones and combinations are almost completely absent and emission bands tend to be narrow and have less overlap than Infrared absorption bands, where rotational fine structure is superimposed on the vibrational transitions. Thus if the sample does not contain too many components, it is possible in a Raman spectrum to find a characteristic band that is free of spectral interference. A standard sample of each component is used to determine the proportionality between peak heights and concentration. If band overlaps do not occur they can be resolved by setting up and solving simultaneous equations under the assumption that the measured intensity at a particular spectral position is made up of contributions from overlapping components which are proportional to their concentrations.

Insitu quantitative measurements for precursor identification has hitherto not been attempted because of inherent problems like :

a) Difficulty in adopting optical methods due to fouling of optical windows by carbon deposition.

b) Perturbation of reaction system in using other methods.

We propose to use the XeCl excimer laser of wavelength 308 nm delivering 4-15 ns long, 500 mJ pulses at 10 Hz for the light source. The collection instrumentation includes ARC Model AM505-6.9 Monochromator with 1800 G/mm holographic grating and stepping motor scanning system and Thorn EMI 9819 QA Model Photomultiplier tube with Fact-50 thermoelectric cooler capable of cooling upto-30^{0} C. A schematic diagram showing the exciting and collection optics is given in Figure 1, while the process schematic is shown in Figure 2.

Y-Rays	X-Rays	UV	Vis	IR	Radio Waves

Y-Rays ..... < 0.006 nm
X-Rays ..... 5 - 0.006 nm
U V ..... 720 - 5 nm
I R ..... 720 nm - 400 um
Vis. ..... 720 -400 nm
Wave Number = No. of Waves per Centimeter = 1/ \

Wave Length of proposed Laser Light = 308 nm = 3080 A
Wave Number = 32467.5 Cm^{-1}
For RAMAN Spectra Excitation of 3400 - 800 Cm^{-1} , the overall range of wave numbers are :

35867.5 or 278.8 nm ..... (+3400)
29067.5 or 344.0 nm ..... (-3400)
33267.5 or 300.6 nm ..... (+ 800)
31667.5 or 315.8 nm ..... (- 800)

For Identical Power, the scattering efficiency increase with respect to using a

Ar Laser operating at 4880 A = 6.2 times
Kr Laser operating at 6471 A = 19.5 times

The only restriction is to ensure that Fluorescence is not excited.

FURTHER WORK PENDING INCLUDE:

- Fabrication of an eight inch stool for lifting the furnace assembly to match the height of the cell with the laser beam.

- Design and fabrication of piping supports for rigidity and aesthetic reasons.

- Transportation and installation of the side table at ERC as per the layout sketch attached. Recheck Leakage.

- Transportation of computer assembly presently with Mr.Amit Inamdar.

- Installation of monochromator, photomultiplier tube assembly, computer, box-car ,integrator, optics and their alignment.

- Transportation of reaction gases and tubing connections.

- Electrical connections and installation of software.

- Dummy run with a known gas and identification through Raman analysis - to confirm compatibility of software.

- Prepare reference Raman Spectral Charts for known mixtures of gases.

- Actual runs for precursor analysis as per attached details.

- Objective No. 6. - Design and execution.

SUMMARY OF CHARACTERISTIC RAMAN FREQUENCIES OF POSSIBLE CONSTITUENTS

FREQUENCY Cm^{-1}	Group	Constituent
3,374	CH Stretch	Acetylene Gas
3,104	Antisymmetric $=CH_2$ Stretch	Ethylene Gas
3,062	CH Stretch	Benzene
3,026	Symmetric $=CH_2$ Stretch	Ethylene Gas
2969-2965	Antisymmetric CH_3 Stretch	n-Alkanes
2929-2912	Antisymmetric CH_2 Stretch	n-Alkanes
2884-2883	Symmetric CH_3 Stretch	n-Alkanes
2861-2849	Symmetric CH_2 Stretch	n-Alkanes
2,172	Symmetric $C\bar{C}-C\bar{C}$ Stretch	Diacetylenes
1,974	$C\bar{C}$ Stretch	Acetylene Gas
1964-1958	Antisymmetric C=C=C Stretch	Allenes
1680-1665	C=C Stretch	Tetra Alkyl Ethylenes
1,679	C=C Stretch	Methylene Cyclobutane
1678-1664	C=C Stretch	Tri Alkyl Ethylenes
1676-1665	C=C Stretch	trans-DialkylEthylenes
1660-1654	C=C Stretch	cis-Dialkyl Ethylenes
1658-1644	C=C Stretch	$R_2C=CH_2$
1,656	C=C Stretch	Cyclohexene
1649-1625	C=C Stretch	Allyl derivatives
1,623	C=C Stretch	Ethylene Gas
1,614	C=C Stretch	Cyclopentene
1,566	C=C Stretch	Cyclobutene
1473-1446	CH_3, CH_2 Deformations	n-Alkanes
1466-1465	CH_3 Deformations	n-Alkanes
1314-1290	In-Plane CH Deformations	trans-DialkylEthylenes
1310-1175	CH_2 Twist & Rock	n-Alkanes
1305-1295	CH_2 In-Phase Twist	n-Alkanes
1,205	C_6H_5-C Vibration	Alkyl Benzenes
1,188	Ring Breathing	Cyclopropane
1150-950	C-C Stretches	n-Alkanes
1,001	Ring Breathing	Cyclobutane
992	Ring Breathing	Benzene
905-837	C-C Skeletal Stretch	n-Alkanes
900-890	Ring Vibration	Alkyl Cyclopentanes
886	Ring Breathing	Cyclopentane
459	Symmetric CCl_4 Stretch	Carbon Tetrachloride

TIME MANAGEMENT

TIME MANAGEMENT SUMMARY

1.	Period under consideration	July 1988 - May 1989
2.	Total number of months	Eleven
3.	Working days per month considered	Twenty
4.	Total number of working days available	220
5.	Total number of experiments conducted (Refer Work Summary)	~116
6.	Assuming one experiment takes one day and assuming every four days of experiment requires one day for cleaning of reactors, total number of days spent for 130 experiments.	116+116/4 =145
7.	Time spent for analysis on SEM (Spare time available on experiment days plus one month)	25 days
8.	Total equipment use time (6 + 7)	170 days
9.	Besides Course Work, the balance time of 50 days were utilized as follows:	

- Familiarization of running of experiment, including substrate preparation, benzene run, reactor baking and catalyst deposition.
- Familiarization of SEM Analysis work including sample preparation, use of EDX for identification of surface elements, dot matrix analysis for catalyst density measurements.
- Trouble shooting in Phase-1 set-up and identification of major problem areas and suggestion of remedial schemes/measures.
- Complete Design and Engineering of modification scheme including General arrangement and piping layout scheme.
- Liaison with Sponsored Research for incorporation of equipment cost head in budget and preparation of revised cash flow document for Sandia Laboratories' approval.
- Procurement work including Vendor identification, cost analysis and paperwork/liaison with all concerned CSU departments for placement of purchase orders for following equipment.

- Mono-chromator/Gratings assembly
- Photomultiplier Tube/Cooled Housing/HV Power Supply Unit.
- Spare Thyratron Switch for laser.
- Laser gases Ar,Xe,HCl.
- Ceramic Reactors.
- Optics and Mountings(part).
- SS Tubing, Fittings and Valves.
- Optical Cell.
- Thermocouples.
- Personal Computer.

Delivery expediting and follow-up activities.

- Organizing Optical Table installation at ERC.
- Equipment down-time due to glassware breakages.
- Assembling of new reactor set-up, leak and pressure testing.
- Examination break.

COST ALLOCATION

COST APPORTIONING

COST HEAD	EQUIPMENT ORDERED-$	TOTAL ESTIMATE-$
SANDIA LABORATORIES		
Monochromator/Gratings	14,915.00	14,915.00
Photomultiplier Tube/ Cooled Housing/ HV Power Supply.	5,187.50	5,187.50
Spare Thyratron Switch	1,922.00	1,922.00
Laser Gases - Xe/HCl/Ar.....	2,375.00	2,375.00
Shipping Cost (Lumpsum).....	1,000.00	1,000.00
Subtotal	25,399.50	25,399.50
AIRFORCE GRANT		
Reactors	980.40	980.40
Optics/Mountings	3,696.00	8,700.00
Tubing/Fittings/Valves	2,500.00	2,500.00
Cell	150.00	150.00
Personal Computer	1,795.00	1,795.00
Thermocouples	50.00	100.00
Shipping Cost (Lumpsum).....	1,000.10	1,000.10
Subtotal	10,171.50	15,225.50
I B M		
Optical Table	-	-
GRAND TOTAL	35,571.00	40,625.00

5. MONITORING THE GROWTH OF CARBON FIBERS USING IN-SITU LASER SPECTROSCOPY

Amit Inamdar, Dinesh Udpa, Carmen Menoni and Carol McConica

A Introduction

Scaling processes up from the lab bench level to production requires knowing the optimal local environment for growth of the fibers or films of interest. This optimal environment must be expressed in terms of the near filament gas composition and temperature as well as the chemical and physical nature of the growing substrate. Our preliminary studies from 1986-1990 were useful for finding flows, temperatures, substrates and nucleating conditions which resulted in high aspect ratio fibers. The conditions at the inlet of the bench scale reactor used in these preliminary studies were known, but not the local conditions which actually resulted in fiber growth. Because processes do not scale in a linear fashion, this current information is not useful in pilot plant design. It is now necessary to find the actual near fiber gas composition and temperature which existed during the runs which gave optimal fiber growth. It is also necessary to determine the actual chemical kinetics (gas composition and temperature dependencies) independent of heat and mass transfer effects so that a pilot plant can be properly designed. Pilot plants always operate with significantly different heat and mass transfer conditions, so achieving the same local chemical condition near the growing fibers with require much different inlet conditions on the pilot reactor than were used on the laboratory scale reactor.

B. Equipment

We have designed and built an apparatus to study the kinetics of low pressure to atmospheric pressure chemical vapor deposition of carbon fibers using in-situ Raman spectroscopy and electrical resistance measurements. The hardware consists of a cylindrically symmetric wire reactor, electronics to heat the wire, monitor its temperature and resistance, a XeCl eximer laser, optics, monochromator/photomultiplier and a boxcar averager. The components are controlled by a PC/AT computer coupled through two serial interfaces to a digital-to-analog converter and a stepping motor driver. Several BASIC programs have been written to control the apparatus, to collect and store data, and to plot and analyze data.

C. Hardware

1. Wire Reactor

The reactor depicted in Figure 1 is built of 2" O.D. 304 stainless steel. It is nickel plated to eliminate reaction with and contamination of the gaseous reactants and products. A 5" long, .005" diameter tungsten wire is held on the axis of the 6" long cylinder by two .25" diameter nickel electrodes. The electrodes pass through the reactor walls via high vacuum, electrically insulating ceramic seals. The wire is heated with direct current resulting from a voltage applied across the electrodes. Resistance of the wire is 0.5 ohms at room temperature and 2.5 ohms

at 400 Celsius. Two quartz windows can be mounted on opposite ends of the cylinder (for absorption spectroscopy) or perpendicularly, as shown, for Raman or fluorescence spectroscopy. A vacuum feedthrough provides the voltage output of a chromel-alumel thermocouple junction cemented to one end of the tungsten wire.

2. Optical System

For Raman spectroscopy, a Lambda-Physik eximer laser is used with XeCl to deliver 100 mJoule pulses of 20 nsec duration (5 MWatt peak power) with wavelength 308.2 nm and 0.4 nm full-width at half-maximum. Repetition rate is adjustable from 1 to 10 pulses per second. All lenses are 50 mm diameter quartz. The first lens focuses the laser beam, propagating parallel to the wire, to a 0.5 mm spot between the wire and the side window. The second lens collects and collimates the scattered light from the molecule-laser interaction region and the third lens focuses that on the entrance slit of the monochromator. The monochromator slits are set at 0.15 mm width and 6 mm height. Since the lens system projects a x3 magnified image of the interaction region, light passing through the entrance slit represents a .05 mm by 2 mm slice of molecules intersected by the beam. By keeping the laser beam and optics fixed and moving the reactor, partial pressures of reactants and products can be monitored versus radial distance from the wire.

The monochrometer is scanned by computer to pass through its exit slit either the Stokes- or AntiStokes-shifted scattered light where it is detected by a photomultiplier tube. For H2 and HF, the Stokes-shifted Raman scattering has a wavelength near 350 nm, well separated from the Rayleigh scattered light at 308.2 nm. 3.

3. Electronics

Control and measurement of experimental parameters requires four electronic modules, all of which are managed by the computer. An Acton Research 747 stepping motor driver scans the monochrometer and a Stanford Research 245 boxcar averager measures the photomultiplier signal. A Stanford Research 240 computer interface with 8 analog input/output channels is used to read: 1) the photomultiplier signal averaged over 100 laser pulses, 2) the temperature of the tungsten wire, 3) the voltage drop across the tungsten wire, and 4) the current through the tungsten wire. The ratio of 3) to 4) is the resistance of the wire. This interface is also used to send an analog signal to a transadmittance amplifier, the fourth electronic component, which controls the current through the wire, and therefore its temperature.

We attempted to adapt and use commercial programmable temperature controllers to maintain the wire at constant temperature, but were unsuccessful as they are designed to switch on and off a fixed alternating current to a heater (in our case a wire with small ratio of mass to surface area). The consequence of this switching and wire size resulted in wildly fluctuating wire temperature, even though the controller, with its limited detection bandwidth, sensed a constant average temperature.

To solve this problem we built a dual input transadmittance amplifier. This circuit translates manually- and/or computer-controlled voltages into large direct currents. The manual control sets a rough, starting value for the current supplied to the tungsten wire while the computer input makes small changes which keep the wire

temperature within one degree Celsius of the set point. This sophisticated control is necessary, not so much because the wire is so small. The circuit is shown in Figure 3.

In the temperature range of interest to this study, thermocouple voltages range from 12 to 18 millivolts. The resolution of our analog-to-digital converter is 5 millivolts
with a range from -10 to +10 volts. To make precise temperature measurements it is necessary to amplify the thermocouple output. For this purpose we have built, on the same circuit board as the transadmittance device, a very high accuracy x500 amplifier with cold-junction compensation and low-pass (< 1 Hz) filtering. This circuit is shown in Figure 4.

D. Software

While software was provided with both the Acton Research stepping motor driver and the Stanford Research computer interface, the two programs are not compatible. Commands to the monochrometer must have an end-of-command indicator, such as carriage-return, whereas commands to the eight analog input/output channels and two digital channels of the Stanford interface cannot have any such suffix. In order to control both units simultaneously we had to write our own software for data acquisition. The programs were written using QuickBASIC 4.5 from Microsoft. Though QuickBASIC programs can be compiled, and therefore executed quickly, it is necessary to run the data acquisition programs uncompiled to prevent loss of commands and data over the 6' serial interface lines to the control units. Data analysis and plotting programs which do not communicate through the serial ports have been written and run well in compiled form.

The following are brief descriptions of programs written to: 1) establish communication with the two incompatible control units, 2) acquire data using the control units, and 3) to analyze stored data. Code listings are included.

1. ARC747 -- Communicate with monochrometer.

   Adapted from TERMINAL.BAS included in the QuickBASIC package, this uses the computer as a "dumb" terminal. Commands are sent to the motor driver with a carriage-return, and replies to status requests are printed on the computer screen.

2. SRS240 -- Communicate with Stanford interface.

   Unable to use the computer as a terminal, due to carriage-returns being fatally uninterpretable by the Stanford interface, this program was written to send "strings" without end-of-command suffixes, read replies, and print them to the screen.

3. RAMAN -- Acquire and plot a Raman spectrum.

   This program prompts user for scan parameters: starting wavelength, scan length, wavelength increment and number of laser shots to average. It initializes the monochrometer motor drive, setting acceleration, velocity and steps for wavelength increment. It initializes Stanford interface to synchronous mode (triggered by laser) and tells it the number of pulses to average. Calculates wavenumber (cm-1) shift from

monochrometer wavelength. Begins scan loop: read Stanford analog input channel #1 to which is connected "average output" of boxcar, plot the data point on the screen, move monochrometer one increment. When all points have been acquired and plotted, rescale the data to fill the screen and return monochrometer to starting wavelength. Write data to floppy disk in drive A.

4. WIRE -- Heat W wire, read temp., voltage and current.

Initialize Stanford interface to asynchronous mode. Prompt user for voltage to send to transadmittance amplifier, wait for temperature to stabilize. Read amplified thermocouple voltage (temperature), voltage drop across W wire, current through wire, and print values to screen.

5. PLOTCAL -- Integrate area under Raman peak.

Read a data file (x,y array) from disk in drive A. Plot data on screen. Use cursor keys to change baseline and limits of integration. Calculate area under Raman peak using trapezoid rule. Print area and peak height to screen.

E. Vacuum reaction chamber

Because the purpose of this project is to understand basic gas/solid chemistry and gas phase chemistry, a reactor was designed which minimizes mass and heat transport effects. It is a differential reactor, in that very little of the reactants are consumed by the very small area. The depositing surface is a fine tungsten wire stretched along the axis of a nickel coated stainless steel cylinder. The local gas composition is monitored with the laser Raman signal of key reactants and products. The laser measurements can be correlated to mass spectroscopy measurements taken with a microprobe placed near the growing filaments. Complex reaction dynamics can be unravelled by making step changes in wire temperature or gas composition land watching the gas phase composition response.

The reactor is plumbed by a turbomolecular pump and/or a corrosion resistant mechanical pump. The lines are stainless steel, but the chamber and the lines to the pumping system are nickel coated. This reactor is built and can be pumped to 10-7 torr. when it is desired to study reactions on flat substrates, a small piece of a wafer will be suspended within the reactor and heated by passing a current through the sample, a standard technique in ultrahigh vacuum studies. Eventually the chamber itself can be replaced with one which can accommodate large sized substrates. The walls of the reactor are kept cold to prevent deposition and growth on the walls and windows of the reactor. For reactants which require a significant residence time at high gas temperatures in order to allow for the homogeneous formation of a precursor, the wire will probably run hotter in this cold wall system in order to achieve the same fiber growth. The gas composition can be monitored as a function of time and distance from the wire with the reactor in batch mode to selectively identify homogeneous and heterogeneous reactions.

F. Gas calibration studies

Calibration curves have been completed for nitrogen, hydrogen and methane from atmospheric pressure down to 3 torr as seen in Figures 5,6 and 7. The signal at one torr is obtained by scanning for 25 A, averaging over 100 samples. For a laser frequency of 10 Hz and a resolution of 0.25 A, the running time is 15 minutes per

sample. A narrower scan width will allow much more frequent sampling. Changing the PMT will give the added sensitivity in the subtorr rang if it is found to be necessary. For the hydrogen calibration, peak area versus hydrogen pressure is linear with a least squares correlation of 0.9994. A subtorr pressure gage has been purchased so that calibrations below 1 torr can begin.

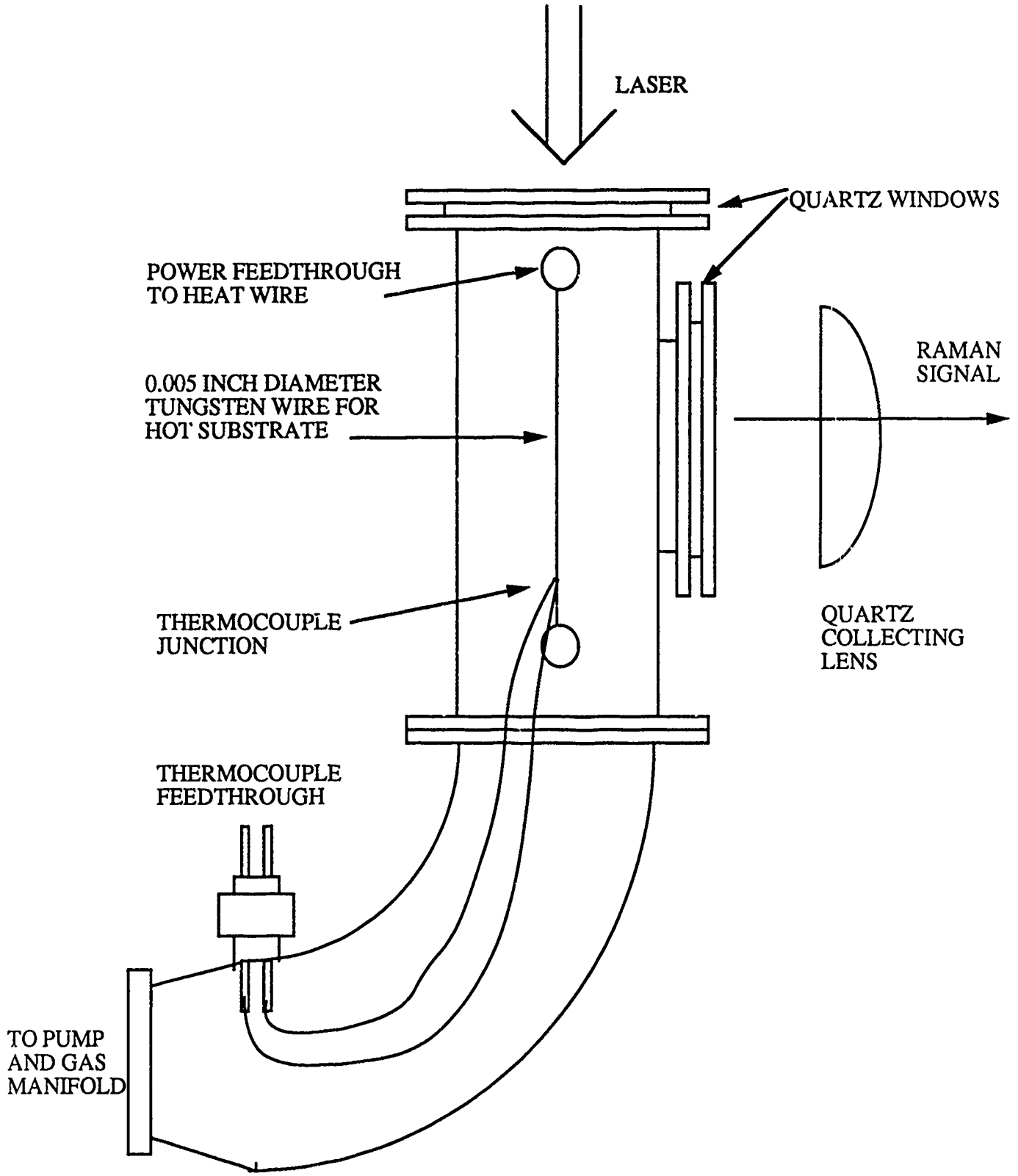

FIGURE 1. Wire CCVD reactor

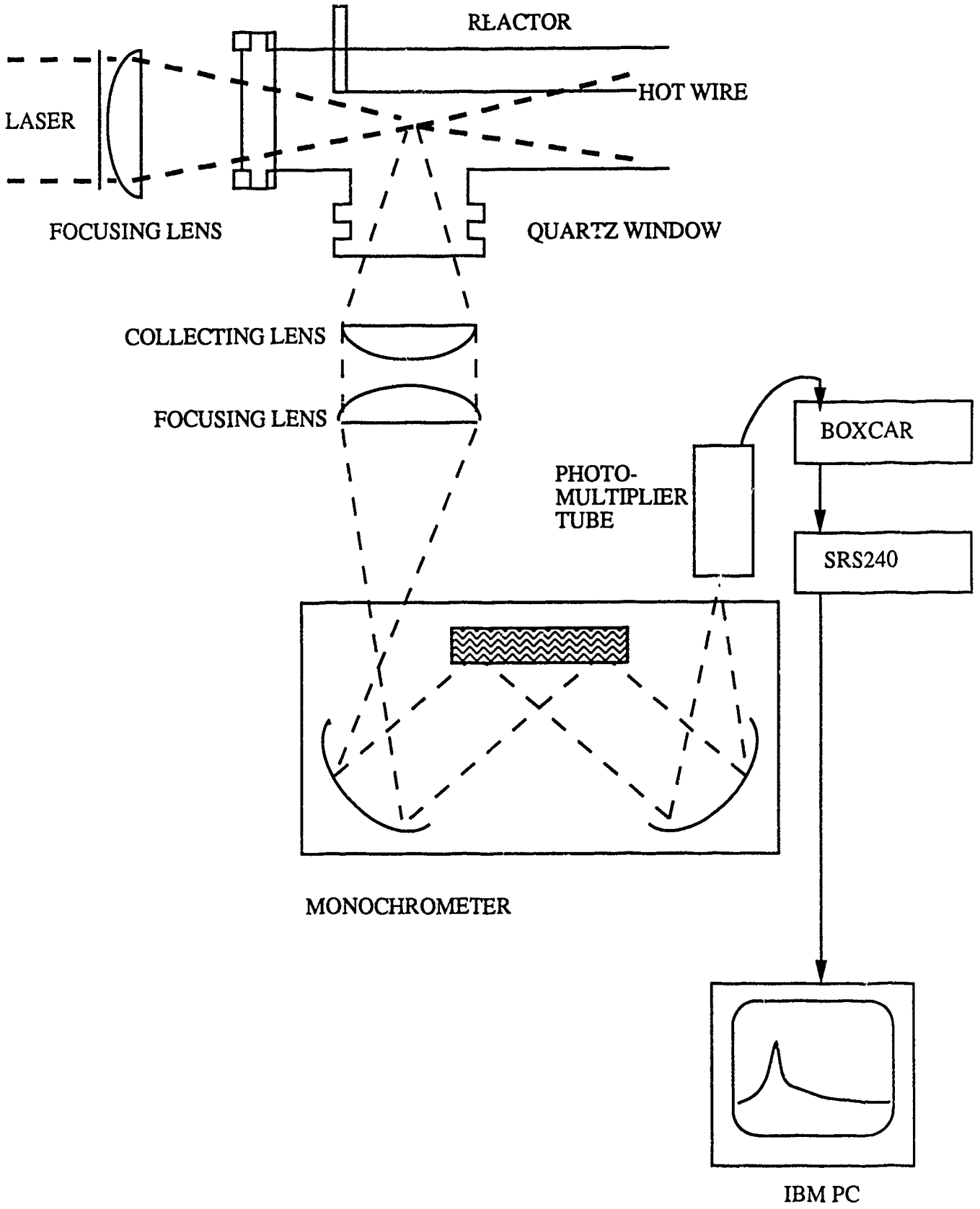

FIG. 2 Optical System for Raman Spectroscopy

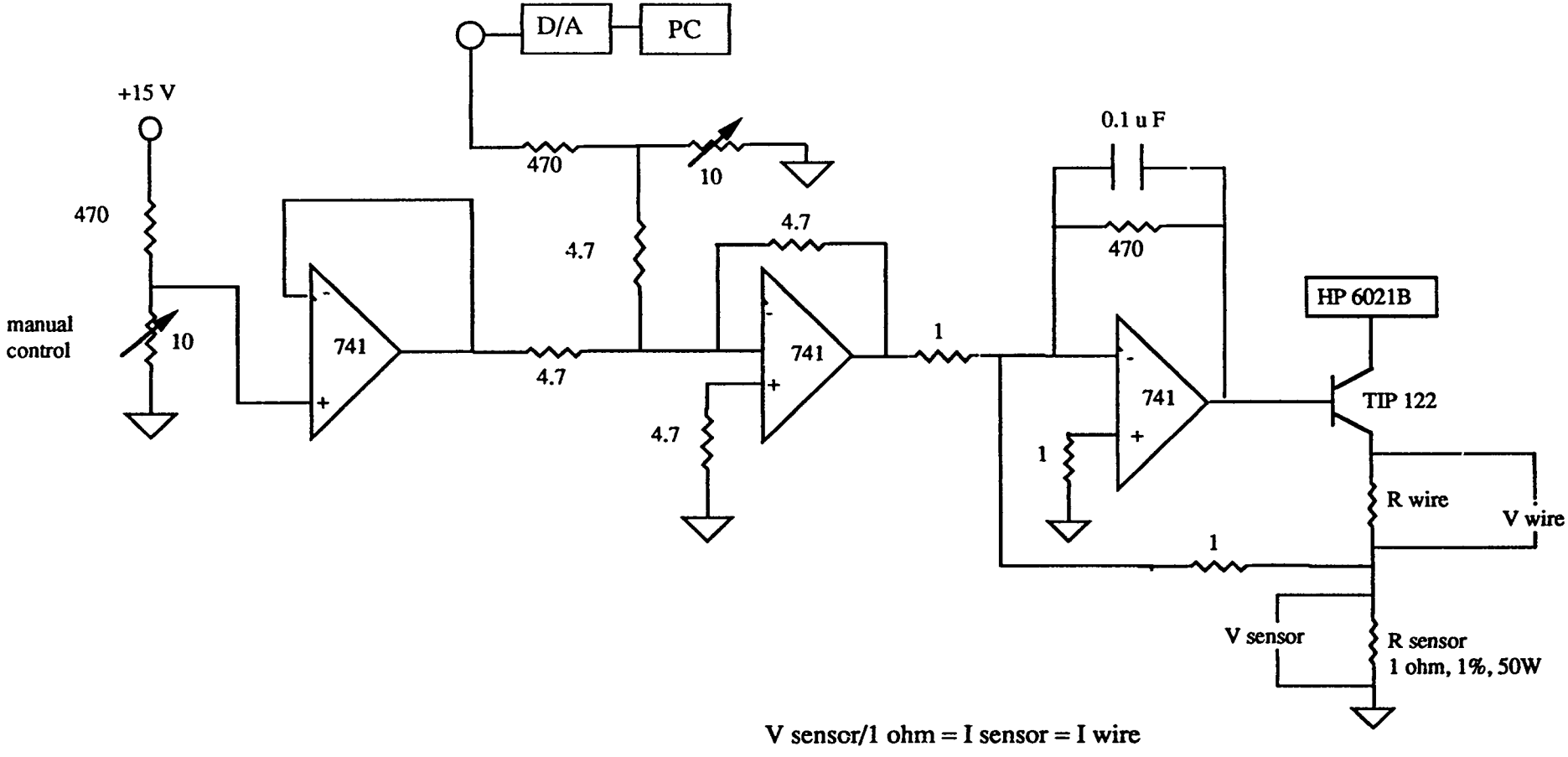

FIGURE 3. Transadmittance Amplifier with manual and computer control. All resistances in kilo-ohms except sensor. HP6012B is a Hewlett Packard constant voltage 1000 W power supply. TIP122 is an NPN Darlington transistor.

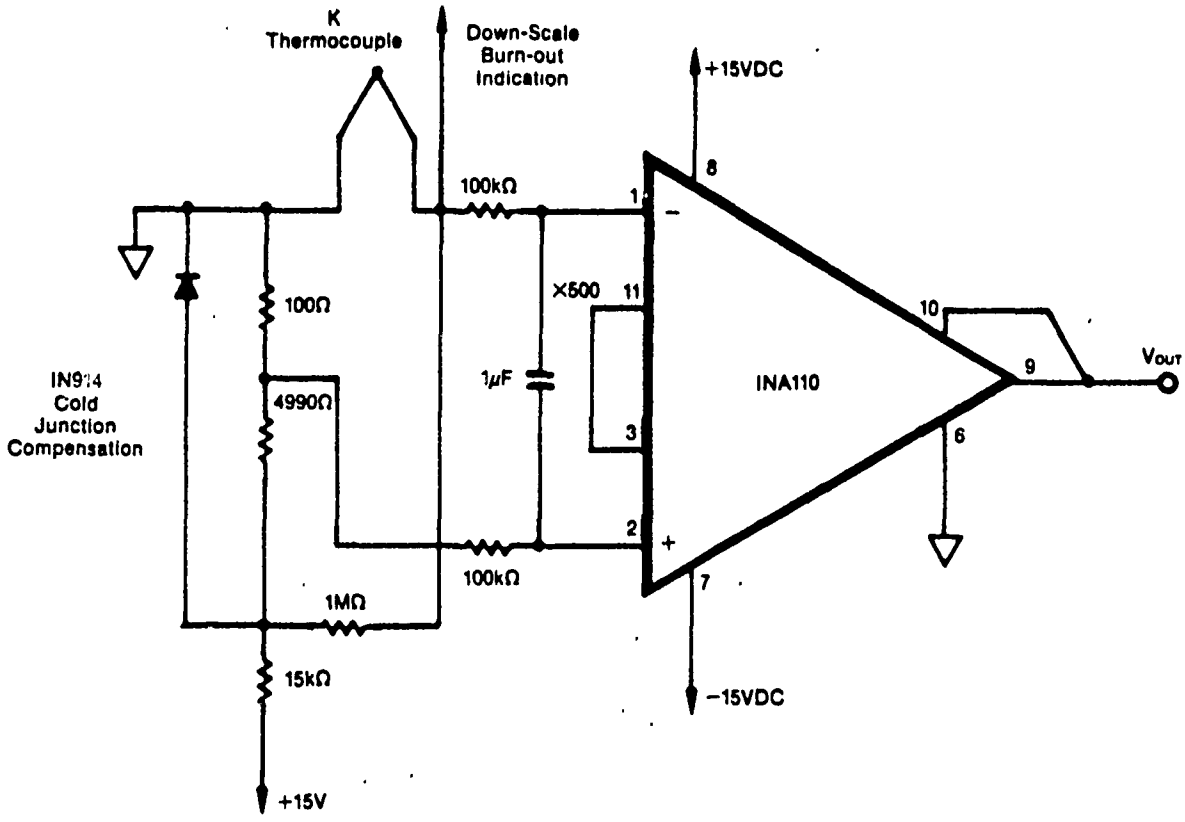

FIGURE 4. Thermocouple Amplifier with Cold Junction Compensation and Input Low-Pass Filtering (<1Hz).

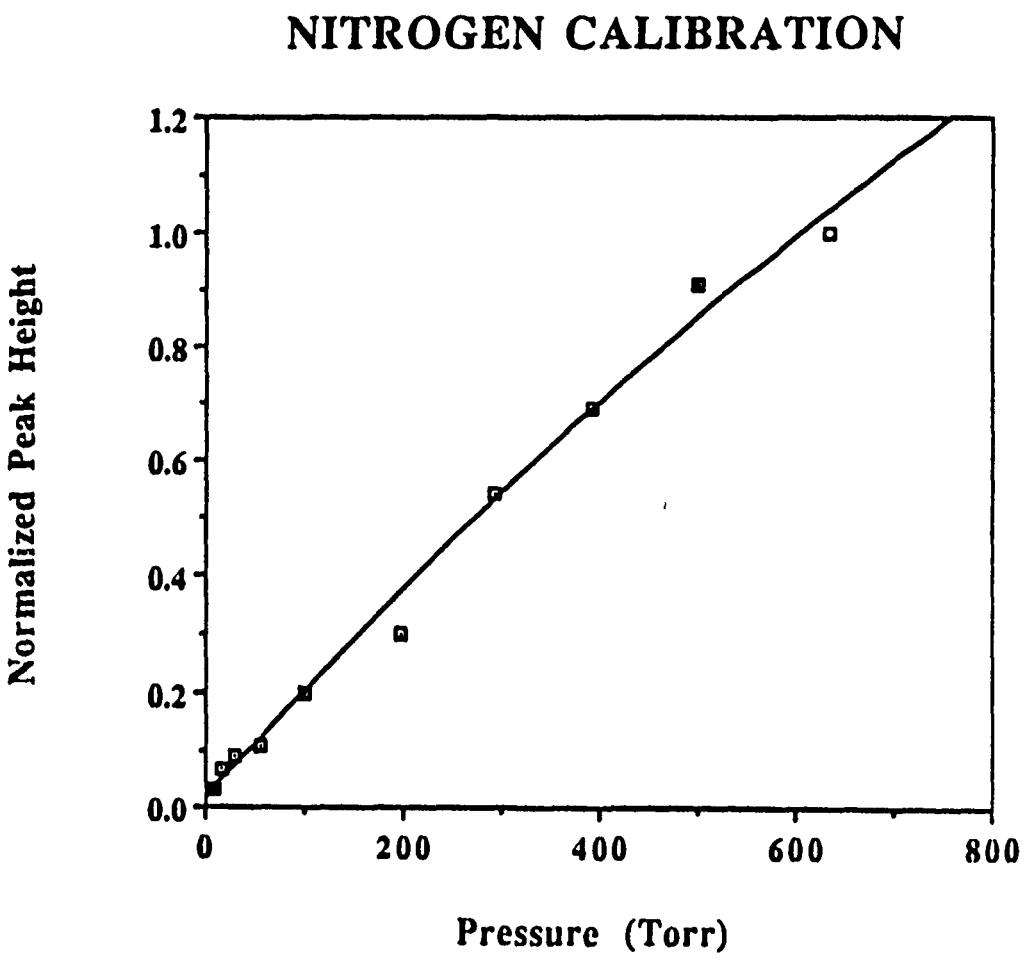

Figure 5. Calibration of Nitrogen Laser Raman Signal versus Pressure

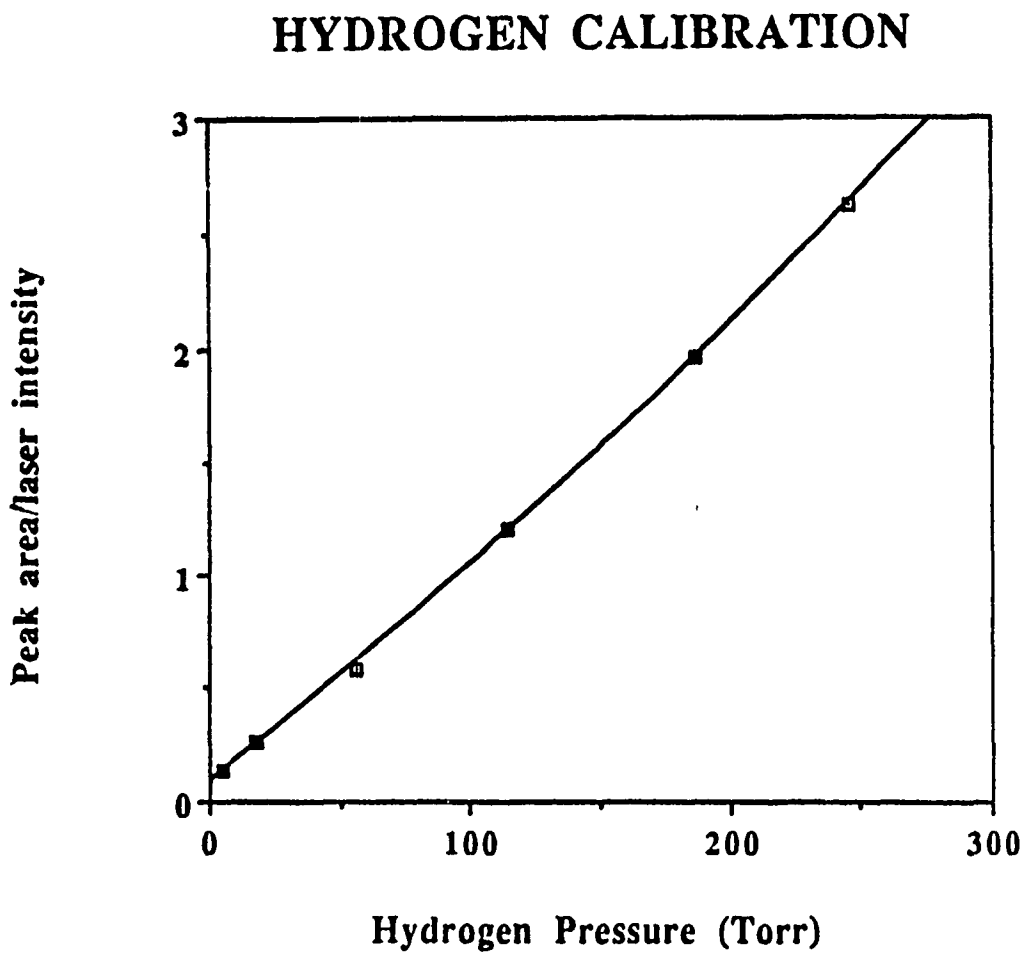

Figure 6. Calibration of Hydrogen Laser Raman Signal versus Pressure

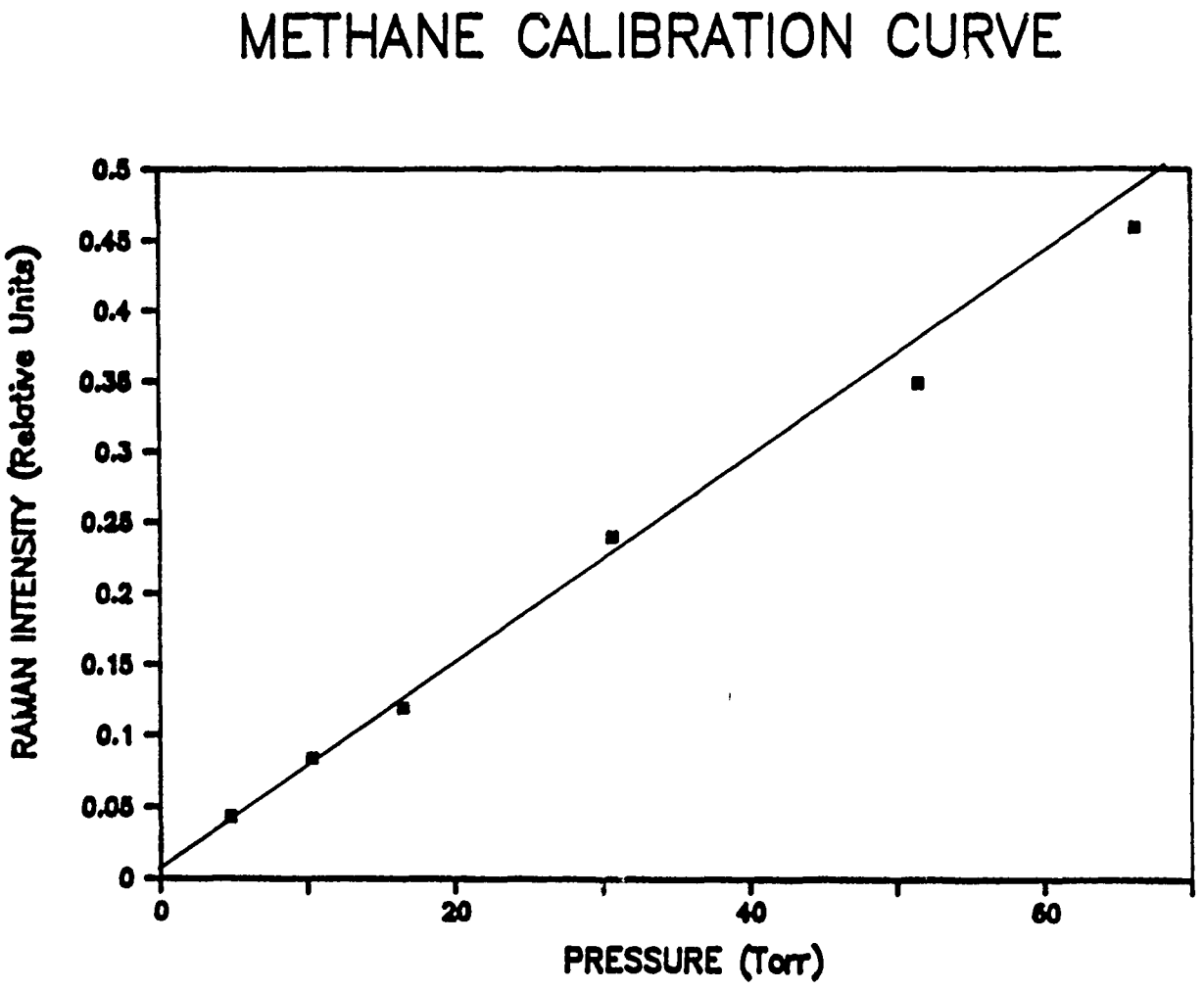

Figure 7. Calibration of Methane Laser Raman Signal versus Pressure

6. ADDITIONAL ACCOMPLISHMENTS

I. X-ray diffraction of CCVD carbon fibers under applied stress

II. Numerical simulation of carbon whisker growth

III. Carbon Boron-Nitride

IV. Other related work completed including a book

I. X-RAY DIFFRACTION OF CCVD CARBON FIBERS UNDER APPLIED STRESS

X-ray diffraction provides important information about the structure of carbon fibers. The inter-layer spacing and the in−plane crystallite size of carbon fibers can be obtained from the diffraction lines and their half width at half-maximum intensity. The diffraction linewidth in the azimuthal direction also measures the preferred orientation of carbon ribbons. This method has been used to characterize CCVD fibers [1] as well as other types of carbon fibers such as ex-PAN fibers [2]. The misorientation angles Φ deduced from the azimuthal linewidth of the (002) diffraction line have been used to calculate the Young's modulus of carbon fibers to test theoretical models [3].

Another phenomenon called "strain stiffening" has been observed especially in CCVD fibers. Young's modulus increases with applied stress by 28% [2] and torsional modulus increases by as much as 100% [4]. They are believed to be due to the improvement of preferred orientation of graphene planes as suggested by Curtis et al., [5]. Because of its capability of providing information about preferred orientation, x−ray diffraction of CCVD fibers under applied stress can be used to distinguish this postulation. Therefore, we felt that it was important to attempt to carry out this experiment.

X-ray diffraction is a well developed technique. Considering a monochromatic x−ray beam of wavelength λ incident on a crystal, diffraction occurs when the scattered wave vector $k_s = 2\pi\hat{k}S/\lambda$ satisfies the condition:

$$\Delta k = (k_S - k_0) = G \tag{1}$$

where $k_0 = 2\pi\hat{k}_0/\lambda$ is the wave vector of the incident beam, G is any reciprocal lattice vector of the crystal.

The inter-layer spacing d_{hkl} between the (hkl) planes are obtained according to Bragg's law:

$$n\lambda = 2d_{hkl}\sin\theta_{hkl} \tag{2}$$

where θ_{hkl} is Bragg angle. The interplanar separation $\tilde{c}$ which is measured by the (002) x−ray diffraction d_{002} indicates the degree of graphitization of a carbon fiber. A parameter called the graphitization index g_p is suggested by Dresselhaus et al., [3]:

$$g_p = (0.344 - \bar{c}) / (0.344 - 0.3354) \quad (3)$$

If the graphene planes were perfectly aligned with the fiber axis which is perpendicular to the x−ray beam in a diffraction experiment, the (002) diffraction would be a sharp dot on the film. The misorientation of these planes results in a spot smeared in the azimuthal direction on the film. Therefore, the misorientation angle Φ is obtained by measuring the half−width at half maximum intensity of (002) peak.

X−ray diffraction study of CCVD carbon fibers was attempted in our lab. The geometry of the experiment is illustrated in Fig. 1. X−ray beam is produced by a molybdenum tube. The fibers are mounted vertically and perpendicular to the x−ray beam. Weights are hung on to the lower end of the fibers through a clamp to apply stress. The figure also shows the schematic of the misorientation angle Φ.

The thin CCVD fibers (~7 μm diameter) are technically important. At first, we used about 100 fiber bundle for the diffraction study. A combination of epoxy and mechanical clamping jigs were employed to hold the fiber bundle (Fig. 2). However, up to 36 hours of exposure of x−ray diffraction did not show any distinguishable patterns. Next attempt was made on 20 thicker (~50 μm diameter each) fiber bundle. Diffraction of (002) spot was obtained but lacked details for quantification with applied stress. A quick calculation indicates that the effective volume of 20 thick fibers is equivalent to more than 500 thin fibers. It is almost impossible to mount this many fibers and maintain a constant stress per fiber. Therefore, conventional x−ray facility is not appropriate for this kind of study. The reasons are: first of all, conventional x−ray tube does not provide enough x−ray flux to obtain a clear pattern for a reasonable exposure. Secondly, the background diffraction is to high to achieve sharp contrast pictures. The only possible method is to use synchrotron radiation which has high x−ray intensity and high monochromaticity to give optimum information in a relatively short exposure. These measurements are extremely important in correlating other mechanical properties of carbon fibers.

II. NUMERICAL SIMULATION OF CARBON WHISKER GROWTH

This work was conducted on a subcontract by Prof. Dimitri D. Vvedensky (The Blackett Laboratory, Imperial College). There is very little reported on the theoretical calculation of whisker/filament growth of carbon fibers. However, considerable progress has been made on the semiconductor technology. Specifically, numerical simulation of molecular beam epitaxial (MBE) growth of semiconductor structures. On a parallel basis to the MBE, attempt was made to numerically simulate the whisker growth of carbon fibers.

Only preliminary progress has been made. Further work is required to complete this research. The following possible pathways to whisker growth have been identified:

* Spiral Defects - We simulated crystal growth under a continuous flux of atoms on a substrate into which we embedded a linear dislocation, with spiral defects at each terminator. This procedure yielded a growth mode similar to that of a whisker, however, the structure generated had a very low height to diameter aspect ratio, unlike those observed experimentally
* Location of Nucleation Centers - Using a considerably simplified algorithm we analyzed a

sputter/redeposition process. Atoms were removed from the surface and redeposited in a random fashion with the exception that a small fraction of surface atoms acted as immovable nucleation centers. Atoms landing upon a nucleation point, become nucleation points; atoms landing adjacent to a nucleation point become fixed atoms - otherwise they remain subject to another sputtering event. This procedure resulted in whiskers with very high aspect ratios and, although somewhat simpler than the previous technique, is more in accord with the experimental situation. The results is shown in Fig. 3.

In a parallel effort we have under taken a major revision of our simulation code, incorporating a considerably more efficient and versatile algorithm. Based upon the generation of random events, driven by cumulative rate equations, this has yielded a two order of magnitude improvement in processing speed. This allows the use of micro rather than super computers, considerably reducing development costs.

Two benefits from the simulation of whisker growth occur from these developments:

* We can study near-equilibrium phenomena, such as whisker growth, as the program rescales its time increment according to the level of surface activity.
* The event generation strategy of the code, facilitates ease of addition of extra events, such as ion−atom scattering, as well as surface diffusion and atom incorporation.

III. CARBON-BORON NITRIDE AND HOPG

1. Properties and Characterization of Codeposited Carbon Boron Nitride and Carbon Materials

A full publication our work on C−BN has been presented in J. Applied Physics 65, 5109−5118 (1989). A reprint has been given in the Appendix. The physical properties of carbon-boron nitride (C−BN) prepared from mixtures of BCl_3, NH_3, and selected hydrocarbons by co−deposition methods have been investigated using x−ray diffraction, electron diffraction, TEM, XPS, Raman scattering, optical reflectivity, thermal conductivity, thermopower, and electrical resistivity. Taken collectively, the results of these experiments indicate that the compression−annealed C−BN materials studied here consist of separated domains of pyrolytic boronated graphite and pyrolytic boron nitride, while as−deposited samples may possibly be a single phase mixture of C, B, and N.

2. Galvanomagnetic Studies of HOPG

In an earlier chapter a program for the growth of straight and thin carbon fibers was described. The technique involved Catalytic Chemical Vapor Deposition (CCVD). Included in the study was a substrate dependent growth. CCVD of carbon fibers were prepared from benzene and hydrogen with Fe catalyst. In one of the studies, effect of employing Highly Oriented Pyrolytic Graphite (HOPG) substrates was carried out. A conflicting observation was made. It was found that the catalyst particle resided perhaps on the surface of substrate rather than on the tip of the filament. Surface examination revealed a lack of catalytic particles after growth. Therefore, an electrical characterization of the HOPG substrates was undertaken to determine the disappearance of the Fe catalyst via diffusion.

The results of resistivity measurements were surprising. The resistivity curve for the modified sample is

shifted downwards and the temperature coefficient becomes more positive indicating that graphitization has occurred. The curve is similar to ones obtained on samples heat treated to 3000°C or higher, but the sample has not been heated above 1100°C! This is similar to the result obtained on CCVD fibers prepared at 700°C with Ni catalyst on Si surfaced (Zhao et al., 1988). It is known that Fe can catalyze graphitization, but the present results are exceptional. It is possible that there is technological significance.

Several samples of HOPG were coated with Fe and heated to temperatures in the range of 800−1000°C. No changes in the resistivity, magnetoresistance or the Hall effect of the magnitude expected were observed. Measurements at 4.2 K and fields up to 15 Tesla also showed no evidence of enhanced graphitization of the HOPG due to Fe diffusion. Therefore, further work is required before any conclusions can be made on the disappearance of the Fe catalyst from the surface of the HOPG substrate during CCVD at ~1000°C, and why there is a large reduction in the resistivity of the catalyzed HOPG compared to the untreated substrate.

IV. OTHER RELATED WORK COMPLETED

1. Book--Graphite Fibers and Filaments

Professor Ian L. Spain was a co−author of a book entitled Graphite Fibers and Filaments that was bound and published during the present contract period. The book describes the preparation, microstructure and defects, electronic structure, lattice, thermal, mechanical, magnetic, electrical and high temperature properties of carbon fibers, together with modifications introduced by intercalation and ion implantation. It concludes with a brief discussion of applications. Particular attention is given to the newly developed vapor−grown fibers, in an effort to elucidate the ultimate capabilities of carbon fiber science and technology.

The list below gives the book chapters.

2. X-Ray Diffraction Data for Graphite to 20 GPa

A paper on high pressure effect on graphite was published during the present contract. (See Appendix.)

3. The Role of Sputter Redeposition in the Growth of Cones and Filaments on Carbon Surfaces During Ion Bombardment

A paper on the growth of carbon filaments using high energy (~1 keV) argon ions was published in the J. Vac. Sci. Technology A8, 3907 (1990). Considerable interest has been shown by other laboratories on this report. The whole paper is given in the Appendix.

REFERENCES

1. G. G. Tibbets and C. P. Beetz Jr., J. Phys. D: Appl. Phys. 20, 292 (1987).
2. H. A. Goldberg, Final Report to U.S. Army Research Office, Contract No. DAAE29-81-C-0016, unpublished (1985).
3. M. S. Dresselhaus, G. Dresselhaus, K. Sugihara, I. L. Spain, and H. A. Goldberg, "Graphite Fibers and Filaments," Springer-Verlag, Berlin (1988).
4. Jianhui Chen and Dinesh Patel, to be submitted.
5. G. J. Curtis, J. M. Milne, and W. N. Reynolds, Nature 220, 1024 (1968).

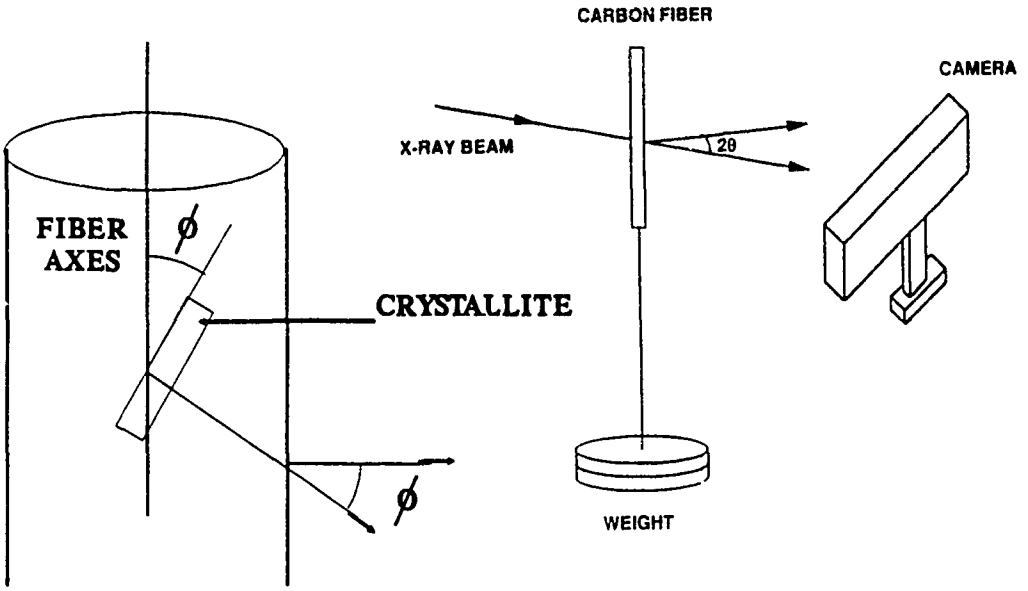

Fig. 1 A schematic diagram of the set up for x-ray diffraction of CCVD carbon fibers under applied tensile stress. A flat plate camera is employed to record the pattern. The inset show the geometry of the crystallite with the fiber axis.

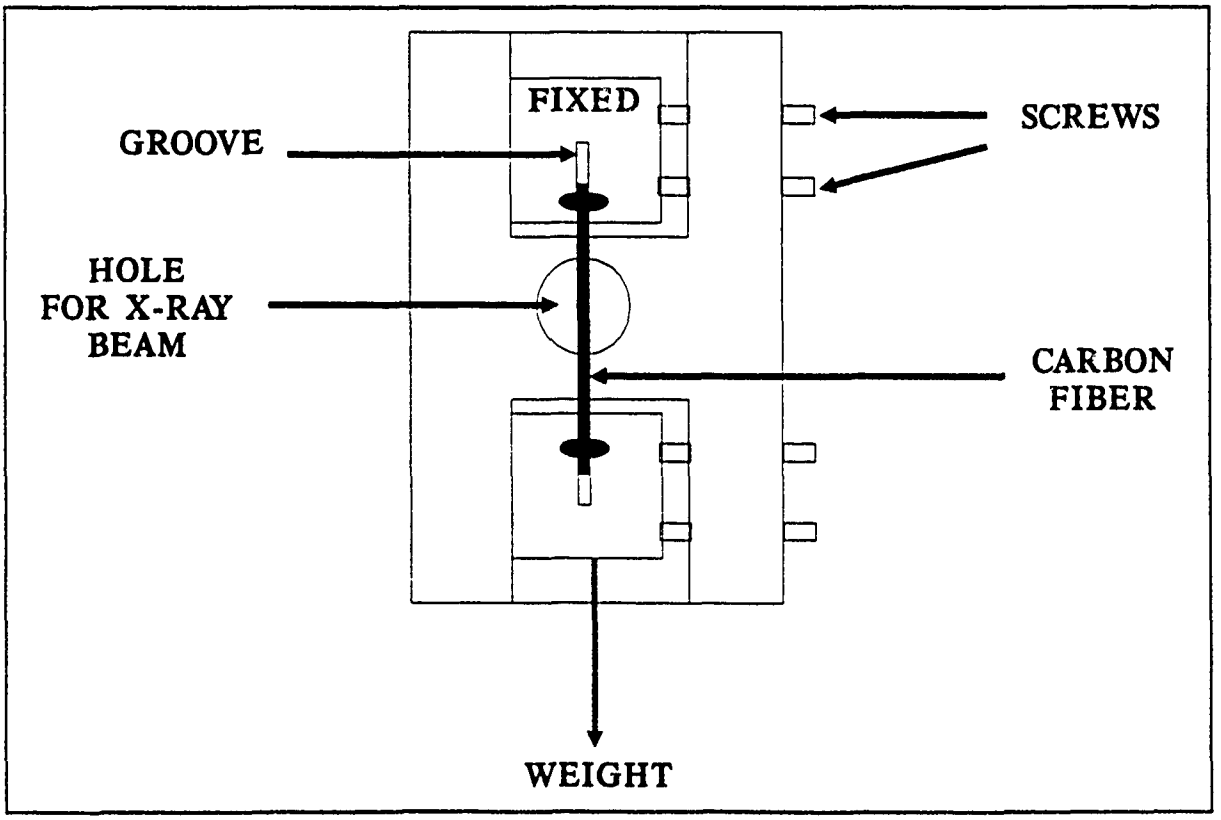

Fig. 2 Sample mount for x-ray diffraction of carbon fiber bundle under applied tensile loading.

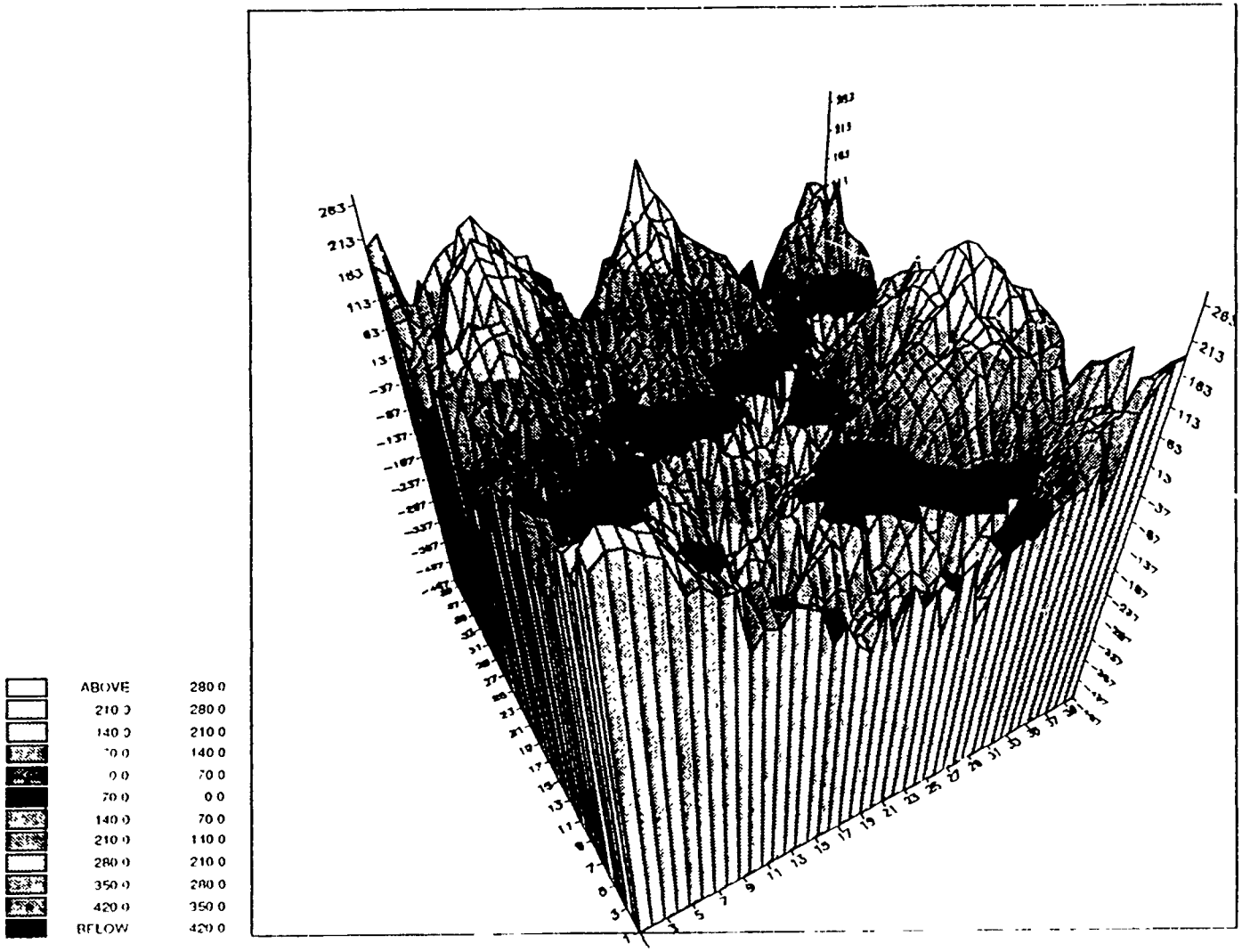

Fig. 3 A computer simulation of carbon whisker growth surface on a substrate.

APPENDIX

ABSTRACTS OF FUTURE PUBLICATIONS

1. Low Frequency Electrical Noise in Carbon Fibers Under Tensile Stress
2. The Electrical Noise of Carbon Fibers- The Dependence on Temperature
3. Temperature Dependent Piezoresistance in Carbon Fibers
4. Diameter Dependent Young's Modulus of Vapor Grown Carbon Fibers.
5. Diameter Dependent Young's modulus of Vapor Grown Carbon Fibers from Loop Test
6. Torsional Modulus of Vapor-deposited Carbon Fibers
7. Thickened ex-PAN Carbon Fibers by Vapor Deposition
8. Relation between structural, elastic and piezo-resistive properties of carbon fibers.
9. Intercalation of VGCF as a function of diameter

PUBLISHED PAPERS

1. The electrical noise of carbon fibers, R. O. Dillon, R. D. Kirby, and I. L. Spain, J. Appl. Phys. 66, 4284, (1989).
2. Electrical noise from carbon fibers, R. O. Dillon, R. D. Kirby, and I. L. Spain, CARBONE 90, Paris, July (1990).
3. Properties and characterization of co-deposited Boron Nitride and carbon materials, A. W. Moore, S. L. Strong, G. L. Dol, M. S. Dresselhaus, I. L. Spain, C. W. Bowers, J. P. Issi, and L. Piraux, J. Appl. Phys. 65, 5109 (1989).
4. The role of sputter redeposition in the growth of cones and filaments on carbon surfaces during ion-bombardment, W. A. Solberg and I. L. Spain; J. Vac. Sci. Tech., A8, 3907 (1990).
5. Graphite nature of chemical-vapor-deposited carbon filaments grown on carbon and Silicon surfaces, Y. X. Zhao, C. W. Bowers, and I. L. Spain; Carbon 26, 291, (1988).
6. X-ray diffraction data for graphite to 20GPa. Y. X. Zhao and I. L. Spain; Phys. Rev. B40, 993, (1989-I).

BOOKS

1. *Graphite Fibers and Filaments*, M. S. Dresselhaus, G. Dresselhaus, K. Sugihara, I. L. Spain, H. A. Goldberg. (Springer Verlag, NY) (1988).

1. **Low Frequency Electrical Noise in Carbon Fibers Under Tensile Stress**

Dinesh Patel and Yves Dumont*
Physics Department, Colorado State University, Fort Collins, CO 80523

R. O. Dillon and R. O. Kirby
Department of Electrical Engineering, University of Nebraska

Max Lake
Applied Sciences, Inc., Yellow Springs, Ohio 45387-0186

ABSTRACT

Electrical noise at low frequency(10-60Hz) have been measured for the first time in carbon fibers whilst they were subjected to tensile stress. The measurements were performed at room temperature. Low modulus ex-PAN carbon fibers showed a small reduction in the noise level for small stress. However, at higher stress the noise level increased gradually until fiber breakage. Measurements were also made on a higher modulus PAN fiber and Catalytic Chemical Vapor Deposited fibers (as-grown and annealed). One expected the fiber microstructure to become more aligned with stress thereby reducing the noise until fiber breaks when the noise would sharply increase. Our results, however, show that the stress dependant noise in these fibers are combination of parameters such as fibril alignment and electronic carriers. Models have been proposed to explain the noise behavior in these fibers.

ACKNOWLEDGEMENTS

This work is dedicated to Professor Ian L. Spain who died September 5, 1990. YD was a part of the team on leave from his graduate program in France. This project was funded by a grant from AFOSR to professor Spain at Colorado State University (grant No. S49620-88-C-0017).

(to be submitted to J. Appl. Phys.)

---

2. **The Electrical Noise of Carbon Fibers- The Dependence on Temperature**

R. A. Dutcher, R. O. Dillon*, R. D. Kirby*, I. L. Spain, and D. Patel
Physics Department, Colorado State University, Fort Collins, CO 80523

* University of Nebraska, Lincoln, Nebraska, NE 68588

ABSTRACT

Low temperature (80-300K) electrical noise have been measured in carbon fibers with varying degree of ordering. This report is an extension of our first publication (Journal of Applied Physics 66, 4284–87 (1989) involving low frequency noise in these fibers. The temperature dependent 1/f noise power spectra in these carbon fibers showed considerable details. Noise power show maxima at 230K and ~300K. These may be interpreted as multilevel electronic states that are probably common to all the fibers. Existing models based on noise measurements on non-fiber systems no not exactly explain our temperature dependence.

ACKNOWLEDGEMENTS

This work was performed under the contract number F49620-88-C-0017. This work was initiated by the late Professor Ian L. Spain and now continued by DP.

(in preparation)

3. **Temperature Dependent Piezoresistance in Carbon Fibers**

D. Patel
Physics Department, Colorado State University, Fort Collins, CO 80523
and
H. A. Goldberg
Celanese Research Company, 86 Morris Avenue, Summit, NJ 07901

ABSTRACT

At room temperature, the piezoresistance(PR) in ex-PAN and pitch based fibers was found to be weakly positive for turbostratic fibers, falling to increasingly negative values as Young's modulus increased. The negative PR was attributed to an electronic contribution to the PR which becomes more important as the graphitization of the fiber increases. At 11K, the amount of negative PR in the high moduli fibers was reduced compared to 300K. No temperature dependence was observed for the low moduli fibers. At 300K, the PR of annealed CCVD high modulus fiber is positive compared to the negative values for high modulus PAN and pitch fibers. The positive PR in this CCVD fiber is due to the high degree of 3D ordering. Here we have observed, for the first time, a positive-to-negative transition in PR at low temperature. This result is an indication that perhaps new phenomenon exist in these annular or tree-ring annealed CCVD fibers.

ACKNOWLEDGEMENTS

The authors wish to thank Ruediger Hennicke (an exchange student) for adapting a cryostat for the low temperature piezoresistance measurements. The present work was performed under a grant from AFOSR (grant No. S49620-88-C-0017).

(in preparation for J. Appl. Phys. or Carbon)

---

4. **Diameter Dependent Young's Modulus of Vapor Grown Carbon Fibers.**

D. B. Church and D. Patel
Physics Department, Colorado State University, Fort Collins, CO 80523

ABSTRACT

A simple yet accurate test apparatus for stress-strain profiling has been developed using linear variable differential transformers. Displacement resolutions of about 2μm can be detected with ease. This is sufficient for single carbon fibers which typically have strain values less than 1%. Young's modulus of vapor grown carbon fibers with varying diameters have been measured successfully. Results show a decrease in the Young's modulus with increasing fiber diameter. A value of 200 ± 15 GPa was obtained for an 8μm sample in agreement with values reported elsewhere, however somewhat lower values < 100 GPa were obtained for larger $\sim 20\mu$m diameter fibers. Step-like stress-strain profiles were recorded on the annealed (>2500°C) vapor grown carbon fibers. All results are discussed in terms of a tree ring morphology of the vapor grown carbon fibers.

ACKNOWLEDGEMENTS

The experimental work was performed by DBC towards a B.Sc. degree in Physics at Colorado State University. This project was funded by a grant from AFOSR grant No. S49620-88-C-0017).

(to be submitted to Rev. Sci. Instrm.)

5. **Diameter Dependent Young's modulus of Vapor Grown Carbon Fibers from Loop Test**

ABSTRACT

Diameter dependent (θ) Young's modulus (E_y), of as-grown CCVD carbon fibers were obtained from a single batch. The measurements were made during loop test of single fiber. Results show decreasing E_y with fiber diameter increasing from 5 to 10μm. Then an increase in E_y with $10<\theta<20\mu$m. Other reports of $dE_y/d\theta$ show a general negative behavior with large range of θ(0-100μm). However, our study for the first time on a single batch of fibers ranging from 5 to 20μm have shown a detailed behavior previously unseen or masked by the large number of measurements. Our interpretations are based on microstructural entities, within the annular morphology of the CCVD carbon fibers. A Matthiessen's type of behavior has been inferred for the E_y, [$E_y=1/(\Sigma\alpha_i/E_i)$].

ACKNOWLEDGEMENTS

The vapor grown fibers were acquired from Applied Sciences, Inc. BG was partially supported by an undergraduate assistance by Colorado State University towards a B.S in Physics. This work was performed under an AFOSR grant No. S49620-88-C-0017.

(in preparation for J. Appl. Phys. or Carbon)_

6. **Torsional Modulus of Vapor-deposited Carbon Fibers**

J. Chen and D. Patel
Physics Department, Colorado State University, Fort Collins, CO 80523

ABSTRACT

The torsional modulus (G) of catalytic chemical vapor-deposited (CCVD) carbon fibers of both as-grown and annealed samples were determined with a torsion pendulum. G is found to be both stress and size dependent. The extrapolated zero-stress value of torsional modulus is 105 $\pm$ 5 GPa for a 5.4 μm diameter as-grown fiber and 200 $\pm$ 10 GPa for a 8.4 μm diameter annealed fiber. G decreases with increasing diameter. These unusually high values of torsional moduli, compared to other types of carbon fibers, are believed to be the results of the tree-ring structural morphology and the degree of graphitization of these CCVD fibers.

ACKNOWLEDGEMENTS

The authors want to thank Y. Lu and D. Church for their efforts in constructing the torsion pendulum. This work is supported by Air Force Office of Scientific Research grant number F49620-88-C-0017.

(to be submitted to Carbon or J. Appl. Phys.)

7. **Thickened ex-PAN Carbon Fibers by Vapor Deposition**

F. Dillon*, C. McConica#, H. Marsh*, I. L. Spain, and D. Patel
Physics Department # Agricultural & Chemical Engineering Department
Colorado State University, Fort Collins, CO 80523

* Present address Northern Carbon Research Lab, University NewCastle Upon, U.K

ABSTRACT

Ex-PAN fibers were thickened to varying degrees by vapor deposition of hydrogen/acetylene gaseous mixtures. The pyrolysis of the hydrogen/acetylene mixture can produce two distinct forms of carbon: (1) vitreous pyrolytic carbon and (2) colloidal soot. The production of vitreous pyrolytic carbon is favored when the partial pressure of acetylene is low. The reaction conditions (partial pressure of acetylene, total gas flow, and time) were varied to optimize the thickening rate and minimize non-uniform growth along the length of the fiber. The same reaction mechanism controlling the thickening of CCVD filaments appears to control this thickening of ex-PAN carbon fibers. Both are composed of concentric rings of pyrolytic carbon. 10-300K temperature dependent electrical resistivity have been obtained. Magnetoresistance measurements at 4.2K and fields up to 15 Tesla have been carried out.

ACKNOWLEDGEMENTS

The samples were prepared here at Colorado State University by FD (an international exchange Ph.D., student). The work was conducted under an AFOSR grant No. F49620-88-C-0017.

(in preparation for Carbon)

Relation between structural, elastic and piezo-resistive properties of carbon fibers.

H. A. Goldberg, F. Haimbach, J. Stamatoff, and

Celanese Research Company, Summit, NJ 87901

I. L. Spain
Physics Department, Colorado State University, Fort Collins, CO 80523

ABSTRACT

The piezo-resistance coefficient of several ex-PAN and pitch carbon fibers has been obtained at room temperature. The coefficient is positive for poorly graphitized fibers with low modulus of Young's modulus, and falls to increasingly negative values as the graphitization index and Young's modulus increases. A model which quanitatively explains the observed trends is presented, based on geometrical and electronic contributions to the coefficient. Structural and mechanical data are presented, allowing the parameters of interest to the above model to be evaluated. The data allow the relationship of Young's modulus to elastic and structural parameters tobe investigated more carefully than has been dene before.

(sumbitted and reviewed by Philosophical Magazine)

= ********* include PC of VGCF paper for CARBON ********

INTERCALATION OF VGCF AS A FUNCTION OF DIAMETER

M. L. Lake and K. K. Brito
Applied Sciences, Inc.
800 Livermore Street
Yellow Springs OH 45387
and
D. Patel and J. Chen
Department of Physics
Colorado State University
Fort Collins CO 80523

INTRODUCTION.

Vapor grown carbon fiber (VGCF) represents a new type of carbon fiber in contrast to pitch-based and PAN-based precursors. Produced from the vapor state by pyrolysis of methane, VGCF has been under limited development in Japan (Shinshu University, Nikkiso, NKK Ltd.) and the United States (General Motors Corporation, Applied Sciences, Inc.) over approximately the past ten years. Owing to the production method of VGCF, it is relatively easy to produce carbon fiber in which the morphology can be varied from virtually amorphous to nearly single crystal graphite. Since heat-treated VGCF closely resembles graphite single crystals in both structure and properties, it provides a unique structure on which to investigate the limits of graphite fiber-based composites. Beyond this, novel chemistry can be applied to improved upon the single crystal limits for properties such as oxidation resistance and electrical resistivity, with possibly acceptable trade-offs in other physical properties. Again, because changes in production phase fibers are prohibitively expensive, these novel approaches have not been extensively explored.

Production of VGCF geometries ranging from fiber diameters of 0.01 μm to 100 μm, and fiber lengths from microns to meters or longer is currently possible. Convenience and economy of production suggest that fiber with diameters lower than those conventionally obtained from pitch or PAN-based precursors could be produced in large quantities, for use in composites for electromagnetic shielding and other electric or electromagnetic applications. While intercalation of fiber with diameters in the 5 to 10 μm range has been shown to produce a decrease in the electrical resistivity of up to a factor of ten, the potential for altering the resistivity of smaller diameter fibers is not well-established.

The electrical resistivity of the fiber is an intrinsic property of the fiber which is useful for assessing the utility of fiber in electrical and electromagnetic applications, as well as in determining the relative degree of graphitization and crystallite size within the fiber. Thus, the resistivity bears implications on other properties of the fiber such as strength, modulus, and thermal conductivity, and can therefore be a useful tool in quality assurance of the fiber production process. While the resistivity should be diameter independent, this is not the observed case both for pristine and intercalated VGCF. In the case of pristine fiber, the resistivity is believed to be influenced by increased strain in the lattice structure of axially-circumferential graphene planes as the diameter decreases. In the case of intercalated fiber this effect is compounded by a depletion layer from which the intercalant escapes following removal of the fiber from the intercalation reaction chamber[1]. The depth of the apparent depletion layer is influenced by degree of graphitic perfection, and is larger for the more graphitic fibers such as VGCF because of the greater order of graphitic planes. The depletion layer can be expected to dominate the resulting resistivity of an intercalated fiber as the diameter of the fiber decreases to values which approach the depth of the depletion layer.

EXPERIMENTAL PROCEDURE.

Four samples of VGCF were prepared. Two samples were composed of pristine and brominated VGCF where the diameters were selected between a range of 10 to 55 μm. The other two samples were made up of fibers with an average diameter of 2.7 μm. Figure 1 is a histogram showing the distribution of diameters for the latter samples as determined by computer-assisted image analysis.

All VGCF samples were heat-treated to 2800 °C for ten minutes. Bromine intercalated VGCF samples were prepared by exposure to a saturated bromine vapor over a nine day period. Following intercalation, the fibers were allowed to degas at room temperature over a three day period while exposed to a gentle flow of dry air.

A four point probe method was used to measure the electrical resistivity of VGCF at room temperature. In conjunction with the resistivity measurements, fiber diameters were measured with a resolution of $\pm$0.3 microns. Sample length was typically 4 to 5 millimeters, with 1 mm contact separation. Micro-circuit type sample mounts were prepared in order to maintain consistency between sample measurements. The ratio between contact size and distance between potential leads was less than 10%. Conducting silver epoxy was used to contact the fibers to the sample mount. Sample currents were kept low to avoid sample heating. Typical currents of 10 μamps were employed in these resistivity measurements. Sample potential was detected with a dc amplifier capable of up to 10^3 gain. For each fiber, 1000 measurements were performed automatically over about 10 minutes, and an average resistivity for that fiber was obtained.

RESULTS AND DISCUSSION.

Room temperature resistivity of pristine and brominated VGCF is shown in figure 2 for fiber ranging from 10 to 55 μm. A noticeable decrease in resistivity was observed for the brominated samples. In fact, a 50% decrease was observed for the brominated samples. There is only a small diameter dependence of the resistivity in these fibers. The scatter in the data is consistent with results on benzene-derived fiber[2] when plotted on a log scale. In the batch of brominated samples, only 10 to 30 μm diameters were available.

Results of the resistivity measurements on a number of smaller (2.7 μm) are shown in figure 3. The pristine fiber has an average resistivity of 309 $\pm$ 100 μ-ohm cm, whereas the brominated set showed an average resistivity of 43 $\pm$ 13 micro-ohm cm for up to 15 samples. For these smaller diameter fibers, the relative scatter in the data are similar to those of the larger fibers.

Figure 4 shows the results of diameter dependent resistivity for all the samples ranging from 2 to 55 μm, both pristine and brominated. This figure shows that there is clearly an increase in the resistivity as the diameter decreases, as expected according to results obtained in references 1 and 2. These data also show a stronger effect from intercalation on the small diameter fibers than on large diameter fibers. This may result from the thinner fibers being easier to brominate than the larger diameter fibers within the same conditions.

The results of the size effect study on benzene derived fibers[2] are shown by the solid line in figure 3. The resistivities of both the pristine and brominated carbon fiber here are lower than the benzene derived fibers. The exception to this is the 2.5 micron pristine fiber. The decrease in resistivity with diameter is described empirically on an exponential form, $\exp(\Theta/\Theta_0)$ for the smaller diameter fibers. For the larger diameters, a $1/\Theta$ dependence was shown for the benzene-derived fibers. Results reported here on the bromine intercalated fibers do not show a $1/\Theta$ dependence, but rather show almost no dependence in the 10 to 50 micron range.

CONCLUSIONS.

A diameter dependent room temperature electrical resistivity has been obtained on pristine and brominated VGCF. Diameters ranged for approximately 2 to 55 microns. There was no significant resistivity dependence on diameter for the 10 to 50 micron diameter samples. However, the fibers in the 2 micron diameter range showed a factor of 6 increase in resistivity compared to the larger fibers. In both sets of brominated samples, the resistivities decreased compared to the pristine samples, with the 2 micron diameter sample showing almost an order of magnitude decrease. These results indicate that while a depletion layer may exist for VGCF which competes with the retention of intercalant within small diameter VGCF, that decreases in electrical resistivity can still be obtained through intercalation.

REFERENCES.

1. J. R. Gaier, Synthetic Metals 34, (1989) 745-750.
2. M. Tahar, M. Dresselhaus, and M. Endo, Carbon, 24, 67 (1986).

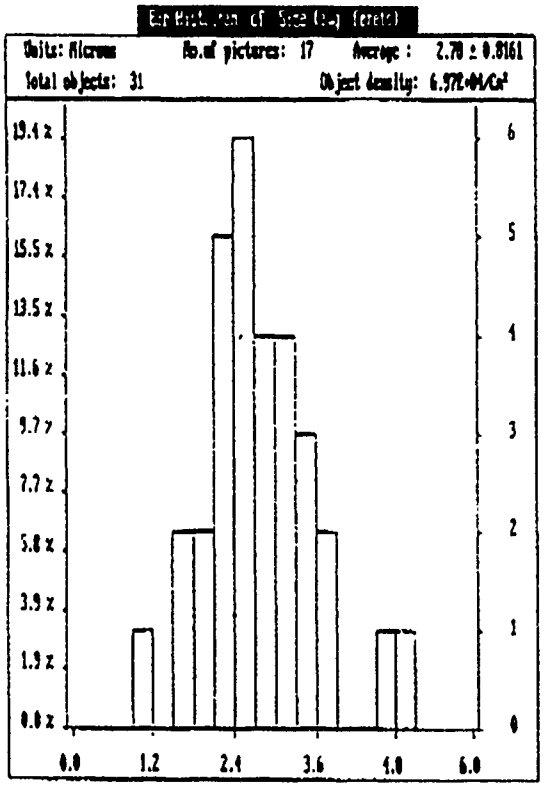

Figure 1 A histogram showing the distribution of fiber diameters.

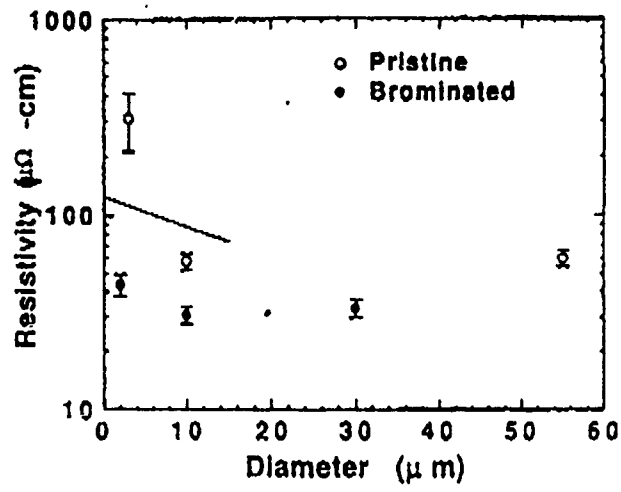

Figure 2 Room temperature resistivity of pristine and brominated VGCF.

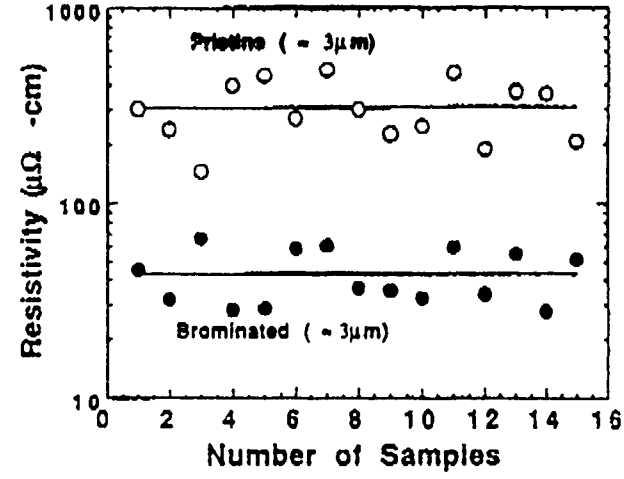

Figure 3 Results of the resistivity measurements on a number of smaller (2.7 μm) fibers.

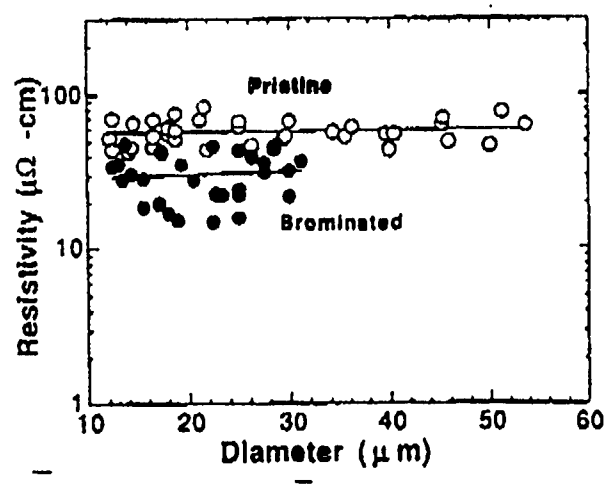

Figure 4 The results of diameter dependent resistivity for all the samples ranging from 2 to 55 μm, both pristine and brominated.

The electrical noise of carbon fibers

R. O. Dillon
Department of Electrical Engineering, University of Nebraska, Lincoln, Nebraska 68588

Roger D. Kirby
Behlen Laboratory of Physics, University of Nebraska, Lincoln, Nebraska 68588

I. L. Spain
Depa.:ment of Physics, Colorado State University, Fort Collins, Colorado 80525

(Received 15 May 1989; accepted for publication 12 July 1989)

The low-frequency excess electrical noise has been measured on carbon fibers with a wide range of crystalline perfection and corresponding electrical and mechanical properties. Fibers include those prepared from ex-PAN and ex-pitch polymers, and a catalytic-chemical vapor deposited filament. The extensional (Young's) moduli of these fibers varied from about 220 to 890 GPa (35–130 Msi), while the electrical resistivities varied from about 19 to 1 $\mu\Omega$ m. The low-frequency electrical noise of each fiber was found to be proportional to I^2 and to vary as $1/f^{\alpha}$, where f is the frequency and α is about 1.15. The most striking feature of the results was the strong dependence of the normalized noise power on the degree of crystalline perfection.

I. INTRODUCTION

Carbon fibers are inhomogeneous materials in which the basic building blocks can be thought of as ribbons. Each ribbon consists of a stack of graphene planes (planes of hexagonal carbon with vacancies and vacancy clusters), and the stacking can be random (turbostratic ordering) or regular (graphitic). The ribbons are roughly aligned along the fiber axis, and the mean misorientation angle is an important parameter which controls the extensional (Young's) modulus. The arrangement of the ribbons across the section of the fiber depends critically on the type of fiber and such parameters as the processing conditions. For instance, ex-PAN fibers usually have a random arrangement, ex-pitch fibers a radial, and catalytic-chemical-vapor-deposited (CCVD) filaments a tree-ring one.[1]

This disorder ensures that scattering of electrons is mainly by defects, except in the most perfect fibers. The degree of perfection can be partially controlled by the maximum temperature of heat treatment to which the fibers are subjected. However, graphitization and other measures of lattice perfection indicate that lattice defects can be removed more easily in the order ex-PAN, ex-pitch, CCVD fibers. An extensive account of the preparation, structure, and properties of carbon fibers can be found in Dresselhaus *et al.*[1]

This paper examines the use of conductivity fluctuations (often referred to as $1/f$ noise) as a probe of the sample perfection. The earlier work of Conner and Owston[2,3] had established that $1/f$ noise was present in the fibers. The present paper examines the fluctuations for a wide range of fibers, and shows that the normalized noise power levels are a strong function of sample perfection.

II. EXPERIMENTAL TECHNIQUES

Fibers were chosen with a wide range of properties, as is summarized in Table I. Ex-Pan fibers had moduli ranging from 220 to 480 GPa (35–70 Msi) for the commercial Celion 3000 and GY-70 types, while a heat-treated experimental one, GY-70 +, had a modulus of 690 GPa (100 Msi). The ex-pitch fibers obtained from AMOCO are designated P-100 (a commercial fiber), P-130X (an experimental fiber), and they had high moduli varying from 690 to 890 GPa (100–130 Msi). Tests were also made on a pitch fiber with an original modulus of 170 GPa (25 Msi), which had been annealed to 2800 °C. Its resistivity (Table I) was consistent with a modulus of about 550 GPa (80 Msi). One P-100 fiber

TABLE I. Fiber properties.

Fiber type	Diameter (μm)	Young's modulus [GPa (Msi)]	Electrical resistivity ($\mu\Omega$ m)
CELION-3000[a]	7.0	220 (35 Msi)	19.0
GY-70[a]	7.0	480 (70 Msi)	5.0
GY-70 +[a] (annealed 3200 °C)	7.0	690 (100 Msi)	3.7
P-25[b] (annealed 2800 °C)	9.5	~550[d] (80 Msi)	4.2
P-100[b]	9.0	690 (100 Msi)	2.88
P-130X[b]	9.1	890 (130 Msi)	1.09
P-100B[c]	8.6	690[d] (100 Msi)	2.40
CCVD	30.2		0.95

[a] Ex-PAN.
[b] Ex-pitch.
[c] Ex-pitch, boronated.
[d] Estimated, not measured.

 0021-8979/89/214284-04$02.40

which had been boronated (P-100B) was tested, since its density of carriers was increased by this process, as shown by Dillon *et al.*[4] Finally, one CCVD filament which had been annealed at 2800 °C was tested. It is emphasized that these fibers have a much wider range of properties than those normally obtained commercially.

The electrical resistivity and electrical noise measurements were made using a standard four-probe setup, with two current leads and two voltage leads. The samples were mounted on specially designed printed circuit boards, with contacts between the samples and copper strips on the board being made with silver paint. The separation of the voltage contacts ranged between 2 and 5 mm, and all contacts were found to be ohmic. A constant current through the sample was maintained using batteries and a series load resistor. The noise voltage across the voltage contacts, after blocking the dc voltage with capacitors, was amplified by a home-built preamplifier (voltage gain 950), then by an Ithaco model 1201 amplifier (typical gain 1000). The output of the Ithaco amplifier was then sent to a -72 dB/oct low-pass active filter to remove the high-frequency portions of the noise spectrum. The amplified and filtered noise voltage $V(t)$ was measured at rates ranging from 300 Hz to 12 kHz using a 12-bit analog-to-digital converter interfaced to a Digital Equipment Corporation LSI-11 computer. These data were then digitally Fourier transformed to obtain the noise voltage spectrum $V(f)$, from which the noise power spectrum

$$S_V(f) = \langle V^2(f) \rangle / \Delta f$$

could be calculated. A more detailed discussion of the experimental techniques can be found in the paper by Fagerquist, Kirby, and Pearlstein.[5] Typically 100 noise power scans were averaged to obtain the resultant noise power spectrum. The noise power spectrum obtained with zero current was subtracted from these spectra in order to eliminate contributions from the associated electronics.

Most spectra were taken using a 300-Hz sampling rate, with a 80-Hz low pass filter to prevent aliasing. Typical noise power spectra for two different currents in a Celion 3000 fiber are shown in Fig. 1. The $1/f$-like rise at low frequencies is apparent in both spectra, and the rapid falloff above 80 Hz is due to the low pass filter. The useful frequency range in these spectra is between 0.6 and 50 Hz, and over this range the magnitudes of the power spectra for each fiber were found to vary as I^2 in each case. Typical results for the dependence of S_V on I^2 are shown in Fig. 2 for fiber GY-70 + at a frequency of 10 Hz.

Figures 3 and 4 show the low-frequency behavior of the noise power spectrum for fiber samples GY-70 and P-100B, respectively. The mechanical and electrical properties of these fibers differ considerably, as indicated in Table I. The points in Figs. 3 and 4 are the measured noise powers, while the solid lines are least-squares fits. The slopes ($-\alpha$) of the fitted curves fall between -1.11 and -1.24, verifying that these samples indeed show $1/f$ noise. It should be noted that the P-100B sample required considerably more current to generate substantial noise than did the GY-70 sample.

III. DISCUSSION

Table II summarizes the results of the noise power measurements on the fiber samples. Column 2 of this table gives the values of α for each fiber sample. Note that the α is near 1.15 for all samples, with the estimated experimental uncertainty in α being ± 0.1. These values of α are similar to those obtained in carbon resistors by Fleetwood, Postel, and Giordano.[6] Column 3 gives S_R, the noise power at 1 Hz multiplied by the sample volume and divided by the current squared. Use of the phenomenological equation of Hooge,[7]

$$S_V(f) = \gamma(V^2/Nf^\alpha),$$

where γ is a constant and N is the number of charge carriers in the sample, together with Ohm's law, shows that this column is proportional to the resistance squared divided by the carrier concentration. Note that S_R decreases by about six orders of magnitude on going from the highly defective fibers to the most perfect fibers. While S_R is most sensitive to fiber perfection, columns 4 and 5 of Table II provide more fundamental information of the source of noise. The quantity S_V in column 4 is the noise power times the sample volume divided by the dc voltage squared, and is proportional to the inverse of the carrier concentration. Column 5 shows

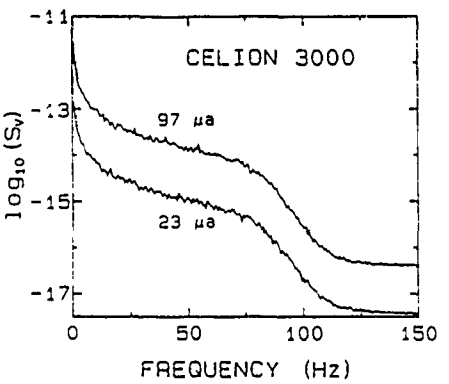

FIG. 1. Log_{10} of the noise power as a function of frequency for two different currents in CELION 3000

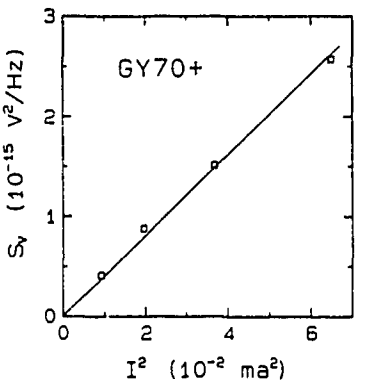

FIG. 2. Noise power vs I^2 for fiber GY-70 + . The points are the measured noise powers, and the solid line is a least-squares fit straight line constrained to pass through the origin.

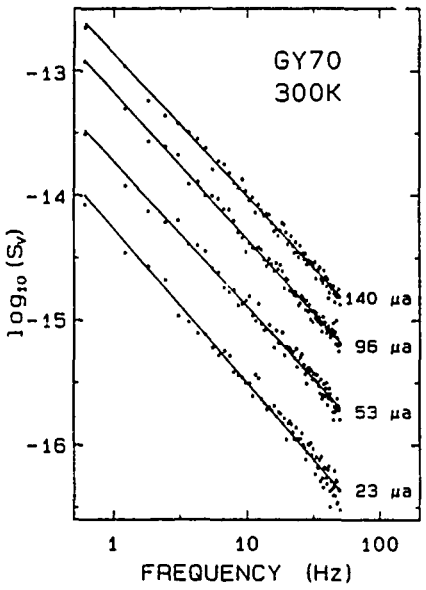

FIG 3 Log_{10} of the noise power vs $\log_{10}$ of the frequency for fiber GY-70 The points are the measured noise powers, and the solid lines are least-squares fits to the data. The values of α obtained from these fits range from 1 15 to 1.24.

S_U, which is defined as S_V divided by the resistance. Since the resistance is inversely proportional to the product of carrier concentration and mobility, S_U is proportional to the mobility. The variations of S_N in column 4 tend to be greater than those of S_U, suggesting that the dependence on carrier concentration is more important than that of mobility in comparing the noise of various fibers.

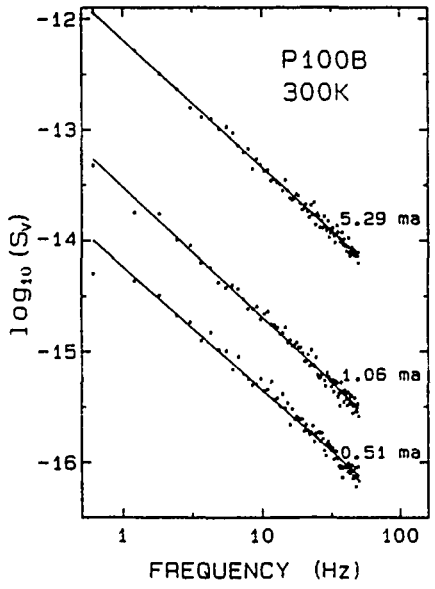

FIG. 4 Log_{10} of the noise power vs $\log_{10}$ of the frequency for fiber P-100B The points are the measured noise powers, and the solid lines are least-squares fits to the data. The values of α obtained from these fits range from 1.11 to 1.17.

TABLE II. Noise power results.

Fiber type	α	S_R (1 Hz) (10^{18} V^2 m^3/Hz A^2)	S_N (1 Hz) (10^{12} m^3/Hz)	S_U (1 Hz) (10^{10} Am^3/Hz V)
CELION-3000	1 13	18.3	14.0	1.2
GY-70	1.18	1.62	0.33	0.47
GY-70 +	1.21	$5\,1\times10^{-2}$	0.12	0.58
P-25	1.14	1.9×10^{-2}	0.051	0.26
P-100	1.19	9.9×10^{-1}	0.069	0.56
P-130X	1.2	3.0×10^{-3}	0.091	1.7
P-100B	1.15	5.5×10^{-3}	0.030	0.22
CCVD	1.2	$3\,6\times10^{-6}$	0.021	5.1

The origin of $1/f$ noise in thin metal films and semiconductors has often been assumed to be due to a distribution of carrier activation energies.[8] Dutta, Dimon, and Horn[9] used temperature dependence measurements of $1/f$ noise in thin Ag films to determine the distribution of activation energies, finding that the distribution was peaked near 1 eV, with a width of 0.4 eV. Fleetwood *et al.*,[6] in their measurements on carbon resistors, also found general agreement with the Dutta–Horn model.[8] Thus, one may speculate the $1/f$ noise in carbon fibers may also be appropriately described by a Dutta–Horn-type model which incorporates a distribution of activation energies. We intend to test this idea by carrying out measurements of the temperature dependence of the noise power in a wide range of carbon fibers. Such measurements may result in a more detailed understanding of the carrier-defect interaction in carbon fibers, and it may in fact be possible to distinguish the types and number of defects in fibers prepared by different methods. Further work is also planned in which electrical noise is studied as a function of tensile stress, at stresses near the tensile limit. Such measurements will presumably give valuable information about the fracture mechanisms, which are not well understood at the present time. In particular, it is not understood completely why the tensile strength does not increase with extensional modulus, as predicted by simple models (see for example, the work by Kelly[10]), while certain whiskers have both high moduli and strengths.[11] It is possible that the noise measurements will probe the fracture processes in unique ways.

ACKNOWLEDGMENTS

Thanks are due to Dr. Ilmar Kalnin of Celanese-Hoechst Research Company for donating the ex-PAN fibers. We also wish to thank Dr. John Barr of Amoco Performance Products Inc. for supplying pitch fibers. This research was partially funded by a grant from AFOSR to Colorado State University (Grant No. S49620-88-C-0017).

[1] M S Dresselhaus, G Dresselhaus, K. Sugihara, I. L. Spain, and H. A Goldberg, *Graphite Fibers and Filaments* (Springer, Berlin, 1988), Vol 5
[2] P C Connor and J. C. Owston, Nature 223, 1146 (1969).

[3]J. C. Owston, J. Phys. D 3, 1615 (1970).
[4]R. O. Dillon, T. Kustka, and S. Backhaus, *Proceedings of the Nineteenth Biennial Conference on Carbon* (American Carbon Society, 1989), p. 262.
[5]R. L. Fagerquist, R. D. Kirby, and E. A. Pearlstein, Phys. Rev. B 39, 5139 (1989).
[6]D. M. Fleetwood, T. Postel, and N. Giordano, J. Appl. Phys 56, 3256 (1984).
[7]See, for example, F. N. Hooge, T. G. Kleinpenning, and L. K. Vandamme, Rep. Prog. Phys. 44, 479 (1981).
[8]P. Dutta and P. M. Horn, Rev. Mod. Phys. 53, 497 (1981).
[9]P. Dutta, P. Dimon, and P. M. Horn, Phys. Rev. Lett. 43, 646 (1979).
[10]A. Kelly, *Strong Solids*, 3rd ed. (Oxford University Press, Oxford, 1983).
[11]R. Bacon, J. Appl. Phys. 31, 283 (1960).

ELECTRICAL NOISE FROM CARBON FIBERS

Rodney O. DILLON*, Roger D. KIRBY+, and Ian L. SPAIN#
*Department of Electrical Engineering, +Behlen Laboratory of Physics, University of Nebraska, Lincoln, NE 68588
#Department of Physics, Colorado State University, Fort Collins, CO 80525

1. INTRODUCTION

The low-frequency excess electrical noise (often referred to as "1/f" noise, where f is the frequency) has been measured on a wide range of carbon fibers and found to be a probe of sample perfection. The fibers include ex-PAN , ex-pitch, a boronated pitch fiber, and a catalytic-chemical-vapor-deposited (CCVD) filament which had been annealed at 2800 C. The sample perfection can be partially controlled by the maximum temperature of heat treatment to which the fibers are subjected. However, graphitization and other measures of lattice perfection indicate that lattice defects can be removed most easily in CCVD fibers, followed in order by ex-pitch and ex-PAN fibers.

2. EXPERIMENTAL TECHNIQUES

The fiber properties are given in Table 1. These properties span a much wider range than those normally obtained commercially. The electrical resistivity and electrical noise measurements were made using a standard four-probe configuration. A constant current was maintained through the outer contacts using batteries and a series load resistor. The noise voltage was filtered, amplified, and converted to digital form. These data were then digitally Fourier transformed to obtain the noise voltage spectrum V(f), from which the noise power spectrum, $S_V(f) = V^2(f) / \Delta f$, was calculated. More experimental details can be found in the paper by Fagerquist et al (1). The useful frequency range in most spectra was between 0.6 and 50 Hz.

3. RESULTS

The magnitudes of the power spectra for each fiber were found to vary as I^2 and as $1/f^{\alpha}$. Table 11 summarizes the results of the noise power measurements. Column 2 of this table gives the values of α for each fiber sample. Note that α is near 1.15 for all samples, with the estimated experimental uncertainty in α being ± 0.1. Column 3 give S_R, the noise power at 1 Hz multiplied by the sample volume and divided by the current squared. Use of the phenomenological equation of Hooge (2),

$$S_V(f) = \gamma(V^2/Nf^{\alpha}), \qquad (1)$$

where γ is a constant and N is the number of charge carriers in the sample, together with Ohm's law, shows that this column is proportional to the resistance squared divided by the carrier concentration. While S_R is most sensitive to fiber perfection, columns 4 and 5 provide more fundamental information on the source of noise. The quantity S_N in column 4 is the noise power times the sample volume divided by the dc voltage squared, and is proportional to the inverse of the carrier concentration. Column 5 shows S_U, which is defined as S_N divided by the resistance, and is proportional to mobility. The variations of S_N is column 4 tend to be greater than those of S_U, suggesting that the dependence on carrier concentration is more important than that of mobility in comparing the noise of various fibers.

We intend to test whether the 1/f noise is due to a distribution of carrier activation energies by measuring the temperature dependence of the noise power in the fibers. We wish to acknowledge partial funding by an AFOSR grant to Colorado State University (Grant No. S49620-88-C-0017)

REFERENCES

1. R.L. Fagerquist, R.D. Kirby, and E.A. Pearlstein, Phys.Rev.B 39, 5139 (1989).
2. See for example, F.N. Hooge, T.G. Kleinpenning, and L.K. Vandamme, Rep. Prog. Phys. 44, 479 (1981).

TABLE I. Fiber properties.

Fiber type	Diameter (μm)	Young's modulus [GPa (Msi)]	Electrical resistivity ($\mu\Omega$ m)
CELION-3000[a]	7.0	228 (35 Msi)	19.0
GY-70[a]	7.0	483 (70 Msi)	5.0
GY-70 +[a] (annealed 3200 °C)	7.0	690 (100 Msi)	3.7
P-25[b] (annealed 2800 °C)	9.5	~552[c] (80 Msi)	4.2
P-100[b]	9.0	690 (100 Msi)	2.88
P-130X[b]	9.1	896 (130 Msi)	1.09
P-100B[c]	8.6	690[c] (100 Msi)	2.40
CCVD	30.2		0.95

[a] Ex-PAN.
[b] Ex-pitch.
[c] Ex-pitch, boronated.
[c] Estimated, not measured.

TABLE II. Noise power results.

Fiber type	α	S_R (1 Hz) (10^{-18} V^2 m^3/Hz A^2)	S_N (1 Hz) (10^{-12} m^3/Hz)	S_U (1 Hz) (10^{-10} Am^3/Hz V)
CELION-3000	1.13	18.3	14.0	1.2
GY-70	1.18	1.62	0.33	0.47
GY-70 +	1.21	5.1×10^{-2}	0.12	0.58
P-25	1.14	1.9×10^{-2}	0.051	0.26
P-100	1.19	9.9×10^{-3}	0.069	0.56
P-130X	1.2	3.0×10^{-3}	0.091	1.7
P-100B	1.15	5.5×10^{-3}	0.030	0.22
CCVD	1.2	3.6×10^{-6}	0.021	5.1

Properties and characterization of codeposited boron nitride and carbon materials

A. W. Moore and S. L. Strong
Union Carbide, Parma Technical Center, Parma, Ohio 44130

G. L. Doll and M. S. Dresselhaus
Department of Physics and Center for Materials Science and Engineering, Massachusetts Institute of Technology, Cambridge, Massachusetts 02139

I. L. Spain and C. W. Bowers
Colorado State University, Fort Collins, Colorado 80523

J. P. Issi and L. Piraux
Université Catholique de Louvain, B-1348, Louvain-la-Neuve, Belgium

(Received 19 October 1988; accepted for publication 9 February 1989)

The physical properties of carbon-boron nitride (C-BN) prepared from mixtures of BCl_3, NH_3, and selected hydrocarbons by codeposition methods have been investigated using x-ray diffraction, electron diffraction, transmission electron spectroscopy, x-ray photoelectron spectroscopy, Raman scattering, optical reflectivity, thermal conductivity, thermopower, and electrical resistivity. Taken collectively, the results of these experiments indicate that the compression-annealed C-BN materials studied here consist of separated domains of pyrolytic boronated graphite and pyrolytic boron nitride, while as-deposited samples may possibly be a single-phase mixture of C, B, and N. As-deposited materials containing more than 20% carbon were found to be more highly oriented than unannealed pyrolytic graphite, and the crystallinity of these materials was greatly enhanced by uniaxial compression annealing. Results of the thermal conductivity, thermopower, and electrical resistivity measurements are consistent with a network of turbostratic graphite BN domains with some conduction paths for charge carrier transport between the domains. Increasing the carbon concentration from 20% to 60% leads to an increased linkage between the conducting domains and a percolation conducting network is established.

I. INTRODUCTION

The preparation of ceramic composites by chemical vapor deposition (CVD) is a topic of increasing interest in materials science since it provides a way to prepare new materials or to improve the properties of existing materials.[1] For example, because of structural similarity of hexagonal boron nitride and graphite, it was thought possible to produce a range of C-BN compounds by codepositing pyrolytic BN and pyrolytic graphite. The preparation of C-BN deposits from mixtures of BCl_3, NH_3, and C_2H_2 at 1700 °C has already been reported.[2,3] Electrical resistivity and infrared (IR) data indicated that these deposits were two-phase mixtures of BN domains and carbon domains. Badzian *et al.*[4] prepared C-BN materials by codeposition of BCl_3, CCl_4, N_2, and H_2 at 1900 °C. The x-ray diffraction measurements were interpreted to indicate that the samples were solid solutions with composition $(BN)_xC_{1-2x}$. The authors thus assumed that their C-BN material was a substitutional alloy at the atomic level, resulting from the substitution of B and N atoms for a pair of carbon atoms in the graphite hexagonal lattice. These authors further reported that their compounds decomposed to boron carbide (B_4C) and graphite when heated to 2200 °C or higher. Kouvetakis *et al.*[5] prepared C-BN materials with graphitelike structures by reacting BCl_3, NH_3, and C_2H_2 at 400–700 °C. They reported that the material had a composition $(BN)_{0.35}C_{0.30}$ and was a semiconductor at room temperature which could be both oxidatively and reductively intercalated. These authors also reported[6] on the preparation of a graphitelike compound of composition BC_3 by reacting benzene with BCl_3 at 800 °C. A similar compound of composition C_5N was obtained[6] by reacting pyridine and chlorine in a silica tube at 800 °C. Besmann[7] used CVD to prepare C-BN materials from mixtures of BCl_3, NH_3, and CH_4 at 1000–1500 °C. Based on x-ray diffraction and Auger electron spectroscopy, he concluded that these mixtures formed an extensive solid solution, but the compositions obtained, e.g., $C_{0.42}BN_{0.29}$ and $C_{1.02}BN_{0.32}$, were far from the C-BN tie line in the phase diagram.

In contrast to the studies of Refs. 2–7, the development of an electrically insulating compound called "boron carbonitride" has been reported.[8,9] This material is produced[8] by hot-pressing mixtures of BN and B_4C and then sintering the mixtures in atmospheres containing N_2, CO_2, H_2O, and O_2.

The possibility of preparing C-BN materials over a range of compositions with a corresponding range of properties offers some unique opportunities for materials science research. The varied accounts of the structure of such compounds found in the literature[2-9] and the importance of these materials for materials processing provided additional motivation for this work. The present study was undertaken to learn more about the structure and properties of C-BN made by codeposition of C and BN and to determine whether the

TABLE II. Properties of some of the as-deposited and compression-annealed C-BN samples.

Sample number	As-deposited: Mosaic spread (deg)	As-deposited: ρ_{dc} ($\mu\Omega$ m) $T = 300$ K	Compression-annealed: Hot press temp. (°C) (nominal)	Thickness (mm): Initial	Thickness (mm): Final	Thickness (mm): % decrease	Compression-annealed: Mosaic spread (deg)	Compression-annealed: ρ_{dc} ($\mu\Omega$ m) $T = 300$ K
8615	24	8–46	2100	0.56	0.56	0	17	
8615			2500	0.56	0.54	3.0	2.7	9
8617	70–72	$> 10^8$	2600	0.81	0.66	19	4	$> 10^8$
8618	35–41	250						
8619	21	9–10	2500	0.72	0 70	3 0	3	2
8619			2600	0.56	0.46	18	2.6–3.5	
8619			2700	0.51	0.41	20	3	
8621	33–48	150–4800						
8622	25–33	8–22						
8623	13–51	30	2600	0.97	0.76	27	6	
8623			2700	0.64	0.51	20	3	
8632	42–46	4–6	2600	1.19	1.07	11	6	5
8632			2700	1.40	1.27	9	4	
8701	26–34	3–5						
8702	29–32	5–7						

ysis was performed on some of the samples and the relative concentrations of C, B, and N were found to vary widely with respect to the sample position in the deposition chamber; however, the elemental abundances were found to be uniform throughout the individual samples. The analysis further shows that the high-carbon deposits were richer in boron than in nitrogen. In Table II values of the sample thicknesses, mosaic spreads of the crystallites, and room-temperature resistivities of the samples are displayed along with the sample identification numbers and carbon content. The room-temperature resistivity (ρ_{dc}) of the as-deposited samples is found to decrease with increasing carbon content from $\rho > 10^8$ $\mu\Omega$ m for $\sim 3\%$ C to $\rho \sim 4$ $\mu\Omega$ m for samples containing 75% C. This reflects the evolution in the electrical properties of the system as the increasing carbon content changes the physical characteristics from BN-like with resistivities typical of wide gap insulators to more conductive, semimetallic graphitic materials.[12]

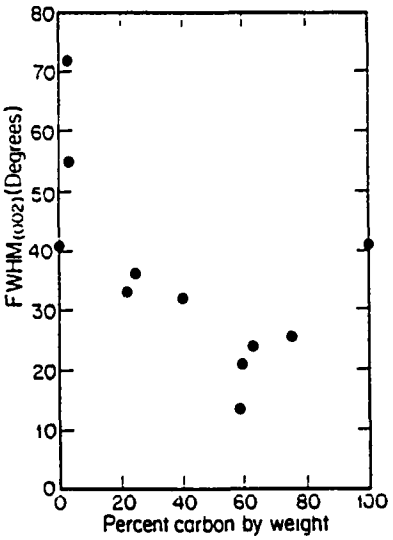

FIG. 2. Mosaic spread for codeposited C-BN samples as a function of carbon content. The mosaic spread is represented by the full width at half maximum intensity of the (002) x-ray reflection.

The effects of uniaxial hot pressing on some of the co-deposited C-BN samples are also examined in Table II. Initial pressings were done at 2100–2300 °C to minimize possible reaction between BN and carbon which might lead to phase changes. Since pressing at these temperatures had no effect on sample appearance or thickness, the pressing temperature was increased to 2500–2700 °C. Pressing under these conditions was found to cause a 10%–20% sample shrinkage in the pressing direction and samples with mirror-like surfaces similar to that of highly oriented pyrolytic graphite (HOPG) were obtained. However, the samples were not as readily cleaved as HOPG, indicating that C-BN possesses stronger interlayer bonds or smaller crystallite dimensions than HOPG. A stronger interlayer bonding is consistent with the formation of interlayer bonds with partly ionic character in BN.

B. X-ray diffraction measurements

The results of the x-ray diffraction study of the structural properties of the C-BN materials are shown in Figs. 2–6. From an analysis of the (00*l*) lattice reflections, the interplanar separation ($c_0/2$) of the as-deposited samples was deduced to be 3.40 ± 0.02 Å and independent of carbon content. This value is typical of turbostratic graphite or turbostratic BN. Compression annealing the sample reduced $c_0/2$ to values of 3.355–3.360 Å, which are typical of HOPG or boronated graphite[13] which exhibit three-dimensional (3D) ordering.

The preferential orientation of the crystallites or the mosaic spreads of the crystallites of the as-deposited samples is

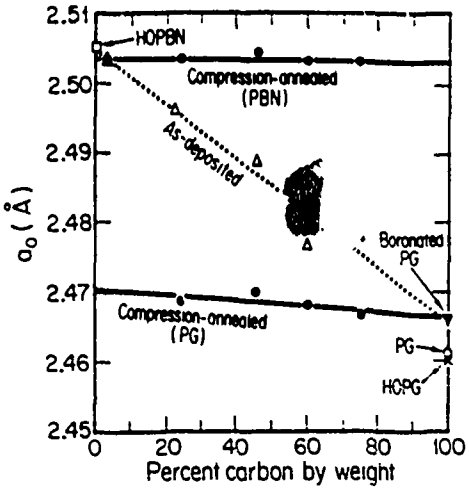

FIG. 6. In-plane lattice parameter (a_0) of the PBN (1) and PG (2) phases of the compression-annealed C-BN materials vs carbon content. Also shown is a plot of a_0 vs % C for the as-deposited C-BN samples. The values of a_0 for pristine HOPBN, HOPG, and PG are noted.

The effects of compression annealing on the crystallinity of a 45% C sample are illustrated by the (110) lattice reflections shown in Figs. 5(a) and 5(b). In Fig. 5(a), a broad line centered near 77° is observed, with a shoulder on the low-angle side of the line just visible. A deconvolution of this line into two separate lines does not yield the PBN and PG diffraction angles shown in Fig. 5(b), but instead yields lattice spacings different from those of PBN and PG. Whereas these data for the compression-annealed samples are consistent with a two-phase mixture of PBN and PG, we conclude that the as-deposited samples may be predominately a single-phase mixture of C, B, and N on an atomic scale.

The a_0 values of the BN and graphite phases as calculated from the (100) and (110) diffraction lines of the as-deposited and compression-annealed samples are plotted versus carbon content in Fig. 6. The PBN and PG phases of the compression-annealed samples are represented by the circles. For the compression-annealed samples, a_0 is constant and independent of carbon content for the PBN phase, while values of a_0 for the PG phase decrease slightly with increasing carbon concentration. Extrapolation of a_0 of the PG phase to 100% C leads to the reported value of the in-plane lattice constant of boronated graphite, slightly greater than that of HOPG.[13] This result is consistent with the chemical analyses in which the concentration of boron was found to be higher than the nitrogen concentration. In boronated graphite, small amounts of boron are substituted for C atoms and occupy regular in-plane lattice sites as opposed to intercalation compounds in which the dopant resides between the C layers. The data for the as-deposited samples show that the a_0 value decreases linearly with increasing carbon content from the PBN value of 2.505 Å to the boronated PG value of 2.466 Å. This linear behavior is again consistent with the identification of the as-deposited samples as a single-phase, homogeneous mixture of C, B, and N.

The x-ray diffraction data failed to detect any phases other than PBN and boronated PG in the C-BN samples which were compression annealed at 2500–2700 °C, although some structural inhomogeneity was observed in some samples. This is a surprising result, because separate pieces of PBN and PG are known to react and form boron carbide at these temperatures.[15] Perhaps the codeposited materials are changing their compositions slowly with temperature with a characteristic time greater than that of the experiment. To learn more about the effects of high-temperature processing on structure and composition, selected samples of C-BN are being annealed and hot pressed at temperatures up to 3000 °C.

C. Raman scattering and optical reflectivity measurements

In Figs. 7(a) and 7(b) we show the backscattered Raman spectra of as-deposited (a) and compression-annealed (b) 60% C samples. The spectrum of the as-deposited material in Fig. 7(a) is characteristic of disordered graphite in that (1) the high-frequency 1580-cm^{-1} E_{2g} line is broad and asymmetric, and (2) there is a broad Gaussian-type line shape near 1360 cm^{-1}. In disordered graphite, the 1360-cm^{-1} feature arises from crystalline disorder which suppresses the $q \approx 0$ Raman selection rules and allows phonons throughout the Brillouin zone to become Raman active.[17] The degree of disorder, or equivalently the in-plane crystallite dimension (L_a), can be quantitatively evaluated by examining the ratio of the integrated intensities of the Raman-allowed to disorder-induced peaks.[18–20] However, hexagonal BN (hBN), which shares the same crystalline structure with graphite, has a Raman-allowed E_{2g} phonon[21] near 1360 cm^{-1}. It is therefore difficult to separate the Raman-allowed BN mode from the graphitic disorder-induced

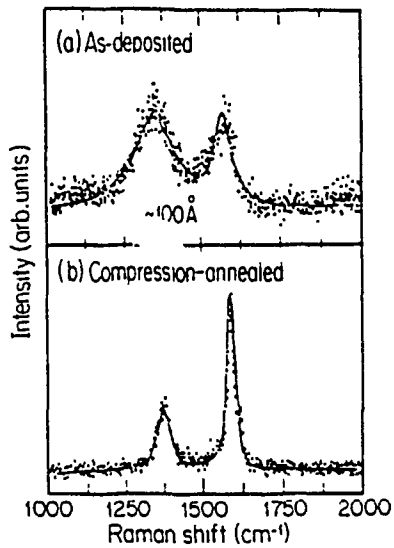

FIG. 7. Raman spectrum for an (a) as-deposited C-BN 60% C sample (No 8615) and (b) compression-annealed sample with the same carbon content. For spectrum (b), $L_a \sim 500$ Å.

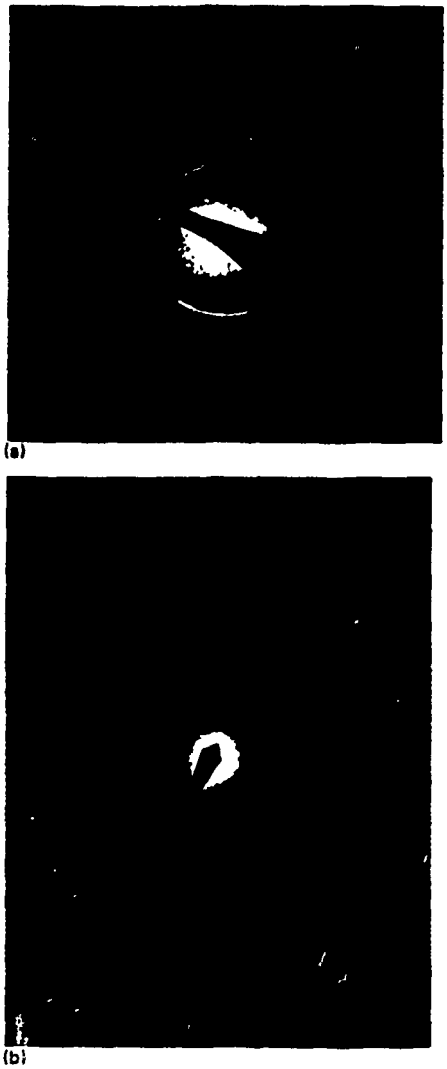

FIG. 9. Selected-area electron diffraction patterns for (a) an as-deposited (No. 8621; 22% C) sample, and (b) a compression-annealed (at 2500 °C and 75 MPa) C-BN (No. 8615; 60% C) sample.

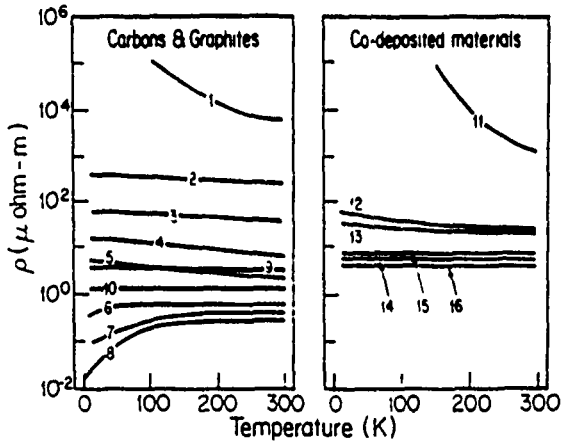

FIG. 10. Temperature dependence of the resistivity ρ for various as-deposited and compression-annealed C-BN samples. A comparison is made with the temperature-dependent resistivities of a variety of other carbons and graphites. (a) Carbon film (see Ref. 12), (2) Glassy carbon (see Ref. 12), (3) lampblack-base carbon (see Ref. 12), (4) petroleum coke carbon (see Ref. 12), (5) pyrolytic carbon as-deposited at 2100 °C (see Ref. 12), (6) graphite whisker (see Ref. 12), (7) HOPG (see Ref. 12), (8) single-crystal graphite (see Ref. 13), (9) pyrolytic carbon – 1% boron (see Ref. 28), (10) 3000 °C heat-treated PG – % boron (see Ref. 28), (11) No. 8621M (24% C) (12) No. 8621 (59%), (13 No 8621B (51% C), (14) No. 22 (75% C), (15) No 8615 (60% C) compression annealed at 2500 °C, (16) No. 8632 (60% C) compression-annealed at 2600 °C

the temperature range $10 < T < 300$ K. Depending on the composition of the samples selected for the measurements in Fig. 10, the room-temperature resistivities varied by a factor of 200. Samples containing 50%–60% carbon had resistivities in the range $5 < \rho < 9\,\mu\Omega$ m, and the resistivity of a given sample was constant over the entire temperature range from $10 < T < 300$ K. This behavior, which is the same as that of boronated PG,[12,28] is thus consistent with the interpretations of the electron energy loss and a_0 measurements showing that the graphite phase in the compression-annealed C-BN samples is saturated with boron. A 24% C as-deposited sample exhibited a sharp increase in resistivity with decreasing temperature. The shape of the resistivity versus temperature curve cannot be explained by electron hopping or by assuming that the sample is a semiconductor. Hall measurements are being made in an effort to better understand the electronic properties and the results will be presented elsewhere. Compression annealing a 60% C sample at 2500 °C was found to reduce the room-temperature value of ρ by about a factor 5, yielding a value of 2 $\mu\Omega$ m, comparable to that for graphitizable carbons with $T_{HT} \approx 2400$ °C (see Fig. 10).

A stoichiometric, substitutional alloy $C_x(BN)_{1-x}$ would be expected to have a band gap varying from ~ 0.04 eV for graphite to ~ 5 eV for BN,[12] in an approximately linear fashion with x. However, several factors can modify the electrical resistivity from that characteristic of an intrinsic semiconductor—principally, lack of stoichiometry, the presence of impurities, lattice disorder, and inhomogeneities. The resistivity results of the compression-annealed samples are consistent with a model in which PG and PBN phases coexist. In particular, curves 14–16 in Fig. 10 suggest that conduction occurs in a boron-saturated phase of turbostratic or graphitic carbon. The independence of the resistivity on temperature arises because the Fermi level is depressed well below the region of band overlap, so that the carrier density is independent of temperature, while the carrier mobility is also temperature independent as a result of scattering from grain boundaries, impurities, and defects. The as-deposited samples (curves 11–13) with higher resistivities and an increasing amount of temperature-dependent resistivity are more difficult to analyze quantitatively.

Measurements of the room-temperature, basal plane resistivity of several C-BN samples are shown in Fig. 11 as a function of carbon content. The ρ values of the as-deposited samples form a smoothly varying curve which extrapolates to HOPBN in the limit of 0% C and to PG in the 100% C limit. Whereas the ρ values of the compression-annealed

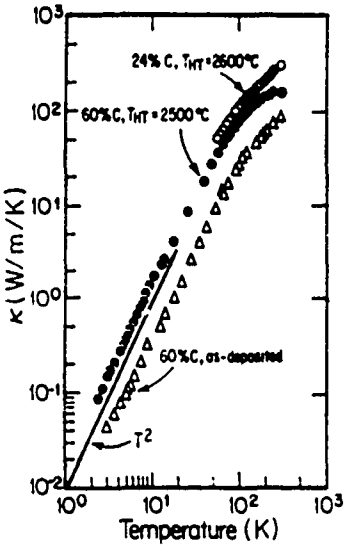

FIG. 13. Temperature dependence of the thermal conductivity $\kappa(T)$ for several C-BN samples including (1) an as-deposited 60% C sample, (2) a compression-annealed 60% C, and (3) a compression-annealed 24% C sample.

deduced, with L_a for the compression-annealed 24% C sample being larger than that of the compression-annealed 60%C sample by about a factor of 2.5. If L_a is dominated by boundary scattering, these results would suggest a growth in domain size with increasing heat treatment temperature T_{HT}. In contrast to the results of $\kappa(T)$ for the C-BN samples, the temperature dependence of $\kappa(T)$ for graphite and BN follows a power law (T^p) at low temperature where $p \sim 2.4$–2.5. This suggests that the C-BN samples are more turbostratic than the most crystalline HOPG and HOPBN materials.

Collectively, these data are consistent with a network of turbostratic graphite and turbostratic BN regions with some electrical conduction paths between the domains. From the thermopower measurements we conclude that a concentration of less than 24% C appears to be too small to link the majority of the conducting domains. Increasing the carbon content leads to an increased linkage between the conducting domains and a percolative conducting network is well established by the time a 60% carbon content is reached. The sample size dependence and the large variability of the resistivity from sample to sample suggests that large sample inhomogeneities persist for carbon concentrations as high at 60% C. The results indicate an inhomogeneous sample on a macroscopic scale, with domains in excess of $\sim 0.1\,\mu$m. Heat treatment appears to increase the domain size, but not the sample homogeneity.

IV. SUMMARY AND CONCLUSIONS

We have shown from a series of independent measurements that the compression-annealed C-BN samples examined in this study are two-phase materials comprised of pure PBN domains and boronated PG domains instead of homogeneous substitutional compounds on an atomic scale as previously reported.[4] Evidence was also given which indicates that the as-deposited samples may be a single-phase mixture of C, B, and N. In addition, evidence from x-ray diffraction, chemical analysis, electron energy loss spectroscopy, and electrical resistivity is presented which suggests that the PG phase of the C-BN samples is boronated. The crystalline orientation of as-deposited samples containing more than 24% C exceeded that of PG, and compression annealing improved the c-axis alignment to nearly that of HOPBN. Structural and optical analysis of the C-BN composites also revealed that compression annealing the as-deposited composites yielded materials with intralayer and interplanar coherence lengths L_a and L_c comparable with those found in HOPBN. The electrical and thermal transport data of the compression-annealed samples were indicative of a percolating conductive network of PG or boronated PG with islands of insulating PBN interspersed. Transport measurements performed on samples of various carbon content interpreted in this manner suggested a percolation threshold to be established for a carbon content between 24% and 60%.

The failure to detect any phases other than boron nitride and boronated graphite in the C-BN samples which were compression-annealed at 2500–2700 °C is a surprising result, because separate pieces of PBN and PG react to form boron carbide at these temperatures.[15] The codeposited materials appear to be slowly changing their composition with temperature and time. Selected samples of C-BN are now being annealed and hot pressed at temperatures up to 3000 °C to learn more about this process.

ACKNOWLEDGMENTS

Thanks are due to T. Kinisky and K. Reuter of Union Carbide's Tarrytown Technical Center for the XPS and analytical electron microscopy data, and to K. Krishnan of the National Center for Electron Spectroscopy for the EELS data. The MIT authors are grateful for support by Air Force Office of Scientific Research (AFOSF) Contract No. F49620-85-C-0147. M. S. Dresselhaus is also a member of the Department of Electrical Engineering and Computer Science at MIT.

[1] T. Hirai and T. Goto, New Mater. (Jpn.) **86**, 231 (1986).
[2] R. J. Diefendorf, U. S. Patent No 3,432,330 (1969).
[3] S. H. Chen and R. J. Diefendorf, in the Proceedings of the 3rd International Carbon Conference, Baden-Baden, June 30–July 4, 1980, pp. 44 (unpublished)
[4] A. R. Badzian, S. Appenheimer, T. Niemyski, and E. Olkusnik, in *Proceedings of the 3rd International Conference on Chemical Vapor Deposition*, edited by F. A. Glaski (American Nuclear Society, Hinsdale, IL, 1972), p. 747.
[5] J. Kouvetakis, R. B. Kaner, M. L. Sattler, and N. Bartlett, Mater. Sci. Bull. 22, 399 (1987).
[6] J. Kouvetakis, R. B. Kaner, M. L. Sattler, and N. Bartlett, J. Chem. Soc. Chem. Commun. 24, 1758 (1986).
[7] T. Bessman, Abstracts of the American Ceramic Society 90th Annual Meeting, Cincinnati, OH, May 1–5, 1988, abstract 164-B-88.
[8] G. V. Samsonov, A. I. Eroshenko, V. I. Ostroverkhov, V. A. Krat, and T. V. Dubovik, Poroshkov Metallurg 120, 46 (1972)
[9] T. V. Dubovik and T. V. Andreeva, Less-Common Metals **117**, 265 (1986).
[10] L. J. van der Pauw, Philips Res. Rep. 13, 1 (1958).
[11] J. Issi, *Intercalation in Layered Materials*, edited by M. S. Dresselhaus (Plenum Press, New York, 1987), p. 347.

The role of sputter redeposition in the growth of cones and filaments on carbon surfaces during ion bombardment*

W. A. Solberg and I. L. Spain[a)]
Department of Physics, Colorado State University, Fort Collins, Colorado 80523

(Received 29 August 1988; accepted 23 June 1990)

Cones topped by filaments with submicron diameters grow on carbon surfaces when they are bombarded with energetic (e.g., 1 keV) argon ions. It is shown that sputter redeposition is an important process by which cone growth occurs. The possible role of hydrogen in poisoning growth sites and increasing the density of cones at higher temperature is discussed. Several experiments are proposed to clarify growth mechanisms.

I. INTRODUCTION

It has been observed[1-3] that cones topped with filaments of submicron diameters and high aspect ratios grow on graphitic carbon surfaces when bombarded by argon ions with energies of ~ 1 keV. The height of the growth features is several times larger than average erosions depths, so that the process is certainly one of growth rather than preferential erosion as in metals. For the remainder of this paper such features will be referred to as cones/filaments (CFs).

The effect of bombardment is initially to smooth carbon surfaces.[3] A rapid period of growth for doses up to $\sim 1.8 \times 10^{19}$ ions/cm^2 is followed by a slower one. The CF surface density remains approximately constant in time, since second generation CFs start growing as first generation ones are being destroyed. A decrease in CF surface density and an increase in volume per CF occurs as beam energy increases, resulting in a liner increase of volume of CFs/unit surface area with increasing beam energy. More recently, the temperature dependence of the surface density of CFs has been shown to increase from zero at -30 °C to a plateau at ~ 300 °C.[4] This increase in surface density is opposite to that observed for the density of erosion features on metal surfaces, resulting from a diffusion-controlled phenomenon.[5] It was also observed[4] that growth features were more conically shaped (i.e., the base dimensions were enhanced) at higher temperature (e.g., 300 °C) than at room temperature, where filament growth was more marked.

A model to account for growth of these CFs has been proposed by Van Vechten *et al.*,[4] based on concepts developed for the growth of AlGaAs layers.[6] The carbon supply to growth sites in this model is mobile surface atoms produced by the bombardment. A defect such as a screw dislocation is postulated as the nucleation center of the growth features, and it was proposed that such dislocations continue to the tips of the filaments. This model accounts for the observation that a small concentration of metallic impurities on the substrate inhibits growth, since the density of nucleation sites becomes too high. However, the model also predicts that the ion current density must exceed a critical value for growth to occur, and this has yet to be observed experimentally. Also, the continued growth of filaments is difficult to envisage with this model, since the distance through which a surface atom must diffuse before arriving at the filament tip would be too long. For this reason the possibility that sputter-redeposition is an important process in growth was examined.

II. THE ROLE OF SPUTTER REDEPOSITION IN GROWTH

A calculation was made for the arrival rate of atoms at a CF growth feature. The calculation was simplified by assuming that a single conical structure was standing on a flat carbon surface of radius R. A cosine θ distribution was assumed for the sputtered atoms, where θ is the angle made by the sputtered atom with the normal to the surface (Fig. 1). The rate of arrival of atoms I at a conical feature distance r from the nucleation center is then

$$I = 4\pi\Phi \int_0^R \int_0^{\pi/2} (r + W/2) \times \cos\theta \arcsin[W(2r/\sin\theta) + W]\, dr\, d\theta,$$

where Φ is the sputtered flux and W is the diameter of the base. This expression was integrated numerically. The parameter R could be varied to account at least approximately for the obscuration effect of other cones, assuming that it took a value approximately equal to the mean distance between cones. The sputter rate of carbon was taken to be 40

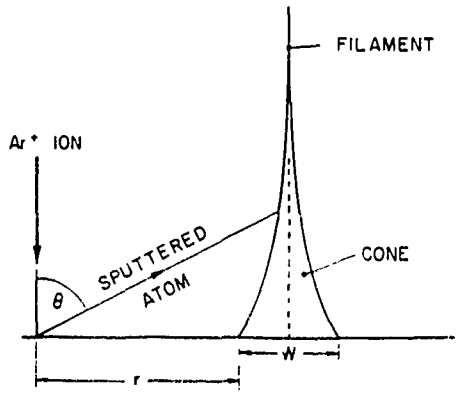

FIG. 1. A sketch of a filament/cone structure showing notation used in the text.

*Published without author corrections

A/min for a beam energy of 500 eV and beam current density of 1 mA/cm^2.[7] Thus, $\sim 5\times10^{17}$ carbon atoms/cm^2 are sputtered off in a time interval of 15 min at a current density of 0.785 mA/cm (typical experimental conditions[2-4]). For this time interval, $\sim 8\times10^{16}$ atoms/cm^2 are deposited in the growth features, or $\sim 15\%$ of the sputtered flux.

The present calculations used published results[1] for the CF dimensions at room temperature and fixed times. The number of carbon atoms arriving from sputter redeposition was then compared to the number needed to produce a cone of these dimensions. The results of the calculation are presented in Table I, where two possible densities are assumed for the carbon in the cones—2.2 and 1.7 g/cm^3. These values correspond to graphite and disordered carbon.[8] It can be seen from the table that sputter redeposition can account for the growth. The overestimation can be accounted for by either (a) shadowing effects of other structures, (b) the assumption that sputtering is from flat surfaces, whereas a high fraction of those arriving at the cones may have originated from surfaces at considerable angles from the plane, and (c) the erosion of atoms on growth features by the impinging ion beam. It is interesting that the overestimation is less severe for the initial growth period (<4 min), where a spurt in growth rates was observed.[4] This is consistent with another mechanism (surface diffusion) being partly responsible for growth. It is noted that sputter redeposition cannot be responsible for initial growth, since a growth feature already has to be present for the sputtered atoms to stick to.

It is possible that the shape difference observed[4] for CFs grown at different temperatures is a direct result of the CF surface density difference. When the CF density is high (higher temperature[4]) the fraction of scattered carbon atoms arriving at a CF from the sides of neighboring ones would be increased. Such ions would consist partly of those reflected from the nearly perpendicular walls of neighboring cones, which would be directed more to the base regions. Also, some carbon atoms would be scattered off a cone onto its base. Thus, the arrival rate at the base would be enhanced by both processes, resulting in a conical structure with enlarged base.

TABLE I. Comparison of the number of atoms redeposited compared to the number needed for growth.

Growth time (min)	Atoms redeposited	Atoms needed: Graphite	Atoms needed: Carbon	H (μm)	W (μm)
4	5.3×10^{16}	1.9×10^{16} (280%)	1.4×10^{16} (370%)	0.1	0.1
15	1.5×10^{17}	2.8×10^{16} (540%)	2.1×10^{16} (700%)	1.5	0.1
60	4.9×10^{17}	9.7×10^{16} (500%)	7.4×10^{16} (660%)	5.4	0.4
120	6.9×10^{17}	2.5×10^{17} (280%)	1.9×10^{17} (360%)	5.0	0.5

Density = 2.235 g/cm^3.
Density = 1.7 g/cm^3.
Experimental data from Ref. 3.

An experiment to establish more positively the role of sputter-redeposition, and to separate it from the nucleation process is to nucleate features at room temperature or higher, then cool the sample below -30 °C, where filaments have not been observed to grow before. If the latter stage of growth is controlled by sputter redeposition, then the CFs should continue to grow. If growth can be sustained satisfactorily in this way, then the shape effect can also be studied by nucleating at different temperatures to obtain varying surface densities. Thus, the role of surface density and temperature on shape can be separated in this way.

III. INHIBITION OF GROWTH AT LOW TEMPERATURE

Growth does not occur below ~ -30 °C and the density of CFs increases with temperature, as noted above.[4] This can be explained on the basis of a temperature-dependent reduction in the density of nucleation sites. A possible contaminant is hydrogen, which is present as H_2O in chambers pumped to 10^{-5} or 10^{-6} Torr used in the experiments.[1-4] Also, hydrogen is present in the surface of graphite samples.[9,10] It is possible that hydrogen (or another contaminant) could poison nucleation sites. At higher temperature the fraction of poisoned sites could decrease from either a thermally activated or ion-assisted process. It is known, for example, that H–C reactions are enhanced by ion bombardment (for a review, see Ref. 9). The optimum temperature for this enhancement is $\sim$800–900 K. It is possible that by the 600 K the fraction of poisoned sites has fallen sufficiently that a plateau is reached in the density of cones/filaments, as observed.[4] Experiments to test this could be:

(1) To ion-bombarded graphite in an ultrahigh vacuum chamber in which H and C–H complexes can be detected as bombardment proceeds at different temperatures. This experiment would have to be carried out with great care.[11]

(2) To repeat the above, but preheat the graphite to 2300 K to drive off hydrogen in the samples before bombardment begins.[11]

(3) To study CF growth under conditions in which hydrogen or other gaseous contaminants are introduced into the vacuum chamber with controlled partial pressures.

(4) The nucleation centers for growth have not yet been identified experimentally. It is known that only certain types of carbon can be used, but the density of CFs is independent of the type of graphite used. It would be interesting to use single crystals with known surface densities of screw dislocations to ascertain whether they correspond to maximum densities of CFs grown on them.

IV. FILAMENT GROWTH

The above models do not account for filament growth on the tips of the cones. One possibility is that growth is associated with the presence of high electric fields near the tips of sharp features. However, it is observed[1] that CFs grow into the ion beam direction rather than the field, which is always perpendicular to the surface. It is possible that growth occurs along the beam direction because sputter loss from the CF is minimized in this way. It would be useful to study the

erosion/growth processes that occur when CFs grown with ions arriving perpendicular to the surface are then exposed to an ion beam at an angle to the perpendicular. Attempts are also being made[12] to model the growth process using computer models. It is hoped that this will lead to a better understanding of the growth processes, and suggest further experiments.

ACKNOWLEDGMENTS

Thanks are due to the Air Force Office of Scientific Research for support of this work through Contracts No. F49620-84-K-0006 and No. F49620-86-C-0083. Thanks are also due to Professor J. A. Van Vechten for helpful discussions.

[a)] Deceased.

[1]J. J. Cuomo and J. M. E. Harper, IBM Tech. Disc. Bull. **20**, 775 (1975).
[2]R. S. Robinson and S. M. Rossnagel, J. Vac. Sci. Technol. **21**, 790 (1982).
[3]J. A. Floro, S. M. Rossnagle, and R. S. Robinson, J. Vac. Sci. Technol. A **1**, 1398 (1983).
[4]J. A. Van Vechten, W A. Solberg, P. E. Batson, J. J Cuomo, and S. M. Rossnagle, J. Cryst. Growth **82**, 289 (1987).
[5]H. R. Kaufman and R. S. Robinson, J. Vac. Sci. Technol. **16**, 175 (1979).
[6]J. A. Van Vechten, J. Cryst. Growth **71**, 326 (1985).
[7]Data from "Chart of Sputter Rates" (Ion Tech., Fort Collins, CO).
[8]See, for example, *Modern Aspects of Graphite Technology*, edited by L. C. F. Blackman (Academic, New York, 1970).
[9]O. Auciello, Rad. Eff. **89**, 63 (1985).
[10]P. C. Stangeby, O. Auciello, and A. A. Haasz, J. Vac. Sci. Technol. A **1**, 1425 (1983).
[11]O. Auciello, A. A. Haasz, and P. C. Stangeby, Phys. Rev. Lett. 783 (1983).
[12]S. Clarke and D. Vvedensky (private communication, 1990).

Carbon Vol 26, No 3, pp 291–293, 1988
Printed in Great Britain.

0008-6223/88 $3.00 + .00

GRAPHITIC NATURE OF CHEMICAL VAPOR-DEPOSITED CARBON FILAMENTS GROWN ON SILICON SURFACES FROM ACETYLENE

Y-X. ZHAO,* C. W. BOWERS,† and I. L. SPAIN
Department of Physics, Colorado State University, Fort Collins, CO 80523, U.S.A.

(*Received* 22 *April* 1987; *accepted in revised form* 2 *September* 1987)

Abstract—Debye–Scherer and diffractometer X-ray studies have been carried out on carbon filaments grown on carbon and silicon surfaces from the catalytic chemical vapor deposition of acetylene on Ni and Fe catalysts. From these data it is concluded that filaments grown on carbon substrates with diameters less than ~0.3 μm are essentially amorphous, or highly disordered, whereas those grown on Si substrates have a partially graphitic, turbostratic structure. Diffraction lines obtained from the cooled catalyst particle at the tip of the filaments grown on carbon surfaces could not be indexed on the basis of known Ni-C compounds.

Key Words—Carbon filaments, acetylene, catalyst, iron, nickel.

1. INTRODUCTION

There are many studies of the growth characteristics and physical properties of carbon filaments grown by catalytic chemical vapor deposition (CCVD) (see for example Refs. 1–6 and citations therein). Tesner *et al.*[7] showed that filaments of small diameter (≤0.1 μm) could be grown from acetylene in the temperature range ~450 to 700°C on nichrome wires. A more recent study of Tibbets[8] has demonstrated that filaments with diameters as small as 5 nm may be grown from natural gas. Filaments of diameters ≤0.1 μm and high aspect ratio are of interest for obscuration applications[9], and the present study was initiated to ascertain if these carbon filaments could be used for this purpose.

Carbon filaments prepared using different gaseous precursors and different catalysts can assume different forms, such as straight, twisted, or helical tubules, etc.[6] Baird *et al.*[10] found that the graphitic nature of filaments prepared from different hydrocarbons could vary appreciably. These authors categorized filaments into graphitic and nongraphitic forms. Filaments prepared from benzene are highly graphitic[11], particularly when grown to diameters greater than 1 μm.

Tibbets[8] assumed that the structure of all filaments was hexagonal carbon with tree-ring morphology. Indirect evidence for this came from the observation that most filaments appear to be hollow. He developed a model to account for this based on an extra strain-energy term in the free energy. He was able to develop a relationship between the ratio of outer to inner diameter as a function of outer diameter that fitted the experiment reasonably well for filaments prepared from natural gas. However, Baker *et al.*[12] showed that the filaments prepared from acetylene consisted of a core that oxidized more easily than the sheath. This core region was presumed to be less crystalline than the sheath, and could possibly be amorphous. The sheath was characterized as a system of hexagonal networks with a scroll-like (or tree-ring) structure. In the particular case of filaments grown from acetylene on carbon substrates, bright-field images were obtained[13] showing the formation of carbon hexagon layers around the catalyst particle.

Baker *et al.*[3] also carried out a study of CCVD growth of carbon filaments on Si surfaces from acetylene using Co, Fe, and Cr catalyst. No references to Ni-catalyzed growth on Si have been found. Major differences were observed for filamentous growth on Si from the three different catalysts. The abnormal growth sequences could not be explained completely, but it was conjectured that Si was to some extent incorporated into the catalyst particle and promoted the precipitation of graphite (see Ref. 14).

No structural determinations for C_2H_2–Ni filaments grown on Si have been reported. Accordingly, an X-ray diffraction study of carbon filaments was carried out to ascertain the structure of submicron diameter filaments and is the subject of this article.

2. EXPERIMENTAL DETAILS

Carbon filaments were grown from acetylene hydrogen mixtures (~ 10:1 ratio) at 1 atm total gas pressure and 850°C on both carbon and silicon substrates. A thin layer (~0.01 μm) of Ni catalyst was evaporated onto the surface forming small diameter spherules when heated in an Ar/H_2 atmosphere to 850°C This process of nucleation of catalyst particles typically took ~15 min after an initial furnace warmup time of ~30 min. After the nucleation

*Permanent address: Department of Physics, Chinese Academy of Science, Peking, China.
†Now at Hughes Aircraft, El Segundo, CA 90245, U.S.A.

time, C_2H_2 was introduced for approximately 30 min, allowing filaments to grow to diameters ≤0.1 μm. Then the hydrocarbon flow was arrested and the furnace allowed to cool with an Ar purge.

In the case of carbon substrates, it was found that the length of the seed nucleation time determined the size of the seeds. A 15-min period at 850°C with the thickness of the film set at 0.01 μm resulted in seed particles of diameter ~0.02 μm, with filaments initially of diameter ~0.03 μm. Some thickening clearly occurred after this initial growth stage.

It was found that the nucleation time could be critical in determining whether or not filaments grew on silicon surfaces at all. Longer times (e.g., 30 min) produced no growth, whereas shorter times (5–15 min) were satisfactory. It was found that Ni_3Si and $NiSi_2$ was forming on the surface, thereby depleting the supply of Ni catalyst particles. This was tested by examining the catalyst particles with Debye–Scherer X-ray techniques.

It was possible to examine the carbon filaments on Si substrates using a diffractometer method. In the case of carbon substrates, it was necessary to remove the filaments to avoid contamination of the diffraction lines by the substrate carbon. A Debye–Scherer camera was used in this case, with CuKα radiation in both instances. Both methods were calibrated by first obtaining diffraction data from carbon fibers (Celanese GY-70) in similar mass quantities to those estimated for the submicron filaments used in the present measurements.

3. EXPERIMENTAL RESULTS

3.1 *Filaments grown on carbon substrates*

A diffractogram was taken of a collection of filaments with mean diameter ~0.08 μm. No hexagonal carbon lines were observed, but sharp lines were obtained (see Table 1) that could be indexed on the basis of an hexagonal cell with $a = 6.17 \pm 0.002$ Å and $c = 16.84 \pm 0.01$ Å. Based on the indexing in Table 1 and the systematic extinctions, the space group was consistent with C6. The lines probably originate from a carbon–nickel compound or alloy, possibly remaining on the surface of the substrate. However, an examination of the phase diagram[15] shows that no known phases can be found with this structure. It is possible that a new metastable phase has been discovered, which has a lower free energy than the stable phases under the conditions of small particle size encountered in this work.

Table 1. X-ray data from C-Ni compound

	$\sin^2\theta$			
d(Å)	Experiment	Calculated	hkl	I/Io
3.035	0.0644	0.0644	111	100
2.479	0.0965	0.0958	114	20
2.253	0.1168	0.1166	204	40
2.089	0.1360	0.1354	205	10
1.968	0.1635	0.1642	123	20
1.871	0.1965	0.1965	009	20

$a = 6.171$ Å, $a/c = 0.366$, $c = 16.84$ Å.

Since the diffraction intensity from compounds related to the Ni catalyst increase in importance as the filament mass decreases, another diffractogram was obtained for filaments with ~0.3 μm diameter. In this case also, no diffraction lines were observed from the carbon. Several attempts to obtain diffraction lines were unsuccessful. It was concluded that the filaments were not hexagonal carbon, but highly disordered (possibly amorphous).

It is stressed that this result is not at variance with the observation of graphite filaments grown from the decomposition of benzene[11], since the filaments in this case were of larger diameter and grown at ~1200°C from a different precursor.

3.2 *Filaments on Si substrate*

Filaments grown in this case were observed in the SEM to be erratic in growth direction, with diameters between ~0.05 and 0.1 μm. The diffractometer trace indicated the presence of hexagonal carbon with $d = 3.40 \pm 0.002$ Å, which is similar to that observed for GY-70 fiber. Using the formula of Maire and Mering[16] relating to d spacing to the degree of graphitization (g)

$$d = 3.354 + 0.086\,(1 - g),$$

g is found to be 0.46 ± 0.02. This is characteristic of a PVC coke heat treated to ~2000°C[17].

Thus, the results suggest that silicon substrates yield carbon filaments with graphitic structure at much lower reaction temperature than those grown on carbon substrates. The reason for this has not been established, but it is possible that a nickel/silicon eutectic is formed (Ref. 14), which is either in a liquid state or close enough to liquid that diffusion rates are enhanced. The eutectic at ~50% Ni (T = 964 and 966°C) are possibilities. The use of eutectics with low melting temperature could be exploited in commercial applications. No trace of silicon could be found where the filaments were examined using EDAX, but this examination did not include the catalyst particle, since no filament ends could be found.

4. CONCLUSIONS

X-ray diffraction data have been obtained on carbon filaments grown by a catalytic chemical vapor deposition technique. The structure of filaments of diameter ~0.1 μm grown on Si were consistent with hexagonal carbon with a degree of graphitization ~0.46. However, no diffraction lines could be obtained from filaments of diameters ~0.08 and 0.3 μm grown on carbon substrates. It is concluded that these filaments are highly disordered, and possibly amorphous. The growth of partially graphitic filaments on silicon surfaces at low reaction tempera-

tures is noteworthy and may be of technological significance. Further work has shown that the growth of these filaments occurs over a fairly narrow range of growth temperatures, and will be reported in detail at a later time.

Acknowledgment—This research was supported by a grant from AFOSR (#F49620-84-K-0006). GY-70 fibers were kindly supplied by Dr. Harris Goldberg of Celanese Research Co. Help with X-ray equipment is gratefully acknowledged from Professors D. Winder and J. Mahan.

REFERENCES

1. T. Koyama, *Carbon* **10**, 757 (1972).
2. R. T. K. Baker, M. A. Barker, P. S. Harris, F. S. Feates and R. J. Waite, *J. Catalysis* **26**, 51 (1972).
3. R. T. K. Baker, P. S. Harris, R. B. Thomas and R. J. Waite, *J. Catalysis* **30**, 86 (1973).
4. M. Endo, T. Koyama and Y. Hihsiyama, *Japan. J. Appl. Phys.* **11**, 2073 (1976).
5. G. G. Tibbets, *Appl. Phys. Lett.* **42**, 666 (1983).
6. A review up to 1978 has been given by R. T. K. Baker and P. S. Harris, *Chem. Phys. Carbon* **14**, 83 (1978).
7. P. A. Tesner, E. Y. Robinovitch, I. S. Rafalkes and E. F. Arefieva, *Carbon* **8**, 435 (1970).
8. G. G. Tibbets, *J. Cryst. Growth* **66**, 632 (1984).
9. Much of the earlier work is classified, but accounts can be obtained in *Proc. 1985 CRDC Conf. on Obscuration and Aeroso! Research*, R. H. Kohl, Assoc. (1985), particularly the paper by N. E. Pederson, P. C. Waterman and J. C. Pederson, p. 551, or *Absorption and Scattering of Light by Small Particles* by C. F. Bohren and D. R. Huffman, Wiley, New York, (1983).
10. T. Baird, J. R. Fryer and B. Grant, *Carbon* **12**, 591 (1971). (See also *Nature* **233**, 329 (1971).)
11. M. Endo, A. Oberlin and T. Koyama, *Japan J. Appl. Phys.* **15**, 1519 (1977).
12. R. T. K. Baker, M. A. Barber, P. S. Harris, F. S. Feates and R. J. Waite, *J. Catalysis* **26**, 51 (1972).
13. M. Raghavan, *Proc. 37th Annual Electron Microscopy Society of America*, p. 484 (1979) (ed. G. W. Bailey).
14. C. Baraniecki, P. Pinchbeck and F. B. Pickering, *Carbon* **7**, 213 (1969).
15. M. Hansen and K. Anderko, *Constitution of Binary Alloys*, McGraw-Hill, New York (1958).
16. J. Maire and J. Mering, *Proc. 4th Biennial American Carbon Conf.*, 345 (1960).
17. For a review, see J. M. Hutcheon, Ch. 1, p. 1 in *Modern Aspects of Graphite Technology*, ed. L. C. F. Blackman, Academic Press, London and New York (1970).

X-ray diffraction data for graphite to 20 GPa

You Xiang Zhao* and Ian L. Spain
Department of Physics, Colorado State University, Fort Collins, Colorado 80523
(Received 22 September 1987; revised manuscript received 19 December 1988)

X-ray diffraction data have been obtained on polycrystalline graphite at pressures up to 20 GPa. A phase transition is observed at ~11 GPa, as evidenced by softening in the interlayer spacing and the observation of new diffraction lines. Below this pressure the variation of the lattice parameters a and c are compared with elastic stiffnesses obtained from ultrasonic measurements. A new value for C_{13} is proposed. The variation $c(P)$ is compared to the recently proposed universal isotherm equation.

INTRODUCTION

Graphite is of considerable experimental and theoretical interest since it is the most highly anisotropic element and is a semimetal. This interest extends to the high-pressure properties of graphite and of its intercalation compounds (see Ref. 1 for a recent review). In spite of this, there is some uncertainty in the compressibilities, which are fundamental to any comparison of experiment and theory (see Ref. 2 for a review).

The crystal structure of graphite is one in which the carbon atoms lie in honeycomb sheets, with extremely strong covalent bonds between the atoms in each sheet. The interlayer bonds are relatively weak, and an *ABAB* . . . stacking sequence results in hexagonal crystal symmetry, *D6h*.[3-5] An alternative *ABCABC* . . . stacking sequence (rhombohedral symmetry) is found in defective graphite, always as a mixture with the hexagonal phase.[6]

As a result of the anisotropy of the crystal structure, the compressibility of graphite is highly anisotropic. The planar Young's modulus is 1020 GPa and is higher than for any other substance, while in the c-axis direction it is only 37 GPa at atomspheric pressure (see Ref. 2). There have been several studies of the compressibilities, and the data are not consistent. The results of piston cylinder,[7-9] precision elastic constant,[10-12] and x-ray diffraction[14,15] measurements are reviewed by Kelly.[2] Representative data from these measurements are shown by him[2] to 2.5 GPa. It can be seen that the discrepancies between different sets of data are considerable. This is probably due in part to problems with pressure scales used, which have been subject to revision (see Ref. 16, for example).

X-ray diffraction data of Lynch and Drickamer[15] indicated that the hexagonal graphite phase persists to the highest pressure obtained in our study. However, Bundy[16] and Aust and Drickamer[17] reported that the resistivity of certain kinds of graphite increased in such a manner at about 14 GPa that a phase transition was occurring. Aust and Drickamer reported the presence of a cubic phase on release of pressure, but a hexagonal phase was reported by Bundy and Kasper after quenching from about 12 GPa and 2000 °C,[18] with diffraction lines recorded in Fig. 1(e). This phase was called hexagonal diamond by them. It should be noted that no *in situ* high-pressure x-ray diffraction measurements have been reported on this tranition either at room or high temperature.

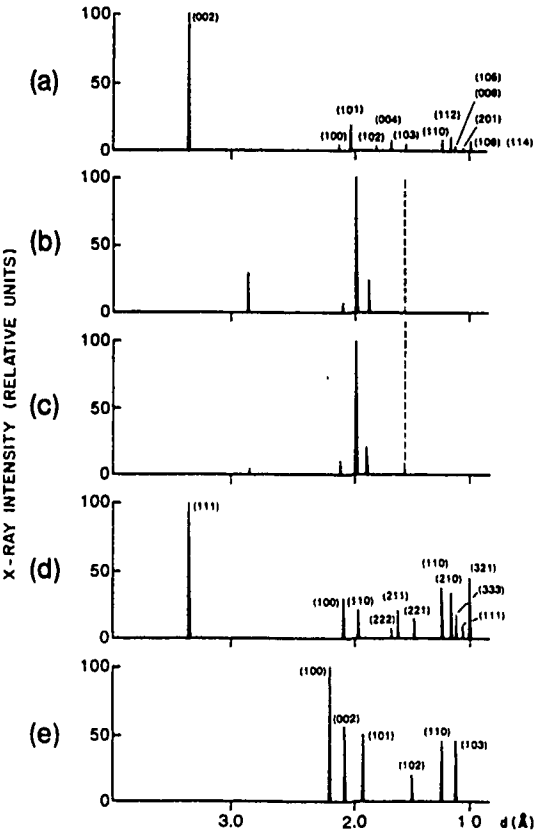

FIG. 1. X-ray diffraction lines for various pressures and comparison with other work: (a) graphite at 0 GPa, (b) pattern obtained at 13.5 GPa, (c) pattern at 16.4 GPa, (d) rhombohedral graphite at 0 GPa, and (e) pattern obtained by Bundy and Kasper at 0 GPa after compression to high pressure. The pattern obtained on release of pressure was an equimixture of (a) and (d). The dashed line represents the window of the diamond-anvil cell.

Most theoretical studies of the compressibilities have used phenomenological models of the interatomic forces.[2] These models appear to describe the compressional elastic constant C_{33} and its variation with pressure reasonably well to 1 GPa, but are inappropriate for describing the shear modulus C_{44}.[19] More recently, an *ab initio* calculation of the internal energy of graphite at high pressure has been made.[20] Such calculations can yield accurate estimates of the compressibilities and high-pressure phases of certain elements.[21] However, the anisotropy of graphite adds further complexity to the calculations, so that graphite can be looked at as a test case for the theoretical models.

The present work was carried out to obtain accurate data on the crystal parameters of graphite at high pressure using modern pressure scales and improved x-ray diffraction techniques compared to earlier work (see Ref. 22 for a review). This is particularly necessary, since it has been observed in the case of several other elements that earlier data could be significantly improved. In the particular case of the data of Lynch and Drickamer,[15] their pressures are probably overestimated increasingly with higher pressure (see Ref. 22), so that curvature in $a(P)$ data is probably a result of this. These data will be compared with empirical and *ab initio* calculations.

EXPERIMENTAL DETAILS

X-ray diffraction experiments were carried out in a diamond-anvil apparatus using a fixed-anode source and photographic detection using a double-film camera.[23] In order to reduce the error of the d spacings as much as possible, the further film was set 100 mm from the sample, allowing diffraction lines to be observed with $2\theta < 32°$. The standard deviations in c/c_0 and a/a_0 were estimated to be 0.001 and 0.002 Å, respectively. However, the diffraction lines were broadened considerably above the transition, so that the uncertainty in diffraction angles increased by a factor of about 2 or 3, and lattice spacings were uncertain because the crystal structure was not known. Exposure times between 5 and 15 days were required to give reasonable intensity, with the longer exposures being required at higher pressure.

Samples were compressed in 4:1 methanol-ethanol solution, which remains close to hydrostatic to 10 GPa,[24] and reasonably hydrostatic to the highest pressure used in our work. Pressure was measured using the ruby-fluorescence scale,[25] with a measurement precision of 0.03 GPa below 10 GPa, falling to about 0.2 GPa at 20 GPa due to line broadening in the nonhydrostatic medium. All measurements were carried out at room temperature (295±2 K).

The sample was a fine-grain polycrystalline graphite (Poco ZXF-5Q) (Ref. 26) which was loaded into the sample cavity of diameter 200 μm with a ratio of sample fluid to sample of about 3:1 to ensure that the diamond anvils did not compact the sample directly. This type of material was chosen after experimentation with other types to give a diffraction pattern with reasonably fine grain. (It is to be noted that the process of grinding single-crystal graphite to small crystallite dimensions compared to the sample cavity diameter of 200 μm produces rhombohedral lines, as noted above.[6])

Two experiments were carried out on different samples, the first to 12 GPa, at which the diffraction lines became weak, and the second to 20 GPa. This second experiment was carried out on a sample in the form of a disk of thickness 50 μm. When used with diamond anvils of culet diameter 650 μm and a hardened Inconel 718 gasket, this ensured that the diamonds did not touch the sample. In the case of an anisotropic material with weak interplanar bonds such as graphite, this can cause preferential alignment. Even so, the intensity was reduced considerably above 10 GPa. The relatively long exposure times needed for graphite are a result of the low atomic-scattering factor, but the decrease in intensity at high pressure must result from other causes, such as the phase transition discussed in the next section.

EXPERIMENTAL RESULTS

Up to about 12 GPa, three diffraction lines of graphite, indexed as (002), (100), and (101), could be observed within the window afforded by the diamond cell and camera. Their intensities (Fig. 1) were in reasonable agreement with standard compilations,[27] except for the (101) line, where our calculations indicate that the ASTM card[27] is in error. Experimental data for a/a_0 and c/c_0 are plotted in Fig. 2, and presented in Table I.

At about 10 GPa, the c-axis parameter softened somewhat (Fig. 2), and at 11.8 GPa a steep decrease in c was observed (see note below). After this softening, one extra diffraction line was observed, becoming stronger as pressure was increased, until the pattern with four diffraction lines was observed at 13.5 GPa [Fig. 1(b)]. The relative intensities of the lines continued to change, with the pattern observed at 16.4 GPa being shown in Fig. 1(c). It is noted that the strongest reflection for graphite, the (002), was weakened, and continued to diminish in intensity to the highest pressure. Assuming that this diffraction line

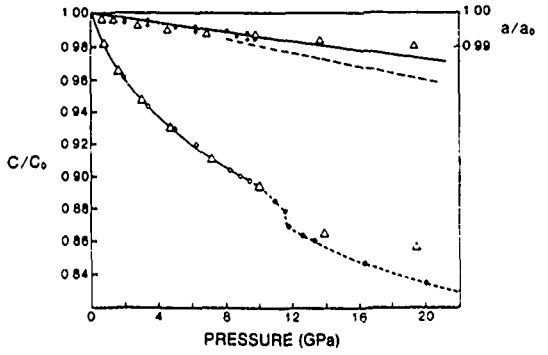

FIG. 2. Present experimental data for the a- and c-axis lattice parameters of graphite to 20 GPa. As explained in the text, the c-axis values above 10 GPa are obtained on the assumption that the line near 3 Å gives the c-axis spacing. The solid line for $a(P)$ is the best fit to the data, the dashed line the prediction using elastic constants from Table I, and the solid triangles the data of Lynch and Drickamer (Ref. 15).

TABLE I. Experimental data for lattice parameters of graphite as a function of pressure.

	P (Gpa)					
	0	2.07	3.5	5.2	6.4	8.2
a (Å)	2.462	2.457	2.455	2.451	2.450	2.448
c (Å)	6.707	6.445	6.324	6.231	6.167	6.060
	8.8	9.5	9.9	11.0	11.6	11.9
a (Å)	2.446	2.445	2.445	2.443	2.442	2.441
c (Å)	6.039	6.022	5.996	5.936	5.892	5.825
	12.7	13.4	16.4	20.0		
a (Å)	2.440	2.439	2.435	2.430		
c (Å)	5.789	5.768	5.764	5.594		

can still be related to the interlayer separation, as for the graphite structure, the decrease in $c(P)$ is plotted in Fig. 2 to 20 GPa. In view of the uncertainty in the structure above about 10 GPa, the a parameter is only plotted to this pressure. If it is assumed that the high-pressure structure is consistent with a mixture of phases, including hexagonal graphite, the values of $a(P)$ deduced from the assumed (100) line lay on a straight line extrapolated from the data shown, but the experimental uncertainty in a was about 0.5%.

DISCUSSION OF RESULTS

The formulas for the volume elastic modulus (bulk modulus) B_v and linear moduli B_a and B_c in terms of the elastic stiffness C_{ij} are

$$B_v = X(C_{11}+C_{12}+2C_{33}-4C_{13})^{-1}\,, \tag{1a}$$

$$B_a = X[2(C_{33}-C_{13})]^{-1}\,, \tag{1b}$$

$$B_c = X(C_{11}+C_{12}-2C_{13})^{-1}\,, \tag{1c}$$

where

$$X = C_{33}(C_{11}+C_{12})-2C_{13}^2\,. \tag{1d}$$

Unfortunately, the error limits in the experimental data (Table II) at $P=1$ atm result in considerably higher uncertainty in the compressibilities than for typical elements:

$$B_a = 1040\pm240 \text{ GPa}\,,$$

$$B_c = 37.0\pm1.6 \text{ GPa}\,,$$

$$B_v = 35.8\pm1.6 \text{ GPa}\,.$$

Table II also includes experimental data of the pressure dependence of the elastic constants, evaluated from their slopes at $P=0$. These data allow an estimate to be made of the pressure–lattice-parameter relationships using empirical relationships such as the Murnaghan equation (see Ref. 13 and later in this paper for a discussion). It is noted that experimental values of the pressure dependence of C_{33}, which is crucial for the variation $c(P)$, differ considerably (Table II).

a-axis compression

The compression of the lattice parameter a is less than 1% at 10 GPa, so that a linear fit to the data, with slope equal to the modulus B_a, is appropriate. For instance, using $B_0=1580$ GPa and $B_0'=5$ with the Murnaghan equation, which should give excellent agreement with data in this limited pressure range ($P/B_0<0.013$), the difference in slopes of $a(P)$ calculated using data points

TABLE II. Elastic constants and their pressure derivatives.

Elastic constant	Experimental value[a] (GPa)	Pressure derivative	Second pressure derivative $(\text{GPa})^{-1}$
C_{11}	1060±20	39[b]	
C_{12}	180±20	11[b]	
C_{13}	15±5	3.1[b]	
C_{33}	36.5±0.1	9.6[b]	-1.3±0.6[b]
		14.7±0.4[c]	-2.9±1[c]
C_{44}	4.5±0.05	0.0023	
		5–10[c]	

[a]Reference 10.
[b]Reference 12.
[c]Reference 11.

at 10 and 20 GPa is less than 1.5%. A second-order fit to the present data, for which $\Delta a/a \approx 0.001$ at 10 GPa and 0.003 at 20 GPa would not be useful. The least-squares fit to the data gives a modulus value of 1580±200 GPa, which is higher than the estimate of 1040±240 GPa based on ultrasonic measurements. The most likely explanation is that the experimental value of C_{13} in Eq.(1b) is incorrect. If the experimental value for $B_a = 1580 \pm 200$ from the present measurements is used together with values of C_{11} and C_{12} from Table I, then the value $C_{13} = 22 \pm 2$ GPa is obtained, which is slightly above the upper error limit of the value obtained by Blakslee *et al.*[10] This contrasts with the negative theoretical estimate for C_{13} obtained by Jansen and Freeman,[20] which would give a much lower value of B_a (i.e., $\lesssim 620$ GPa). It is noted that an analysis of the bulk modulus B_a can give a more accurate value for C_{13} than ultrasonic measurements.

The present data can also be compared to covalent-bond models which give the variation of lattice parameters with pressure.[28] However, the input data for these models are the elastic constants, and the predicted variation for $a(P)$ is indistinguishable from that of the linear fit to the data because the range of reduced pressure is so small.

c-axis compression

The *c*-axis compression is higher than 10% at 10 GPa, so that equations of state based on the value of C_{33} and its pressure derivative at $P=0$ are inadequate to describe the data. A universal form for the isotherm of solids has been recently proposed.[29–31] It has also been shown[31] that the limiting forms as V/V_0 approaches zero of several empirical equations are identical with that of the new equation:

$$P(X) = B_0[3(1-X)/X^2]\exp[\zeta(1-X)] , \qquad (2)$$

where B_0 is the bulk modulus at $P=0$, X is the reduced volume, V/V_0, and ζ is the pressure derivative of the bulk modulus at $P=0$. Accordingly, a plot of $\ln[P(X)X^2/3(1-X)]$ versus $1-X$ should give a straight line of intercept equal to $\ln B_0$ and slope ζ. Although this equation was derived for isotropic metals, it is instructive to test it with the present data.

Figure 3 plots the experimental data in this form (solid curve). The phase transition is clearly seen, and is similar to curves obtained for other transforming materials.[3] The intercept gives a bulk modulus of 30.8±2 GPa, which is significantly less than the accepted value of $B_c = 35.8 \pm 1.6$ GPa derived from elastic constants. As seen from Eq. (1a), this could be due to errors in C_{11}, C_{12}, C_{13}, and C_{33} or to the inapplicability of Eq. (2) to an anisotropic material. The results discussed below suggest that the accepted value of C_{33} is reasonable. Since B_c does not depend strongly on C_{13}, whose value has been fixed from B_a, and the parameters C_{11} or C_{12} are known accurately from ultrasonic data (Table I), the present data point to a limitation in the applicability of Eq. (2).

The data are plotted in an alternative form in Fig. 3,

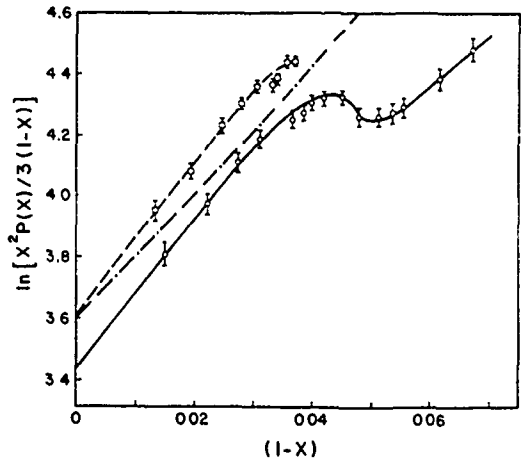

FIG. 3. Plot of $\ln[X^2P(X)/3(1-X)]$ vs $1-X$ (the units of P are GPa). The open circles are for $X^3 = V/V_0$, fitted with the solid line, the squares are for $X'^3 = C/C_0$, fitted with a dashed line, and the dotted-dashed line is for the Lennard-Jones equation (3), with $C_{33} = 36.5$ GPa.

where X is replaced by $X' = c/c_0$ with a dashed line. In this case the relatively unimportant contribution from in-plane contraction is neglected. The intercept equals the acoustic value of $B_c = 37$ GPa within experimental error, but the initial slope (25±3) is much higher than either of the previous determinations from velocity measurements (see Table I). This is consistent with fitting $P(c/c_0)$ data in Fig. 2 to empirical equations, in which it is found that the ultrasonic data of Ref. 12, with a higher value of C'_{33}, give c/c_0 values which fit the data more nearly than using values from Ref. 11. The discrepancy between the $P(c/c_0)$ values using data from Ref. 12 and the experimental data is in the direction that a higher value of C'_{33} is called for.

A Lennard-Jones interplanar potential model is often used for graphite, giving good agreement with thermal and elastic data.[32] The resulting isotherm equation, assuming negligible *a*-axis contraction, is[2]

$$P = \frac{C_{33}}{6}\left[\left(\frac{c_0}{c}\right)^4 - \left(\frac{c_0}{c}\right)^{10}\right] . \qquad (3)$$

This equation is plotted in Fig. 3 as the dotted-dashed line, using $B_c = C_{33} = 36.5$ GPa. It can be seen that the line is straight at low compressions, but bows upwards at higher values, consistent with the pressure derivative C'_{33} increasing with pressure. The initial slope is 19.7, which is considerably larger than either of the values estimated from elastic data (Table I), but lower than that required to fit the present data.

Phase transition at high pressure

Both the softening of the interlayer forces near 12 GPa (Figs. 1 and 2) and changes in the diffraction pattern [Figs. 1(b) and 1(c)] argue for a phase transition near this pressure. It was not possible to assign a structure to the

high-pressure phase, but it was possible to rule out the possibility of its being hexagonal diamond,[18] particularly since this phase was not obtained on release of pressure, but an approximately equivolume mixture of hexagonal and rhombohedral graphite. It is possible that the phase transition is related to that observed in resistivity measurements[16,17] if allowance is made for differences in pressure scales.[22] Unfortunately, shock data have been aimed at a higher pressure and temperature range. Recent measurements[33] of higher precision still show considerable scatter at pressures between 10 and 20 GPa, so that a transition such as that observed here cannot be confirmed from these data.

The question of the origin of the softening can only be answered by obtaining data on higher-index peaks. This can be obtained, in principle, by using synchrotron radiation. An experiment on a single crystal of graphite in a compressing medium such as argon using synchrotron radiation is recommended. Such measurements would also be invaluable for increasing the precision of measurement of $a(P)$, and of determining a precise value of C_{13}.

CONCLUSIONS

X-ray diffraction data have been obtained on polycrystalline graphite to 20 GPa, from which it was deduced that a phase transition occurred at ~ 11 GPa, which accounts for a discontinuity found in previous resistivity measurements. A mixture of hexagonal and rhombohedral graphite was found on release of pressure, so that the high-pressure phase was probably planar, and not related to the formation of three-dimensional bonds, as found in metastable phases at higher pressure and temperature. It was not possible to specify the high-pressure phase from the limited data available.

The data to about 10 GPa were analyzed to give $a(P)$ and $c(P)$. These data were then analyzed in terms of a function proposed as a universal isotherm. It was found that the in-plane modulus B_a was higher than the value based on elastic stiffnesses, and allowed a new value of C_{13} to be proposed.

ACKNOWLEDGMENTS

Thanks are due to the U.S. Air Force Office of Scientific Research for (Contract No. F49620-84-K-006) supporting this work. The assistance of Carmen Rocca, Charles Bowers, and Donald Trock is gratefully acknowledged. Thanks are also due to Henri Jansen for providing a copy of his work prior to publication and for pointing out an error in our analysis of C_{13}, and to Dr. John Shaner for communicating results of his work prior to publication.

---

*On leave from Institute of Physics, Chinese Academy of Science, Beijing, China.

[1]R. Clarke and C. Uher, Adv. Phys. **33**, 469 (1984).
[2]B. T. Kelly, *The Physics of Graphite* (Applied Science Publishers, London, 1981).
[3]A. W. Hull, Phys. Rev. **10**, 661 (1917).
[4]J. D. Bernal, Proc. Phys. Soc. London, Sect. A **106**, 749 (1924).
[5]O. Hassel and H. Mark, Z. Phys. 18, 291 (1924).
[6]H. Lipson and A. R Stokes, Proc. Phys. Soc. London, Sect. A **181**, 101 (1942).
[7]T. W. Richards, J. Am. Chem. Soc. 1934 (1915).
[8]J. Basset, Compt. Rend. **213**, 829 (1941).
[9]P. W. Bridgman, Proc. Am. Acad. Arts Sci. **76**, 9 (1945); **76**, 55 (1945).
[10]O. L. Blakslee, D. G. Proctor, E. J. Seldin, G. B. Spence, and T. Weng, J. Appl. Phys. **41**, 3373 (1970).
[11]J. F. Green, P Bolsaitis, and I. L. Spain, J. Phys. Chem. Solids **34**, 1927 (1973)
[12]W. B. Gauster and I. J. Fritz, J. Appl. Phys. **45**, 3309 (1974).
[13]L. Knopff, in *High Pressure Physics and Chemistry*, edited by R. S. Bradley (Wiley, New York, 1951), p. 227.
[14]S. S. Kabalkina and L F. Vereschagin, Dokl. Akad. Nauk SSSR **131**, 300 (1960) [Sov. Phys.—Dokl. **5**, 373 (1960)].
[15]R. W. Lynch and H.G. Drickamer, J. Chem. Phys. **44**, 181 (1966).
[16]F. P. Bundy, J. Chem. Phys. **38**, 631 (1963).
[17]R. B. Aust and H. G. Drickamer, Science **140**, 817 (1963).
[18]F. P. Bundy and J. S. Kasper, J. Chem. Phys. **46**, 3437 (1967).
[19]J. F. Green and I. L. Spain, Phys. Rev. B **11**, 3935 (1975).
[20]H. J. F. Jansen and A. J. Freeman, Phys. Rev. B **35**, 8207 (1987).
[21]M. L. Cohen, Science **234**, 549 (1986).
[22]A. Jayaraman, Rev. Mod. Phys. **55**, 65 (1983).
[23]I. L. Spain, D. R. Black, Z. L. D. Merkle, J. Z. Hu, and C. S. Menoni, High Temp. High Pressures **16**, 507 (1985), and references therein.
[24]G. J. Piermarini, S. Block, and J. S. Barnett, J. Appl. Phys. **44**, 5377 (1973).
[25]J. D. Barnett, S. Block, and G. J. Piermarini, Rev. Sci. Instrum. **44**, 1 (1973).
[26]Poco Graphite Inc., Dekatur, TX 76243, Type ZXF-5Q.
[27]American Society for Testing Materials, Philadelphia, PA, Crystallographic Data, Card 12-212.
[28]V. N. Zharkov and V. A. Kalinin, *Equations of State for Solids at High Pressures and Temperatures* (Consultants Bureau, New York, 1970).
[29]P. Vinet, J. Ferrante, J. R. Smith, and J. H. Rose, J. Phys. C **19**, L467 (1986).
[30]P. Vinet, J. Ferrante, J. H. Rose, and J. R. Smith, J. Geophys. Res. **92**, 9319 (1987).
[31]H. Schlosser and J. Ferrante, Phys. Rev. B **37**, 4351 (1988).
[32]B. T. Kelly and P. L. Walker, Carbon **8**, 211 (1970).
[33]J. Shaner (unpublished data), of Los Alamos Scientific Laboratory, communicated privately.

M. S. Dresselhaus · G. Dresselhaus
K. Sugihara · I. L. Spain · H. A. Goldberg

Graphite Fibers and Filaments

With 226 Figures

Springer-Verlag Berlin Heidelberg New York
London Paris Tokyo

A29

Professor Dr. Mildred S. Dresselhaus
Dr. Gene Dresselhaus
Dr. Ko Sugihara
Massachusetts Institute of Technology,
Cambridge, MA 02139, USA

Professor Dr. Ian L. Spain
Colorado State University,
Fort Collins, CO 80523, USA

Dr. Harris A. Goldberg
Celanese Hoechst Corp.
Summit, NJ 07901, USA

Guest Editor: Professor Dr., Dres. h. c. Manuel Cardona
Max-Planck-Institut für Festkörperforschung, Heisenbergstrasse 1
D-7000 Stuttgart 80, Fed. Rep. of Germany

Series Editors:

Prof. Dr. *K.A. Müller*
IBM, Zurich Research Lab.
CH-8803 Rüschlikon, Switzerland

Prof. Dr. *U. Gonser*
Fachbereich 12.1
Werkstoffwissenschaften
Universität des Saarlandes
D-6600 Saarbrücken, FRG

Dr. *M.B. Panish*
AT&T Bell Laboratories,
600 Mountain Avenue,
Murray Hill, NJ 07974, USA

Dr. *A. Mooradian*
Leader of the Quantum Electronics Group, MIT,
Lincoln Laboratory, P.O. Box 73,
Lexington, MA 02173, USA

Prof. *H. Sakaki*
Institute of Industrial Science,
University of Tokyo,
7-22-1 Roppongi Minato-ku,
Tokyo 106, Japan

ISBN 3-540-18938-6 Springer-Verlag Berlin Heidelberg New York
ISBN 0-387-18938-6 Springer-Verlag New York Berlin Heidelberg

Library of Congress Cataloging-in-Publication Data. Dresselhaus, M.S. Graphite fibers and filaments (Springer series in materials science ; v. 5) Bibliography: p. Includes index. 1. Graphite fibers. I. Title. II. Series. TA455.G7D74 1988 620.1'93 88-4593

Printing: Druckhaus Beltz, 6944 Hemsbach/Bergstr.
Binding: J. Schäffer GmbH & Co. KG, 6718 Grünstadt
2153/3150-543210

Contents